



A11103 432418

NIST
PUBLICATIONS

U.S. DEPARTMENT OF COMMERCE
National Bureau of Standards

NIST Special Publication 789

*Proceedings of the International Symposium on
Correlation and Polarization in Electronic
and Atomic Collisions*

Paul A. Neill, Kurt H. Becker, Michael H. Kelley, Editors

QC
100
.U57
#789
1990
C.2

Research Information Center
Gaithersburg, MD 20899

[illegible]

NISTC
48100
U57
=789
1990
0.2

NIST Special Publication 789

*Proceedings of the International Symposium on
Correlation and Polarization in Electronic
and Atomic Collisions*

Held August 2-4, 1989 at Stevens Institute of Technology, Hoboken, NJ

Edited by

Paul A. Neill

Department of Physics
University of Nevada
Reno, Nevada

Kurt H. Becker

Department of Physics
City College of New York
New York, NY

Michael H. Kelley

Electron and Optical Physics Division
National Institute of Standards and Technology
Gaithersburg, MD



June 1990

U.S. Department of Commerce
Robert A. Mosbacher, Secretary

National Institute of Standards and Technology
John W. Lyons, Director

National Institute of Standards
and Technology
Special Publication 789
Natl. Inst. Stand. Technol.
Spec. Publ. 789
163 pages (June 1990)
CODEN: NSPUE2

U.S. Government Printing Office
Washington: 1990

For sale by the Superintendent
of Documents
U.S. Government Printing Office
Washington, DC 20402

Preface

The International Symposium on Correlation and Polarization in Electronic and Atomic Collisions was held at the Stevens Institute of Technology, Hoboken, NJ on August 2-4, 1989. A gathering together of colleagues is always a pleasurable occasion and it was a particular pleasure for Kurt Becker, Mike Kelley and myself to organize this Symposium.

The previous meeting, held in Belfast, UK (1987), extended the scope of the Symposium to include ion-atom and atom-atom collisions. This was reflected in the Symposium title which was modified to replace the term "electron-atom collisions" with "electronic and atomic collisions." The Hoboken meeting maintained this expanded subject area and included several talks in more loosely related areas. The attendance of 66 scientists represented 16 countries and the talks described the work of 23 research groups from 9 countries.

The opening address was given by Professor Joachim Kessler (University of Munster). This was followed by 23 invited talks and closing remarks by Professor Benjamin Bederson (New York University).

We would like to thank the speakers for giving permission to publish their contributions to the meeting. A special thanks to those who reformatted their text at my request. The organizers wish to acknowledge the sponsorship of the American Physical Society and financial support from the U.S. National Science Foundation, the National Institute of Standards and Technology and the U.S. Department of Energy, Office of Energy Research, Division of Chemical Sciences. We would also like to thank the people of the Office of Center Operations at the Stevens Institute of Technology.

Finally we wish to express our regret at the loss of our colleague Klaus Jost. Klaus was a talented scientist with a warm personality and will be missed by the community. We dedicate these proceedings to his memory.

Paul Neill
University of Nevada, Reno
March 1990

In the same way that I am often referred to as the "head" of the group, Klaus was the "heart."


J. Kessler, August 3, 1989

In Memory of Klaus Jost

The Proceedings of this Symposium are dedicated to Dr. Klaus Jost who died of a heart attack in Münster, Germany, on 15 July 1989 at age of 52. Klaus Jost had been in the field of electron-atom collisions since 1959, when he joined my group at Karlsruhe as my first graduate student. His achievements and his advice were invaluable for the success of this group in the following 30 years. Not only did the results of his Ph.D. thesis become well known and were frequently reproduced (e.g., in Massey-Burhop, *Electronic and Ionic Impact Phenomena*, Vol. I, p. 356 and 357, or the front page of *Physics Today*, Nov. 1969), but his later achievements, like a convenient type of electrostatic spectrometer or very careful and reliable absolute cross-section measurements, were also highly appreciated by workers in the field. The latter work was done after he had accompanied me to Münster in 1971 where he belonged to the small number of people who built up from scratch an experimental atomic physics group. He assumed increasing responsibility for the management of this group and played a central role in it. When we had the Symposium on Polarization and Correlation in Electron-Atom Collisions in 1983 in Münster he was one of the three organizers.

One of the reasons for my high respect of Jost is that his main object was not his personal career, but rather to do very good physics and to help others to do so. Although he published a number of fine papers he never succumbed to the publish- or -perish ideology, and instead of publishing piecemeal papers he always waited until all the results were really ripe. His pleasant personality and his helpfulness made him very popular both with students and colleagues.

The loss of Jost is a terrible shock for my group – it is impossible to replace him. The reaction of the participants of this Symposium showed the high reputation he had among his peers. I am very grateful that I had the privilege of having Klaus Jost's company for a long period of my life.


(Joachim Kessler)

Disclaimer

Certain commercial equipment, instruments, or materials are identified in individual contributions to these proceedings in order to adequately specify the experimental procedures. Such identification does not imply recommendation or endorsement by the National Institute of Standards and Technology, nor does it imply that the materials or equipment identified are necessarily the best available for the purpose.

Contents

Preface	iii
In Memory of Klaus Jost	v
A Choice of Open Problems in Polarisation and Correlation in Electronic and Atomic Collisions <i>J. Kessler</i>	1
Extracting Dynamics from Collision-Induced Polarization <i>U. Fano</i>	7
Correlations in (e, 2e) Experiments. Recent Results on Inner and Outer Shells <i>G. Stefani, L. Avaldi & R. Camilloni</i>	16
Theoretical Atomic Physics Code Development at Los Alamos <i>R.E.H. Clark & J. Abdallah, Jr.</i>	22
Systematic Investigations of Mott Polarimetry with Very Thin Gold Films <i>M.A. Khakoo, J.A. Brand, W.M.K.P. Wijayaratna & T.J. Gay</i>	28
Polarization Correlation Effects in the Two-Photon Decay of Metastable Atomic Deuterium <i>A. Duncan</i>	34
Electron Impact Excitation of the $n=3$ States of Helium and $5s^3P_1$ State of Krypton <i>A. Crowe</i>	39
Orientation and Alignment in Electron Collisions with Sodium <i>P.J.O. Teubner, R.E. Scholten & G.F. Shen</i>	45
Theoretical Interpretation of the Associative Ionization Reaction between Laser Excited Sodium Atoms: Atomic and Molecular Points of View <i>A. Henriët & F. Masnou-Seeuws</i>	51
Detailed Study of Polarization Effects on the Associative Ionization in $\text{Na}(3p) - \text{Na}(3p)$ Collisions <i>H.A.J. Meijer</i>	58
Excitation and Ionization of Atoms - What We Can Learn by Using Polarized Collision Partners <i>K. Bartschat</i>	64

Alignment and Orientation in Simply-Structured Atomic Collision Complexes <i>R. Hippler</i>	70
Is the "Classical" Double Scattering Less Accurate for Calibrating Mott Polarimeters than Recently Proposed Methods? <i>K. Jost (Delivered by A. Gellrich)</i>	76
Low Energy Electron Scattering by $3^2P_{3/2}$ Sodium <i>L. Vušković</i>	83
The Effects of a Finite Scattering Volume on the Determination of Electron Impact Coherence Parameters <i>P.W. Zetner, S. Trajmar & G. Csanak</i>	89
Spin Dependence in Electron Impact Ionization of Atomic Hydrogen <i>M.S. Lubell, D.M. Crowe, X.Q. Guo, F.C. Tang, A. Vasilakis, J. Slevin & M. Eminyan</i>	95
Progress on Spin Detectors and Spin-Polarized Electron Scattering from Na at NIST <i>J.J. McClelland</i>	102
Coherences between Autoionizing States of Different Excitation Energies <i>H.G.M. Heideman</i>	110
Stokes Parameter Measurements in the Heavy Rare Gases <i>J.W. McConkey, P.J.M. van der Burgt, J.J. Corr & P. Plessis</i>	115
Spin-Polarized Electron Impact Ionization of Atoms <i>G. Baum, P. Freienstein, L. Frost, B. Granitza, W. Raith & H. Steidl</i>	121
"Spin-Orbit" Effects in Inelastic Electron-Atom Collisions: Are Experiments in Conflict with Theoretical Models? <i>G.F. Hanne</i>	128
Optical Analysis of Electron Impact Induced Excited State-Excited State Transitions in Alkali Atoms <i>B.J. Stumpf</i>	134
The Stepwise Excitation Coincidence Technique <i>M.C. Standage, W.R. MacGillivray, A.J. Murray & C.J. Webb</i>	141
Summary of Symposium Proceedings — Some Impressions and Observations <i>B. Bederson</i>	147
List of Attendees	155

OPENING ADDRESS

A CHOICE OF OPEN PROBLEMS IN POLARISATION AND CORRELATION IN ELECTRONIC AND ATOMIC COLLISIONS

Joachim Kessler

Physikalisches Institut, Universität Münster,
D-4400 Münster, Wilhelm-Klemm-Str. 10, West Germany

I have been privileged to deliver the official opening address of what promises to become a very stimulating Conference, because the Organizing Committee – Drs. Kurt Becker, Mike Kelley, and Paul Neill – was very successful in persuading a number of internationally renowned speakers to give a review of their field.

This symposium has become one of the traditional satellite meetings to the ICPEAC which does not mean, of course, that the topics discussed here are traditional. On the contrary, the Symposium is focused on novel information obtained by advanced techniques such as coincidence methods and polarization experiments. Keywords of the previous conferences were polarization (of photons and electrons), correlation (of atomic-collision products), coherence, alignment, and orientation. But when you compare the titles of the previous symposia, you find that they differ a little bit from each other, which indicates that the emphasis has been varied. The terms "correlation" and "polarization" have changed places from time to time, and at the Belfast meeting 1987 the "electron-atom" collisions have been substituted by "electronic and atomic" collisions. This indicates that at Belfast the scope of the program was extended to include ion-atom and atom-atom collisions which has been maintained at the present conference.

Such slight shifts of the emphasis may partly help to answer a question which was occasionally discussed by some of the active participants. Does it really make sense to have such a conference every two years? Needless to say, 100 people or so produce a lot of new data within a period of two years. But couldn't these be presented at the ICPEAC just as well? Is there really a good reason for an extra symposium not only from time to time but every two years? Or is the main reason that such meetings tend to develop their own dynamics and that once they have been started they jump into a stable rhythm? Shifting the emphasis of the symposium makes it certainly easier to find a positive answer to this question.

Still, I do not think that a positive answer can be taken for granted. It depends

very much on what one expects from a conference of this type and this depends on the individual viewpoint. I can only give my personal view. I always found it a great advantage of the Polarization and Correlation Symposium that it is the proper place for discussing open problems and controversial questions. In Münster we have developed into a rather big group over the years, and when it came to the question of what to present at the ICPEAC and what at this Symposium, then I felt that we should present clear-cut results which speak for themselves at the ICPEAC. Results, however, which we would like to discuss in great detail with close colleagues from other groups should be presented at the satellite meeting. Examples are results that differ from those of other groups or whose interpretation is not clear.

The Polarization and Correlation Symposium has always been a forum for discussing such problematic or controversial issues. Let me briefly mention some points of that type we dealt with in the past and highlight some of the problems we certainly have to discuss at the present conference. At the Münster Symposium in 1983 S. Trajmar's group presented an experiment on superelastic electron scattering from laser-excited barium atoms where they found an unexpected asymmetry.¹ Despite careful systematic changes of the parameters of the experiment, the asymmetry did not vanish. A broad discussion of this controversial question was quite important, because it was not at all clear whether this was a new effect which was as yet unexplained or, more likely, an unresolved experimental artifact which – and that is why it was important – might affect other similar measurements as well. It seems that tomorrow we will get the final answer to this open question.

Another debate was opened by M. Lubell at the Münster Symposium, and it may persist for a few more years. It concerns the accuracy of electron polarimetry by Mott scattering. This point came up because of major advances in polarized-electron sources with the result that the accuracy of many experiments with polarized electrons is no longer limited by statistics but rather by the value of the electron polarization. As a consequence, the determination of the accuracy of an electron-polarization measurement has assumed a much higher degree of importance than before, when the papers of different groups varied considerably in the accuracy they claimed for their polarization measurements. Conservative uncertainties were $\pm 5\%$, more optimistic groups claimed uncertainties down to $\pm 1\%$. Since I could never understand why the rules of Mott scattering for polarization analysis should be so different in some other groups than they are in Münster I was quite relieved to hear that also the careful experimental analysis by Fletcher, Gay,

and Lubell² showed that, for basic reasons, the overall uncertainty of Mott polarimetry is restricted to at least $\pm 5\%$.

This is one of the reasons why the discussion of electron polarimetry has revived in the past few years and why new methods for polarization analysis have been suggested. In Münster we have focused much attention on this problem. We found that optical polarization analysis utilizing the polarization of helium impact radiation that is produced by polarized electrons is a very accurate method of electron polarimetry. It has been suggested by T. Gay a few years ago and is discussed in a broader context in the contribution by K. Jost. In Münster we are very upset because we lost K. Jost, one of my most competent co-workers, shortly before going to the ICPEAC. His talk will be presented by A. Gellrich. Incidentally, it is interesting to note that the discussion of electron-polarization techniques now centers on the polarization detectors and that the discussion of polarized-electron sources which had revived after the discovery of the Fano effect and the GaAs source has slowed down. This is reflected by three topics on polarization analyzers and none on sources in our program. It seems that the GaAs source will be the standard source technique for a longer period of time and that the hope to find materials even more suitable than GaAs will not be fulfilled for a while. The Fano effect, on the other hand, turned out to be a valuable tool for studying photoionization processes and is nowadays rather a topic of synchrotron radiation conferences than of this symposium. That is an example of how things can develop in directions not anticipated at their beginning.

Let me continue my list of controversial problems with an example from the field of electron-photon coincidences. I am not going to take up again the well-known problem of angular-momentum transfer $\langle L_{\perp} \rangle$ in electron-impact excitation. There were different views on the interpretation of the angular dependence of $\langle L_{\perp} \rangle$; the semi-classical interpretation originally suggested by Kohmoto and Fano³ and favored by many experimentalists was opposed by several theorists. I think the debate has come to a certain conclusion, though I am not so sure whether it is really over. From the various open problems of electron-photon coincidences I would like to point out one, in which we are involved ourselves.

If you excite an atomic state by electron impact then you have certain restrictions due to reflection symmetry. As a consequence, the waist of the charge cloud of an excited P state must have zero height,⁴ i.e., it does not look like in Fig. 1b, but the waist goes down to the origin of the coordinate system like in Fig. 1a, if there are no spin-dependent forces that flip the electron spins in the excitation process. If you do have spin flips, then

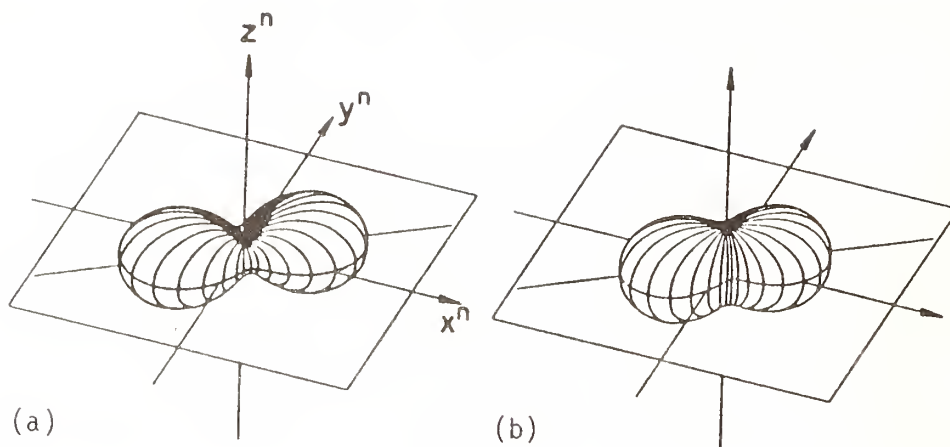


Fig. 1. Collisionally induced charge cloud in P-state atom; (a) without spin flip, (b) with spin flip. (From ref. 4)

reflection symmetry still holds for the whole system electron plus atom, while the individual wave functions will change their symmetry character. In this case the height of the waist becomes different from zero corresponding to an oscillator along the z axis, so that light emitted in the y direction has not only a linear polarization component along the x axis but also an incoherent component along z . In other words the corresponding linear light polarization, usually denoted by P_4 , is smaller than 1. An equivalent way to express this is to say that the density-matrix element ρ_{00} , which corresponds to excitation of the sub-level with the magnetic quantum number $M = 0$, is no longer zero. Briefly, $\rho_{00} \neq 0$ or $P_4 < 1$ indicate spin flips, i.e., the significance of spin-dependent interactions. That is why electron-photon coincidences are one way of studying spin-dependent interactions in electron-atom collisions.

Another more direct way are experiments with polarized electrons where the spin flips can be directly observed by electron-polarization measurements. The point I want to make here is that there are some controversial results of the two methods. From the electron polarization experiments made over the past 2 decades one knows quite well where spin-dependent interactions do or do not play a role. One knows, for instance, that spin interactions of the scattered electrons have negligible effects for small scattering angles at medium energies. This is in accordance with simple models and also with sophisticated calculations. On the other hand, there are recent electron-photon coincidence measurements by several groups yielding significant values of ρ_{00} , i.e. significant spin interaction,

at such angles and energies. This is certainly puzzling and the question of artifacts is raised again. Since in Münster we are involved in both electron polarization and electron-photon coincidence measurements, G.F. Hanne will try to shed some light upon this dark point, and I think that also J.W. McConkey will address this problem.

From the examples given it might appear that puzzling problems occur only in involved processes like coincidence experiments or polarization phenomena. But this is not at all true. Let me quote from a paper by Callaway and McDowell⁵ saying: "One purpose of this Comment is to remind our colleagues, both theorists and experimentalists, that while it is of great interest to measure or calculate such esoteric parameters as spin-flip ratios, differential cross sections and orientation and alignment parameters, we are still unable to give a satisfactory answer to the simple question 'What is the absolute value of the cross section (for electron impact excitation of a specific energy level in atomic hydrogen) at a specified energy?' We find that the uncertainties are of the order of 20% at some energies for the simplest cases, of at least a factor of two in other apparently simple cases..." .

Somewhat later I discussed in a Comment⁶ why in a perfect scattering experiment, which yields the complete set of observables describing the collision process, it is usually the cross sections that are the weakest point. At least in those investigations that have been done with heavy atoms in the past few years it was clearly the cross sections that had the largest experimental and theoretical uncertainties. A similar problem in which the Adelaide group is involved are serious discrepancies between experimental and theoretical cross sections occurring with sodium but not with other atoms, even though the experimental and theoretical methods applied to the various targets are the same.

Given this situation, you hear the question between the lines I quoted before: does it make sense that you study all those esoteric parameters as long as we have problems with such fundamental parameters as cross sections? To me the answer becomes clear when I look at the development of collision physics in the past 2 decades. When the first experimental results on electron-photon coincidences, (2,2e), or spin polarization were published, most of them could not be interpreted quantitatively within the framework of the existing theoretical approaches, which had been focused on the calculation of cross sections. The novel, much more detailed experimental data were an immense challenge for theory resulting in great advances of the theoretical methods. In my own field, for instance, it was impossible a decade ago to obtain reliable theoretical results for electron collisions with heavy atoms where the different kinds of spin interaction simultaneously

play a role. Today one finds relativistic approaches including exchange and charge-cloud polarization which yield reliable theoretical data for quite complex processes of which K. Bartschat will give some examples tomorrow. The wealth of the so-called esoteric experimental data put theories to a very stringent quantitative test so that only the most reliable of them can survive. And these give usually a better description of cross sections as well, even in cases where this is not necessarily anticipated. An example for this was given by McEachran and Stauffer⁷ at the previous symposium, where they discussed cross sections for electron scattering from heavy atoms at low energies, where one has Ramsauer minima below 1 eV. They showed that even at these low energies a relativistic theory based on the Dirac equation gives much better results for the Ramsauer minima than non-relativistic approaches. Generally speaking, I feel that the elaborate experimental and theoretical methods which are discussed at our symposium enabled us to make a quantum jump in the quantitative understanding of collision processes.

The few examples, which I picked out according to my personal preference, show that we will have more than enough problems to discuss here. It seems that our Australian friends feel that this will also be the case in 2 years because they are planning the next symposium in 1991. I cannot foresee whether the group of people assembled here will continue to produce a sufficient number of exciting problems to have another stimulating symposium 4 years from now in Europe. Perhaps Ben Bederson can make a good guess when he will close the symposium and when all of us will be much better informed than we are today.

References

1. D.F. Register, S. Trajmar, G. Csanak, S.W. Jensen, M.A. Fineman and R.T. Poe, Phys. Rev. A **28**, 151 (1983)
2. G.D. Fletcher, T.J. Gay and M.S. Lubell, Phys. Rev. A **34**, 911 (1986)
3. M. Kohmoto and U. Fano, J. Phys. B **14**, L 447 (1981)
4. N. Andersen, J.W. Gallagher and I.V. Hertel, Physics Reports **165**, 1 (1988)
5. J. Callaway and M.R.C. McDowell, Comments At. Mol. Phys. **13**, 19 (1983)
6. J. Kessler, Comments At. Mol. Phys. **18**, 279 (1986)
7. R.P. McEachran and A.D. Stauffer, in "Correlation and Polarization in Electronic and Atomic Collisions" (A. Crowe and M.R.H. Rudge eds.) p. 183. World Scientific, Singapore 1988

EXTRACTING DYNAMICS FROM COLLISION-INDUCED POLARIZATION

U. Fano

Dept. of Physics & James Franck Inst.
University of Chicago, Chicago, IL 60637

1. INTRODUCTION

The polarization generated by collision depends on the dynamics of the collision process but also on incidental aspects of the experimental designs. Identification of the relevant dynamics and evaluation of its essential parameters require one to disentangle these parameters from raw collision data, a task common to many theoretical studies.¹ C.W. Lee's report to the 4th Symposium^{2,3} has contributed many important elements of the polarization dynamics, but has still fallen short of the actual extraction of dynamical parameters. Intervening progress toward Lee's goal is reported here.

The essential parameters of interest are elements of the scattering (or equivalently of the transition or the reaction) matrix, preferably freed from magnetic quantum numbers -- and thus made rotationally invariant -- through the Wigner-Eckart theorem. Polarization and cross section measurements are represented by *real* numbers and expressed as quadratic -- more properly, bilinear -- functions of the dynamical parameters, among which the scattering and transition matrix elements are *complex*. Moreover the measurements are obtained at sets of scattering angles, whereas the rows and columns of dynamical matrices are labeled by angular momentum quantum numbers. Disentangling dynamical parameters requires thus some combination of expansion into spherical harmonics with unraveling of bilinear equations. It seems

likely at this time that this unraveling should precede the harmonic expansion.

The initial step appears trivial for the prototype collision



where cross section and orientation data are familiarly translated into a pair of real parameters $\{\lambda(\theta), \chi(\theta)\}$,⁴ linearization is obtained here simply by using $\sqrt{\lambda}$ and $\sqrt{1-\lambda}$ instead of λ . A full disentangling (or "inversion") procedure is otherwise nontrivial; its development through Lee's and later contributions remains fragmentary. Lee's papers have since been extended to alignment parameters of process (1)⁵ but this advance remains peripheral to the main task because orientation and alignment measurements bear on the same parameters $\{\lambda, \chi\}$ in this case.

2. SUBTRACTION OF LONG RANGE CONTRIBUTIONS

Long range interactions between projectile and target contribute heavily to cross sections and polarizations for charged-particle collisions. On the other hand their contribution through each partial wave component with large orbital momentum remains small and can be evaluated accurately in the Born approximation. Moreover the aggregate Born contribution of all partial waves is represented compactly in terms of the "form factor", i.e., of the Fourier transform of the charge distribution of a target's excitation of interest; this parameter is obtained readily from theory or by measurements on collisions by very fast charged particles.

Recalling that the contributions of long range interactions cause inelastic cross sections to peak sharply at small scattering angles, one anticipates a slow convergence of their expansions in spherical harmonics. There results a requirement to consider *large sets* of dynamical parameters. This substantial inconvenience can, however, be removed by two devices, namely:

a) Replacement of the total angular momentum J of projectile + target, which ranges to infinity, by the angular momentum transfer j_t which does not exceed the sum of the target's angular momenta in its initial and final states. This device, used throughout by Lee,^{2,3} also limits the *difference* of the initial and final projectile orbital momenta but does not restrict their magnitudes.

b) Evaluation of the dynamical parameters corresponding to large orbital momenta by the Born approximation, which is accurate in that range and is readily applied as noted above. The relevant procedure⁶ is outlined below.

An analysis of the Born approximation's contribution to the cross section and orientation in the process (1) has been presented previously for purposes of illustration.³ Each of the observed quantities was viewed in Ref. 3 (IV) as proportional to a squared element of transition matrix, $|T(\theta)|^2$, T itself being the sum of a Born term T^B and of a residual term T^R . Contributions to $|T(\theta)|^2$ consist then of three components labeled as BB, RR and I(BR) -- where I stand for "interference" -- adding up to a "total". (The BB contribution to the orientation vanishes, of course, but I(BR) does not).

Ref. 6 proceeds in the same manner for the dynamical parameters whose *indirect* connection to experimental data is the subject of this report. Each of these parameters is cast as an "exact" transition matrix element T^{ex} , labeled by rotationally invariant angular momentum quantum numbers, and is viewed as the sum of two contributions

$$T^{ex} = T^B + T^R \equiv T^B + (T^{ex} - T^B). \quad (2)$$

T^B itself is constructed in terms of the form factor for the relevant transitions of the collision target, a quantity measured or calculated for collisions of very fast charged particles, that is, *without* any allowance for projectile-target exchange interactions or other corrections

appropriate to lower energy transitions. Such corrections are thus incorporated in T^R , whose convergence to zero with increasing orbital momenta is thereby hampered but still readily tractable.

3. UNRAVELING BILINEAR EQUATIONS

An initial approach to determine the dynamical parameters of process (1) by adapting the analytical machinery of Ref. 3, complemented by subtraction of the Born contribution, has been made by John Bohn in 1988.⁷ Its numerical implementation proved, however, unstable. Bohn initiated then a more flexible procedure applicable to inelastic electron impact on any target with zero angular momentum.⁸

Flexibility stems from unraveling initially a set of intermediate parameters, namely, the probability amplitudes of excitation to specific states $|j_t m_t\rangle$, designated by $\{a_{j_t m_t}(\theta)\}$ as in the review by N. Andersen et al.⁴ The index j_t of this amplitude can be omitted since it represents the specific angular momentum of the excited target, its dependence on the scattering angle θ is preserved in the unraveling process. The set of observable tensorial parameters of the excited target, $\langle T_q^{(k)} \rangle_{j_t \theta}$, equals a bilinear expression in $\{a_{m_t}(\theta), a_{m_t}^*(\theta)\}$. This approach thus unravels the bilinear expression *before* expanding it into spherical harmonics, in contrast to the Lee-Fano procedure of expanding the $\langle T_q^{(k)} \rangle_\theta$ directly.⁷

Bohn noted that the subset of parameters with cylindrical symmetry about the collision axis, $\{\langle T_0^{(k)} \rangle_{j_t \theta}\}$ consists of j_t+1 nonzero elements with $\{k=0,2,\dots,2j_t\}$, whose values are linear combination of $\{|a_{m_t}(\theta)|^2\}$ with $\{m_t=0,1,\dots,j_t\}$. [Negative values of m_t are not independent owing to reflection symmetry through the scattering plane]. The amplitude moduli $|a_{m_t}(\theta)|$ are thus determined from the observables $\langle T_0^{(k)} \rangle_{j_t \theta}$ by solving a linear system of j_t+1

inhomogeneous equations.

The phase differences among the $\{a_{m_i}(\theta)\}$ are to be determined next from the observables $\{T_q^{(k)}\}_{j,\theta}$, with nonzero $q=-k, -k+1, \dots -1, 1, 2, \dots k$, each of them represented as a superposition of

$$a_{m_i}(\theta)a_{m_i+q}^*(\theta) \equiv |a_{m_i}| |a_{m_i+q}| \exp i(\chi_{m_i}(\theta) - \chi_{m_i+q}(\theta)). \quad (3)$$

Measurement of the $\langle T_q^{(k)} \rangle_{j,\theta}$ parameters suffices in fact to determine the sines and cosines of all the phase differences. [The remaining "arbitrary" phase of the $\{a_{m_i}\}$ reflects a convention on the states $|j_i m_i\rangle$].

The desired invariant dynamical parameters, indicated in Ref 3 (III) by $(L_A L_B |S(j_i) l_a l_b)$, where $L_A=0$ and $L_B=j_i$ in our case, are finally constructed from the coefficients of the expansions of the $a_{m_i}(\theta)$ into associated Legendre functions $P_{j_i m_i}(\theta)$. Specifically they are given by Eqs. (2) and (4) of Kohmoto and Fano⁹ as linear functions of these coefficients and of Wigner coefficients for additions of angular momentum vectors $\vec{l}_a = \vec{l}_b + \vec{j}_i$, $\vec{L}_B = \vec{L}_A + \vec{j}_i$.

Extensions of this procedure to targets with nonzero angular momentum, to account for electron spin effects and to deal with projectiles other than electrons, remain to be developed. The following should, however, be anticipated with regard to asymmetric targets with nonzero angular momentum. Determination of the full set of relevant dynamical parameters implies maximal experimental knowledge of the collision variables, including the target's polarization *before* as well as after the collision. (The initial polarization can be controlled by appropriate preparation of the target). Less-than-maximal knowledge of the target's $\langle T_q^{(k)} \rangle$ (or of projectile spin polarization) implies in turn a reduction in the number of equations available to determine the dynamical parameters.¹⁰

Preliminary Calculations

Practical aspects of the procedure outlined in this Section have been explored in recent weeks by A. Chakravorty and X.C. Pan, utilizing data on process (1) from various sources to evaluate the dynamical parameters $(L_A L_B | S(j_t) | l_a l_b)$. [The S and T matrices coincide here for inelastic processes]. Interpolation and extrapolation of data from different authors and at different angles proved necessary to provide a consistent set of input data. The procedure appears workable but considerable experience and skill may prove essential to its sound and effective application.

A particular difficulty emerged in the selection of T^B matrix elements. T^B values obtained from form factors yield a cross section at $\theta=0^\circ$ about 40% in excess of the experimental value at 80eV. Scaling them down to match experiment at $\theta=0^\circ$ distorts the fitting of $S(j_t)$, since the departure from Born at 80eV depends on the angle θ . Convergence of $T^{ex} - T^B$ has thus required the fitting of ≥ 9 harmonics; dispensing with scaling, on the other hand, avoided a major kink in the dependence of $S(j_t)$ on l_a , but may slow down its convergence. It remains obscure which among these or other versions of the procedure may lead to a more substantive interpretation of experimental evidence. On the other hand the very raising of specific issues appears to open new vistas.

$$\langle L_B L_A | S(J_t) | l_a l_b \rangle = |S| e^{i\phi}$$

$$(L_B = 1, L_A = 0, j_t = 1)$$

Unscaled Born

$(l_b=l_a-1)$	$ S $ (a.u.)	ϕ (rad)	$(l_b=l_a+1)$	$ S $ (a.u.)	ϕ (rad)
0			0	0.12	0.07
1	0.11	0	1	0.18	1.07
2	0.13	3.19	2	0.16	1.41
3	0.26	3.65	3	0.13	1.25
4	0.26	3.68	4	0.11	1.23
5	0.22	3.66	5	0.09	1.40
6	0.16	3.75	6	0.07	1.71
7	0.11	3.92	7	0.05	1.91
8	0.08	4.09	8	0.02	1.94
9	0.05	4.08	9	0.01	1.09
10	0.03	3.74	10	0.01	0.95

Scaled Born

$(l_b=l_a-1)$	$ S $ (a.u.)	ϕ (rad)	$(l_b=l_a+1)$	$ S $ (a.u.)	ϕ (rad)
0			0	0.17	0.05
1	0.18	0	1	0.22	0.80
2	0.06	3.25	2	0.18	1.06
3	0.20	3.85	3	0.16	0.90
4	0.21	3.85	4	0.13	0.87
5	0.17	3.85	5	0.10	0.99
6	0.12	4.03	6	0.07	1.19
7	0.09	4.30	7	0.05	1.18
8	0.07	4.60	8	0.03	0.70
9	0.04	4.76	9	0.03	0.29
10	0.02	4.78	10	0.02	0.38

Remarks:

- 1) Smooth convergence of $|S|$ as l_a increases
- 2) Sensitivity of ϕ to precision of input.

4. INTERPRETATION OF THE DYNAMICS

The extraction of dynamical parameters discussed here aims at providing a transparent interpretation of the observed polarizations. Qualitative aspects of the polarization, e.g., the induced target orientation being perpendicular to the scattering plane and the alignment tensor being symmetric under reflection through that plane, follow from symmetry considerations.⁴ More detailed aspects, typically the *sign* of the orientation, depend on dynamical features that have not yet been identified fully.

Fragmentary interpretations of the orientation sign have dealt thus far mainly with semi-classical aspects of collision, such as the curvature of the projectile's trajectory. On the other hand quantum mechanical interpretations would generally center on the analysis of transitions between (time dependent) stationary states. Some relevant aspects of the dynamical parameters $(L_A L_B |S(j_i)| l_a l_b)$, namely, identification of their bilinear combinations that are real or purely imaginary, as well as even or odd under a certain permutation of their indices, have been noted in Ref. 3 (III). This permutation bears on the dynamical propensity toward a *decrease* of the *orbital* momentum about the center of motion of projectile and target accompanying target *excitation* at the expense of the projectile's *kinetic energy*. This kind of analysis looks promising but has not yet been pursued to sufficient depth.

ACKNOWLEDGEMENT

The work leading to this report has been supported by NSF Grant PHY-86-10129 and includes contributions by John Bohn, Alak Chakravorty and Xiao-Chuan Pan.

REFERENCES

1. A prototype extraction of basic parameters from experimental data is seen in the representation of Rydberg series of spectral levels through its limit and its quantum defect, parameters whose accuracy appears more significant than that of individual levels. Additional examples are stressed in U. Fano and A.R.P. Rau, *Atomic Collisions and Spectra* (Academic, Orlando 1986).
2. C.W. Lee, in *4th Intern'l Symp. on Polarization and Correlations in Electronic and Atomic Collisions*,
3. C.W. Lee et al., Phys. Rev. A: I 33, 921 (1986); II 34, 959 (1986); III 36, 66 (1987); IV 36, 74 (1987); V 39, 5 (1989).
4. See, e.g., N. Andersen *et al.* Physics Reports 165, 1 (1988).
5. R. Venugopalan, B.S. Honors Thesis, U. of Chicago (1987), unpublished.
6. X.C. Pan and U. Fano, Phys. Rev. 39, 4502 (1989).
7. J. Bohn, B.S. Honors Thesis, U. of Chicago (1988), unpublished.
8. J. Bohn, to be published
9. M. Kohmoto and U. Fano, J. Phys. B. 14, L447 (1981).
10. "Maximal knowledge" of tensorial parameters $\langle T_q^{(k)} \rangle$ may be provided indirectly, e.g., by magnetic polarization of a target in a thermal bath. In this case statistical mechanics determines the nonzero values of the $\langle T_q^{(k)} \rangle$ with $q=0$ corresponding to axial symmetry about the field direction; this symmetry causes parameters with $q \neq 0$ to vanish under conditions of thermal equilibrium [see, e.g., U. Fano, Rev. Mod. Phys. 29, 74 (1957) sec. 4g].

CORRELATIONS IN (e,2e) EXPERIMENTS. RECENT RESULTS ON INNER AND OUTER SHELLS

G. Stefani

Dipartimento di Matematica e Fisica, Universita' di Camerino, 62032 Camerino, Italy

L. Avaldi and R. Camilloni

Istituto di Metodologie Avanzate Inorganiche CNR
Area della Ricerca di Roma. CP 10 00016 Monterotondo, Italy

Introduction

Among the electron impact ionisation experiments the (e,2e) experiments measure triple differential cross sections (TDCS), in as much as they consist of measuring simultaneously the energy E_0 of the incident electron, the energies E_a and E_b of the two escaping electrons and the probability that these coincidence pairs are emitted into solid angles around the directions (θ_a, ϕ_a) and (θ_b, ϕ_b) .¹ The electron-electron coincidence technique has been largely applied to obtain structural data on atoms and molecules and to perform studies on the collision dynamics. The technique also turned out to be a good mean to investigate ee-correlations. Two classes of ee-correlations can be recognized to be relevant in a (e,2e) process: i) ee-correlations present in the isolated atom or molecule under consideration, in the initial ground state or/and in the final ionic state. They manifest themselves mainly as satellite lines in the coincidence energy spectrum; ii) ee-correlations that are switched on during the ionising collision. They involve the free electrons, interacting with each other or with the bound atomic electrons. Inclusion of these latter correlations has proved in a few cases to be essential in calculating the correct shapes of the angular distributions and the size of the cross section. Depending on the kinematics of the experiment, the structural aspect of the information can be privileged with respect to the dynamical one, or viceversa. Most of the work done to investigate electronic correlations has been concentrated on outer shells of atoms and molecules, studying the satellite peaks and their angular distributions in symmetric kinematics ($E_a = E_b$). In these experiments the high energy incident electron undergoes a high momentum transfer (K) collision, thus essentially interac-

ting with a single target electron, removing it and leaving the residual ion in a given quantum state (impulsive ionisation).² Under these conditions are the initial and final state correlations (ISC and FSC respectively) of kind i) to be investigated. On the other hand, high/medium energy and low momentum transfer scattering ($E_0 > 5$ I.P., $E_a \gg E_b$) must involve grazing collisions, with the incident electron interacting with the target system as a whole. These latter kinematics are more suitable for dynamical studies. Asymmetric (e,2e) experiments were recently carried out on both valence and inner-valence atomic orbitals. Post Collisional Interactions (PCI) and Continuum Final State Correlations (CFSC) were evidenced by these investigations.^{1,3}

The present paper will be confined to report on some recent experiments performed in asymmetric kinematics (incident energy larger than 1 KeV) aimed at investigating ionisation dynamics and ee-correlation effects for either core and outer electrons.

Inner shell TDCS

There is interest in measuring the TDCS for inner shell ionisation because it is expected to produce detailed information on the many-body response of an atomic or molecular system to the change of the potential when the ionised system relaxes. Until now the smallness of the cross section and the limitations imposed by the "unavoidable" accidental coincidences have hampered extensive studies on inner shells to be carried out.

Here, the measurements of the TDCS for the ionisation of C 1s in the molecule C_2H_2 are reported. The (e,2e) experiments were performed in asymmetric conditions at small scattering angle, with a scattered

electron energy (E_{α}) of 1500 eV, and low ejected electron energies (9.6 and 41.0 eV).⁴ In particular the (e,2e) technique was applied for the first time to the ionisation of an inner orbital upon kinematics where resonant channels are expected to be relevant with respect to the direct ionisation.

Several dynamical effects were observed in the measured TDCS. The angular distribution, reported in Fig. 1, shows a large recoil lobe and severe deviation of the symmetry axis of both recoil and binary peak maxima from the momentum transfer direction. The disagreement with 1st Born predictions is more pronounced than for the outer shell ionisation performed in similar kinematic conditions. In particular, the recoil intensity is shifted to form smaller angles with the incident beam direction. This latter finding is in contrast with what is usually observed.¹ Finally, the transition energy of the (e,2e) peak is found to be shifted, for the first time, with respect to the correspondent XPS transition.⁵ The amplitude of the shift decreases with increasing the slow electron energy as shown by the insert of Fig. 2.

The angular distribution of the TDCS is not accounted by a dipolar approximation which, instead, would account for the equal intensity of the two opposite lobes and which was found to be adequate in describing the DDCS for similar molecules upon similar kinematics.⁶ On the basis of the results of the extensive theoretical work done for the outer shell ionisation and because of the localisation of the core orbital it is argued that the description of the free electrons wave functions in the region of small r is crucial to the description of the process (Distorted Waves and approximations beyond 1st-order).

Furthermore, a suitable model for inner-shell ionisation should take into account the rearrangement of the residual ion, that for light atoms ends up in the emission of Auger electrons. When the primary ionisation event is close to threshold, the ejected electron, slowly receding in the ion field, and the fast Auger electron can exchange energy and momentum. As a consequence of this kind of post collision interaction (PCI), a shift of the (e,2e) peak and distortion of the angular distribution is expected. A semiclassical model⁷ predicts an energy exchan-

ge from the slow electron to the Auger insufficient to account for the "apparent" shift of the (e,2e) peak in the energy separation spectrum. It amounts to 0.46 ± 0.23 eV at 9.6 eV ejected energy. A tentative explanation for the extra contribution asks for a non Frank-Condon unresolved vibrational structure shifting the centroid of the peak. The vibrational excitation in core level ionisation accompanies the spatial redistribution of the outer electronic charge. The possibility of a non Frank-Condon distribution is based on the following observations: i) the C 1s ionisation, at the energies above threshold of our experiment, proceeds through resonant $\sigma_{1s} \rightarrow K_b \sigma_u$ channels that are expected to take into account up to 30% of the total intensity; ii) strong non Franck-Condon effects have been already observed in the photoionisation of the valence $1\sigma_u$ orbital whenever a resonant channel becomes dominant in the ionisation process.⁸ The presence of such channels would also contribute to the distortion observed in the TDCS angular distributions

Correlations and satellite structures

The satellite peaks present in the ionization of the valence orbitals provide evidence for the presence of ee-correlations in the target. The Ar 3s ionisation spectrum can be considered a prototype one, because it is characterized by a rich satellite structure due to correlations in both the initial and the final states, and because it has been extensively investigated by photoionisation and impulsive (e,2e) experiments. He is the other limiting case, where the correlations are present only in the initial state.

The (e,2e) experiments on these systems, that are reported in this paper, have been performed upon asymmetric kinematics, intermediate between the impulsive and dipolar regimes. Aim of this work is to study the satellite intensity as a function of the momentum transfer (K) in the collision.

Argon

The satellite spectrum from 35 eV up and above the Ar $^{++}$ ionisation threshold has been measured at an incident energy of 1 Kev and at a fixed ejected electron

energy of 120 eV.¹⁰ The measurements have been performed at three different values of the scattering angle, in order to span K values from 1.3 a.u. up to the Bethe ridge value of 3.0 a.u., where the collisions are known to belong to the binary regime. The satellite spectrum shows several unresolved broad structures and, by using a model function deduced from the main $3p^{-1}$ line, the spectrum was deconvoluted into three main peaks. The relative intensities, obtained as best fit parameters, are reported in Fig. 3 versus (a) the recoil momentum, $q=K_0-(K_a+K_b)$ and (b) the momentum transfer K . Previous symmetric (e,2e) results are also shown in the figure. For the most intense structure, whose centroid is at 38.5 eV, the relative intensity is found to be independent on the ionization kinematics. This structure is known to be dominated by a transition belonging to the 2S manifold.² The discrepancy between the intensity measured by (e,2e) and XPS experiments, already observed in previous work, is confirmed.

On the contrary, the intensities of the peaks centered at 36.5 and 41.3 eV show a monotonic dependence on K . This behaviour is explained with a sizeable contribution from transitions belonging to the 2D and 2P manifolds, which are not due to final state correlations. It has to be noted that previous symmetric (e,2e) experiments assigned these peaks to 2S states. Because states with 2D and 2P final configurations can be accessed not only due to initial state correlations, but also as a consequence of continuum final state correlations, their excitation probability may depend on the kinematics of the collision. The presence of such contributions results also from a recent symmetric (e,2e) experiment.¹¹ In this latter study a dependence on the recoil momentum, q , of the relative intensity of the satellite structures is also evidenced.

Helium

The ionisation of helium to the $n=2$ excited state of He^+ has been studied by measuring the angular dependence of the TDCS, for both the binary and the recoil lobe, and comparing the shapes of the cross section with those relative to the final ground state $He^+ n=1$. The asymmetric kinematics are characterized by high energy, $E_0=1544.5$ eV for $n=1$ and $E_0=1585.4$

eV for $n=2$, small momentum transfer, $K \approx 0.8$ a.u., corresponding to 4° for the scattering angle and 20 eV for the kinetic energy of the ejected electron. In these kinematics the collisional regime is out of the Bethe ridge and approaches the dipolar one. The transition energy spectrum is investigated in a region free from resonances. The TDCS is shown in Fig. 3. The most striking feature is the intense recoil lobe present in the $n=2$ TDCS. Furthermore, while the angular distribution for the $n=1$ state is well symmetric around the K direction, the binary and recoil lobes for the $n=2$ state deviate from the K symmetry by 10° and 25° respectively. Because the velocities of the outgoing electrons are exactly the same in the two cases, the deviation can not be ascribed to the effect of long range repulsive interaction between the electrons. What is to be understood is why the interactions of the free incoming and outgoing electrons with the residual core (nucleus+electron) are enhanced when the ion is left in the excited state. The transition to the $n=2$ final state is made possible because of the presence of ee-correlations in the ground state of helium. The $n=2$ momentum distribution measured by previous symmetric (e,2e) experiments,¹² indicates an average $\langle q \rangle$ value larger than the one associated to the $n=1$ final state. Larger $\langle q \rangle$ usually means lower $\langle r \rangle$, hence a higher probability for large angle elastic scattering on the nucleus can be expected.

The ratio $\sigma(n=2)/\sigma(n=1)$ for the recoil lobes has been reported as a function of the recoil momentum q measured in the experiment. At the lower q the values of the ratio are slightly smaller than those measured by symmetric (e,2e) experiments, while with increasing q a much steeper rise is observed. This different behaviour clearly indicates that, although the width of the angular distribution of ejected electrons is basically determined by the electron momentum density of the initial state, the momentum balance q measured in asymmetric conditions can not be identified with the momentum exchanged by the bound electron, unless Bethe ridge conditions are fulfilled. In general this q balance is a collective quantity and it is influenced by the overall distortion of the electron wavefunctions.¹³

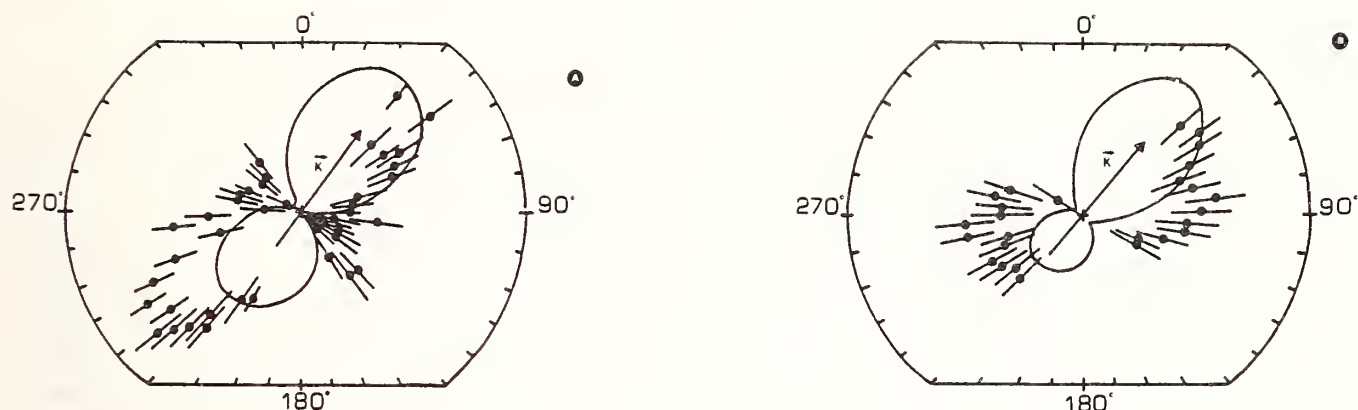


Figure 1. The $(e,2e)$ angular distribution for the ionisation of $C\ 1s$ in C_2H_2 , versus θ_b . (a) $E_0=1801.2$ eV, $E_b=9.6$ eV, $\theta_a=4^\circ$, $K=1.26$ a.u.; (b) $E_0=1832.4$ eV, $E_b=41.0$ eV, $\theta_a=5^\circ$ and $K=1.46$ a.u. The energy E_a is 1500.0 eV in both the figures. Full lines: 1st Born model [formula (3) from Ref. 14].

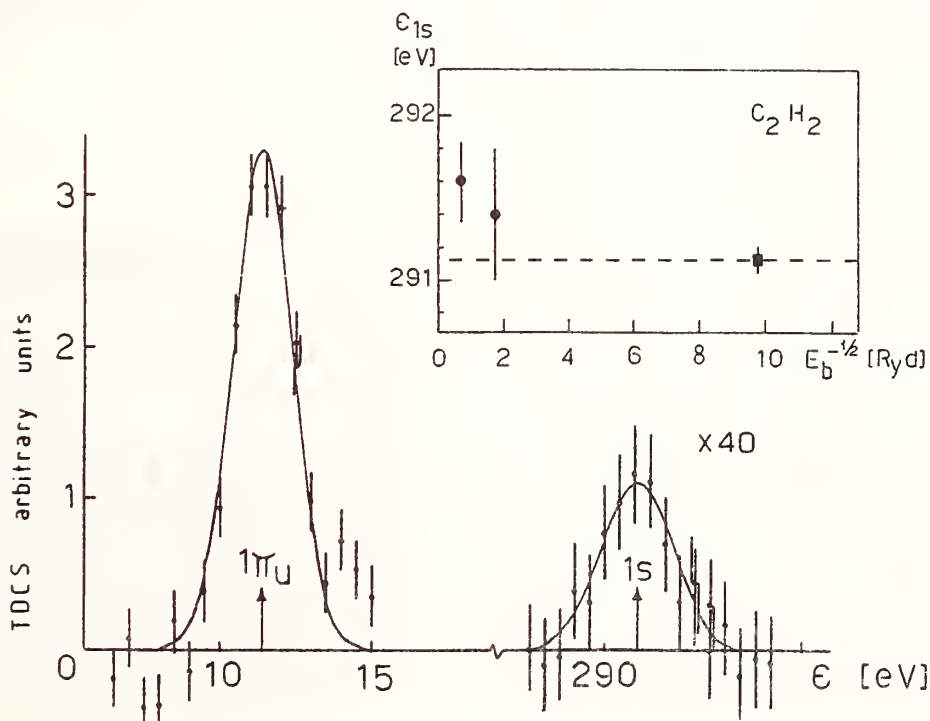


Figure 2. The $(e,2e)$ energy separation spectrum. Kinematics as in Fig. 1(a), θ_b fixed at 60° . In the insert the centroids of the $1s$ peak (\bullet) are reported versus E_b together with the $1s$ binding energy (\blacksquare) measured by XPS.

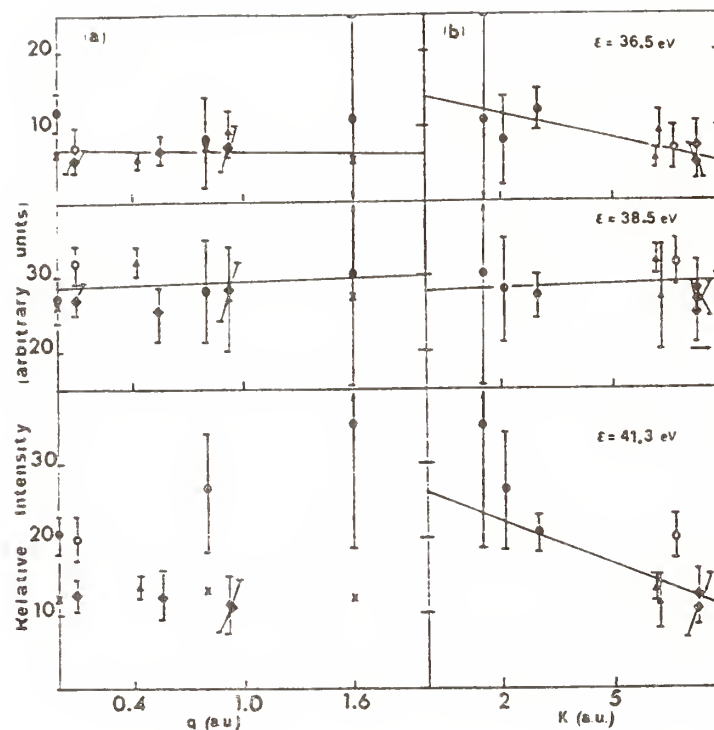


Figure 3. Relative intensity of the three main features of the Ar 3s satellite spectrum plotted versus q (a) and K (b). The transition $\text{Ar } 3s^{-1}$ is assumed to be 100. Experimental data: (\bullet) from Ref. 10, (\circ) Ref. 15, (\blacktriangle) Ref. 16, (\blacklozenge) Ref. 17. Crosses: theoretical predictions, Ref. 18. Arrow: XPS value. Straight lines: least-squares fits to the data.

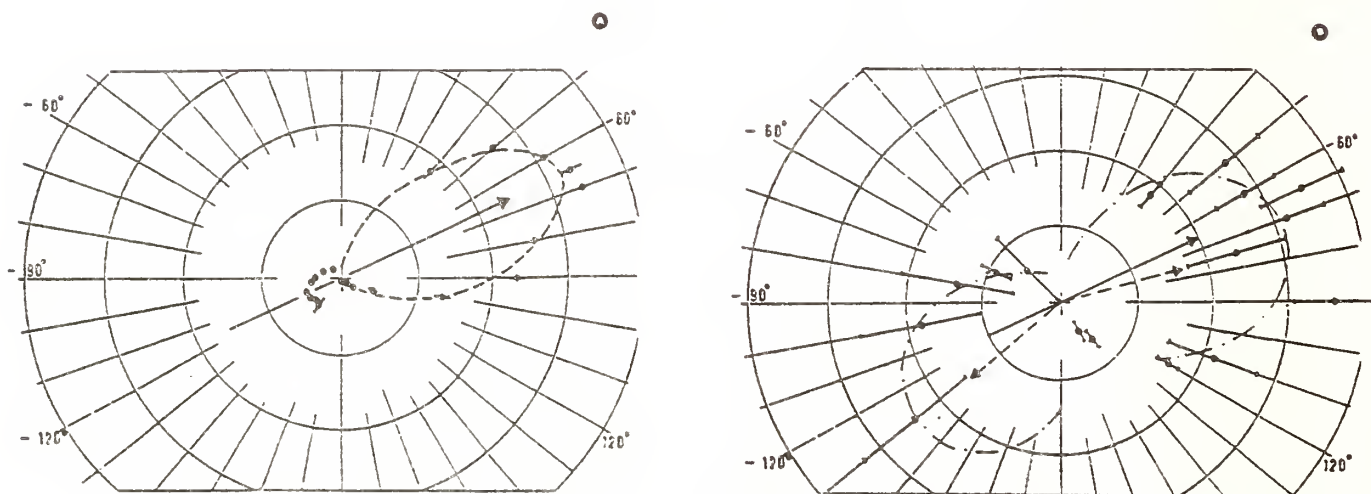


Figure 4. The $(e, 2e)$ angular distribution in helium, versus θ_b with $E_0=1580 \text{ eV}$, $E_a=1500 \text{ eV}$, $\theta_a=4^\circ$, $K=0.8 \text{ a.u.}$. In (a) the final state is $\text{He}^+ n=1$, in (b) $n=2$. The dashed lines are fitting curves to the data.

References

1. H. Ehrhardt, G. Knoth, P. Schlemmer and K. Jung, *Z. Phys.* D, 3 (1986).
2. I.E. McCarthy and E. Weigold, *Rep. Progr. Phys.* 51, 288 (1988).
3. G. Stefani, *Proceedings of the XV International Conference on the Physics of Electronic and Atomic Collisions*, Brighton, United Kingdom, 1987, edited by H.B. Gilbody, W.R. Newell, F.H. Read and A.C.H. Smith (North Holland, Amsterdam, 1988), p.163 and references therein quoted.
4. L. Avaldi, R. Camilloni and G. Stefani, submitted to *Phys. Rev.* A (1989) and *Book of Abstracts of Third European Conference on Atomic and Molecular Physics*, Bordeaux 1989, Editor A. Salin, (published by EPS).
5. R.G. Cavell, *J. Electron Spectrosc. Relat. Phenom.* 6, 281 (1975).
6. P. Letardi, R. Camilloni and G. Stefani *Phys. Rev.* B, (1989), to be published.
7. R.B. Barker and H.W. Berry, *Phys. Rev.* 51, 14 (1966).
8. D. Lynch, M.T. Lee, R.R. Lucchese and V. McKoy, *J. Chem. Phys.* 80, 1907 (1984).
9. J.L. Dehmer, A.C. Parr and S.H. Southworth, in *Synchrotron Radiation Handbook*, Vol. 2, edited by G.V. Marr (North Holland, Amsterdam, 1987).
10. L. Avaldi, R. Camilloni and G. Stefani, *Phys. Rev.* A, (1989) to be published.
11. I.E. McCarthy, R. Pascual, P. Storer and E. Weigold, to be published.
12. J.P.D. Cook, I.E. McCarthy, A.T. Stelbovics and E. Weigold, *J. Phys.* B17, 2339 (1984).
13. A.D. Smith, M.A. Coplan, D.J. Chornay, J.H. Moore, J.A. Tossell, J. Mrozek, V.H. Smith and N.S. Chant, *J. Phys.* B19, 969 (1986).
14. Yu.V. Popov and E.K. Shabalina, *J. Phys.* B19, L855 (1986).
15. K.T. Leung and C.E. Brion, *Chem. Phys.* 82, 87 (1983).
16. I.E. McCarthy and E. Weigold, *Phys. Rev.* A31, 160 (1985).
17. J.F. Williams, *J. Phys.* B11, 2015 (1978).
18. I.E. McCarthy, private communication 1988.

THEORETICAL ATOMIC PHYSICS CODE DEVELOPMENT AT LOS ALAMOS

R. E. H. Clark and J. Abdallah, Jr.

LOS ALAMOS NATIONAL LABORATORY

Recently, several computer codes for calculation of various types of atomic physics data have been developed at the Los Alamos National Laboratory. The purpose of the code development was to provide a set of codes that are very easy to use, will provide results for any ion or atom, use the best possible theory within the constraints of reasonable running time, and provide great flexibility to the user. The codes relevant to this meeting are the CATS¹ atomic structure code based on Cowan's² Hartree-Fock method, the ACE³ collisional excitation code which can calculate collisional data in the distorted wave approximation (DWA) of Mann⁴ or via first order many body theory (FOMBT), and the TAPS⁵ code which can display various quantities from CATS and ACE and can provide differential cross sections (DCS) and electron impact coherence parameters (EICP).

For the three codes, CATS, ACE, and TAPS, a brief description of the theory will be presented. Following this will be a presentation of the method of using the codes. Finally, several examples of DCS and EICP calculations using various approximations available in ACE will be given.

The atomic structure code, CATS, is based on Cowan's² Hartree-Fock method. Radial wave functions are calculated in the single configuration Hartree-Fock approximation. Configuration interaction and intermediate coupling mixing is brought in through perturbation theory. The calculation of the

radial wave functions is a non-relativistic calculation except that the mass and Darwin terms can be included. Quantities calculated by the CATS code include the radial wave functions, energy levels, oscillator strengths and, optionally, plane wave Born collision strengths. The CATS code is run via commands. The following set of commands will generate atomic structure data for neutral barium:

```

open bal
ion 56 1
rcf
6s2
6p2
6s1 6p1
6p1 5d1
/
run
end

```

All data calculated by CATS is placed on a random access file for easy retrieval by the ACE and TAPS codes.

The collisional excitation code, ACE, reads the atomic structure data from the random access file prepared by the CATS code. The radial wave functions for the target states can be generated in the Hartree-Fock or Hartree-statistical-exchange approximations of Cowan² with or without the inclusion of the mass and Darwin terms. The ACE code

also contains subroutines to generate hydrogenic bound state wave functions for comparison purposes. The continuum wave functions can be calculated in the DWA method of Mann⁴ or via FOMBT^{6,7} theory. Subroutines are available to calculate Coulomb functions for comparison purposes. A variety of local exchange potentials are available. Unitarization of the reactance matrix can be turned on and off. Mixing in the target states is included. If requested, the scattering amplitude will be written to a file for use in the TAPS code for DCS and EICP calculations. The ACE code is also run by commands. The following set of commands will calculate cross-section data for neutral barium:

```
files bal
seq 4
setl 1 5
setle 1 5
0.0
2.24
eunits ev
e 20 50
lmax 250
dcs t
thetalin 37 0 180
go
end
```

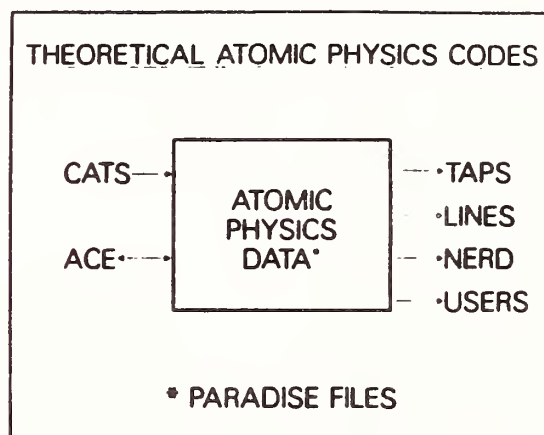
All data from the ACE code is also written to a random access file.

The display code, TAPS, reads data generated from the CATS and ACE codes. It displays selected data in either text or graphic form. Sums and averages over fine structure levels and LS terms can be performed to provide data for LS terms and configurations. The TAPS code can use the scattering amplitude generated by the ACE code to calculate DCS's and EICP's. Various sets of EICP's are written to different files which are named Blum, Fano, Hertel, and Stokes for obvious reasons.⁸⁻¹¹ The TAPS code is also run by

commands. The following set of commands will generate DCS's and EICP's for barium:

```
file adam
ion 56 1 4
dcs
cop
end
```

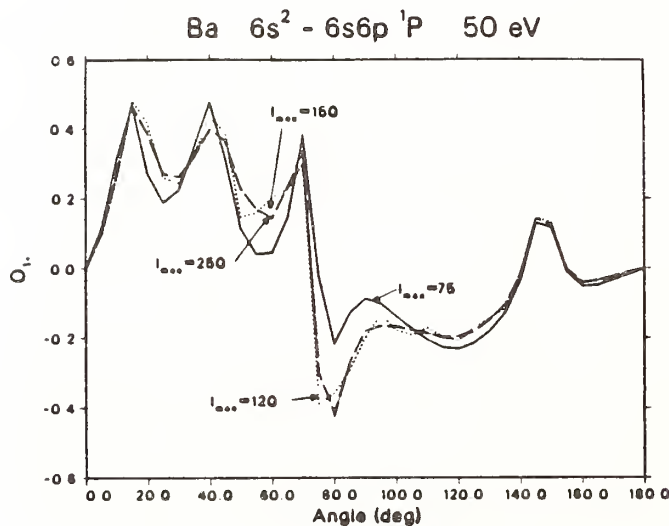
The following figure shows a schematic diagram of the system of codes:



Central to the system is the data file. The arrows indicate that the CATS code writes data to the file, the ACE code reads and writes data, and the other codes read various data. The LINES code generates synthetic spectra and the NERD code is a non LTE code; these two codes will not be discussed further here.

The sets of commands can be sent to the CATS, ACE, and TAPS codes either through interactive use of the computer terminal or through a text file. Full descriptions of all commands are available in the manuals.^{1,3,5} Running the three codes with these sets of commands will ultimately produce DCS's and EICP's for the $6s^2$ - $6s6p$ 1P_1 transition in neutral barium. The CATS run takes ~ 30 sec,

ACE takes ~ 180 sec and TAPS takes ~ 1 sec of Cray-1 time for this test case. Scattering calculations were performed at 20 and 50 eV with 250 partial waves at each energy. The setl command in ACE was used to select the $6s^2-6s6p\ ^1P_1$ transition. Other level to level transitions may easily be selected. Tables 1-4 show samples of the EICP's for barium. Table 1 shows the EICP's from the blum file for 50 eV. Table 3 shows the corresponding fano file; Table 3 shows the hertel file; Table 4 shows the stokes file. The transition energy for barium $6s^2-6s6p\ ^1P_1$ is 2.4 eV so that 50 eV electron energy corresponds to over 20 times the threshold energy. This requires a large number of partial waves for convergence. The following figure shows the orientation parameter for different numbers of partial waves for this case.



Excitation to a specific magnetic sublevel can also be calculated from our codes. From these, polarization fractions can be obtained. Table IV is taken from Ref. 12. It shows collision strengths to magnetic sublevels for neon-like molybdenum (Mo^{+32}) calculated with the fully relativistic code of Zhang et al.¹² compared with the present results. The collision strengths and cross section are related by

$$Q = \frac{\pi a_0^2}{w_i E(R_y)} \Omega$$

where Q is the cross section, a_0 is the Bohr radius, w_i is the statistical weight of the initial state, $E(R_y)$ is the impact electron energy in rydbergs and Ω is the collision strength.

In summary, we have developed a set of computer codes for atomic physics calculations at Los Alamos. These codes can calculate a large variety of data with a minimum of effort on the part of the user. In particular, DCS's and EICP's can be readily obtained for arbitrary ions or atoms. Currently, the theory consists of non-relativistic Hartree-Fock structure calculations and non relativistic DWA or FOMBT collisional calculations.

This work was performed under the auspices of the U.S. Department of Energy.

REFERENCES

1. J. Abdallah, Jr., R. E. H. Clark, and R. D. Cowan, Los Alamos Manual LA-11436-M Vol. I (1988).
2. R. D. Cowan, *Theory of Atomic Structure and Spectra* (University of California, Press, Berkeley and Los Angeles, 1981).
3. R. E. H. Clark, J. Abdallah, Jr., G. Csanak, J. B. Mann, and R. D. Cowan, Los Alamos Manual LA-11436-M Vol. II (1988).
4. J. B. Mann, *At. Data Nuc. Data Tables*, 29, 407 (1983).
5. R. E. H. Clark, J. Abdallah, Jr., and S. P. Kramer, Los Alamos Manual LA-11436-M Vol. III (1988).
6. G. Csanak, H. S. Taylor, and R. Yaris, *Phys. Rev. A*, 3, 1322 (1971).

7. G. Csanak, H. S. Taylor, and R. Yaris, *Adv. At. Mol. Phys.*, 7, 287 (1971).
8. K. Blum, F. J. da Paixão, and G. Csanak, *J. Phys. B*, 13, L257 (1980).
9. U. Fano and J. Macek, *Rev. Mod. Phys.*, 45, 553 (1973).
10. H. W. Hermann and I. V. Hertel, *Comm. At. Mol. Phys.*, 12, 61 (1982); *ibid* 12, 127 (1982).
11. N. Andersen, J. W. Gallagher, and I. V. Hertel, *Phys. Repts.* 165, 1 (1988).
12. H. L. Zhang, D. H. Sampson, and R. E. H. Clark, *Phys. Rev. A*, (submitted 1989).

Table 1. Blum file for barium at 50 eV.

start	i1,i2,e=	1	5	5.0000e+01	
c	theta	lambda	chi	cos delta	cos eps
0.0000e+00	1.0000e+00	0.0000e+00	0.0000e+00	0.0000e+00	0.0000e+00
5.0000e+00	4.4039e-02	-5.0521e-01	1.0000e+00	1.0000e+00	1.0000e+00
1.0000e+01	7.7861e-02	-1.6153e+00	1.0000e+00	1.0000e+00	1.0000e+00
1.5000e+01	3.3075e-01	-1.4757e+00	9.9999e-01	9.9999e-01	9.9999e-01
2.0000e+01	4.7757e-01	-8.8734e-01	1.0000e+00	9.9999e-01	9.9999e-01
2.5000e+01	4.1853e-01	-5.8229e-01	1.0000e+00	1.0000e+00	1.0000e+00
3.0000e+01	3.9709e-01	-5.6558e-01	9.9998e-01	9.9999e-01	9.9999e-01

Table 2. Fano file for barium at 50 eV.

start	i1,i2,e=	1	5	5.0000e+01	
c	theta	o1-	a1+	a0	a2+
0.0000e+00	0.0000e+00	0.0000e+00	-1.0000e+00	0.0000e+00	0.0000e+00
5.0000e+00	9.9306e-02	1.7955e-01	4.3394e-01	-4.7798e-01	
1.0000e+01	2.6769e-01	-1.1917e-02	3.8321e-01	-4.6107e-01	
1.5000e+01	4.6835e-01	4.4672e-02	3.8755e-03	-3.3462e-01	
2.0000e+01	3.8731e-01	3.1542e-01	-2.1635e-01	-2.6121e-01	
2.5000e+01	2.7129e-01	4.1202e-01	-1.2780e-01	-2.9073e-01	
3.0000e+01	2.6221e-01	4.1310e-01	-9.5639e-02	-3.0145e-01	

Table 3. Hertel file for barium at 50 eV.

start	i1,i2,e=	1	5	5.0000e+01			
c	theta	rho00	p1 +	gamma(rad)	gamma(deg)	l perp +	l perp
0.0000e+00	9.5363e-10	1.0000e+00	-4.3672e-05	-2.5022e-03	0.0000e+00	0.0000e+00	0.0000e+00
5.0000e+00	4.5688e-08	9.8008e-01	-1.3832e+00	-7.9253e+01	1.9861e-01	1.9861e-01	1.9861e-01
1.0000e+01	7.0877e-07	8.4461e-01	1.5567e+00	8.9191e+01	5.3538e-01	5.3538e-01	5.3538e-01
1.5000e+01	2.5547e-06	3.5009e-01	-1.4418e+00	-8.2607e+01	9.3671e-01	9.3671e-01	9.3671e-01
2.0000e+01	1.7246e-06	6.3243e-01	-8.2089e-01	-4.7034e+01	7.7462e-01	7.7462e-01	7.7462e-01
2.5000e+01	9.3473e-07	8.4000e-01	-8.8300e-01	-5.0592e+01	5.4259e-01	5.4259e-01	5.4259e-01
3.0000e+01	2.0884e-06	8.5145e-01	-9.0747e-01	-5.1994e+01	5.2442e-01	5.2442e-01	5.2442e-01

Table 4. Stokes file for barium at 50 eV.

start	i1,i2,e=	1	5	5.0000e+01	
c	theta	p1	p2	p3	
0.0000e+00	1.0000e+00	-8.7344e-05	0.0000e+00		
5.0000e+00	-9.1192e-01	-3.5910e-01	-1.9861e-01		
1.0000e+01	-8.4428e-01	2.3834e-02	-5.3538e-01		
1.5000e+01	-3.3850e-01	-8.9344e-02	-9.3671e-01		
2.0000e+01	-4.4860e-02	-6.3084e-01	-7.7462e-01		
2.5000e+01	-1.6294e-01	-8.2404e-01	-5.4259e-01		
3.0000e+01	-2.0581e-01	-8.2621e-01	-5.2442e-01		

TABLE IV. Comparison of results for the collision strengths for excitation from the ground level to the magnetic sublevels M_f of the excited odd parity levels with $n = 3$ and $J_f = 1$ in neon-like molybdenum. In each case upper entries are the present fully relativistic results and the second entries are from the code of Ref. 13. Numbers in square brackets designate powers of 10 by which adjacent entries should be multiplied.

Excited Level	M_f	E_f (Ry)				
		10	50	200	500	1000
$2p3s \ ^1P_1$ or $(2p_{3/2}3s_{1/2})_1$	0	3.43[-4] 3.47[-4]	4.65[-4] 4.80[-4]	8.99[-4] 9.20[-4]	1.48[-3] 1.46[-3]	2.00[-3] 1.87[-3]
	1	1.11[-4] 1.08[-4]	1.28[-4] 1.29[-4]	2.30[-4] 2.36[-4]	4.85[-4] 5.03[-4]	8.85[-4] 9.13[-4]
$2p3s \ ^3P_1$ or $(2p_{1/2}3s_{1/2})_1$	0	2.36[-4] 2.67[-4]	3.06[-4] 3.56[-4]	5.61[-4] 6.60[-4]	9.17[-4] 1.05[-3]	1.24[-3] 1.36[-3]
	1	1.19[-4] 1.23[-4]	1.23[-4] 1.32[-4]	1.65[-4] 1.89[-4]	3.00[-4] 3.56[-4]	5.31[-4] 6.32[-4]
$2p3d \ ^3P_1$ or $(2p_{3/2}3d_{3/2})_1$	0	2.14[-4] 2.06[-4]	1.76[-4] 1.67[-4]	1.08[-4] 9.86[-5]	6.90[-5] 5.77[-5]	5.25[-5] 3.81[-5]
	1	7.94[-4] 8.03[-4]	6.30[-4] 6.35[-4]	3.13[-4] 3.11[-4]	1.23[-4] 1.19[-4]	5.72[-5] 4.93[-5]
$2p3d \ ^3D_1$ or $(2p_{3/2}3d_{5/2})_1$	0	1.36[-2] 1.37[-2]	1.61[-2] 1.62[-2]	2.33[-2] 2.31[-2]	3.11[-2] 2.99[-2]	3.75[-2] 3.43[-2]
	1	6.03[-3] 5.91[-3]	6.61[-3] 6.50[-3]	8.95[-3] 8.84[-3]	1.37[-2] 1.37[-2]	2.06[-2] 2.06[-2]
$2p3d \ ^1P_1$ or $(2p_{1/2}3d_{3/2})_1$	0	1.15[-2] 1.18[-2]	1.36[-2] 1.39[-2]	1.97[-2] 1.99[-2]	2.65[-2] 2.62[-2]	3.22[-2] 3.03[-2]
	1	5.00[-3] 4.97[-3]	5.49[-3] 5.46[-3]	7.44[-3] 7.44[-3]	1.14[-2] 1.16[-2]	1.73[-2] 1.76[-2]
$2s3p \ ^3P_1$ or $(2s_{1/2}3p_{1/2})_1$	0	2.50[-4] 2.22[-4]	3.37[-4] 3.01[-4]	6.45[-4] 5.79[-4]	1.08[-3] 9.47[-4]	1.48[-3] 1.26[-3]
	1	1.56[-4] 1.46[-4]	1.57[-4] 1.44[-4]	1.93[-4] 1.73[-4]	3.31[-4] 3.00[-4]	5.82[-4] 5.35[-4]
$2s3p \ ^1P_1$ or $(2s_{1/2}3p_{3/2})_1$	0	6.30[-4] 7.75[-4]	8.78[-4] 1.05[-3]	1.74[-3] 2.00[-3]	2.97[-3] 3.25[-3]	4.13[-3] 4.30[-3]
	1	1.93[-4] 2.32[-4]	2.33[-4] 2.80[-4]	4.17[-4] 4.89[-4]	8.59[-4] 9.97[-4]	1.58[-3] 1.82[-3]

Systematic Investigations of Mott Polarimetry with Very Thin Gold Films *.

M.A.Khakoo, J.A.Brand, W.M.K.P.Wijayarathna and T.J.Gay .

Physics Department, University of Missouri-Rolla, Rolla, MO 65401 .

INTRODUCTION.

The precision determination of the absolute spin polarisation of a collimated beam of electrons by double scattering measurements has been the subject of considerable interest in the past¹. Recently the Munster group² have used an optical helium polarimeter³ to calibrate a Mott polarimeter absolutely to better than $\pm 1\%$, providing that the accuracy of the helium polarimeter is only limited by the statistical precision in the determination of the circular polarisation of the emitted light and the η_2/P theoretical analysing power². The question of the absolute precision of the helium polarimeter still remains experimentally untested.

A complementary problem is to determine the ultimate precision of a retarding potential Mott polarimeter, if possible, to better than 1%. This problem has been carefully considered by Fletcher et al.⁴, who experimentally demonstrated a limitation of $\pm 5\%$ absolute accuracy in their Mott scattering experiments. This limitation was "a consequence of foil thickness dependence of the Mott asymmetry ($\pm 3\%$) and the theoretical uncertainties in the calculations of the Sherman function ($\pm 2\%$)"⁴.

One motivation for making a sub-1% relative Mott asymmetry measurement is to determine the absolute Sherman function for Mott scattering at a given incident electron energy to a considerably higher precision than present theory allows, using the helium polarimeter as the absolute standard. Of course, agreement between the two methods, using available theoretical values of the Sherman function, will give us increased confidence that our assumption of absolute accuracy for the helium technique is justified.

However, in order to improve the present state of Mott scattering measurements a clearer understanding of multiple and plural scattering is required to quantify the present disagreements between theory and experiments. For example, a Monte-Carlo calculation⁵ of elastic plural electron scattering in gold films showed that the asymmetry for films of, e.g., 200Å at the incident electron energy of 30keV should be reduced by as much as 50% by plural elastic scattering in the film, a fact which is not in agreement with existing Mott asymmetry measurements⁸.

It is to shed new light on this particular aspect of Mott scattering from gold films that this work is aimed.

EXPERIMENTAL APPARATUS.

The Rolla polarised electron source consists of a continuously cesiated NEA-GaAs photoemission source pumped by a GaAlAs solid-state laser (7960Å). The laser was $\approx 95\%$

circularly polarised by using an achromatic $\lambda/4$ plate. The source was found to be extremely stable for periods in excess of several months, with an average electron spin polarisation of $\approx 30\%$. The electrons were transversely polarised via a 90° electrostatic spherical bender, collimated and transported into the Mott chamber by cylindrical electron lenses. Base pressures in the source and Mott chambers were typically 4×10^{-11} torr and 2×10^{-9} torr, respectively, rising to 1×10^{-10} torr and 1×10^{-8} torr during experimental runs.

The Mott detector (Farago/Rice design⁶) was UHV compatible and had two high resolution retarding potential detectors at $\pm 120^\circ$ scattering angles. The design of the retarding optics included (among other collimating apertures) two apertures 2mm in diameter placed 6mm apart where the retarding potential was applied, to produce a spatially well defined retarding potential. The retardation optics performed with an energy resolution of ± 1.5 eV FWHM. The angular resolution of the detection system was $\pm 0.3^\circ$ FWHM. After the retardation optics the scattered electrons were accelerated to kinetic energies ≥ 135 eV at the entrance nose cone of the channeltron detectors in an effort to minimise systematic variations of the detection efficiency as a function of energy loss. Five gold films vacuum-evaporated onto Formvar were used. A bare Formvar foil was included for background determination purposes. The gold film thicknesses were 10, 25, 50, 100 and 200 Å. The relative error in film thickness is estimated at $\pm 8\%$.

The electron beam was dumped into a 150mm long, 25mm diameter Faraday cup and the current was continuously monitored using an electrometer connected by an IEEE bus to a personal computer. The computer controlled a stepper motor which rotated the $\lambda/4$ plate to reverse the electron spin polarisation as well as a ramp voltage output ($\pm 2000 \pm 10$ mV) for the retarding potential detectors. The Mott scattering asymmetry is evaluated by taking the counts in the left (L) and right (R) detectors for four orthogonal positions of the $\lambda/4$ plate, corrected for Formvar and X-ray backgrounds. The left-right asymmetry, A, is given by

$$A = (1 - \xi) / (1 + \xi) \quad (1)$$

where

$$\xi = \frac{1}{2} \{ (L^+ R^-) / (R^+ L^-) \} . \quad (2)$$

The \pm superscripts represent spin-up/down electrons, respectively. This method of evaluating A eliminates instrumental asymmetries⁶. The asymmetry is related to the Sherman function, S, (provided no plural scattering processes are present) by

$$A = S \cdot P_e \quad (3)$$

where P_e is the transverse electron spin polarisation.

For all the measurements of signal + background a corresponding background run was made using the Formvar foil (corrected for the variation of the electron current and taking into account the transmission of the foil in question). This was crucial to reduce systematic errors in the experiment since background scattering due to Formvar could be a significant fraction of that due to scattering from the gold. At worst this was approximately 23% for a 10Å film at 20keV incident electron energy and 1300eV maximum energy loss (retarding voltage).

Using this system, Mott scattering asymmetries were measured at various incident electron energies from 20 to 120 keV as a function of film thickness and maximum energy loss. Asymmetry vs. film thickness measurements were carried over periods not exceeding a day to normalise the different asymmetry values to a fixed electron spin polarisation. It was observed that the electron spin polarisation did not vary by greater than 1% over this period.

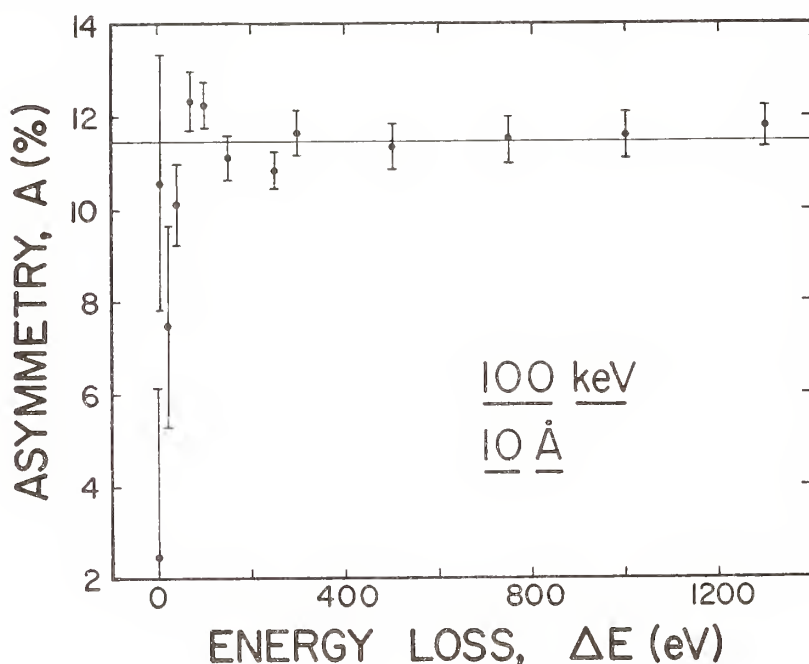


Figure 1. Mott asymmetry vs. maximum energy loss for 10Å film thickness at an incident electron energy of 100keV, showing the lack of dependence of asymmetry on energy loss. See text for details.

RESULTS.

Figure 1 shows the asymmetry plotted against maximum energy loss (retarding voltage) for our 10Å gold film at the incident electron energy of 100keV. From figure 1 it can be seen that the asymmetry vs. maximum energy loss is effectively flat with a nominal slope of $-1(\pm 2.3) \times 10^{-6} \text{ V}^{-1}$. This implies the absence of multiple inelastic scattering i.e. the asymmetry remains within $\pm 0.1\%$ for an asymmetry of 0.1. More importantly, it implies that using a retarding Mott polarimeter at 100keV to make foil thickness measurements of the asymmetry at non-zero

energy loss retardation values will yield the correct extrapolated asymmetry free from multiple scattering. This is an advantage since the larger energy loss retardation values provide correspondingly higher electron count rates due to improved transmission through the retarding optics. We have used this fact to make relative asymmetry foil thickness measurements (following the analysis of Fletcher et al.⁴) to an accuracy of $\pm 0.7\%$, i.e. considerably better than that of Fletcher et al ($\pm 3\%$). Details of this analysis are lengthy and will not be described here, but will be presented at the meeting.

With the retardation at 4eV energy loss (which essentially limits us to observing elastically scattered electrons only) we have made relative measurements of Mott scattering asymmetry vs. film thickness vs. incident electron energy. These data are shown in figure 2. The

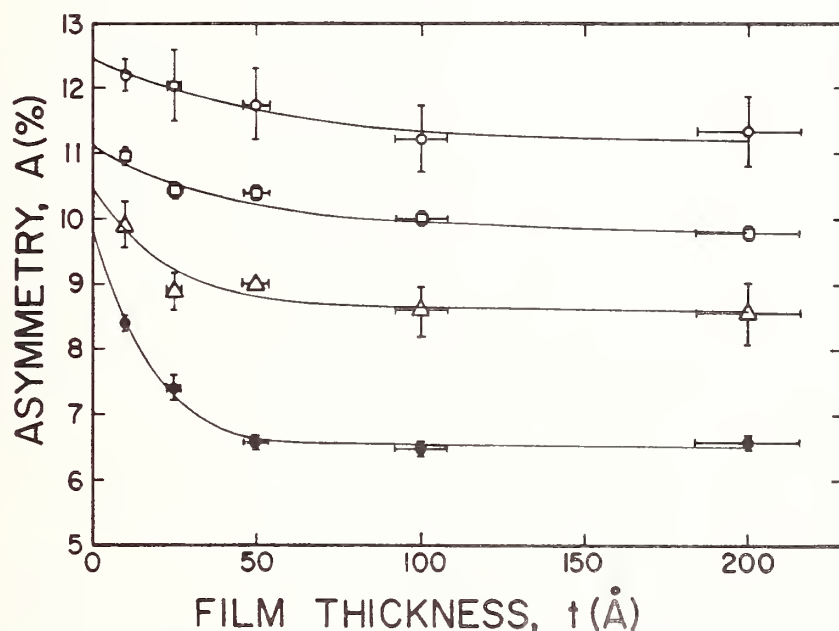


Figure 2. Mott asymmetry vs. film thickness for various E_i values. Key:- \circ $E_i = 100$ keV, \square $E_i = 60$ keV, \triangle $E_i = 40$ keV, \bullet $E_i = 20$ keV. The curves are fits to the experimental points using equations 4 and 5.

curves are our semi-empirical extrapolations derived from the observations of Hnizdo⁵. For a given value of incident electron energy (E_i) his Monte-Carlo calculations showed that the film thickness (t) dependence of the asymmetry A for elastically scattered electrons can be described by

$$A(t) = A(t=0)/(1 + b(E_i) \cdot t), \quad (4)$$

where b is independent of foil thickness. However, since he did not account for inelastic processes in attenuating elastically scattered electrons emerging deeper in the film, a modification of equation 4, replacing t with an effective film thickness t' given by

$$t' = b(E_i) \cdot L \cdot (1 - \exp(-t/L)) \quad (5)$$

is required. L is the mean free path for inelastic scattering. The term $1 - \exp(-t/L)$ is the reduction of elastic electrons by inelastic scattering as a function of film thickness. The validity of equation 5 can be observed in figure 3, where the observed intensity of elastically scattered electrons are plotted against film thickness for several E_i values.

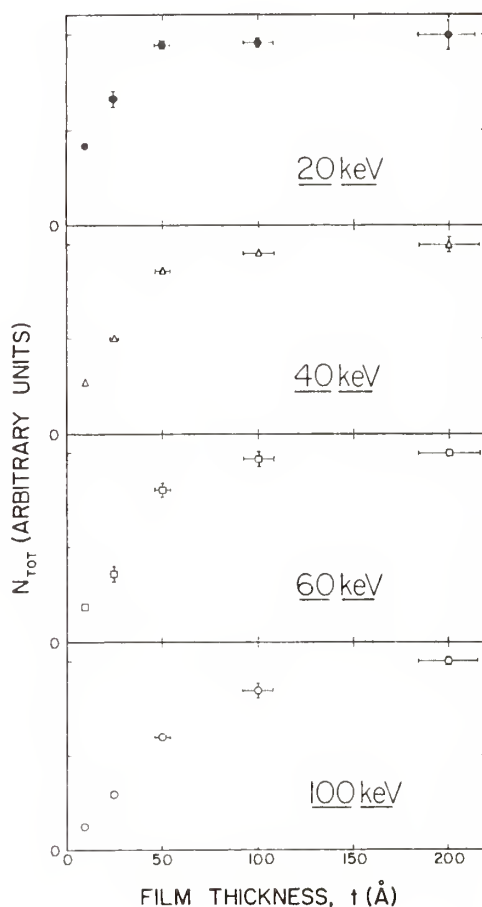


Figure 3. N_{tot} (count rate of scattered electrons) vs. film thickness for the maximum energy loss value of 4eV (essentially only elastic electrons are detected) and various E_i values. See text for details.

It is clear from figure 3 that, eg., at 20keV incident electron energy, the 100Å film is infinitely thick for elastic scattering processes, a fact that is also clearly borne out in the film thickness dependence of the Mott scattering asymmetry which effectively bottoms out at this film thickness. This is due to the fact that the inelastic mean free path is short enough ($L \approx 20\text{\AA}$ at 20keV) to stop deeply penetrating electrons from emerging elastically from the gold film at the scattering angle of 120° .

Normalising the 100keV extrapolated asymmetry to the Sherman function value of 0.394 of Ross and Fink⁷ gives (using the film thickness extrapolated values at the other lower energies) the values of $S(20\text{keV}) = 0.312 \pm 0.014$, $S(40\text{keV}) = 0.333 \pm 0.010$, and $S(60\text{keV}) = 0.353 \pm 0.008$, in good agreement with theory. The experiment of Campbell et al.⁸ which made erroneous asymmetry vs. energy loss extrapolations is the only other measurement which shows similar agreement with theory. We have correctly modified their S values based strictly on the assumptions of their paper and find that at 20keV, for example, this corrected value falls 6.6% lower than theory, showing indeed that their data did, like all other previous experiments, suffer from plural scattering.

In conclusion, the above work strongly suggests that in the near future it will be possible to make an absolute determination of the Sherman functions for Mott scattering from a solid target, using the helium polarimeter as a calibration standard, to a sub-1% precision and hence extend the precision of absolute Mott polarimetry to an accuracy better than that provided by present theoretical values of these Sherman functions.

* Supported by the NSF (Grant PHY-8602066)

REFERENCES

- (1) See for example H.Boersch et al.(1971) Nucl.Phys. A163, 625
and H.Hopster and D.L.Abraham (1988) Rev.Sci.Inst. 59, 49
- (2) M.Uhrig et al.(1989) Rev.Sci.Inst. 60, 872
- (3) T.J.Gay (1983) J.Phys.B.Atom.Mol.Phys. 16, L553
- (4) G.D.Fletcher et al.(1986) Phys.Rev. A34, 911
- (5) V.Hnizdo (1973) Nucl.Inst.Methods 109, 503
- (6) L.A.Hodge et al.(1979) Rev.Sci.Inst. 50, 5
- (7) A.Ross and M.Fink (1988) Phys.Rev A38, 911
- (8) D.M.Campbell et al.(1985) J.Phys.E Sci.Inst. 18, 664

POLARIZATION CORRELATION EFFECTS IN THE TWO-PHOTON DECAY OF METASTABLE ATOMIC DEUTERIUM

A J Duncan

Atomic Physics Laboratory, University of Stirling,
Stirling FK9 4LA, Scotland

Over the past few years a series of measurements^{1,2,3} have been carried out to investigate the polarization correlation properties of the two photons emitted in the decay of metastable atomic deuterium. In the first of these experiments in which two polarizers were placed diametrically one on either side of the source, the measurements verified the quantum mechanical predictions and violated Bell's inequality⁴ thus ruling out a local realistic interpretation of the results. However, because of the low detection efficiency of the photomultipliers only a small sample of the photon pairs emitted by the source was detected leaving open the possibility that, in some way, a biased sample of pairs was detected. The assumption that such a bias does not exist is known as the no-enhancement assumption.⁵ If this assumption is not made Garuccio and Selleri,⁶ for example, have shown that it is easy to explain the results of all existing two polarizer experiments in local realistic terms by attributing to a photon an additional (hidden) parameter which determines its probability of detection. However, their model leads to a direct conflict with the predictions of quantum mechanics in experiments in which an additional linear polarizer is inserted on one side of the source. Such an experiment with an additional linear polarizer has now been completed³ and the results once again have been shown to be in good agreement with quantum mechanics and to rule out local realistic interpretations of the kind suggested by Garuccio and Selleri. In addition, in evaluating the quantum mechanical prediction an interesting question is raised regarding the coherence length to be attributed before detection to single photons which are an integral part of a two-photon excitation.

In this experiment the polarization correlation properties of the two-photon radiation from a metastable atomic deuterium source are investigated using three pile-of-plates polarizers as shown in Fig 1.

With the transmission axis of polarizer a held fixed in the x direction, the transmission axis of polarizer b is rotated through an angle β in one sense and the transmission axis of polarizer a' through an angle α' in the opposite sense. The ratio $R(\beta, \alpha')/R(\beta, \infty)$ is then measured as a function of the angle α' for various

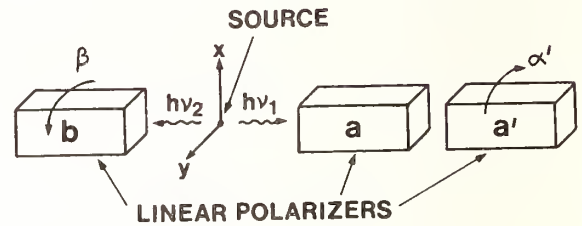


FIG 1. Diagram to illustrate the three-polarizer experiment. The source consists of a beam of metastable atomic deuterium, the two-photon radiation from which is detected and analyzed by a conventional electronic coincidence technique.

angles β , where $R(\beta, \alpha')$ is the rate of coincident detection of photon pairs with all the polarizer plates in place, while $R(\beta, \infty)$ is the rate with the plates of polarizer a' removed. If the action of the polarizers a, a' and b on the state vectors of the photons which are incident upon them is represented, respectively, by the 2x2 matrices A, A' and B, then, according to quantum mechanics, the ratio $R(\beta, \alpha')/R(\beta, \infty)$ is obtained from the 4x4 density matrix ρ representing the two-photon state by the formula

$$\frac{R(\beta, \alpha')}{R(\beta, \infty)} = \frac{\text{Trace}[A'A \otimes B \rho (A'A \otimes B)^\dagger]}{\text{Trace}[A \otimes B \rho (A \otimes B)^\dagger]} \quad (1)$$

or alternatively

$$\frac{R(\beta, \alpha')}{R(\beta, \infty)} = \frac{\text{Trace}_1(A'A \rho_{\text{eff}} A^\dagger A^\dagger)}{\text{Trace}_1(A \rho_{\text{eff}} A^\dagger)} \quad (2)$$

In expression (2) the traces are taken only over the polarization variables of photon 1 (on the right in Fig 1) and ρ_{eff} , the effective density matrix obtained by taking the trace over the polarization variables of photon 2 (on the left in Fig 1), is given by

$$\rho_{\text{eff}} = \text{Trace}_2(B \rho B^\dagger). \quad (3)$$

In a sense then, expression (2) demonstrates that, for a given two-photon state, the polarization properties of

photon 2 on the right can be considered to be determined by the properties and setting of the polarizer b on the left. If M_A and m_A are the transmission efficiencies (the moduli squared of the transmission amplitudes) for light polarized parallel to (the wanted component) and perpendicular to (the unwanted component) the transmission axis of polarizer a, respectively, with similar definitions for M_B , m_B , $M_{A'}$ and $m_{A'}$, then from either expression (1) or (2)

$$R(\beta, \alpha') / R(\beta, \infty) = F + G(\beta) \cos 2\alpha' - H(\beta) \sin 2\alpha' \cos \phi \quad (4)$$

where $F = 1/2 (M_{A'} + m_{A'})$,

$$G(\beta) = 1/2 (M_{A'} - m_{A'}) [(M_A P - m_A Q) / (M_A P + m_A Q)]$$

$$H(\beta) = (M_A m_A)^{1/2} [(M_B - m_B)(M_{A'} - m_{A'}) / 2(M_A P + m_A Q)] \sin 2\beta$$

with $P = 1/2 [(M_B + m_B) + (M_B - m_B) \cos 2\beta]$

and $Q = 1/2 [(M_B + m_B) - (M_B - m_B) \cos 2\beta]$.

The term $H(\beta) \sin 2\alpha' \cos \phi$ is of particular interest and results from the interference between the wanted light and the unwanted light passing through polarizer a. The angle ϕ represents the relative phase between the complex transmission amplitudes for wanted and unwanted light through polarizer a, and, for light passing directly (ie without internal reflections) through the polarizer, it would be expected that $\phi = 0^\circ$, $\cos \phi = 1$. However, in practice, the effect of internal reflections between the polarizer plates cannot be ignored. It is assumed that the contribution of internal reflections to the wanted component is negligibly small since they occur near to Brewster's angle, but a significant part of the unwanted component does arise from these reflections. However, because of the small random deviations of the plate alignment from Brewster's angle, the lack of parallelism of the surfaces of the individual plates and the imperfect polish of the plate surfaces (only 2λ at 243nm) it is unlikely that the component of the unwanted light resulting from internal reflections will interfere with the light passing straight through the polarizers irrespective of the coherence length to be associated with the photons passing through each polarizer. It can be argued that this coherence length is extremely short since the source has a large bandwidth (121.5nm - ∞) with wavelengths in the range 185nm to 355nm being detected in practice. Taking the coherence length $l_c = \lambda^2 / \Delta\lambda$ where λ is the mean wavelength and $\Delta\lambda$ the bandwidth gives $l_c \approx 350$ nm, which is of the order of the wavelength of the radiation itself. With such a short coherence length, interference

of the internally reflected light with the straight through component would thus not take place. If such interference does not in fact occur then the factor $(M_A m_A)^{1/2}$ in the expression for $H(\beta)$ must be modified to $(M_A h_A)^{1/2}$ where h_A represents the transmission efficiency for the unwanted component not resulting from internal reflections. The quantity h_A is wavelength dependent and may be calculated from a knowledge of the optical properties of the polarizer plates and the spectral distribution of the source to have the value 0.0182. In a subsidiary experiment described elsewhere¹ the following values were found for the transmission efficiencies $M_A = M_B = 0.908 \pm 0.013$, $m_A = m_B = 0.0299 \pm 0.0020$, $M_{A'} = 0.938 \pm 0.010$, $m_{A'} = 0.040 \pm 0.002$. In practice, however, since the ratio $R(\beta, \alpha') / R(\beta, \infty)$ is wavelength dependent, and depends nonlinearly on wavelength dependent transmission efficiencies a wavelength averaged value was computed. The result of these calculations is shown as the quantum mechanical prediction in Figs 2 and 3 but the curves do not, in fact, differ significantly from those obtained by direct substitution in expression (4) of the measured transmission efficiencies quoted above.

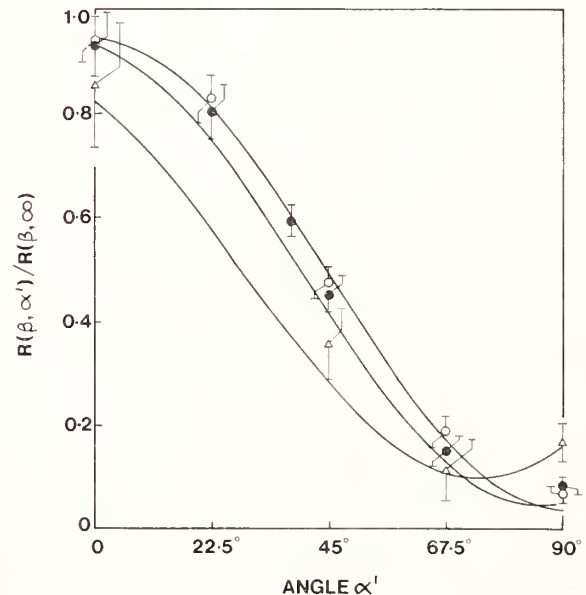


FIG 2. Variation of the ratio $R(\beta, \alpha') / R(\beta, \infty)$ as a function of α' for $\beta = 0^\circ$ (O), 33° (●), and 67.5° (Δ). The solid curves represent the quantum-mechanical predictions.

The experimental results for $\beta=0^\circ$, 33° and 67.5° are shown in Fig 2 and, clearly, within the limits of experimental error, agree well with the theoretical predictions.

Also, referring to equation (4), it is clear that the ratio $R(\beta, \alpha')/R(\beta, \infty)$ should not be symmetrical with respect to a change in the sign of angle α' because of the presence of interference between the wanted and unwanted components of radiation transmitted through polarizer a. To investigate this prediction an additional measurement was made for $\beta = 67.5^\circ$, $\alpha' = -45^\circ$ and the result is shown, in comparison to the result for positive α' , in Fig 3 along with the corresponding quantum mechanical prediction.

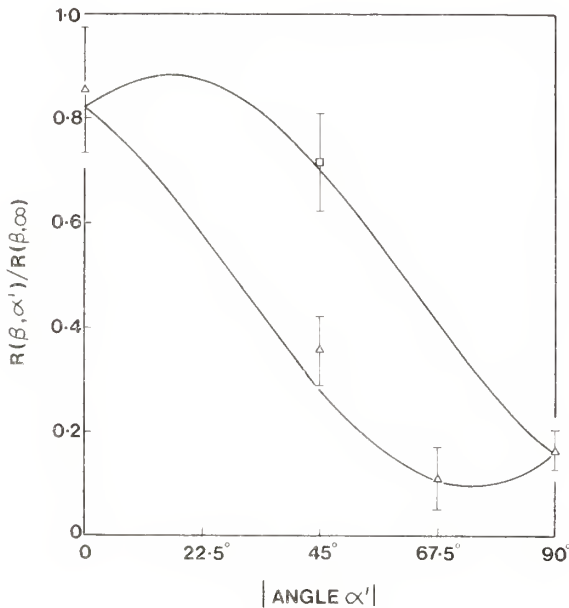


FIG 3. The ratio $R(\beta, \alpha')/R(\beta, \infty)$ as a function of α' for $\beta=67.5^\circ$. The upper (lower) curve is the theoretical result for $\alpha' < 0$ ($\alpha' > 0$). The experimental points are marked \square for $\alpha' < 0$, \triangle for $\alpha' > 0$.

These results are also of interest because of their relevance to the suggestion by Garuccio and Selleri,⁶ based on a particular class of local realistic models, that a finite difference might exist, in this situation, between the predictions of quantum mechanics and local realistic theories involving enhanced photon detection made possible by the low detection efficiency of photomultipliers. In this class of theories, capable of explaining all existing two-polarizer experiments, Garuccio and Selleri postulate that a detection vector $\underline{\lambda}$ in addition to a polarization vector \underline{l} is to be attributed to each photon of the pair emitted by a two-photon

source. The detection vector $\underline{\lambda}$ is assumed to be unaffected by passage through a linear polarizer and the probability of detection of a photon is assumed to depend on the angle between \underline{l} and $\underline{\lambda}$. Using this approach, for the parameters of the present experiment the theory of Garuccio and Selleri set an upper limit of 0.413 on the ratio $R(33^\circ, 38^\circ)/R(33^\circ, \infty)$ whereas the actual experimental point has the value 0.585 ± 0.029 violating their prediction by over six standard deviations. More recently, Selleri⁷ taking other factors into account set an upper limit of 0.514 on the ratio which is still, however violated by the experimental result by almost three standard deviations. The three polarizer experiment, therefore, provides strong evidence against the possibility of enhancement in the detection process depending on the existence of an additional (hidden) parameter, and appears to rule out the class of local realistic theories proposed by Garuccio and Selleri.

Experiments have also been carried out to investigate the effect of a weak electric field on the polarization correlation properties of the two photon radiation. Unfortunately, although the theory of the two-photon decay of metastable atomic hydrogen was developed some time ago,^{8,9} and the effect of an electric field on the lifetime of metastable atomic hydrogen is well known,¹⁰ no theoretical treatment exists to describe the effect of an electric or magnetic field on the polarization correlation properties of the two-photon radiation emitted by metastable atomic hydrogen or deuterium. It is perhaps interesting to note, however, that some theoretical and experimental work has been carried out with reference to the polarization correlation properties of the two photons emitted in cascade by excited calcium atoms in a magnetic field.¹¹

In the case of atomic hydrogen or deuterium the matrix element describing the two-photon decay in the absence of fields is in the form

$$\sum_j \left[\frac{\langle \psi_f | \underline{l} \cdot \hat{e}_1 | \psi_j \rangle \langle \psi_j | \underline{l} \cdot \hat{e}_2 | \psi_i \rangle}{W_i - W_j - \hbar \nu_2} + \frac{\langle \psi_f | \underline{l} \cdot \hat{e}_2 | \psi_j \rangle \langle \psi_j | \underline{l} \cdot \hat{e}_1 | \psi_i \rangle}{W_i - W_j - \hbar \nu_1} \right]$$

where $|\psi_i\rangle$ and $|\psi_f\rangle$ represent the initial (2S) and final (1S) state of the atom, W_i and W_f the initial and final energies and W_j the energy of the virtual intermediate states which are the P states of the atom. The unit vectors \hat{e}_1 and \hat{e}_2 are in the directions of polarization of the two photons of frequencies ν_1 and ν_2 . At first sight then, on examination of the matrix element it might seem unlikely that a weak electric and/or magnetic field would have any significant effect on the two-photon decay process since W_i and W_f will only change by a small amount in

However, it is possible that angular momentum effects could be very sensitive to the presence of a field since it will remove the degeneracy of the virtual intermediate states $|\psi_j\rangle$ and may result in a substantial change in the polarization state of the two photons. The characterization of the polarization state of the two photons, of course, requires in general the specification of 15 independent elements of a 4×4 Hermitian matrix, although, in practice, this number will normally be reduced by various symmetry requirements. Also, in the usual arrangement¹ with polarizers placed diametrically on either side of the source, say on the left and on the right, as has already been demonstrated in equations (2) and (3) the polarization properties of the radiation on the right detected in coincidence with that on the left can be expressed³ in terms of an effective 2×2 density matrix whose three independent elements depend on the two-photon polarization state and the setting and properties of the polarizer on the left. Measurements of the effective density matrix for one type and setting of the polarizer on the left then gives partial information on the two-photon polarization state. The complete specification can be obtained by a series of measurements of this kind with different types and settings of polarizers on the left.

In a preliminary experiment,¹² referring to Fig 1, polarizer a' was removed. Polarizer b was fixed with its transmission axis in the x direction while polarizer a was rotated through an angle α relative to the x axis in the same sense as for angle α' in the three-polarizer experiment. An electric field of 30 Vcm^{-1} was applied to the source in the x direction by means of electric field plates of the Spiess¹³ design with transverse dimensions $10 \text{ mm} \times 22 \text{ mm}$ placed a distance 13 mm apart. The measured variation with angle α of the ratio $R(\alpha)/R(\infty)$, where $R(\alpha)$ is the coincidence rate with the transmission axis of polarizer a at angle α and $R(\infty)$ is the rate with the plates of both polarizers removed, is shown in Fig 4, along with the experimental results and theoretical predictions in the absence of the electric field.

An additional measurement for $\alpha = -45^\circ$ gave $R(-45^\circ)/R(\infty) = 0.87 \pm 0.30$. Measurements of right hand and left hand circular polarization were also carried out by placing a quarter-wave plate in front of polarizer a. As a result, the following values for the three effective Stokes' parameters were obtained.

$$P_1 = [I(45^\circ) - I(-45^\circ)] / [I(45^\circ) + I(-45^\circ)] = -0.248 \pm 0.170$$

$$P_2 = [I(\text{RHC}) - I(\text{LHC})] / [I(\text{RHC}) + I(\text{LHC})] = 0.014 \pm 0.159$$

$$P_3 = [I(0^\circ) - I(90^\circ)] / [I(0^\circ) + I(90^\circ)] = 0.932 \pm 0.366$$

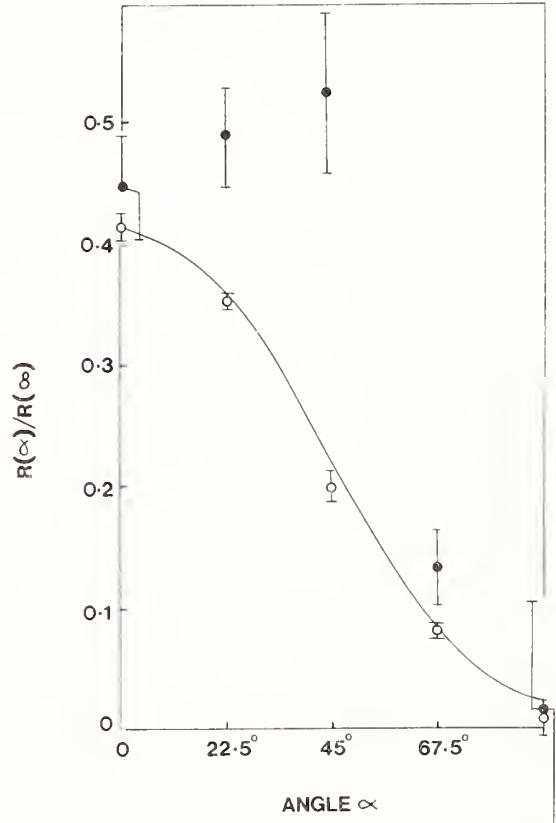


FIG 4. Variation of the ratio $R(\alpha)/R(\infty)$ as a function of α for zero electric field (O) and for an electric field of 30 Vcm^{-1} (●). The solid curve represents the theoretical prediction for zero electric field.

The preliminary nature of these results must be emphasized. For a definite conclusion to be drawn the measurements need to be repeated and extended. However, if they are confirmed these observations would represent an essentially new effect in atomic physics.

Acknowledgements

The author wishes to acknowledge the collaboration with his colleagues, H J Beyer, T Haji-Hassan, H Kleinpopp, E Merzbacher and W Perrie. In particular, he wishes to thank T Haji-Hassan for his agreeing to the presentation of unpublished results from his thesis.

References

1. W Perrie, A J Duncan, H J Beyer and H Kleinpoppen, Phys.Rev.Lett., 54, 1790 (1985).
2. T Haji-Hassan, A J Duncan, W Perrie, H J Beyer (1987)
3. T Haji-Hassan, A J Duncan, W Perrie, H Kleinpoppen and E Merzbacher, Phys.Rev.Lett., 62, 237 (1989).
4. J S Bell, Physics (N.Y.) 1, 195 (1964).
5. J F Clauser and M A Horne, Phys.Rev.D., 10, 526 (1974).
6. A Garuccio and F Selleri, Phys.Lett.A, 103, 99 (1984).
7. F Selleri, private communication.
8. M Göppert-Mayer, Ann.Phys.(N.Y.) 9, 273 (1931).
9. G Breit and E Teller, Astrophys.J. 91, 215 (1940).
10. G W F Drake and R B Grimley, Phys.Rev.A 8, 157 (1973).
11. A Aspect, J Dalibard, P Grangier and G Roger, Opt.Commun. 49, 429 (1984).
12. T Haji-Hassan, PhD Thesis, University of Stirling, 1988 (unpublished).
13. G Spiess, A Valance and P Pradel, Phys.Rev.A. 6, 746 (1972).

ELECTRON IMPACT EXCITATION OF THE $n = 3$ STATES OF HELIUM AND $5s^3P_1$ STATE OF KRYPTON

Albert Crowe

Department of Pure and Applied Physics
The Queen's University of Belfast
Northern Ireland, UK

Since the original angular correlation measurements of Eminyan et al¹, excitation of the 2^1P state of helium has been studied extensively using this technique and more recently the polarisation correlation technique. There has been a correspondingly large number of theoretical studies of this state. Although there are still major quantitative discrepancies between theory and experiment over wide ranges of both energy and angle for the 2^1P state, the emphasis of studies of this type in helium has recently switched to the $n = 3$ states. Experimental studies have been reported from Stirling, Utrecht, Perth and Belfast while theoretical work on these states has been reported using the first-order many body theory (FOMBT), distorted wave Born approximation (DWBA) and the R-matrix approach.

The four $n = 3$ states, $1^1P, 3^1P, 1^1D, 3^1D$, have now been studied experimentally over limited ranges of energy and angle. The 3^1P studies date back to 1976 with the angular correlation studies of Eminyan et al² and the polarisation correlation studies of Standage and Kleinpoppen³. Studies of the other three states are more recent.

The data have been analysed using the (λ, χ) parameterization of Eminyan et al¹ or alternatively in terms of the charge cloud and angular momentum description⁴ ($P_{lin}, L_{\perp}, \gamma, \rho_{00}$). The experimental techniques involve measurement of either the angular correlation between the scattered electron and the photon arising from the decay of the excited state or the polarisation of the radiation in coincidence with the scattered electron. Both the angular correlation technique and a measurement of the linear polarisation (the Stokes parameters P_1, P_2) of the radiation emitted perpendicular to the scattering plane map out the shape of the charge cloud in the scattering plane. The angular momentum transferred to the atom during the excitation process can only be obtained from a measurement of the circular polarisation, P_3 , of the radiation emitted in that direction. Additionally, for the D states, there exists the possibility of exciting a dipole

perpendicular to the scattering plane and so complete information on the excitation can only be determined by a linear polarisation measurement, P_4 , in the scattering plane. For the triplet states, allowance for the fine structure depolarisation of the radiation must be taken into account in determination of the above parameters from the data.

Excitation of the 3^1P state

To avoid complications, this state is best studied by observation of the 501.6 nm (3^1P-2^1S) radiation rather than the 53.7 nm (3^1P-1^1S) photons⁵. The Stirling group^{2 3 6 7} have made measurements of both linear and circular polarisation at energies of 50, 80, 120 and 160 eV for angles in the range 27.5° to 105° while Beijers et al⁸ have measured the circular polarisation at 50, 60 and 80 eV. Recent angular and polarisation correlation measurements in this laboratory^{5,9} have concentrated on the lower energy range, 26.5 and 29.6 eV, where comparison can be made with R-matrix calculations¹⁰. While these calculations are in qualitative agreement with the experimental results for the Stokes parameters P_1, P_2 and P_3 and hence with the linear polarisation P_{lin} and angular momentum transfer L_{\perp} , there is a curious discrepancy with the data for the charge cloud alignment angle γ . γ values are determined directly from the minimum positions of the angular correlations and are related to the measured linear polarisations P_1 and P_2 through the relationship

$$\gamma = \frac{1}{2} \tan^{-1} (P_2/P_1)$$

Figure 1 shows the experimental and theoretical values of γ as a function of electron scattering angle at 29.6 eV and 26.5 eV. To highlight the different variations, the experimental data are plotted on a scale 0 to -180° while the theoretical values are shown over the range $-90 < \gamma < +90^\circ$. Theoretically there is an initial rotation of the charge cloud to negative angles, in qualitative agreement with experiment, followed by a rotation to

positive angles. Experimentally the charge cloud continues to rotate more towards negative angles before reaching a minimum.

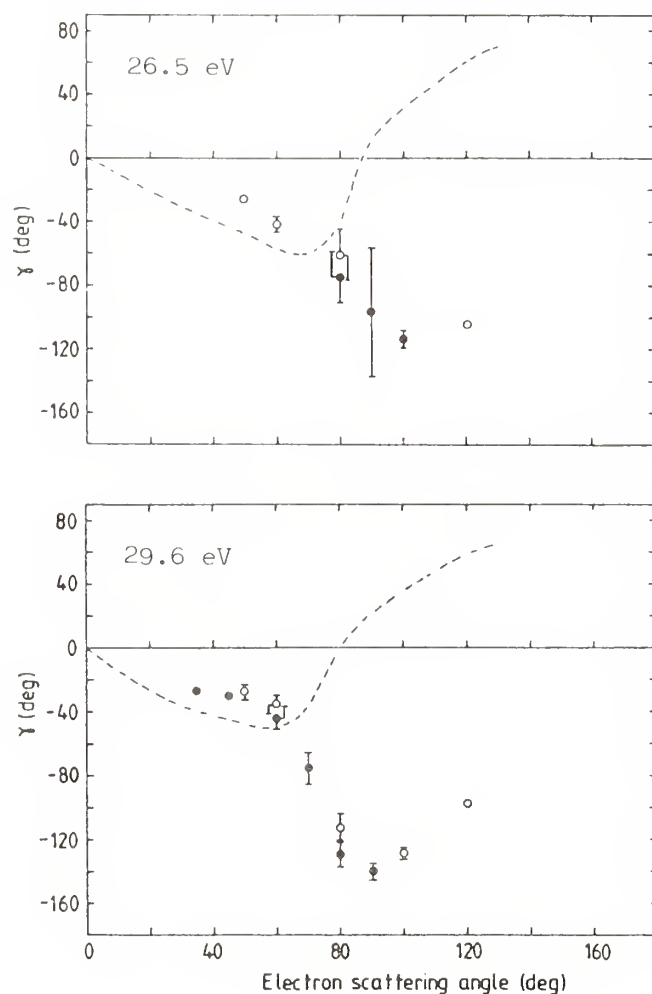


Fig. 1.

- Angular Correlation data⁵
- Polarisation Correlation data⁹
- 19-state R matrix¹⁰

Excitation of the 3^3P state

The situation up to the last meeting in this series was discussed by Beyer¹¹. Since then we have measured¹² both angular and polarisation correlations for the 3^3P state at 29.6 eV. Very recently these have been complemented with 19-state R-matrix calculations.

Figure 2 shows the measured values of P_1 , P_2 , P_3 obtained using both experimental techniques compared with the 5-state R-matrix calculation for the 2^3P state¹³ and the 19-state R-matrix calculation¹⁰ for the 3^3P state at 29.6 eV. The negative values of P_1 at 40 and 60° are not predicted theoretically,

although the 19-state calculation gives a much lower positive value than the 5-state for the 2^3P state. Theory predicts a double hump structure for P_3 which is also seen in the experiment although displaced in angle and much less pronounced.

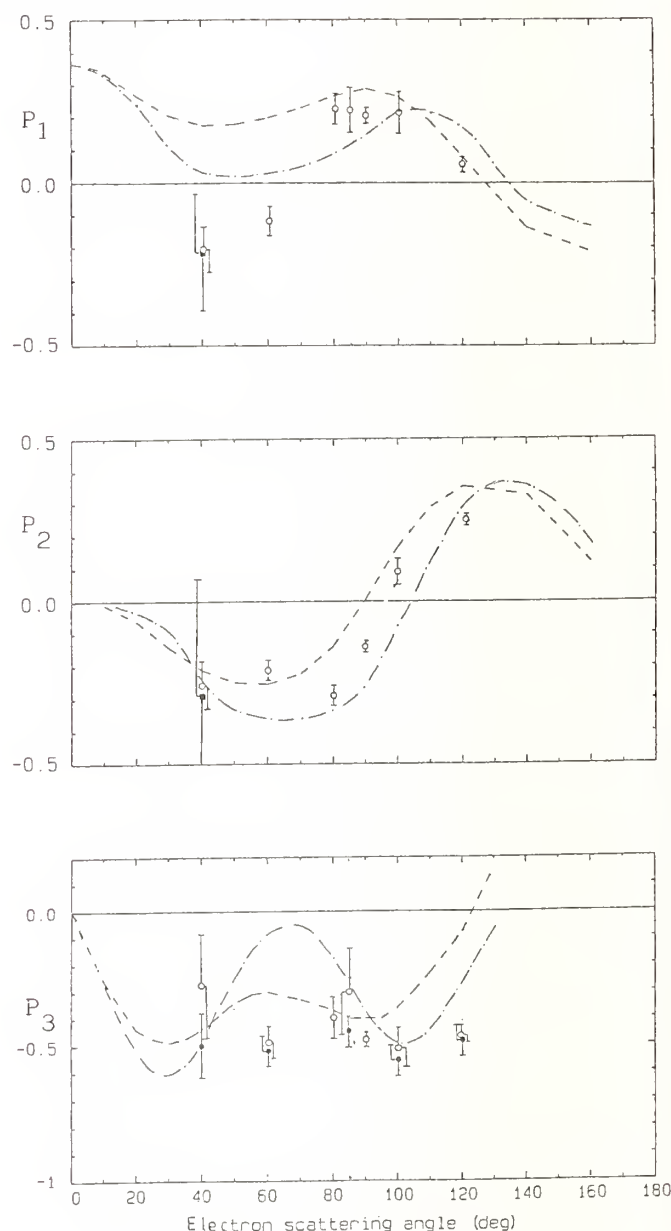


Fig. 2.

- Angular Correlation data¹²
- Polarisation Correlation data
- 5-state R matrix¹³ (2^3P)
- .- 19-state R matrix¹⁰ (3^3P)

Excitation of the 3¹D state

At the last meeting considerable interest¹⁴ was focused on new results¹⁵ which indicated that the sign of the circular polarisation P_3 was positive for small scattering angles, in contrast to that measured for the P states. This was in qualitative agreement with the FOMBT of Cartwright and Csanak¹⁶ but in disagreement with the 10 channel eikonal approximation results of Mansky and Flannery¹⁷ and the excited state potential DWBA results of Bartschat and Madison¹⁸. Although preliminary data from this laboratory¹⁹ confirmed the sign of P_3 as measured by Beijers et al, both groups, after careful evaluation of the $\lambda/4$ plates used to determine the circular polarisation, agree that the sign is in fact negative²⁰, as for the P states, for small scattering angles and energies around 40 eV.

Figure 3 shows the measured values of the circular polarisation at an incident energy of 40 eV compared with the DWBA and FOMBT calculations. It can be seen that although there is qualitative agreement between the excited state DWBA theory and experiment, there is a lack of quantitative agreement.

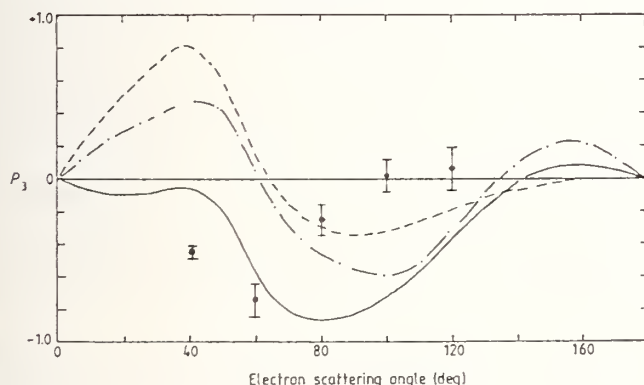


Fig 3.

- Present data
- FOMBT¹⁶
- DWBA-EP¹⁸
- DWBA-GP¹⁸

Measurements of the linear polarisations P_1 , P_2 and P_4 and the circular polarisation P_3 are presently being carried out for the 3¹D state at both 29.6 eV and 40 eV, enabling all four parameters describing the charge cloud to be determined. The height parameter ρ_{00} , calculated from the linear polarisations P_1 and P_4 using the relation

$$\rho_{00} = \frac{3(1+P_1)(1-P_4)}{2(4-(1-P_1)(1-P_4))}$$

is shown in Figure 4 at an incident electron energy of 29.6 eV. At all angles the measured values of ρ_{00} are small. The 10-state eikonal approximation of Mansky and Flannery¹⁷ gives values just greater than 0.2 in the range $40 < \theta < 80^\circ$. The deconvoluted $n=3$ electron-cascade photon angular correlation data of van Linden van den Heuvell et al²⁷ indicates a value of 0.4 at 35° at this energy.

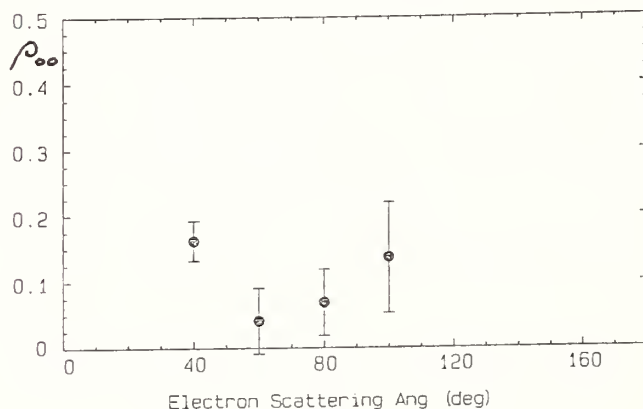


Fig 4.

Present data @ 29.6 eV

Excitation of the 3³D state

Like the 3³P state, both angular and polarisation correlation measurements on the 3³D state are made difficult by the large fine structure depolarisation of the emitted radiation. The 3³D state depolarisation factors are 71/150 and 43/54 for the linear and circular polarisations respectively.

Measurements of the Stokes parameters P_1 , P_2 , P_3 have recently been reported²¹ from this laboratory at 40 eV. The results are shown in Figure 5 and compared with the only available calculation at this energy¹⁸ and the preliminary experimental data of Beyer¹¹. The effect of the large depolarisation on the measured linear polarisations P_1 and P_2 is obvious from their small values. The P_1 value of Beyer agrees well with the present measurements while the DWBA calculations disagree strongly with experiment at large scattering angles. It is a general feature of all the correlation studies for the $n=3$ states that the greatest discrepancies between theory and experiment exist for P_1 . The DWBA calculations predict very small values of P_2 compared with experiment, while the opposite is true for P_3 .

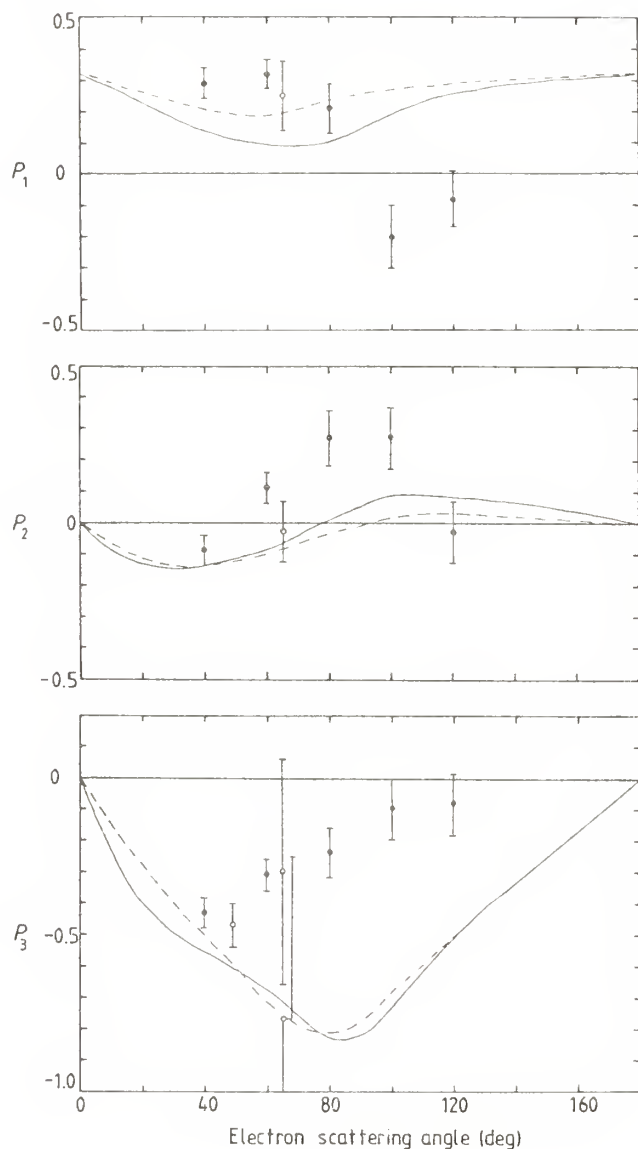
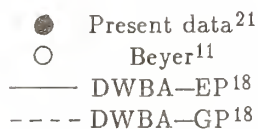


Fig 5.



Excitation of the $4p^5 ({}^2P_{3/2}) 5s^3P_1$ state of krypton

We have measured double angular correlations for the $4p^5 ({}^2P_{3/2}) 5s^3P_1$ state of krypton at 15, 30 and 60 eV over a wide range of electron scattering angles.

Two significant results are obtained.

(1) Excellent agreement is obtained with the DWBA results of Bartschat and Madison²², particularly for the most directly measurable parameters. Figure 6 shows, as an example, the situation for the alignment angle γ corresponding to the position of the angular

correlation minimum at an energy of 30 eV. This seems a surprising result when contrasted with the situation in helium, but may be a result of the dominance of the central potential in the krypton case.

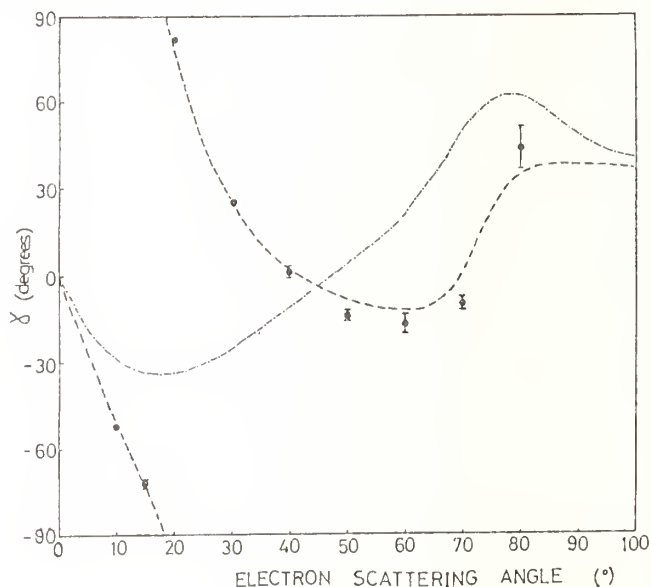
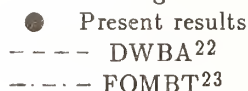


Fig 6.



(2) The rapid variation of the λ parameter (Figure 7) in the region of a differential cross section minimum (Figure 8) at 60 eV. Experiments are now in progress to examine this phenomena at other electron energies.

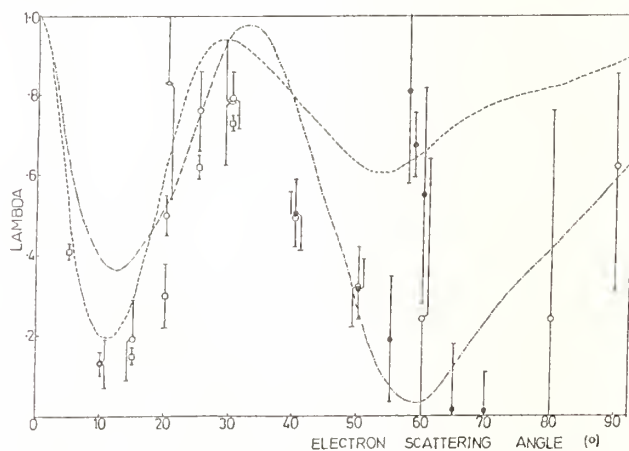
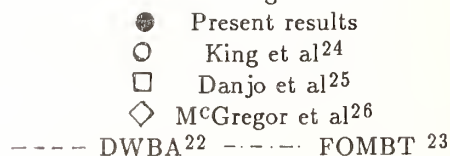


Fig 7.



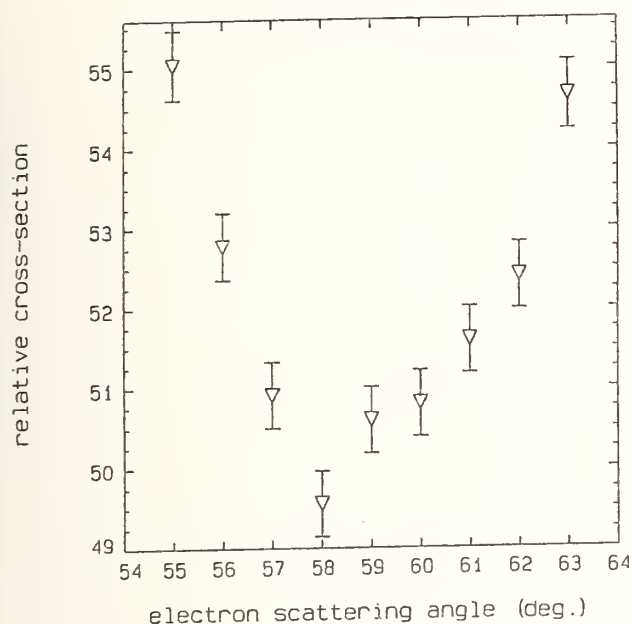


Figure 8.

Acknowledgments

This work has been supported by the United Kingdom Science and Engineering Research Council. The contribution of B.P. Donnelly, S.F. Gough, P.B. Murray, and P.A. Neill to the work in this laboratory is gratefully acknowledged.

References

- 1 M. Eminyan, K.B. McAdam, J. Slevin and H. Kleinpoppen, *Phys Rev Lett* **31**, 576 (1973).
- 2 M. Eminyan, K.B. McAdam, J. Slevin, M.C. Standage and H. Kleinpoppen, *J Phys B* **8**, 2058 (1975).
- 3 M.C. Standage and H. Kleinpoppen, *Phys Rev Lett* **36**, 577 (1976).
- 4 N. Andersen, J.W. Gallagher and I.V. Hertel, *Phys Rep* **165**, 1 (1988).
- 5 P.A. Neill and A. Crowe, *J Phys B* **21**, 1879 (1988).
- 6 K.S. Ibraheim, H.J. Beyer and H. Kleinpoppen, *Proc 2nd ECAMP, Amsterdam*, ed. A.E. de Vries and M.J. van der Wiel, p 298 (1985); *Proc 14th ICPEAC, Palo Alto*, ed. M.J. Coggiola et al, p 118 (1985).

- 7 H.J. Beyer, K. Blum, H.A. Silim, M.C. Standage and H. Kleinpoppen, *J Phys B* **21**, 2953 (1988).
- 8 J.P.M. Beijers, J.P. van den Brink, J. van Eck and H.G.M. Heideman, *J Phys B* **19**, L581 (1986).
- 9 P.A. Neill, B.P. Donnelly and A. Crowe, *J Phys B* **22**, 1417 (1989).
- 10 W.C. Fon, private communication.
- 11 H.J. Beyer, *Correlation and Polarisation in Electronic and Atomic Collisions*, ed. A. Crowe and M.R.H. Rudge, p 324 (1988).
- 12 B.P. Donnelly, P.A. Neill and A. Crowe, *J Phys B* **21**, L321 (1988).
- 13 W.C. Fon, K.A. Berrington, P.G. Burke and A.E. Kingston, *J Phys B* **12**, 1861 (1979).
- 14 G. Csanak and D.C. Cartwright, *Correlation and Polarisation in Electronic and Atomic Collisions*, ed. A. Crowe and M.R.H. Rudge, p 31 (1988).
- 15 J.P.M. Beijers, S.J. Doornenbal, J. van Eck and H.G.M. Heideman, *J Phys B* **20**, 6617 (1987).
- 16 D.C. Cartwright and G. Csanak, *J Phys B* **20**, L583 (1987).
- 17 E.J. Mansky and M.R. Flannery, *J Phys B* **20**, L235 (1987).
- 18 K. Bartschat and D.H. Madison, *J Phys B* **21**, 153 (1988).
- 19 B.P. Donnelly and A. Crowe, *J Phys B* **21**, L637 (1988).
- 20 H. Batelaan, J. van Eck and H.G.M. Heideman, *J Phys B* **21**, L741 (1988).
- 21 B.P. Donnelly and A. Crowe, *J. Phys B* **21**, L697 (1988).
- 22 K. Bartschat and D.H. Madison, *J Phys B* **20**, 5839 (1987).
- 23 G.D. Meneses, F.J. da Paixao and N.T. Padial, *Phys Rev A* **32**, 156 (1985).
- 24 S.J. King, P.A. Neill and A. Crowe, *J Phys B* **18**, L589 (1985).

25 A. Danjo, T.Koike, K.Kani, H. Sugahara, A. Takahashi and H. Nishimura, J Phys B 18, L595 (1985).

26 I. McGregor, D. Hils, R. Hippler, N.A. Malik, J.F. Williams, A.A.Zaidi and H. Kleinpoppen, J Phys B 15, L411 (1982).

27 H.B. van Linden van den Heuvell, E.M. Gasteren, J. van Eck and H.G.M. Heideman, J Phys B 16, 1619 (1983).

Orientation and Alignment in Electron Collisions with Sodium

P.J.O. Teubner, R.E. Scholten and G.F. Shen

Institute for Atomic Studies,
School of Physical Sciences,
The Flinders University of South Australia,
Bedford Park, South Australia, 5042, Australia

The electron impact of the 3^2P state in sodium provides a particularly fertile ground for the study of electron scattering from atoms. Whereas the analytical wave functions of the atomic states are not known as they are for atomic hydrogen, the very strong coupling between the ground and the first excited state suggests that only a few states will be required in a close coupling solution of the scattering problem. This description which was first alluded to by Seaton¹, was subsequently refined by Moores and Norcross² and most recently has been applied in depth by McCarthy and coworkers³.

When the Flinders coupled channels theory is tested against the experimental differential cross section⁴, the results are perhaps inconclusive. For example at an incident energy of 22.1eV, there is excellent agreement out to 15° but the theory overestimates the cross section at larger angles. As the energy increases the agreement between theory and experiment deteriorates. This observation has led Mitroy *et al.*³ to question the validity of the experiments. We note that the theoretical predictions are essentially invariant with respect to the inclusion of more states in the model and by the use of an optical model³.

Teubner *et al.*⁴ went to considerable effort to identify and remove possible systematic errors in their experiments. The data were taken in the form of angular distributions and were normalised to the total differential cross sections of Enemark and Gallagher⁵. The distributions are very strongly peaked in the forward direction. For example at 22.1eV, 75% of the integral cross section comes from the angular range $0^\circ \leq \theta_e \leq 10^\circ$. Thus this technique requires measurements at very small scattering angles with the consequent additional experimental problems of possible detector saturation and interference by the incident electron beam. These problems were identified by Teubner *et al.*⁴ and were solved. The success can be inferred by the excellent agreement between theory and experiment. What causes the lack of accord at larger angles? Are there systematic errors in the experiments?

It is appropriate to ask for another test of the theory. This in part prompted the electron photon coincidence experiments of the Flinders group at several energies. In these experiments, electrons which had excited the 3^2P state and the photons arising from the decay of the state were detected in coincidence after the polarisation states of the photons were analysed. The photons were detected normal to the scattering plane and a complete Stokes parameter analysis was performed⁶. The data from these experiments can be used not only to observe the shape, alignment and orientation of the excited atomic state but also, through the concept of the reduced total polarisation $|\bar{P}|$, the role of spin in the collision can be studied.

Figure 1 shows the values of \bar{P}_1 , measured by electron photon coincidence techniques, compared with the predictions of the 4 state close coupling theory of Mitroy *et al.*³ and with the superelastic scattering data of Hertel and coworkers⁷. Although the coincidence measurements support the

theory out to 15° , the quality of the experimental data at the largest angle studied makes any further comparison difficult. In any event it has already been observed that the kinematic region of interest lies beyond 15° at 22.1eV. There are *a priori* reasons why the kinematic range of coincidence experiments is limited. It can be shown⁸ that the counting time required to obtain data of a specified relative error is proportional to the ratio $\frac{Q}{\sigma}$ where Q is the total cross section and σ the differential cross section. At 22.1eV, $\sigma(30^\circ)$ is 130 times less than $\sigma(10^\circ)$. Thus it is unrealistic to use this technique at larger angles where the theoretical interest is greatest.

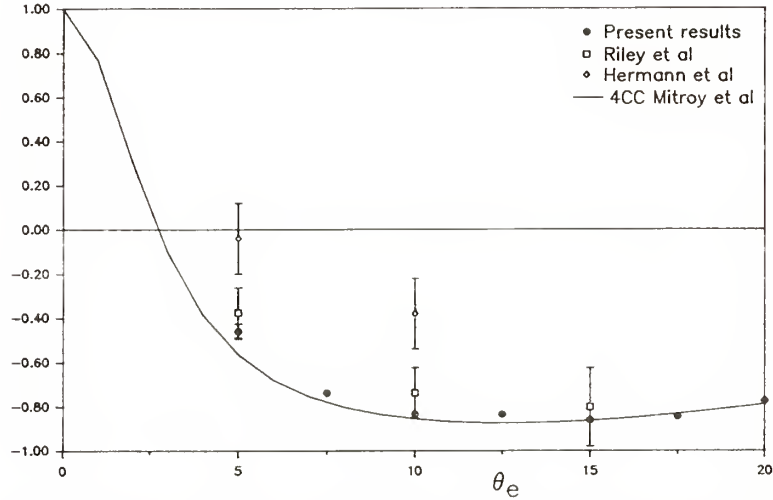
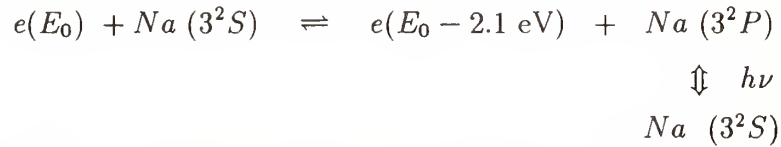


Figure 1. A comparison between \bar{P}_1 from coincidence experiments with theoretical predictions at forward angles at 22.1eV.

The optical pumping technique developed by Hertel and coworkers⁷ appears to offer a solution to this experimental problem. Time reversal invariance ensures that the data derived from optical pumping experiments are equivalent to those which can be obtained from coincidence experiments. That is



Whilst the data shown in figure 1 do not appear to support this premise, there is no doubt about its validity.

In these experiments, radiation from a laser is used to pump a beam of ground state sodium atoms from a specific HFS level ($\bar{F} = 2$) to the $F = 3$ level of the $3^2P_{3/2}$ state. An electron beam of energy 20eV is introduced into the interaction region and an electron spectrometer views the region of overlap of the electron, sodium and laser beams. The laser beam is introduced normal to the scattering plane. Electrons which have gained 2.1eV of energy in the collision are analysed by the electron spectrometer and detected in a channel electron multiplier. The superelastic count rate is then measured as a function of the polarisation state of the laser beam.

The equivalent Stokes parameters

$$P_1 = \frac{I(0^\circ) - I(90^\circ)}{I(0^\circ) + I(90^\circ)} \\ P_2 = \frac{I(45^\circ) - I(135^\circ)}{I(45^\circ) + I(135^\circ)} \quad (1)$$

$$P_3 = \frac{I(RHC) - I(LHC)}{I(RHC) + I(LHC)}$$

can be measured, where $I(\alpha)$ is the count rate when the laser beam is polarised at an angle α with respect to the outgoing electron beam direction.

Such measurements depend on the orientation and alignment of the sodium atoms induced by the laser beam. These effects can be measured by appropriate observations⁹ of the fluorescence radiation from the sodium beam and the appropriate corrections made. The resulting reduced polarisations \bar{P}_i are related to the measured values P_i by

$$\begin{aligned} \bar{P}_{1,2} &= \frac{a_0^{ph} - 60}{3a_0^{ph}} P_{1,2} \\ \bar{P}_3 &= \frac{2 + \frac{a_0^{ph}}{15}}{O_0^{ph}} P_3 \end{aligned} \quad (2)$$

where the laser induced alignment and orientation parameters of the atomic beam are a_0^{ph} and O_0^{ph} respectively.

It is possible to compare the measured values \bar{P}_i with the theory. Figure 2 shows a comparison of the linear component \bar{P}_1 with the predictions of the theory of Mitroy *et al.*³. It is clear that there is excellent agreement with theory out to about 20°. At larger angles the agreement is poor. A similar effect is observed with the other linear component \bar{P}_2 . This lack of agreement is consistent with the description provided by the differential cross section.

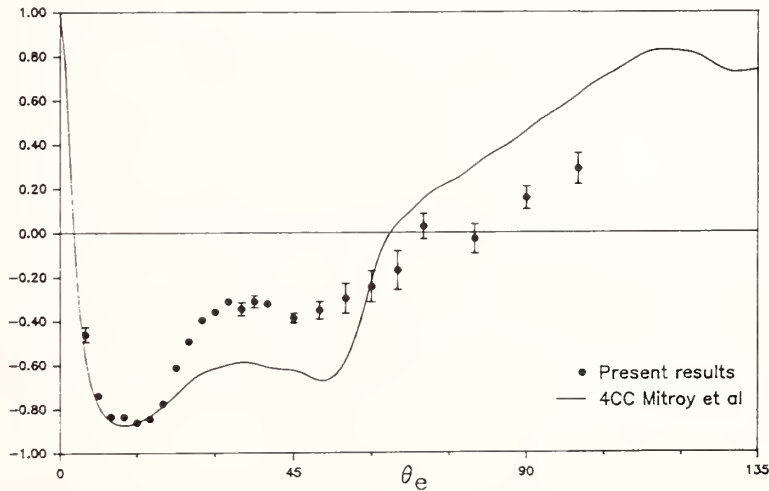


Figure 2. \bar{P}_1 as a function of scattering angle from optical pumping experiments at 20eV.

A clearer picture of the dynamics¹⁰ of the scattering process can be gained from the alignment angle γ , the total linear polarisation \bar{P}_ℓ and the angular momentum L_\perp transferred normal to the scattering plane. These parameters are related to those in equation (2) by¹⁰

$$\begin{aligned} \gamma &= \frac{1}{2} \arg(\bar{P}_1 + i\bar{P}_2) \\ \bar{P}_\ell &= [\bar{P}_1^2 + \bar{P}_2^2]^{\frac{1}{2}} \\ \text{and } L_\perp &= -\bar{P}_3 \end{aligned}$$

The angle γ measures the angle between the major axis of the charge cloud and the incident electron beam direction. The shape of the charge cloud is measured by \bar{P}_ℓ in that the relative length and width are given by $\frac{1+\bar{P}_\ell}{2}$ and $\frac{1-\bar{P}_\ell}{2}$ respectively.

Measurements of the angle γ are shown in figure 3 where they are compared with those predicted by the coupled channels theory of Mitroy *et al.*³, the distorted wave polarised orbital theory of Kennedy *et al.*¹¹ and with the First Born approximation. Also shown are the results of the coincidence experiments of Riley *et al.*⁶ and the previous superelastic results of Hermann *et al.*⁷.

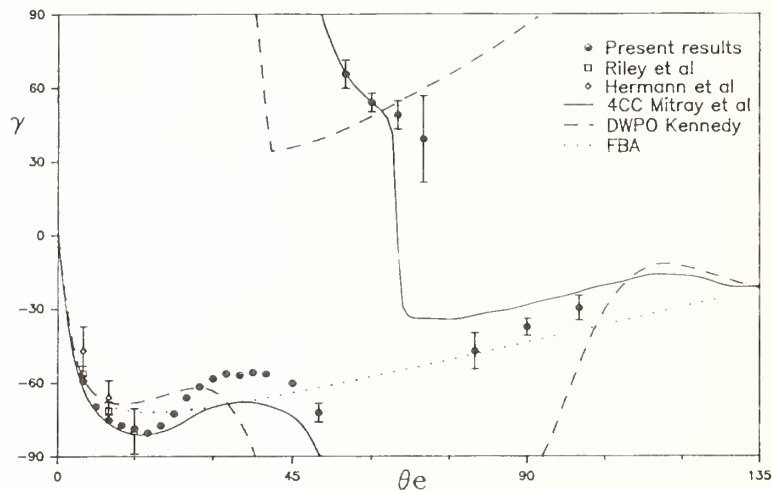


Figure 3. γ as a function of electron scattering angle compared with theory at 20eV.

It is immediately apparent that the results derived from the superelastic experiments are far superior to that from the coincidence experiments. The kinematic range covered by the present measurements covers the whole region of interest which is dictated by the theory. It is also clear that the DWPO theory of Kennedy *et al.*¹¹ is inadequate at all but the most forward of scattering angles. This observation differs from the conclusion of Riley *et al.*⁶ and reinforces the well known problem of forming conclusions based on limited data. The problems with the Born approximation are also obvious. They appear to agree with the coincidence measurements for $\theta_e \leq 15^\circ$ but this is a measure of the quality of the data rather than an indication of any deep physical significance.

The agreement between the coupled channels theory and experiment is better for γ than for either of the components \bar{P}_1 and \bar{P}_2 . Although the prediction by the theory of the change of quadrant is spectacular, there are significant differences in the range $20^\circ < \theta_e < 50^\circ$ and around the minimum in the differential cross section. Whilst it is undeniably true that γ gives a clearer physical picture of the collision, it is a ratio measurement and the individual components \bar{P}_i are a more sensitive test of the theory.

Figure 4 shows a comparison of the results of the measurement of \bar{P}_ℓ with those predicted by the theory. The theory appears generally to be supported out to a scattering angle $\theta_e \simeq 45^\circ$ but there are serious discrepancies for angles greater than this.

The angular momentum transferred normal to the scattering plane is shown in figure 5. Again there is a significant difference between experiment and the coupled channels theory for scattering angles greater than about 45° .

The data shown in figures 2-5 demonstrate that the problems which the coupled channels theory had in describing the backward angle behaviour of the differential cross section are still present when a more sensitive test of the theory are applied.

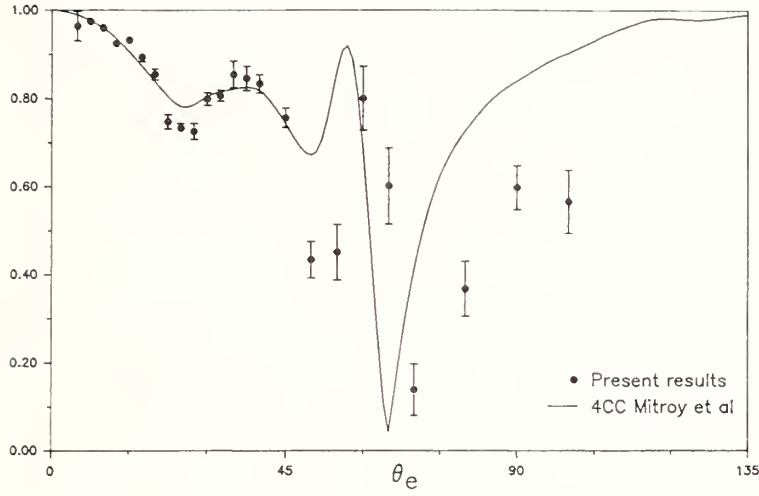


Figure 4. P_L as a function of electron scattering angle compares with theory³ at 20eV.

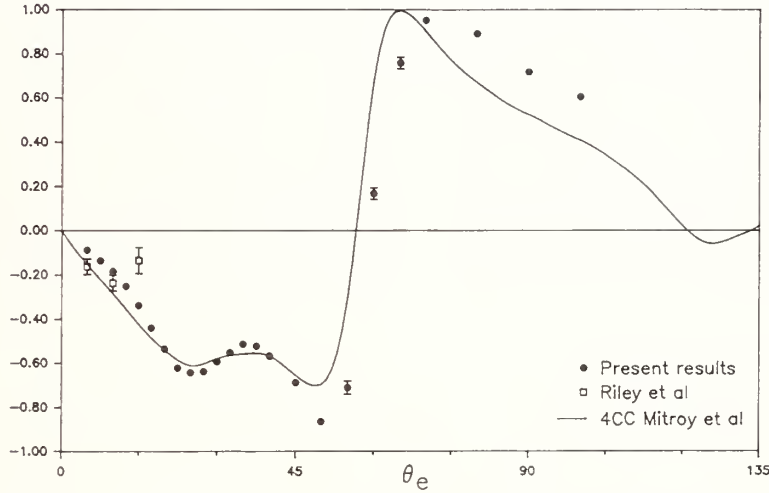


Figure 5. \bar{P}_3 as a function of electron scattering angle compared with a coupled channels theory⁴.

One can speculate about possible shortcomings of the theory. For example if exchange was not adequately described, this influence would be more apparent at backward angles. This hypothesis can be probed by comparing the total reduced polarisation $|\bar{P}|$ with that predicted by the theory.

$$|\bar{P}| = [\bar{P}_1^2 + \bar{P}_2^2 + \bar{P}_3^2]^{\frac{1}{2}}$$

and $|\bar{P}| = 1$ is a test of the coherence of the collision. It can be shown¹² that, *inter alia*, the coherent excitation of a doublet state implies that exchange scattering can be ignored.

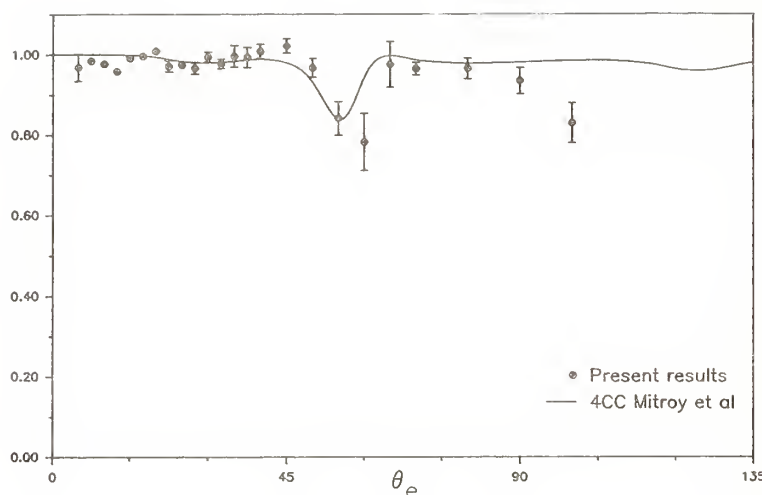


Figure 6. A comparison between measured values of $|\bar{P}|$ and theory³.

Figure 6 shows the results of the present measurement of $|\bar{P}|$ compared with the predictions of the coupled channels theory. Overall the agreement is excellent including the onset of the loss of coherence at about 60° . This corresponds to the minimum in the differential cross section and the fact that the theory does not reproduce the point at 60° may simple reflect a slight shift in the predicted minimum of the differential cross section. Consequently it would appear that the difference between theory and experiment cannot be explained on the basis of exchange.

The variety of experimental evidence presented in the current study clearly demonstrates that there are significant problems in the coupled channels theory. Tempting though it may be to retain the concept of few state coupled channel calculation to describe the excitation of the 3^2P state in sodium, the present results show that this model does not provide a complete picture of the collision process.

References

1. M. Seaton, Proc. Phys. Soc. Lond. A **68**, 457 (1955).
2. D.L. Moores and D.W. Norcross, J. Phys. B **5**, 1482 (1972).
3. J. Mitroy, I.E. McCarthy and A.T. Stelbovics, J. Phys. B **20**, 4827, (1987).
4. P.J.O. Teubner, J.L. Riley, M.J. Brunger and S.J. Buckman, J. Phys. B **19**, 3313 (1986).
5. E.A. Enemark and A. Gallagher, Phys. Rev. A **6**, 192 (1972).
6. J.L. Riley, P.J.O. Teubner and M.J. Brunger, Phys. Rev. A **31**, 1959 (1985).
7. H.W. Hermann, I.V. Hertel, W. Reiland, A. Stamatović and W. Stoll, J. Phys. B **10**, 251 (1977).
8. J.L. Riley, Ph.D. Thesis, The Flinders University of South Australia (1984) - unpublished.
9. A. Fischer and I.V. Hertel, Z. Phys. A **304**, 103 (1982).
10. N. Andersen, J.W. Gallagher and I.V. Hertel, Phys. Rep. **165**, 1 (1988).
11. J.V. Kennedy, V.P. Myerscough and M.R.C. McDowell, J. Phys. B **10**, 3759 (1977).
12. H.W. Hermann and I.V. Hertel, Comments At. Mol. Phys. **12**, 127 (1982).

Theoretical interpretation of the associative ionization reaction between laser excited sodium atoms : Atomic and Molecular points of view

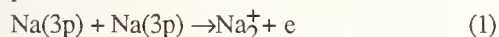
Anne HENRIET⁺ and Françoise MASNOU-SEEUWS

*Laboratoire des Collisions Atomiques et Moléculaires, Bât. 351, Université Paris-Sud
91405 ORSAY Cedex France*

The experiments on associative ionization between two laser excited alkali atoms have demonstrated that the ion signal markedly depends upon the angle between the atomic beam and the polarization vector of the exciting laser light. In the atomic point of view, first developed by Nienhuis, this angular dependence is analyzed to determine which initial preparation of the two atoms is the most favourable. In the molecular point of view, the problem of the autoionization of the Na₂ molecule is treated so as to know which molecular symmetry is the most favourable one. The first order MQDT treatment proposed by Giusti (1980) for dissociative recombination is applied to the present problem. Two-electron calculations for the intermediate Rydberg states of Na₂ are used to define a diabatic representation, where dissociative doubly excited states Q_j are interacting with mono-excited Rydberg series, converging to the Na₂⁺ ground state X. The ionization probability is controlled by the strength of this electronic coupling and by the position of the crossing between the Q_j and the X curves. The cross sections may thus differ considerably from one molecular symmetry to another, explaining the strong anisotropy observed experimentally. A link between both points of view has been established by Jones and Dahler who considered a sudden change from atomic to molecular "Hund's case a" representation at infinite internuclear distances. Although some aspects of the problem still have to be clarified, the conclusion is that the associative ionization reaction is more likely to proceed when the two atoms are prepared in Zeeman sublevels $j=3/2$, $m_j=1/2$ or $-1/2$ and form a molecular state of $^3\Sigma_u^+$ symmetry.

Introduction

During the past few years, many experimental results have become available for the associative ionization (AI) reaction between two laser excited alkali atoms, in particular for the reaction



The results can be summarized as follows :

1) The value of the total cross-section^{1,2} is of the order of 1 \AA^2 at room temperature, that is more than one order of magnitude smaller than the geometrical cross-section : the minimum of the Na₂⁺ ground state potential curve being located around 7 a.u., one should expect a geometrical cross-section of 43 \AA^2 . An unexpectedly large increase of the cross-section is apparently observed at ultracold temperatures³.

2) A strong anisotropy effect is observed^{4,5} when the two atoms are excited using polarized laser light. The ion signal can vary by a factor of two when the polarization vector of the laser is turned by 90°. Detailed results concerning the sodium measurements using linearly or circularly polarised light are presented in the following talk by H. A.J. Meijer. It is remarkable that a similar conclusion is obtained⁶ when two potassium atoms are considered.

3) In the latter case however, a competition with the K⁺K⁻ exit channel is observed.

The interpretation of such experiments is a challenge for the theoreticians : being a particularly simple

example for the formation of a chemical bond, the associative ionization reaction presents a fundamental interest. In the initial state, all the electrons are bound while the relative motion of the two atoms is free ; in the final state the vibrational motion of the two nuclei is bound while a free outgoing electron is taking off the excess energy and eventually some part of the angular momentum. The major difficulty lies in the treatment of bound-continuum interactions which involves a very large number of molecular states.

However, the strong dependence of the observed ion signal as a function of the initial preparation of the two atoms indicates that some molecular symmetries should be more favourable than the others for the molecular autoionization process. In order to analyze this symmetry effect, one can adopt two points of view :

1) An "atomic" point of view, first developed by Nienhuis⁷, analyses the experimental signal so as to determine the relative value of the cross-sections for a given initial state, when the two atoms are prepared in particular Zeeman sublevels. The question therefore is : *in which Zeeman sublevels should we prepare the two atoms in order to get the maximum signal ?*

2) A molecular point of view, in which the autoionization of the Na₂ molecule is considered. Among the twelve molecular states which are correlated to the Na(3p)+Na(3p) dissociation limit, ten may contribute to the reaction (1) (the two others being Σ^- states, a symmetry which is not possible for the final state). The question then is : for which of those ten states is the autoionization process most probable ?

The link between the atomic and molecular points of view then needs to be established. In the work of Jones and Dahler⁹, this is done by assuming a sudden change of coupling at large internuclear distances from the $|j\ m_j\rangle$ atomic states to the molecular states corresponding to Hund's case "a".

2. Atomic point of view : analysis of the measurements in terms of Nienhuis' theory.

Let us consider a collision event where in the initial state two atoms are prepared in Zeeman sublevels $|j_1\ m_1\rangle |j_2\ m_2\rangle$ and collide with relative velocity V_i and angular momentum J . In the final state, a Na_2^+ molecular ion is formed in a ro-vibrational level $|v, J'\rangle$ while an electron escapes with a final velocity V_f :
 $[\text{Na}(3p\ j_1\ m_1) + \text{Na}(3p\ j_2\ m_2)] (V_i, J)$

$$\rightarrow \text{Na}_2^+(v, J') + e(V_f) \quad (2)$$

We shall call : $|\alpha\rangle = |j_1\ m_1\rangle |j_2\ m_2\rangle$ the initial state of the two atoms and $f(\alpha, V_i, J \rightarrow v, J', V_f)$ the probability amplitude for this collision..

Let us consider an experiment where the angle between the polarization axis of the laser light (direction of polarization for σ radiation, propagation direction for π radiation) and the atomic beam is θ . The number of ions detected per unit time, $R(\theta)$, can be computed from the trace of the product of two matrices :

$$R(\theta) = \text{Tr}[G \cdot \rho] \quad (3)$$

where ρ is the product of the density matrices of the two atoms and depends both upon the polarization of the light (linear, circular) and upon the angle θ . G is a detection operator defined as :

$$\langle \alpha | G | \alpha' \rangle = \left\{ \mu_f V_f / \mu_i \sum_{J'} \sum_v \right. \quad (4)$$

$$\left. \int \{ f(\alpha, V_i, J \rightarrow v, J', V_f) f^*(\alpha', V_i, J \rightarrow v, J', V_f) d(V_f / |V_f|) \} \right\}_{\text{av}}$$

In (4), μ_f and μ_i are the reduced masses in the final and in the initial state respectively, the average is performed over the distribution of the initial relative velocities, the summation is over all possible rotational and vibrational states of the final molecular ion and the integration is over the direction of the velocity of the ejected electron. The diagonal elements of G are simply rate constants for the formation of a molecular ion starting from two atoms prepared in a given combination of Zeeman sublevels $|\alpha\rangle$. The non diagonal matrix elements are less obvious coherence terms corresponding to an interference between the contributions to the ionization process starting from two different initial states $|\alpha\rangle$ and $|\alpha'\rangle$ of the two atoms.

By expanding the two matrices ρ and G in spherical tensors with appropriate quantization axis, Nienhuis finds that $R(\theta)$ can be expressed as a combination of a limited number of independent parameters. For instance, in the case of the excitation of the $F=2 \rightarrow 3$ hyperfine component of the D_2 line with linearly polarized light, $R(\theta)$ has only three Fourier components :

$$R(\theta) = R_0 + R_1 \cos(\theta) + R_2 \cos(2\theta) \quad (5)$$

depending upon five independent parameters, among which three are combinations of the diagonal matrix elements of the G matrix and two are coherence terms. Assuming that the latter may be neglected, it is possible to determine from experiment three quantities A, B, C :

$$\begin{aligned} A &= 1/2 [K(3/2, 3/2) + K(3/2, -3/2)] \\ B &= 1/2 [K(3/2, 1/2) + K(3/2, -1/2)] \\ C &= 1/2 [K(1/2, 1/2) + K(1/2, -1/2)] \end{aligned} \quad (6)$$

where the rate constant $K(m_1, m_2)$ is defined as :

$$K(m_1, m_2) = \langle j_1=3/2, m_1 ; j_2=3/2, m_2 | G | j_1=3/2, m_1 ; j_2=3/2, m_2 \rangle \quad (7)$$

Both in the case of $\text{Na}(3p) + \text{Na}(3p)^4$ and $K(4p) + K(4p)^6$ collisions the Fourier analysis of the signal indicates that the associative ionization reaction is favoured when the two atoms are prepared in Zeeman sublevels with $m_j = +1/2$ or $-1/2$. However, as will be discussed by H. Meijer, the coherence terms should not be neglected.

More information about the collision process can be obtained by varying the polarization of the exciting light : the Fourier analysis of the ion signal, in the most general case, contains also terms in $\cos(3\theta)$. The results are discussed by H. Meijer.

Future work should discuss the validity of the representation of the operators in a subspace restricted to the 6×6 sublevels of the two $3p$ atomic configurations : calculations by Kowalczyk¹⁰ indeed predict a long range ($R=30$ a.u) avoided crossing between the potential curves correlated to $\text{Na}(3p) + \text{Na}(3p)$ and one potential curve correlated to $\text{Na}(3s) + \text{Na}(4d)$.

3. From atomic to molecular point of view : analysis of the measurements in terms of Jones and Dahler' theory.

A simple model for the formation of molecular orbitals from atomic orbitals consists in assuming a sudden decoupling of the spin of the two atomic valence electrons at infinite internuclear distance, the orbital momentum being then coupled to the internuclear axis. The atomic states with $m_j=3/2$ or $-3/2$ will then give π orbitals, while the states with $m_j=1/2$ or $-1/2$ will lead to σ and π orbitals.

$$\begin{aligned} |j\ m_j\rangle &\rightarrow |l\ m_l\ s\ m_s\rangle \\ |3/2\ 3/2\rangle &\rightarrow |1\ 1\ 1/2\ 1/2\rangle \quad (8) \\ |3/2\ 1/2\rangle &\rightarrow \sqrt{2/3} |1\ 0\ 1/2\ 1/2\rangle \\ &\quad + \sqrt{1/3} |1\ 1\ 1/2\ -1/2\rangle \end{aligned}$$

It is then easy to predict which molecular states are formed for an initial preparation of the two atoms in particular Zeeman sublevels. This is done in Table 1, extracted from ref 11.

Table 1. Population of the various molecular states from the atomic states assuming a sudden change of coupling from atomic to molecular Hund's case a.

m ₁	$\frac{3}{2}$	$\frac{1}{2}$	$-\frac{1}{2}$	$-\frac{3}{2}$
m ₂				
$\frac{3}{2}$		$(\frac{1}{3})^3 \Pi_u$	$(\frac{1}{6})^3 \Pi_g$	$(\frac{1}{4})^3 \Sigma_u^+(\pi^2)$
	$3\Delta_u$	$(\frac{1}{3})^3 \Pi_g$	$(\frac{1}{6})^3 \Pi_u$	$(\frac{1}{4})^3 \Sigma_g^-$
			$(\frac{1}{6})^1 \Pi_g$	$(\frac{1}{4})^1 \Sigma_u^-$
		$(\frac{1}{6})^1 \Delta_g$	$(\frac{1}{6})^1 \Pi_u$	
			$(\frac{1}{6})^3 \Sigma_g^-$	$(\frac{1}{4})^1 \Sigma_g^+(\pi^2)$
		$(\frac{1}{6})^3 \Delta_u$	$(\frac{1}{6})^3 \Sigma_u^+(\pi^2)$	
$\frac{1}{2}$			$(\frac{2}{9})^1 \Sigma_g^+(\sigma^2)$	$(\frac{1}{6})^3 \Pi_g$
		$(\frac{4}{9})^3 \Sigma_u^+(\sigma^2)$	$(\frac{2}{9})^3 \Sigma_u^+(\sigma^2)$	$(\frac{1}{6})^3 \Pi_u$
		$(\frac{1}{9})^3 \Delta_u$	$(\frac{2}{9})^3 \Pi_u$	
		$(\frac{1}{9})^1 \Pi_g$	$(\frac{2}{9})^3 \Pi_g$	$(\frac{1}{6})^1 \Pi_g$
		$(\frac{1}{9})^3 \Pi_g$	$(\frac{1}{36})^3 \Sigma_u^+(\pi^2)$	$(\frac{1}{6})^1 \Pi_u$
		$(\frac{1}{9})^1 \Pi_u$	$(\frac{1}{36})^3 \Sigma_g^-(\pi^2)$	$(\frac{1}{6})^3 \Sigma_g^-$
			$(\frac{1}{36})^1 \Sigma_u^-$	$(\frac{1}{6})^3 \Sigma_u^+(\pi^2)$
		$(\frac{1}{9})^3 \Pi_u$	$(\frac{1}{36})^1 \Sigma_g^+(\pi^2)$	
$-\frac{1}{2}$			$(\frac{4}{9})^3 \Sigma_u^+(\sigma^2)$	$(\frac{1}{3})^3 \Pi_u$
			$(\frac{1}{9})^3 \Delta_u$	
			$(\frac{1}{9})^1 \Pi_g$	$(\frac{1}{3})^3 \Pi_g$
			$(\frac{1}{9})^3 \Pi_g$	
			$(\frac{1}{9})^1 \Pi_u$	$(\frac{1}{6})^1 \Delta_g$
			$(\frac{1}{9})^3 \Pi_u$	$(\frac{1}{6})^3 \Delta_u$
$-\frac{3}{2}$				$3\Delta_u$

For some symmetries two states are correlated to Na(3p)+Na(3p), one formed with two σ orbitals and the other with two π orbitals. It appears clearly that the molecular states of $^3\Sigma_u^+$ symmetry constructed with two σ orbitals can be formed only when the two atoms are prepared with a magnetic quantum number $|m_1| = |m_2| = 1/2$.

In the work of Jones and Dahler⁹, the ion signal $R(\theta)$ is determined as a sum from the contributions $R_i(\theta)$ of the various symmetries weighted by the population of each molecular state $li>$. Such populations a_i are easily determined from the matrix density ρ by the transformation described above. The coherence terms are neglected.

$$R(\theta) = \sum_i a_i R_i(\theta) \quad (9)$$

The angular dependance of the various $R_i(\theta)$ is analyzed, the contribution of Δ states being neglected. The conclusion is that the experimental results for the Na(3p) + Na(3p) associative ionization process can be interpreted as due to a dominant contribution of the $^3\Sigma_u^+$ symmetry together with a weaker contribution of the $^1\Sigma_g^+(\pi^2)$, $^3\Pi_u$, $^1\Pi_u$, molecular symmetries.

Future work should also consider the Δ states, which according to the experimental work of Wang et al¹² are contributing to the reaction.

We shall now discuss the determination of the autoionization probability for the various molecular potential curves.

4. Molecular point of view : treatment of the autoionization of the Na₂ molecule

One of the main difficulties in treating the associative ionization problem is the large number of channels that are involved. We know that of the twelve molecular potential curves correlated to the Na(3p) + Na(3p) dissociation limit, ten may contribute to the reaction (1). Such curves are embedded in the Rydberg series converging to the various Na(3s) + Na(nl) limits : the (3s + 5s) and (3s + 4d) limits are respectively 92 meV under and 70 meV above the doubly excited limit. Turning now to the reaction region, the full treatment of the autoionization problem for a given molecular symmetry requires in principle the consideration of an infinite number of states, corresponding to molecular Rydberg series.

We shall see that this complexity can greatly be reduced by use of a multichannel quantum defect (MQDT) approach¹³.

We first compute the potential energy curves of the Na₂ molecule : as the final state of the reaction (1) involves Na₂⁺, it is also necessary to describe the molecular ion. Due to the weak bonding energy of the sodium valence electron compared to the core electrons, a model potential treatment should be satisfactory¹⁴. The Na₂⁺ ion is then treated as an effective one-electron system, and the Na₂ molecule as an effective two-electron system. We treat the core-polarization effects via effective operators¹⁵, the interaction between one electron and one core being represented by a parametric potential fitted to the sodium experimental spectrum¹⁶. Fine structure effects are neglected in this treatment.

In a first step, the Na₂⁺ orbitals χ_p are evaluated accurately by solving the one electron Schrödinger equation

in a space defined by a large basis set of generalized Slater orbitals in prolate spheroidal coordinates¹⁷. The potential curves for the ground and first excited states of the Na_2^+ molecular ion are displayed in Fig. 1.

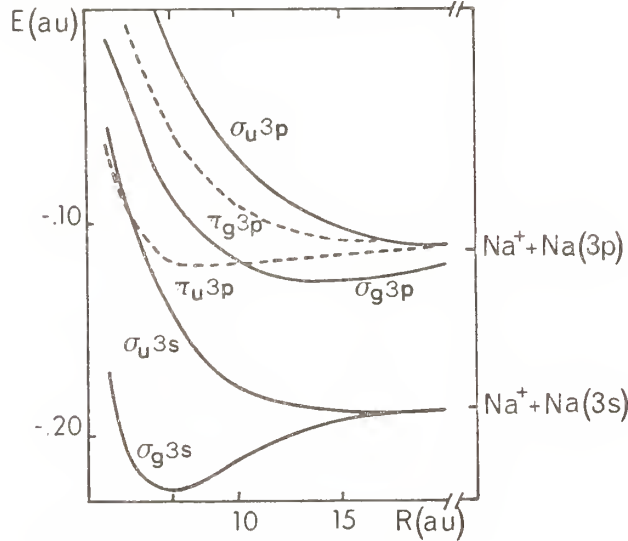


Figure 1. Potential curves for Na_2^+ .

We next solve the Na_2 problem by expanding the two electron wavefunction in antisymmetrized products of two Na_2^+ orbitals χ_p and χ_q :

$$\mathcal{F}(1,2) = \sum_i a_i \left\{ \chi_p^i(1) \chi_q^i(2) \pm \chi_p^i(2) \chi_q^i(1) \right\} \quad (11)$$

We have chosen to perform a numerical evaluation of the two-electron integrals¹⁸. An expansion on 30 configurations for the Σ symmetry, 20 for the π symmetry, is sufficient to obtain, by diagonalization of the full hamiltonian $\mathcal{H}(1,2,R)$, the various adiabatic potential curves of Na_2 ¹⁹ with an accuracy which can be assessed by comparing to spectroscopic data. The conclusion¹⁴ is that the energies are presently determined to within 200 cm^{-1} (24 meV) and the position of the minima to within 0.1 Å. Moreover, an independent check of the calculations is the good agreement obtained with the potential curves computed by Jeung²⁰ up to the $3s + 5s$ dissociation limit using an *ab initio* pseudo-potential treatment with a gaussian orbitals basis set.

As some adiabatic potential curves display many avoided crossings, the Rydberg series being strongly perturbed by a doubly excited state, it appears more convenient to use a *diabatic* representation.

The procedure, first introduced by O'Malley¹⁶ to treat autoionizing atomic states, consists in diagonalizing the two electron hamiltonian $\mathcal{H}(1,2,R)$ by dividing the configuration space, for a given molecular symmetry, into two subspaces:

i) in one subspace, hereafter named \mathcal{P} , we consider configurations such that one electron stays on the bonding $\sigma_g 3s$ Na_2^+ orbital. Partial diagonalization in \mathcal{P} yields

regular Rydberg series converging to the Na_2^+ ground state X. For all the states $|P_i^k\rangle$ of a series k, the ionization energies are obtained by the Rydberg formula:

$$\langle P_i^k | \mathcal{H}(1,2,R) | P_j^k \rangle > -E_X(R) = \delta_{ij} \mathcal{R} / (n_i^k - \mu_k(R))^2 \quad (12)$$

In (12), $E_X(R)$ is the energy of the Na_2^+ ground state, \mathcal{R} is the Rydberg constant, n_i^k an integer number increasing by one unit from the state $|i\rangle$ to the next upper one, and $\mu_k(R)$ is indeed independent of the index i. Such states correspond to a Rydberg electron moving in the field of a ground state Na_2^+ core.

ii) in another subspace, hereafter named \mathcal{Q} , we consider doubly excited configurations, such that both electrons occupy excited Na_2^+ orbitals. Partial diagonalization in \mathcal{Q} yields doubly excited potential curves, corresponding to Rydberg series converging to an excited state of Na_2^+ or more generally to a linear combination of such excited states.

In order to avoid an incorrect dissociation, we have modified the subspace \mathcal{Q} into \mathcal{Q}' by orthogonalization to the lowest state obtained in (i). For most symmetries, this procedure causes a minor modification of the Q_j states. An example of such states is displayed on Fig.2. for the $^3\Sigma_u^+$ symmetry.

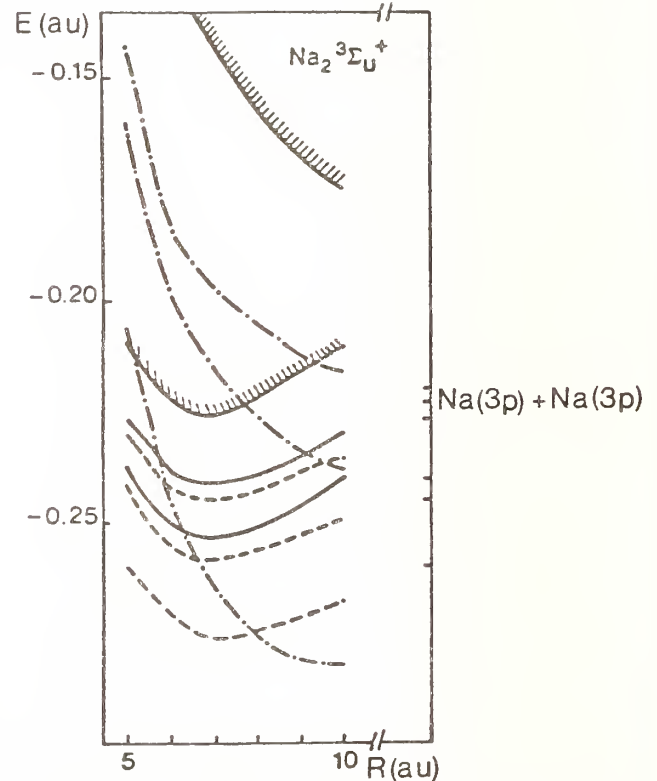


Figure 2. Diabatic potential curves for $\text{Na}_2 \ ^3\Sigma_u^+$. dashed lines, "p" Rydberg series; solid lines "f" Rydberg

series ; dash-dotted line, doubly excited states. The shadowed curves correspond to the ground and first excited states of Na_2^+ .

After this block diagonalization, the electronic hamiltonian $\mathcal{H}(1,2,R)$ has non zero matrix elements between a state of \mathcal{P} and a state of \mathcal{Q} . As the states of \mathcal{P} are grouped in Rydberg series, there exists²² a scaling law for such matrix elements :

$$\langle P_i^k | \mathcal{H}(1,2,R) | Q_j \rangle = (n_i^k - \mu_k(R))^{-3/2} \mathcal{V}_{jk}(R) \quad (13)$$

where the reduced interaction $\mathcal{V}_{jk}(R)$ may be considered as a constant along a Rydberg series. Examples for this scaling law are displayed in table 2. We should note that the scaling law is no longer valid for $R > 10$ a.u when the two atoms begin to part and that the reduced interaction is a slowly varying function of the internuclear distance.

Table 2. Example of a scaling law for the interaction of the second doubly excited state of $3\Sigma_u^+$ symmetry with two levels of a Rydberg series in the mono-excited space \mathcal{P}

$R = 5$	$n_i - \mu_i(R)$	3.90	4.90
	$\mathcal{V}_{jk}(R)$	0.048	0.046
$R = 6$	$n_i - \mu_i(R)$	3.88	4.89
	$\mathcal{V}_{jk}(R)$	0.044	0.042
$R = 7$	$n_i - \mu_i(R)$	3.80	4.81
	$\mathcal{V}_{jk}(R)$	0.049	0.044
$R = 8$	$n_i - \mu_i(R)$	3.78	4.78
	$\mathcal{V}_{jk}(R)$	0.048	0.043
$R = 10$	$n_i - \mu_i(R)$	3.63	4.66
	$\mathcal{V}_{jk}(R)$	0.049	0.037

The associative ionization can therefore be understood as a two electron process, where in the initial state one electron occupies an excited antibonding Na_2^+ orbital, the other electron occupying a Rydberg orbital. The transfer of the inner electron towards the ground state Na_2^+ orbital yields enough energy ($> 2\text{eV}$ at equilibrium) to enable the second electron to escape.

We have considered separately two groups of doubly excited states, hereafter labelled A and B. The group A contains the second doubly excited state of each symmetry which, for internuclear distances $R > 10$ a.u., is mainly described by configurations containing two of the four orbitals correlated to $\text{Na}^+ + \text{Na}(3p)$. The group B contains the first excited state of each symmetry, which for $R > 10$ a.u. is mainly described by a configuration involving the $\sigma_u 3s$ orbital. The corresponding potential curves are displayed on Fig.3 and 4 respectively.

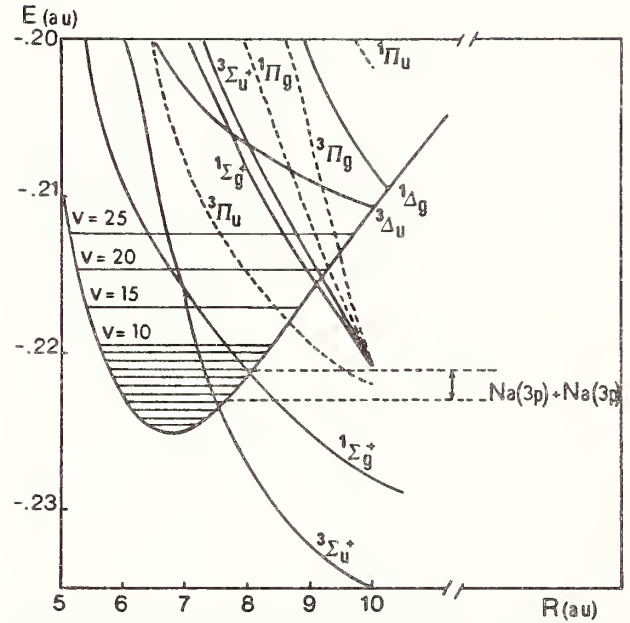


Figure 3 Doubly excited states of Na_2 correlated to the $3p+3p$ dissociation limit.

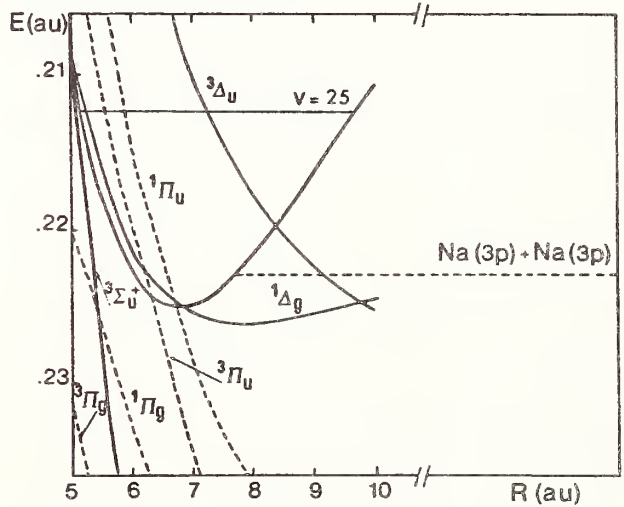
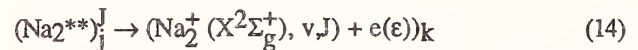


Figure 4. Doubly excited states of Na_2 corresponding for each symmetry to the lowest state in the subspace \mathcal{Q} . They are correlated at infinity to an ionic curve. The $1\Sigma_g^+$ curve is lower and not visible on the figure.

Following Giusti¹³ the autoionization of a molecule can be described in the framework of a MQDT treatment. Let us consider the ionization of the doubly excited state Q_j resulting into a continuum state corresponding to the extrapolation of the Rydberg series k .



We assume that the angular momentum $\hbar\sqrt{J(J+1)}$ of the heavy particle motion is conserved. The corresponding

cross-section may be evaluated, in the weak coupling approximation, by :

$$\sigma_{jk}(E) = \frac{\pi}{2\mu E} r \sum_{J=0}^{J_{\max}} (2J+1) a_{jk}^J(E) \quad (15)$$

In Eq(15), E is the collision energy, r the multiplicity ratio between the final and the initial state, J the partial wave and $a_{jk}^J(E)$ a dimensionless quantity such that :

$$a_{jk}^J(E) = \sum_{v=0}^{v_{\max}} \frac{4 |\xi_{vj}^{jk}|^2}{[1 + \sum_w |\xi_{wj}^{jk}|^2]} \quad (16)$$

$$\xi_{vj}^{jk} = \pi \int \chi_{vJ}(R) \psi_{jk}(R) f_j^j(E, R) dR \quad (17)$$

In (16), the summation is over the vibrational levels of Na_2^+ which may be populated through the reaction (14) at energy E . In (17), χ_{vJ}^J is the vibrational wavefunction in the final state, $\psi_{jk}(R)$ the reduced interaction defined in the Eq(13) and $f_j^j(E, R)$ the radial wavefunction associated to the relative motion of the two atoms interacting with the potential $Q_j(R)$ for given energy E and angular momentum $\hbar\sqrt{J(J+1)}$. As $\psi_{jk}(R)$ is a slowly varying function of R (see table 2) the autoionization process finally depends of quantities which can be estimated as :

$$\xi_{vj}^{jk} = \pi \overline{\psi_{jk}} \int \chi_{vJ}(R) f_j^j(E, R) dR \quad (18)$$

In (18) $\overline{\psi_{jk}}$ is an average value and the integral is merely the *overlap* between the radial wavefunctions describing the nuclear motion in the initial and in the final state.

The autoionization probability is thus controlled both by the strength of the electronic coupling and by the Franck-Condon factor for the initial and final nuclear wavefunctions. Such factors depend markedly upon the relative position of the Na_2^+ ground state potential curve $X(R)$ and of the doubly excited curve $Q_j(R)$. We have reported in Fig.5 the vibrational wave functions χ_{vJ} for various levels of the molecular ion together with continuum functions $f_j^j(E, R)$ computed at 0.07 eV both for crossing and for non crossing potential curves. *Even in the case of a strong electronic coupling*, the autoionization process can hardly take place for any value of the vibrational quantum number v when the two curves are not crossing. It is also negligible for the vibrational numbers $v \leq 3$ when the crossing is located at internuclear distances $R > 8$ a.u.

We may therefore predict a strong selectivity of the autoionization process at low collision energy E in favour of molecular symmetries leading to a doubly excited diabatic curve presenting a crossing with the Na_2^+ ground state potential curve close to the minimum.

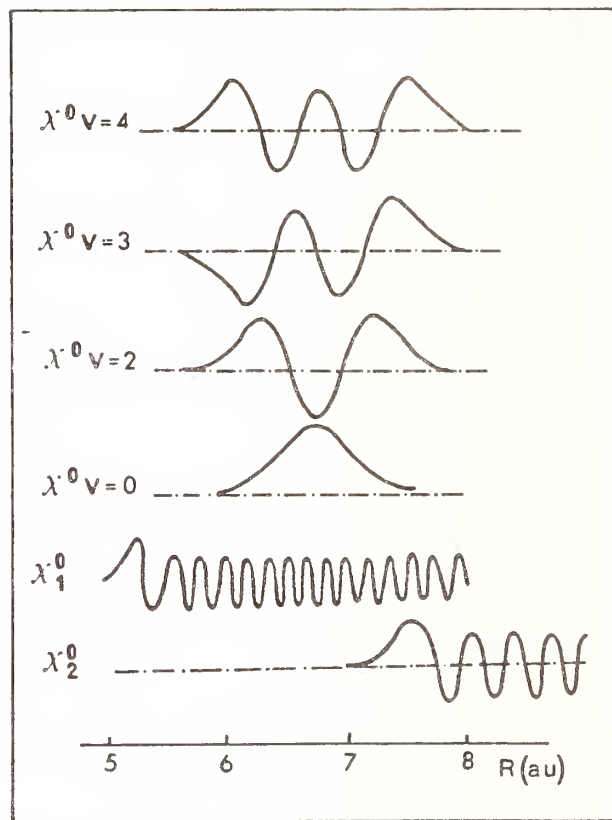


Figure 5. Wavefunctions for the nuclear motion in the final state (vibrational functions χ_v^J computed for $J=0$) and in the initial state in the case of 1) a non crossing curve $Q_j(R)$ 2) the crossing curve Q_A discussed in text.

Considering the group A of states, displayed in Fig.3, we see that one of the two $^3\Sigma_u^+$ curves, hereafter labelled Q_A , crosses the X curve at $R = 7.5$ a.u. A $^1\Sigma_g^+$ curve, hereafter labelled Q_B , is crossing the X curve at $R = 8.1$ a.u. The autoionization via a $^3\Pi_u$ state necessitates a collision energy $E \geq 0.14$ eV. Therefore we may conclude that for $E < 0.14$ eV, autoionization proceeds preferentially via Σ molecular states. For $E < 0.054$ eV, the Q_A $^3\Sigma_u^+$ channel is the only possible one. Such a conclusion is in agreement with the experimental findings^{4,5}, and with the analysis of Jones and Dahler⁹ (see above), provided that we may assume an adiabatic correlation of the Q_A state to a state of the separated atoms with two σ orbitals. The $^3\Sigma_u^+$ states of the group A are constructed mainly with the $(\sigma_g 3p \sigma_u 3p)$ and $(\pi_g 3p \pi_u 3p)$ configurations. There is a crossing at $R = 13$ a.u between the energies of those two configurations, the first one being lower at large distances. The comparison with the experimental results could indicate that this crossing is adiabatic. However, a correct treatment of the population sharing from the states of the separated atoms to the molecular states has to be considered. In the case of the $^1\Sigma_g^+$ curve, the discussion is even more

complicated, as four configurations $(\sigma_g 3p)^2 (\sigma_u 3p)^2 (\pi_g 3p)^2$ and $(\pi_u 3p)^2$ should be considered.

Assuming that in the group A of states only the $^3\Sigma_u^+$ Q_A state can be populated, and that there is a statistical population of the Q_A state of $\frac{3}{12}$ from the $Na(3p) + Na(3p)$

limit, the r factor in (15) being $\frac{4}{3}$, we find a cross section of 12 \AA^2 at 0.03 eV, 18 \AA^2 at 0.05 eV, while the experimental cross section^{1,2} is of the order of 1 \AA^2 . In our calculations J_{\max} is the maximum rotational number for a given value of v and we have considered an arbitrary extrapolation of the Q_A curve to the separated atoms. The presence of a small long-range barrier would change the results.

We also predict a selective population of the levels $v=2$ and $v=3$.

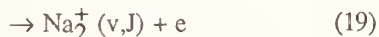
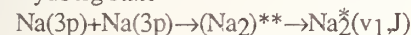
Turning now to the group B of states (see Fig.4) we see that provided they may be populated from the $Na(3p) + Na(3p)$ dissociation limit, the $^1\Delta_g$, $^3\Delta_u$, $^1\Pi_u$ and $^3\Pi_u$ doubly excited states *could also contribute to the ionization process*. For instance the $^1\Delta_g$ state is mainly represented by the $(\pi_g 3p \pi_u 3p)$ configuration at short distances, which has a smaller energy than the $(\sigma_u 3s \delta_g 3d)$ configuration. Although this situation is reversed at large distances, we may note that the states of the group B should be correlated to ionic Na^+-Na^- states, the Na^- ion being excited into Π and Δ states.

A detailed treatment of the correlation between the atomic representation at large R and the diabatic molecular representation at small R is therefore required

5. Discussion

It is thus possible to treat the autoionization of the Na_2 molecule by considering the interaction of dissociative doubly excited states with mono-excited Rydberg series. Several points of this treatment still need to be refined :

- i) the potential curves are required to better accuracy. *Ab initio* calculations by W. Meyer and colleagues in Kaiserslautern offer hope for an improvement in the future.
- ii) the MQDT evaluation of the K matrix should be extended to second order, including the indirect ionization process via vibrational autoionization of a mono-excited Rydberg state



Such work is presently in progress.

Nevertheless, the qualitative conclusion that a $^3\Sigma_u^+$ doubly excited state is mainly responsible for the auto-ionization process is consistent with the Nienhuis' interpretation of the angular dependence of the experimental ion signal showing that, for collision energies $E \approx 0.1-0.3$ eV, the reaction (1) is favoured when both atoms are prepared in a $\frac{3}{2} \frac{1}{2} >$ Zeeman sublevel. It also agrees with

the conclusion of Jones and Dahler⁹ who assume a sudden change of coupling at infinite internuclear distances.

At lower collision energies, the hypothesis of a sudden decoupling of the spin is no longer justified and a *correct treatment of the connection between the atomic state representation in the asymptotic region and the diabatic molecular representation in the autoionization region should be realized in a near future.*

¹Present address : Laboratoire des interactions ioniques et moléculaires. Université d'Aix-Marseille 1 - Centre Saint Jérôme, 13397 MARSEILLE Cedex 13

Acknowledgements.

The authors wish to acknowledge for the stimulating collaboration with A Giusti-Suzor and O.Dulieu and the discussions with N.Andersen, H.A.J. Meijer, R.Morgenstern, J. Weiner and R. Mc Carroll.

References.

1. J. Huennekens and A. Gallagher, Phys.Rev.A **28**, 1276 (1983)
2. R. Bonanno, J. Boulmer and J. Weiner, Phys.A **28**, 604 (1983)
R. Bonanno, J. Boulmer and J. Weiner, Comments At.Mol.Phys. **16**, 109 (1985)
3. P.L. Gould, P.P. Lett, P.S.Julienne, W.P.Phillips, H.R.Thorsheim and J.Weiner, Phys.Rev.Lett. **60**, 788 (1988)
4. J.G. Kircz, R. Morgenstern, and G. Nienhuis, Phys.Rev.Lett. **48**, 610 (1982)
5. M.X. Wang, J. Keller, J. Boulmer and J. Weiner Phys.Rev.A **34**, 4497 (1986)
6. L.Brencher, B.Nawracala and H.Pauly, Z.Phys.D. **10**, 211(1988)
7. G.Nienhuis, Phys.Rev.A **26**, 3137(1982) and XIV ICPEAC invited papers
8. A.Henriet and F.Masnou-Seeuws submitted to Z.Phys.D.(1989)
9. D.M. Jones and J.S Dahler, Phys.Rev.A **35**, 3688 (1987)
10. P. Kowalczyk J.Phys.B. **17** 817 (1984)
11. A.Henriet, thesis, Orsay, unpublished (1988)
12. M.X. Wang, J. Keller, J. Boulmer and J. Weiner Phys.Rev.A **35** 934 (1987)
13. A. Giusti J.Phys.B **13** 3867 (1980)
14. A Dalgarno, Atomic physics, vol.4 (Plenum Press, New York 1975) pp 325-334
15. C Bottcher and A. Dalgarno, Proc. Roy Soc Lond. A **340** 187 (1974)
16. M. Klapisch, Comput.Phys.Commun. **2** 239 (1971)
17. A. Henriet J.Phys.B. **18** 3085 (1985)
18. A. Henriet, C. Le Sech and F. Masnou-Seeuws, Chem.Phys.Lett. **158** 389 (1989)
19. A.Henriet and F. Masnou-Seeuws J.Phys.B. **21** L339 (1988) and J.Phys.B. in press (1989)
20. G.H.J. Jeung Phys.Rev.A **35** 26 (1987)
21. T. O'Malley Adv.At.Mol.Phys. **7** 223 (1971)
22. M.J. Seaton Rep.Prog.Phys. **46** 167 (1983)

Detailed study of polarization effects on the Associative Ionization in Na(3p) - Na(3p) collisions

H.A.J. Meijer

Fachbereich Physik, Universität Kaiserslautern, FRG

1) Introduction

In recent years many groups have investigated associative ionization occurring in (thermal) collisions between two laser excited Na(3p) atoms:



which is one of the possible reactions that occur during such a collision. Fig. 1 shows schematically a few of the molec-

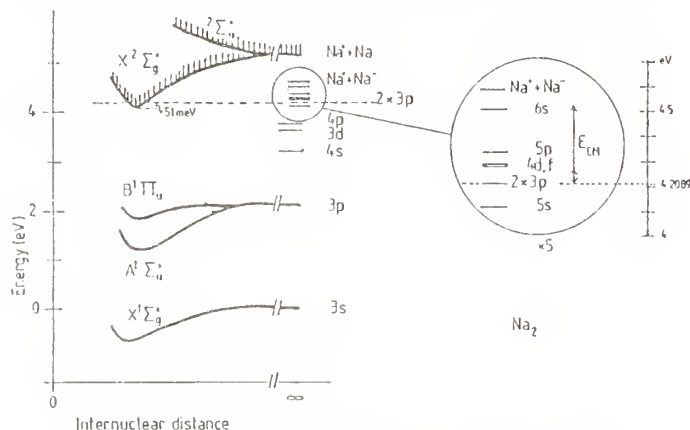


Fig. 1 Some potential curves for Na₂

ular curves of the Na dimer and their dissociation limits. This limit for 3p + 3p lies just above the minimum of the Na₂⁺ potential. Kircz et al. [1] were the first to show that the cross section for (1) depends strongly on the polarization of the collision partners. After this publication, several groups investigated the polarization, as well as the collision velocity dependence [2,3,4]. Aim of this study is twofold:

First, we want to produce many accurate and mutually consistent data on process (1), so that comparison with theory is meaningful.

Second, we want to demonstrate a complete experiment, in the sense that in the given geometry of the experiment the maximum amount of information becomes available. In order to achieve these goals, a highly automatized apparatus has been developed, in which many checks have been incorporated, especially concerning the laser

and atomic polarization, and the laser intensity. To describe the experimental results, we use the theoretical analysis of Nienhuis [5], which formulates the experimental results in terms of atomic states, i.e. as a function of the initially prepared situation. No assumptions are made yet about the transition from atomic to molecular states.

2) Experiment

The experimental setup is shown schematically in fig. 2. Two counterrunning thermal beams of Na are intersected at nearly right angles (87°) by light from a cw dye laser, tuned to the $F_l = 2 - F_u = 3$ hyperfine component of the Na(3²S_{1/2} → 3²P_{3/2}) transition. The laser beam is expanded and directed through a rectangular diaphragm, resulting in a spatially homogeneous laser spot of (hwx) 9 x 5 mm. After it has traversed the Na beams the laser beam is directed into its own path. The rectangular laser spot defines the interaction region, where ions can be formed according to process (1). The total Na density in the interaction region is about 1·10¹⁰ cm⁻³. All ions created in the interaction region are extracted by a weak electric field and are counted by a high current channeltron. The fluorescence light is monitored by five photodiodes at various angles, allowing us to keep track of the atomic density and the atomic polarization (see.

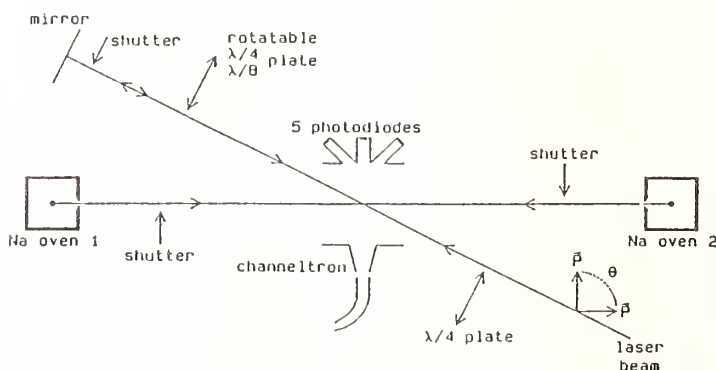


Fig. 2 Schematic overview of the apparatus

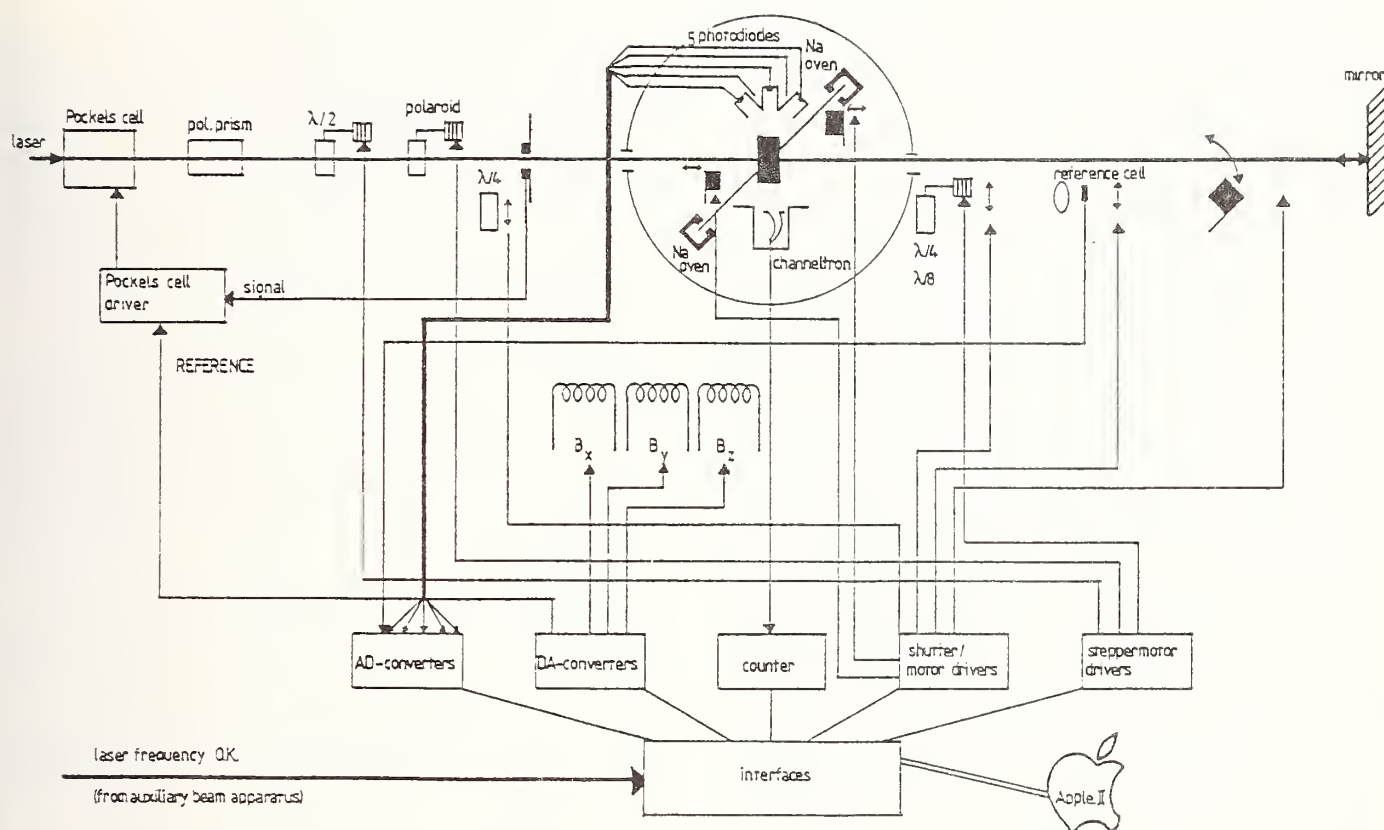


Fig. 3 Overview of the automation of the experiment.

2.2). The laser intensity has been chosen only $8 \pm 2 \text{ mW/cm}^2$, i.e. far from saturation, in order to keep the so-called trapping effect caused by the hyperfine splitting of Na as small as possible. Such a trapping effect would introduce a spurious velocity dependence of the cross section and, even worse, could influence the prepared polarization of the excited atoms significantly [7,8]. The magnetic field in the collision center can be varied between $0 \pm 5 \text{ mG}$ and $\geq 2 \text{ G}$, in arbitrary direction. Normally it is kept 0 mG (i.e. the earth's magnetic field compensated), since magnetic fields influence the atomic polarization. However, we can also deliberately introduce this influence, thereby having to our disposal an additional tool to vary the polarization [7].

We excite atomic beam 2 by the incoming laser, and atomic beam 1 by the reflected one, using the Doppler shift introduced by the crossing angle of 87° . By varying the laser (detuning) frequency we can select the velocity class of atoms excited in both atomic beams, and thus the collision velocity of excited atoms. This

method requires an excellent long-time frequency stabilization, which is performed in a separate apparatus using a third laser [9].

Furthermore, the selective excitation of the atomic beams 2 and 1 by the direct and reflected laser beam, respectively, implies that the polarization of atoms in beam 1 can be made different from the polarization of those in beam 2, simply by changing the laser polarization of the reflected beam. To take full advantage of this possibility we use in the incident laser beam a rotatable $\lambda/2$ plate in combination with a polaroid, to rotate the polarization vector. Also, a $\lambda/4$ plate can be installed, in order to prepare circularly polarized light. For changing the polarization of the reflected beam we use either a rotatable $\lambda/4$ plate or a rotatable $\lambda/8$ plate. Since the laser beam passes these retardation plates twice they act as a $\lambda/2$ and a $\lambda/4$ plate, respectively.

By using the appropriate combination of these retardation plates, we can choose either linear polarization with the polarization vector at arbitrary direction,

or circular polarization with arbitrary helicity, and this independently for the direct and the reflected beam.

The experimental setup is completely automatized. Fig. 3 shows an overview. The photodiodes and the ion counting system are read, and the magnetic fields are set automatically. Furthermore, a "laser okay" signal, coming from the laser stabilization apparatus, is interpreted: measurements are stopped during the time this signal is "not okay". All retardation plates are mounted on computer-driven stepper motors; two of them can be moved in and out of the beam by means of DC-motor driven translators, again computer controlled. Finally, also the shutters for the atomic beams and the reflected laser beam are computer operated. They are needed to separate the ion signal resulting from a collision between atoms from different beams (so-called head-head collisions) from the signals from collisions between atoms within one beam (head-tail collisions). Furthermore, they allow us to measure the fluorescence light (and thus the relative density and the polarization) of the two atomic beams separately, and finally we can correct for the small "cross-over" excitation (i.e. the direct (reflected) laser beam exciting a small amount of the atoms from beam 1 (2)).

Two very crucial points in the experiment need further explanation:

2.1) The laser intensity stabilization

Apart from small, random fluctuations in the laser intensity, which increase only the random noise in the measurements, the rotation of one or more retardation plates in the beam also introduces a systematical angle-dependent variation in

the laser intensity, and thus in the ion signal (which is quadratically dependent on the intensity!). Since we are looking for angle-dependent variation in the ion signal caused by polarization dependence of reaction (1), it is clear that this effect could influence the measurements to a large extent. Therefore we developed a computer operated intensity stabilization system, shown in fig. 4. It is based on a Pockels cell in combination with a polarizer. In order to use this device as a stabilization system, it needs a feedback signal. However, in our system with a direct and a reflected laser beam, and a variable polarization, this signal has to be realized in a complicated way. Two photodiodes on the sides of the slit diaphragm monitor the laser light intensity. Still, their signal is not suited for stabilization since a rotation of the $\lambda/2$ plate varies the intensity in the center of the spot different from that at the sides. Furthermore, variations in the reflected beam would not be accounted for at all.

Our solution is the following: Before the start of a measurement at a certain position of the retardation plates, another photodiode is shifted automatically into the beam, just in front of the mirror. Our computer measures this signal and it adjusts this signal to a certain preselected value (corresponding to the irradiance desired in the experiment), by changing the reference signal for the Pockels cell. The feedback system itself will keep the signal of the photodiodes on the slit equal to that reference signal, thereby compensating for random fluctuations in the laser intensity during a measurement. The photodiode in front of the mirror is shifted out of the beam again, and the measurement itself

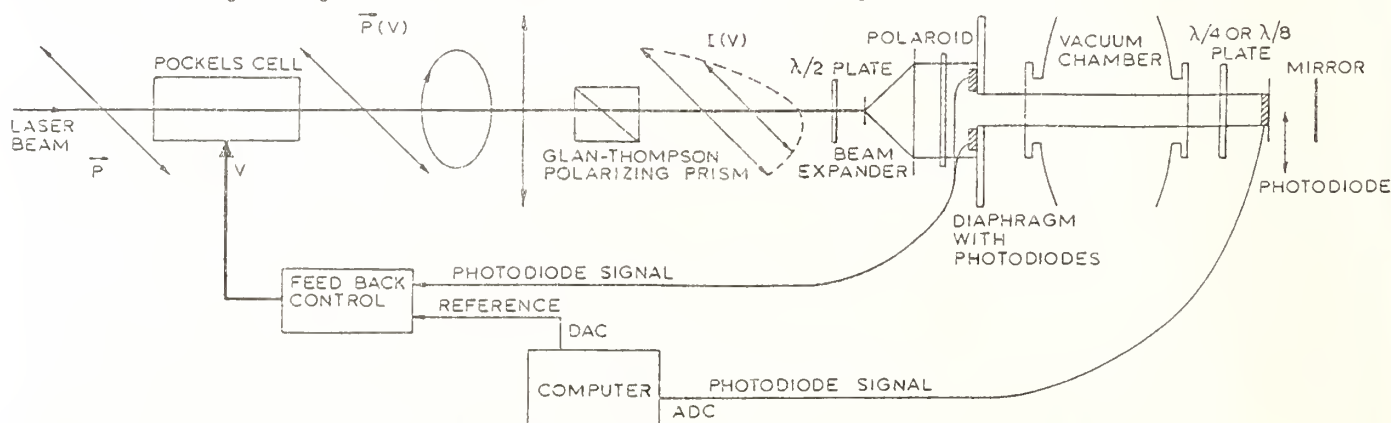


Fig. 4 The laser intensity stabilization system.

starts. After finishing the measurements at that certain position of the retardation plates the photodiode is moved into the beam again and checks the intensity. If the check is satisfactory the retardation plates are rotated to a new position and the procedure starts again.

2.2) Atomic polarization and density of excited atoms

In order to analyze the data we need to know the relative density of atoms. Furthermore we want to check the atomic polarization. In principle, the emitted fluorescence light contains this information:

$$I_f = \eta n_e \frac{(n_{-1}+n_1)(1+\cos^2\phi) + 2n_0\sin^2\phi}{(n_{-1}+n_0+n_1)} \quad (2)$$

with η the overall detection efficiency, n_e the total density of excited atoms, and n_{-1}, n_0 and n_1 the density of atoms in the magnetic sublevels $M = -1, 0, 1$, respectively. Finally, ϕ is the angle between the detector and the polarization direction. Using our five photodiodes, we are able to measure ηn_e , the relative density of excited atoms during one measurement series, as well as the ratio $(n_{-1}+n_1)/n_0$. The latter was compared to the theoretically expected value. In some cases there were significant deviations, which were caused by a bad polarization quality of the reflected laser beam. (In fact the polarization quality of the reflected laser beam can be checked only in this indirect, but very reliable way.) Different measurement series have in principle somewhat different η 's. Therefore, every measurement series must contain several measurements, at which both atoms are excited with linearly polarized light, at an angle $\theta=0^\circ$. Comparison of these measurements learnt that η varied by no more than $\pm 10\%$. After correcting for these variations, the measurement series are now comparable to each other within 5% (for more details see [7,8]).

3) THEORY

The process of associative ionization can be characterized by ionization amplitudes

$f(M_A M_B)$ which depend on the magnetic quantum numbers M_A and M_B of the colliding atoms. Absolute square values of these amplitudes represent cross sections $\sigma(M_A M_B) = |f(M_A M_B)|^2$, and the observed ion rate can be written (in a somewhat simplified form):

$$R = \sum_{M_A M'_A} \sum_{M_B M'_B} f(M_A M_B) f^*(M'_A M'_B) \rho_{M_A M'_A} \rho_{M_B M'_B} \quad (3)$$

where $\rho_{M_A M'_A}$ and $\rho_{M_B M'_B}$ are elements of the density matrix ρ of the excited atoms A and B. We define the detection operator G:

$$\langle M'_A M'_B | G | M_A M_B \rangle = f(M_A M_B) f^*(M'_A M'_B) \quad (4)$$

This G contains all information that can be extracted out of a measurement with this specific geometry. For each basis of M states the diagonal elements of G are connected to cross sections $\sigma(M_A M_B)$, whereas the off-diagonal ones represent coherence terms, connected to ionization amplitude products $f(M_A M_B) f^*(M'_A M'_B)$ for which $M_A \neq M'_A$ or $M_B \neq M'_B$. However, there is no principal difference between this contributions, and they convert into each other if one selects another basis of atomic M-states. We chose our basis such that the z-axis of the coordinate frame is the internuclear axis. This makes our results easier comparable to theoretical potential curves. The elaborate computations following from this choice can be much reduced by expansion of the density matrices and of G in spherical tensors [5,7,8]. The analysis shows that for our geometry there are 8 independent contributions (4 cross sections and 4 coherence terms) to the ion signal if we assume that the influence of the electron spin can be neglected (L-picture). If not (J-picture), this number is doubled (6 cross sections and 10 coherence terms). The maximum amount of independent parameters we can deduce out of our experiments with arbitrary combinations of linearly and circularly polarized light is 7. However, if we use the magnetic field as an additional tool for influencing the atomic polarization, we can increase this

number to 8. The measurement types we have to perform are indicated in fig. 5, together with the expected dependence of the ion signal on the polarization angle θ (linearly polarized light) and/or on the helicity (+/-).

case	Atom 1	Atom 2	θ -dependent terms		
			$\cos 2\theta$	$\cos 4\theta$	$\sin 2\theta$
$R(\theta, \theta)$			+	+	-
$R(\theta, -\theta)$			+	+	-
$R(\theta, 0^\circ)$			+	-	-
$R(\theta, 90^\circ)$			+	-	-
R^{++}			-	-	-
R^{+-}			-	-	-
$R(\theta, +)$			+	-	+

Fig. 5 The various detection schemes.

4) MEASUREMENTS AND RESULTS

We performed all 7 measurement types, each at about 15 different collision velocities. Figs. 6 and 7 show some examples ($R(\theta, \theta)/R(\theta, -\theta)$ and $R(\theta, +)$, respectively). Fitting the results provides us with an overdetermined set of Fourier coefficients for all collision velocities. Via a least squares analysis we can get the results for 7 cross sections and coherence terms, as well as perform a check on internal consistency [7,8]. Together with the results for the magnetic field dependence [6] we end up with all 8 cross sections and coherence terms for the L-picture. However, one cross section is significantly negative, which means that the L-picture is not valid. Therefore we have to present our final results in the J-picture, which we unfor-

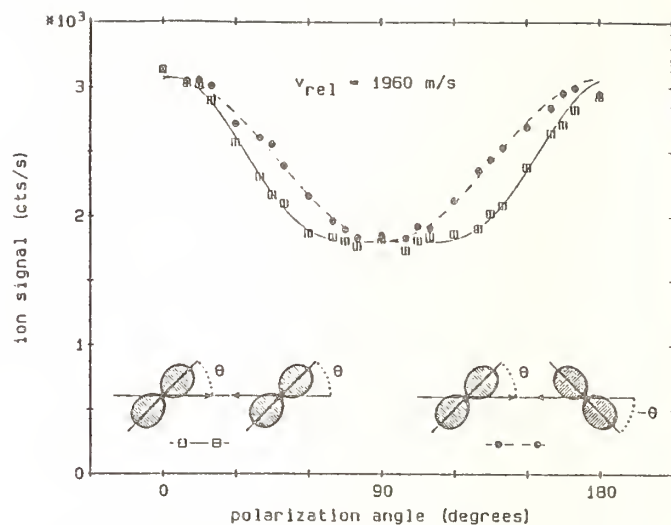


Fig. 6 Example of a measurement with linearly polarized light.

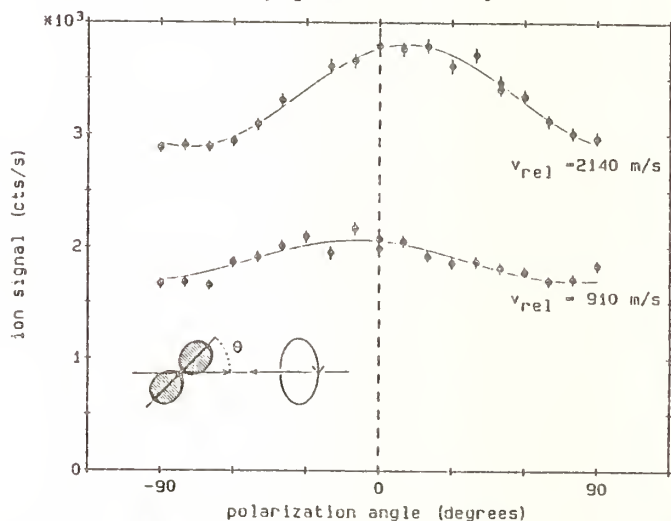


Fig. 7 Measurements with a combination of linearly and circularly polarized light.

tunately could not determine completely. Fig. 8 shows the three (average) cross sections. Furthermore we could determine two coherence terms, both gradually increasing from ≈ 0 arb.un. at 1000 m/s to ≈ 200 arb.un. at 2200 m/s. (For detailed information see [7,8].)

5) CONCLUSIONS

5.1) The associative ionization

Our most important conclusion is that the L-picture description, which has hitherto been used because of its simplicity, definitely is not valid at collision velocities below 2000 m/s. This means that the description of the process must involve the electron spin and/or possibly also other Na nl states.

Comparison with theoretical potential curves is still preliminary, since important work on them is still in progress [10,11]. Also the significance of (the velocity dependence of) some coherence terms is not yet clear.

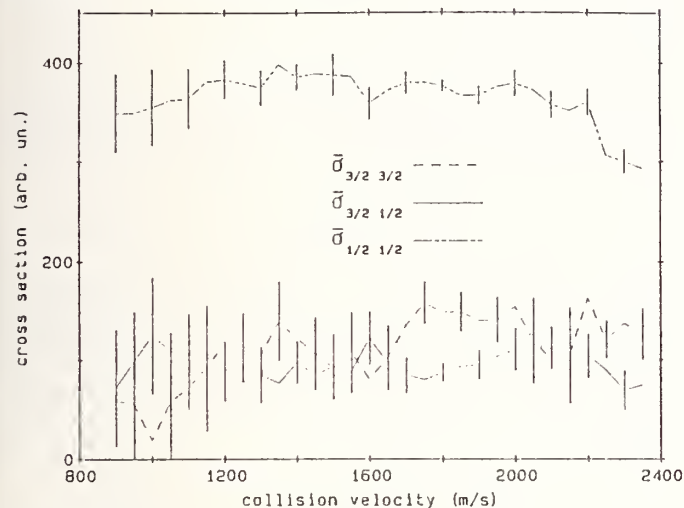


Fig. 8 The final results for the cross sections, with $\bar{\sigma}_{ij} = (\sigma_{ij} + \sigma_{i-j})/2$

So for the time being, our conclusions are restricted to what fig.8 directly shows, namely that the situation in which the major axis of the charge cloud points along the internuclear axis is most favorable for associative ionization in the collision velocity range we investigated.

Our measurements also provide us with data at much lower collision velocities: the "head-tail" signal, taking place at $v = 200$ - 400 m/s. Although in this case we are restricted to measurements at which both atoms are excited with the same laser beam and thus with the same polarization, we might still be able to extract additional information out of these measurements. This will be done in a separate publication [12].

5.2) The detection scheme

We demonstrated a detection scheme for possible complete analysis of detection matrices, which is certainly not restricted to our case study of $\text{Na}(3p) + \text{Na}(3p)$. In fact, the latter system appears not to be the best choice, since in our collision velocity range we must use the J-picture with more parameters than we possibly can determine experimentally.

A better case study would be a $^1P-^1P$ system, e.g. $\text{Ba}(6s6p) + \text{Ba}(6s6p)$.

REFERENCES

- [1] J.G. Kircz, R. Morgenstern and G. Nienhuis, Phys.Rev.Lett. 48 (1982), 610.
- [2] H.A.J. Meijer, H.P. van der Meulen, R. Morgenstern, I.V. Hertel, E. Meyer, H. Schmidt and R. Witte, Phys.Rev. A33 (1986), 1421.
- [3] E.W. Rothe, R. Theyunni, C.P. Reck and C.C. Tung, Phys.Rev. A31 (1985), 1362 and A33 (1986), 1426(E).
- [4] M.-X. Wang, J. Keller, J. Boulmer and J. Weiner, Phys.Rev. A35 (1987), 934; M.-X. Wang, M.S. de Vries and J. Weiner, Phys. Rev. A33 (1986), 765.
- [5] G. Nienhuis, Phys.Rev. A26 (1982), 3137.
- [6] H.A.J. Meijer, Th. Zeegers, T.J.C. Pelgrim, H.G.M. Heideman and R. Morgenstern, J.Chem.Phys. 90 (1989), 729.
- [7] H.A.J. Meijer, T.J.C. Pelgrim, H.G.M. Heideman, R. Morgenstern and N. Andersen, J.Chem.Phys. 90 (1989), 738.
- [8] H.A.J. Meijer, thesis, Utrecht, 1988 (in English, available on request).
- [9] H.A.J. Meijer, H.P. van der Meulen, F. Ditewig, C.J. Wisman and R. Morgenstern, J.Phys.E:Sci.Instrum. 20 (1987), 305.
- [10] A. Henriët, thesis, Orsay, 1988 (in French); A. Henriët and F. Masnou-Seeuws, J.Phys.B 21 (1988), L339; Z.Phys:d (subm.)
- [11] I. Schmidt and W. Meyer, to be published; I. Schmidt, thesis, Kaiserslautern, 1989 (in German).
- [12] H.A.J. Meijer, to be published.

Excitation and Ionization of Atoms — What We Can Learn by Using Polarized Collision Partners

Klaus Bartschat

Department of Physics and Astronomy, Drake University,
Des Moines, Iowa 50311, U.S.A.

1. Introduction

Recent progress in experimental techniques has enabled very detailed testing of theoretical models for atomic collision processes. The preparation of spin polarized projectile beams with narrow energy distribution as well as the construction of sources for polarized target atoms is now a particularly feasible endeavor in several laboratories. Despite this progress, however, the so-called “complete” experiments are still extremely difficult to perform. This is due to the (often) very large number of independent parameters that have to be measured with a high degree of accuracy in order to extract the scattering amplitudes from experimental data; in fact, this requires the solution of the nonlinear system of equations that relates these scattering amplitudes to the individual observables determined in the experiments.

The question therefore arises what information is really contained in a given observable and which parameters should be measured to obtain information about the various effects that determine the outcome of a collision process. A comparison between experimental and theoretical data for these parameters should then allow a profound judgement about the reliability of the individual theoretical approaches.

In the present work, the above questions are addressed as follows. We begin with a brief outline of a general density matrix theory for the scattering of possibly spin polarized projectiles from also polarized targets. In particular, we will concentrate on the systematic derivation of the reduced density matrices which must be used in the description of almost all realistic experiments. Furthermore, some important observables will be introduced, and numerical results for these parameters will be compared with recent experimental data. In detail, we will concentrate on i) the change of an initial projectile polarization through the scattering process, ii) the light emitted in atomic transitions after excitation by polarized electrons, and iii) the ionization of spin polarized target atoms by also polarized projectiles. A more complete treatment of the present topic has been given in ref. [1].

2. General Density Matrix Theory

In studying the scattering of spin- $\frac{1}{2}$ particles with initial linear momentum \mathbf{k}_0 and spin component m_0 (with regard to a given quantization axis) from a target with total angular momentum J_0 and spin component M_0 , we are generally interested in transitions to a final state with momentum \mathbf{k}_1 , spin component m_1 , and a target state with J_1 and M_1 . The

pure initial and final states are denoted by $|J_0 M_0; \mathbf{k}_0 m_0\rangle$ and $|J_1 M_1; \mathbf{k}_1 m_1\rangle$, respectively. The above transition is described by scattering amplitudes

$$f(M_1 m_1; M_0 m_0) \equiv \langle J_1 M_1; \mathbf{k}_1 m_1 | T | J_0 M_0; \mathbf{k}_0 m_0 \rangle \quad (1)$$

where T is the transition operator. In order to keep the notation as simple as possible, we have omitted the arguments \mathbf{k}_0 and \mathbf{k}_1 as well as J_0 and J_1 in the scattering amplitudes.

We can now write the density matrix of the initial state as

$$\rho_{in} = \rho_{in}^p \times \rho_{in}^t = \sum_{m'_0 m_0 M'_0 M_0} \rho_{m'_0 m_0} \rho_{M'_0 M_0} |J_0 M'_0; \mathbf{k}_0 m'_0\rangle \langle J_0 M_0; \mathbf{k}_0 m_0| \quad (2)$$

where the symbol \times denotes the direct product. The elements $\rho_{m'_0 m_0}$ and $\rho_{M'_0 M_0}$ characterize the preparation density matrix of the projectiles (“p”) and the target (“t”), respectively. Note that by using the direct product, we implicitly assume an independent preparation of both systems. This is the normal case in practice, but a formal generalization is straightforward. Following Blum [2], the density matrix elements of the final state are obtained as

$$[\rho_{out}(\theta)]_{m'_1 m_1}^{M'_1 M_1} = \sum_{m'_0 m_0 M'_0 M_0} \rho_{m'_0 m_0} \rho_{M'_0 M_0} f(M'_1 m'_1; M'_0 m'_0) f^*(M_1 m_1; M_0 m_0) \quad (3)$$

where the star denotes the complex conjugate quantity and θ is the scattering angle, i.e., the angle between \mathbf{k}_0 and \mathbf{k}_1 . These density matrix elements contain the total information which can be obtained from the scattering process for a given set of elements $\rho_{m'_0 m_0} \rho_{M'_0 M_0}$ describing the initial state. The two sets are related to each other through the scattering amplitudes, but it should be noted that generally the elements of the outgoing density matrix cannot be factorized in parts describing the target and the projectile separately (see also Blum [2], Chapter 3). In the above formulation, a so-called “complete experiment”, i.e., the determination of all independent scattering amplitudes, is equivalent to the knowledge of all possible density matrix elements of ρ_{out} for all possible initial states described by ρ_{in} . Apart from a few exceptions (see, for example, Berger and Kessler [3]), however, such experiments can hardly be performed in reality.

Before going into more details, we point out the main advantage of the density matrix formalism. It is essentially the possibility to describe *real experimental facts* in a *systematic* way. The initial state in basically every experiment is described by a mixture of pure states, and in the final state not all possible quantum numbers are determined simultaneously. While the first experimental restriction is accounted for through the preparation density matrix in eqns. (2) and (3), respectively, a so-called “reduced” density matrix has to be introduced in the theory to accommodate the second limitation. Some important examples will be discussed in the following.

2.1 Generalized STU-Parameters

We will now specialize eqns. (2) and (3) to the scattering of spin polarized spin- $\frac{1}{2}$ particles from unpolarized targets. In addition, we will assume that only the polarization of the projectiles is measured after the collision process. In this case, the initial density matrix elements of the target are given by $\rho_{M'_0 M_0} = \frac{1}{2J_0+1} \delta_{M'_0 M_0}$, and the reduced spin density matrix elements $\rho_{m'_1 m_1}(\theta)$ of the scattered projectiles are obtained by summing over $M'_1 = M_1$ in eqn. (3). The next step is a detailed analysis of the geometrical and dynamical symmetries contained in these reduced density matrix elements, with the final result shown in fig. 1. If parity conservation is assumed, the above spin density matrix is described by eight independent parameters — the *absolute* differential cross section σ_u and the seven *relative* parameters S_P , S_A , T_x , T_y , T_z , U_{xz} and U_{zx} . In terms of these “generalized STU-parameters”, the projectile spin polarization \mathbf{P}' after the scattering is given by

$$\mathbf{P}' = \frac{(S_P + T_y P_y)\hat{y} + (T_x P_x + U_{zx} P_z)\hat{x} + (T_z P_z - U_{xz} P_x)\hat{z}}{1 + S_A P_y} \quad (4)$$

which is a generalization of eqn. (3.78) of Kessler [4].

The following geometries are particularly suitable for the experimental determination of the individual parameters: to begin with, σ_u and S_P can be measured with *unpolarized* projectiles while a *transverse polarization perpendicular to the scattering plane* ($\mathbf{P} = P_y \hat{y}$) is needed to obtain S_A and T_y . Finally, the measurement of T_x , U_{zx} , T_z and U_{xz} requires a *transversal projectile polarization in the scattering plane* ($\mathbf{P} = P_x \hat{x}$) and also a *longitudinal component* ($\mathbf{P} = P_z \hat{z}$).

Finally, it should be noted that in the presence of explicitly spin dependent forces such as the spin-orbit interaction, a “complete experiment” can only be performed for $J_0 = 0 \rightarrow J_1 = 0$ transitions, if nothing but the projectile polarization is prepared before the collision and measured thereafter. In this special case, the number of independent parameters is reduced to four — sufficient to determine the magnitudes of and the relative phase between the “direct” amplitude f and the “spin-flip” amplitude g [4]. In all cases involving

non-vanishing target angular momenta, however, there are at least six independent complex scattering amplitudes. Hence, the magnitudes and relative phases cannot be determined uniquely in the above arrangement. On the other hand, the neglect of explicitly spin dependent forces (for example, in the approximation of the pure “fine structure effect” [5]) will reduce the number of independent scattering amplitudes and may lead to symmetry relations between the above generalized STU-parameters [1]. The experimental and theoretical test of such relationships can then provide a detailed test about the importance of these spin dependent forces.

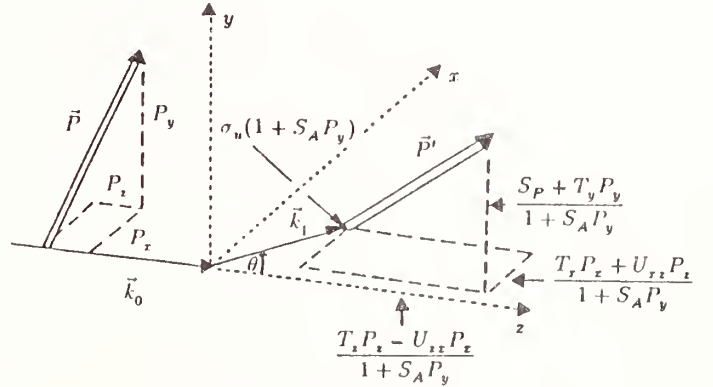


Figure 1: Physical meaning of the generalized STU-parameters: apart from the differential cross section σ_u for the scattering of unpolarized projectiles from unpolarized targets, we show the polarization function S_P , the asymmetry function S_A , the contraction parameters T_x , T_y , T_z and finally the parameters U_{xz} and U_{zx} that determine the rotation of a polarization component in the scattering plane.

2.2 Electron-Photon Coincidences and Integrated Stokes Parameters

Another important case are the electron-photon coincidence experiments, where (up to now) the final projectile polarization has not been observed directly (in some special cases, however, it can be calculated from experimental data through certain linear combinations of scattering amplitudes [6]). Hence, reduced density matrix elements $\rho_{M'_1 M_1}(\theta)$ can be constructed from eqn. (3) by summing incoherently over the unobserved final spins ($m'_1 = m_1$). These matrix elements describe the target state after the collision, but they simultaneously depend on the projectile scattering angle θ . They can therefore be determined either in coincidence experiments or via laser-assisted superelastic scattering processes which provide the equivalent information [7].

However, if the scattered projectiles are not observed at all, we can construct “integrated” reduced density matrix elements $\rho_{M'_1 M_1}$ by integrating over all scattering angles.

In this report, we will concentrate on these elements which can be experimentally determined by measuring the so-called "integrated" Stokes' parameters. The cases of highest practical interest are the following:

- i) Transversely polarized electrons ($\mathbf{P} = P_y \hat{e}_y$) incident along the z-axis and observation of the light in the y-direction defined by the incident electron polarization. In this case, we can observe the following integrated Stokes' parameters:

the degree of linear polarization with respect to the z and x axes

$$\eta_3 = P_1 \equiv \frac{I(0^\circ) - I(90^\circ)}{I(0^\circ) + I(90^\circ)} \quad (5a)$$

where $I(\beta)$ denotes the intensity transmitted by a Nicol prism oriented at an angle β with respect to the z-axis; the linear polarization

$$\eta_1 = P_2 \equiv \frac{I(45^\circ) - I(135^\circ)}{I(45^\circ) + I(135^\circ)} \quad (5b)$$

and the circular light polarization

$$\eta_2 = -P_3 \equiv \frac{I_+ - I_-}{I_+ + I_-} \quad (5c)$$

where I_+ and I_- are the intensities of light transmitted by polarization filters which only admit photons with positive (I_+) and negative (I_-) helicity, respectively. In eqns. (5), the η 's correspond to the notation used, for example, by Blum [2] while the P 's are the light polarizations defined by Born and Wolf [8].

- ii) Longitudinally polarized electrons ($\mathbf{P} = P_z \hat{e}_z$) and observation of the light along the z-direction. For symmetry reasons, only the circular light polarization $\eta_2 = -P_3$ can be different from zero in this case. In our earlier work [9], it has been shown that for $J_0 = 0^{\text{even}} \rightarrow J_1 = 1^{\text{odd}}$ transitions the circular light polarization η_2/P_y is always positive, provided explicitly spin dependent effects can be neglected completely. It was therefore not very surprising to find large deviations from these predictions for electron-mercury scattering [10-12], in particular because of the "intermediate coupling" character of the atomic wavefunctions. A more meaningful statement about the importance of spin dependent effects on the continuum electron can therefore be made for electron-alkali scattering which has been examined experimentally in the Mainz and Münster groups [13-15]. In fact, we have recently shown [16] that in the "LS-approximation" (only spin-flips through exchange processes), the various integrated Stokes' parameters are not independent of each other. This allows not only a *qualitative*, but also a *quantitative* test of the importance of explicitly spin dependent effects, as will be shown below.

2.3 Electron Impact Ionization with Polarized Particles

Our last example considers experiments where polarized atoms are ionized (or excited) by polarized electrons, but only the total ionization (or excitation) cross sections are measured. As before, the preparation density matrix of the collision partners is described by eqn. (2). From eqn. (3), we can then construct a reduced density matrix by summing over $m'_1 = m_1$, integrating over all possible directions of $\hat{\mathbf{k}}_1$ and, for excitation, by also summing over $M'_1 = M_1$. For ionization processes, however, the latter summation has to be split into a sum over $M'_f = M_f$, i.e., the magnetic sublevels of the residual ion, and a second integration over all electron ejection angles.

In explicit numerical calculations, these steps must be performed consecutively. It is, however, possible to make some general statements about the overall structure of the final result. If we denote the cross section for parallel projectile and target polarizations (P_e and P_A) by $Q_{\uparrow\uparrow}$ and for antiparallel polarizations by $Q_{\uparrow\downarrow}$, the cross section can be written as [17]

$$Q_{\uparrow\uparrow} = Q_u - P_e P_A Q_{pol} \quad (6a)$$

$$Q_{\uparrow\downarrow} = Q_u + P_e P_A Q_{pol} \quad (6b)$$

where Q_u is the contribution originating from unpolarized collision partners while Q_{pol} denotes the part depending on the spin polarization. A spin asymmetry can then be defined by

$$A \equiv \frac{1}{P_e P_A} \frac{Q_{\uparrow\downarrow} - Q_{\uparrow\uparrow}}{Q_{\uparrow\downarrow} + Q_{\uparrow\uparrow}} = \frac{Q_{pol}}{Q_u} \quad (7)$$

which allows the determination of the individual contributions to the total cross section.

The usefulness of this parameter in testing theoretical models can be seen as follows. In many numerical treatments, the ionization cross sections are written as [18]

$$Q_u \equiv Q_d + Q_e - \alpha Q_{int} \quad (8)$$

thus containing a direct (Q_d), an exchange (Q_e) and an "interference" contribution (αQ_{int}). It can also be shown [17] that the cross section Q_{pol} introduced in eqns. (6) is identical to the interference cross section αQ_{int} . Various methods have been used to predict the above contributions via numerical calculations. In particular, Younger [18] successfully applied the so-called "maximum interference approximation" with $\alpha \equiv 1$. This approximation *minimizes* the total cross section while it *maximizes* the asymmetry parameter in eqn. (7). Since only the interference contribution appears in the numerator, the above asymmetry is expected to be more sensitive to the exchange part than the total cross section. This is another example of how the use of polarized collision partners can allow a more detailed test of theoretical models.

3. Example Results

3.1 Generalized STU-Parameters for Electron Impact Excitation

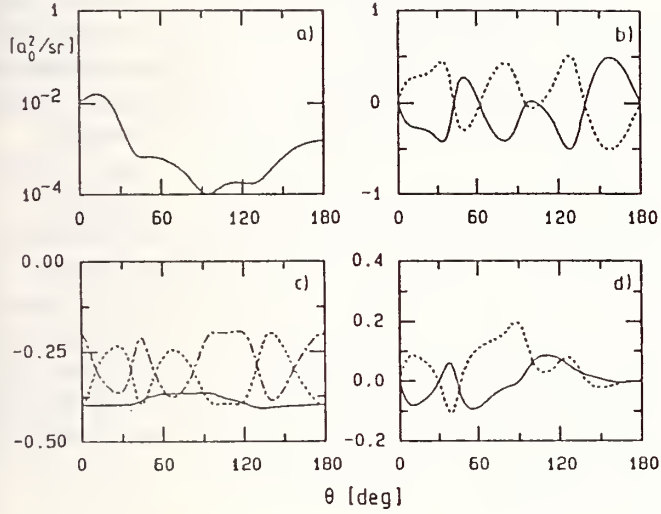


Figure 2: DWBA results [19] for the differential cross section and the generalized STU-parameters for excitation of the $[5p^5 6s]^3P_2^o$ -state in xenon for an incident electron energy of 40 eV. a) absolute differential cross section σ ; b) polarization function S_P (—) and asymmetry function S_A (----); c) contraction functions T_y (—), T_z (----) and T_x (- · - ·); d) rotation functions U_{xz} (—) and U_{zx} (----).

In fig. 2, we present the differential cross section and the generalized STU-parameters for electron impact excitation of the $[5p^5 6s]^3P_2^o$ -state in xenon for an incident energy of 40 eV. There are no experimental data for comparison, but the theoretical curves obtained using the DWBA approach [19] exhibit the following interesting symmetry properties:

$$S_P \simeq -S_A \quad (9a)$$

$$T_y \simeq -0.4 \quad (9b)$$

$$T_x + T_z \simeq -0.6 \quad (9c)$$

$$U_{xz} \simeq -U_{zx} \quad (9d)$$

It is indeed possible to derive these relationships by using the approximations of the pure fine-structure effect where the energy splitting of the multiplet as well as the spin-orbit interaction between the continuum electron and the target nucleus are neglected and spin-dependent effects are only taken into account by an algebraic recoupling procedure [5]. This approximation may be roughly valid for the above case; however, experimental tests of the symmetry predictions as well as the actual theoretical values are highly desirable.

3.2 Integrated Stokes' Parameters for Electron – Alkali Scattering

As mentioned above, it can be shown that in the absence of explicitly spin dependent forces (LS-approximation), the integrated Stokes' parameters introduced in eqns. (5) are not independent of each other [16]. Hence, a *quantitative* test of this approximation can be performed by comparing the predicted correlations either directly with experimental data or by using theoretical results obtained with the inclusion of the above effects. We have tested the predictions of the LS-approximation against the results of the R-matrix (close-coupling) calculation by Scott *et al* [20]. This calculation explicitly included the most important relativistic effect, namely the one-electron spin-orbit term of the Breit-Pauli hamiltonian (Bethe and Salpeter [21]). We can therefore expect at least some disagreement between the predictions of the LS-approximation and the numerical results. The magnitude of these deviations should give an indication about the importance of the spin-orbit interaction on the excitation process.

Table 1

Stokes' parameters for e – Cs scattering

	energy [eV]	"exact"	calculated
$\eta_3^y(\frac{3}{2})[\%]$	1.63	9.044	
$\eta_1^y(\frac{3}{2})/P_y[\%]$	1.63	0.121	
$\eta_2^y(\frac{3}{2})/P_y[\%]$	1.63	17.040	
$\eta_2^y(\frac{1}{2})/P_y[\%]$	1.63	-12.083	
$\eta_2^z(\frac{3}{2})/P_z[\%]$	1.63	14.738	13.288
$\eta_2^z(\frac{1}{2})/P_z[\%]$	1.63	8.120	6.521
$\eta_3^y(\frac{3}{2})[\%]$	2.04	8.049	
$\eta_1^y(\frac{3}{2})/P_y[\%]$	2.04	- 0.122	
$\eta_2^y(\frac{3}{2})/P_y[\%]$	2.04	18.014	
$\eta_2^y(\frac{1}{2})/P_y[\%]$	2.04	-11.985	
$\eta_2^z(\frac{3}{2})/P_z[\%]$	2.04	14.340	14.623
$\eta_2^z(\frac{1}{2})/P_z[\%]$	2.04	6.984	5.123

Table 1 summarises the results obtained for the Stokes' parameters of the light emitted in the transitions $(6p)^2P_{3/2}^o \rightarrow (6s)^2S_{1/2}^e$ and $(6p)^2P_{1/2}^o \rightarrow (6s)^2S_{1/2}^e$ in cesium after excitation by polarized electrons [16]; the superscript in the η 's indicates the direction of observation, and the total angular momentum J_1 of the excited target state is given in brackets. The column labelled "exact" corresponds to the results obtained directly from the K-matrices of the above calculation (also see Nagy *et al* [22]) while the column labelled

"calculated" contains the results for $\eta_2^z(\frac{3}{2})/P_z$ and $\eta_2^z(\frac{1}{2})/P_z$ obtained by determining the necessary three independent variables from the other Stokes' parameters and using them to calculate these light polarizations. It can be seen that the deviations between the "exact" and the "calculated" values are quite significant in some cases (up to almost 30%). This is most likely due to the very complicated resonance structure in the above near-threshold energy region. In any case, these numbers illustrate that the widely used conceptions of "singlet" and "triplet" or "direct" and "exchange" scattering are only valid to a limited extent for this collision system.

3.3 Ionization Asymmetries

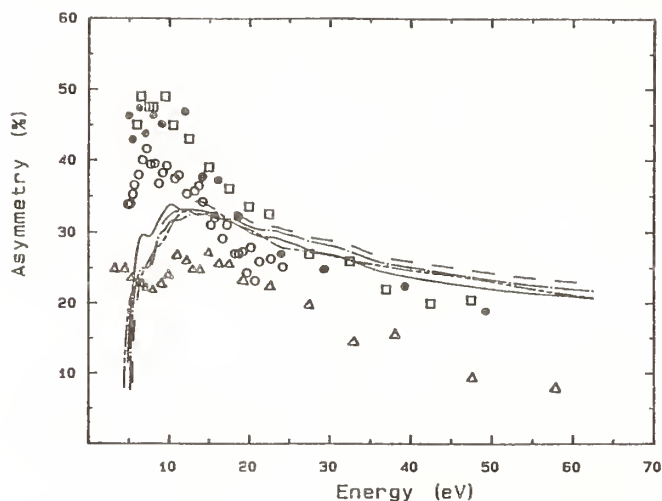


Figure 3: Spin asymmetry A for electron impact ionization as a function of the incident electron energy. The theoretical results were obtained in a DWBA approach combined with the "maximum interference approximation" [23]. The individual curves for the initial states $[1s2s]^3S^e$ of helium (—), $[1s2s]^2S^e$ of lithium (— — —), $[2p^63s]^2S^e$ of sodium (— · —) and $[3p^64s]^2S^e$ of potassium (— - -) are compared with the experimental data of the Bielefeld group (\square , lithium [24]; \bullet , sodium [24]; Δ , potassium [24]; \circ , helium [25]).

In fig. 3, we show results for the ionization asymmetry A defined in eqn. (7) for the ground states of the alkali atoms lithium, sodium and potassium as well as for the excited $[1s2s^3S^e]$ state of helium. The theoretical values were obtained using the DWBA-method in connection with the "maximum interference approximation" [23]. While the agreement with the experimental data of the Bielefeld group [24,25] is quite satisfactory at higher collision energies, there are significant discrepancies between theory and experiment near the ionization threshold. Since the theoretical values lie *below* the experimental data in this region, this result indicates a fundamental problem with the DWBA-approach (recall that the "maximum interference approximation" already maximizes the theoretical asymmetry in this

calculation). Hence, the more detailed experiment involving polarized collision partners revealed again some defects in a theoretical approach which is rather successful in the description of the total cross section for unpolarized particles.

Finally, we note that the theoretical results look very similar for all four targets investigated in this study while the experimental data for potassium differ significantly from those for the other systems. Some possible explanations for this feature have been proposed, however, more work is required before a definite conclusion can be drawn.

4. Summary

In this report, we have shown how polarized collision partners can be used for detailed testing of theoretical models. A quantitative test for the importance of explicitly spin dependent forces has been proposed. Finally, it was shown that the "maximum interference approximation" which has been used very successfully to predict total ionization cross sections, exhibits significant defects when applied to the calculation of spin dependent ionization asymmetries.

Acknowledgments

I would like to thank Professors G. Baum, K. Blum, M. Fink, G.F. Hanne, J. Kessler, W. Raith and H. Steidl for stimulating discussions on various topics. Financial support from the Deutsche Forschungsgemeinschaft in Sonderforschungsbereich 216, the NATO under grant #86/353 and the Research Corporation under grant #C-2640 is gratefully acknowledged.

References

- [1] K. Bartschat, Physics Reports (1989), in press
- [2] K. Blum: **Density Matrix Theory and Applications** (Plenum, New York 1981)
- [3] O. Berger and J. Kessler, J. Phys. B **19** (1986), 3539
- [4] J. Kessler: **Polarized Electrons**, 2nd edition (Springer, Berlin 1985)
- [5] G.F. Hanne, Phys. Rep. **95** (1983), 95
- [6] J. Goeke, G.F. Hanne and J. Kessler, Phys. Rev. Lett. **61** (1988), 58
- [7] I.V. Hertel, M.H. Kelley and J.J. McClelland, Z. Phys. D **6** (1987), 163
- [8] Born and Wolf: **Principles of Optics**, 4th edition (Pergamon, New York 1970)
- [9] K. Bartschat and K. Blum, Z. Phys. A **304** (1982), 85
- [10] A. Wolcke, K. Bartschat, K. Blum, G.F. Hanne and J. Kessler, J. Phys. B **16** (1983), 639
- [11] K. Bartschat, N.S. Scott, K. Blum and P.G. Burke, J. Phys. B **17** (1984), 269
- [12] K. Bartschat and P.G. Burke, J. Phys. B **19** (1986), 1231
- [13] N. Ludwig, A. Bauch, P. Nass, E. Reichert and W. Welker (1986), Z. Phys. D **4**, 177

- [14] P. Nass, M. Eller, N. Ludwig, E. Reichert and M. Weber-sinke (1989), Z. Phys. D **11**, 71
- [15] F. Eschen, G.F. Hanne, K. Jost and J. Kessler (1989), J. Phys. B **22** (1989), in press
- [16] K. Bartschat, J. Phys. B **22** (1989), in press
- [17] G. Baum, E. Kisker, W. Raith, W. Schröder, U. Sillmen and D. Zenses, J. Phys. B **14** (1981), 4377
- [18] S.M. Younger, Phys. Rev. A **22** (1980), 111
- [19] K. Bartschat and D.H. Madison, J. Phys. B **21** (1988), 2621
- [20] N.S. Scott, K. Bartschat, P.G. Burke, O. Nagy and W.B. Eissner, J. Phys. B **17** (1984), 3775
- [21] H.A. Bethe and E.E. Salpeter: **Quantum Mechanics of One- and Two-Electron Atoms** (Springer, Berlin 1957)
- [22] O. Nagy, K. Bartschat, K. Blum, P.G. Burke and N.S. Scott, J. Phys. B **17** (1984), L527
- [23] K. Bartschat, J. Phys. B **22** (1989), submitted
- [24] G. Baum, M. Moede, W. Raith and W. Schröder, J. Phys. B **18** (1985), 531
- [25] J. Taborski, G. Baum, M. Fink, W. Raith and H. Steidl in: **Verhandlungen der Deutschen Physikalischen Gesellschaft** (Spring-Meeting Bonn 1988)

ALIGNMENT AND ORIENTATION IN SIMPLY-STRUCTURED ATOMIC COLLISION COMPLEXES

Rainer Hippler

Fakultät für Physik, Universität Bielefeld, D-4800 Bielefeld 1, Fed. Rep. Germany

Electronic processes in simply-structured atomic collision complexes are of fundamental importance for our understanding of collision dynamics and also of practical relevance for a variety of experimental fields including fusion technology and astrophysics. In continuation of our previous work¹⁻² we are currently investigating alignment and orientation in such collision systems. We concentrate our investigations on the excitation of atomic hydrogen to the H(2p) state either by direct or by charge changing processes. The quantities of interest here are the so-called alignment A_{20} and the orientation O_1 .³ The alignment A_{20} provides detailed information about the relative population of the H(2p_m) magnetic substates; it is defined as⁴

$$A_{20} = \frac{\sigma_1 - \sigma_0}{\sigma(2p)} \quad (1)$$

where σ_0 and σ_1 ($=\sigma_{-1}$) are the total cross sections for excitation into the H(2p₀) and H(2p₁) magnetic substates, respectively, and $\sigma(2p) = \sigma_0 + 2\sigma_1$. Experimentally, A_{20} is obtained from a measurement of the linear polarization P_1 of Lyman- α radiation emitted during the decay of the excited H(2p) state to the H(1s) ground state. Here we define the degree of linear polarization P_1 as

$$P_1 = \frac{I_{\parallel} - I_{\perp}}{I_{\parallel} + I_{\perp}} \quad (2)$$

and where I_{\parallel} and I_{\perp} are the intensities of Lyman- α radiation with electric vector parallel and perpendicular, respectively, to the incident projectile direction (z-direction). The orientation O_1 is a measure of the transferred angular momentum $\langle L_y \rangle$ in a direction perpendicular to the scattering plane,

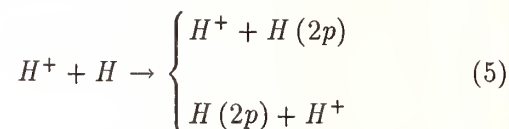
$$O_1 = -\frac{1}{2} \langle L_y \rangle, \quad (3)$$

and where the scattering plane (x-z plane) is defined by the directions of the incident and scattered projectile. The transferred angular momentum in a given direction is directly related to the circular polarisation P_3 ,

$$P_3 = \frac{I(-) - I(+)}{I(-) + I(+)} \quad (4)$$

in the same direction. $I(-)$ and $I(+)$ denote the intensity of circularly polarized light with negative and positive helicity, respectively.

For the simplest one-electron system, H(2p) excitation in



collisions is predicted to proceed at low incident velocities v through a united-atom 2p σ -2p π rotational coupling in the transiently formed quasi-molecule (Fig. 1). This should lead to population of the H(2p_{±1}) magnetic substates only.

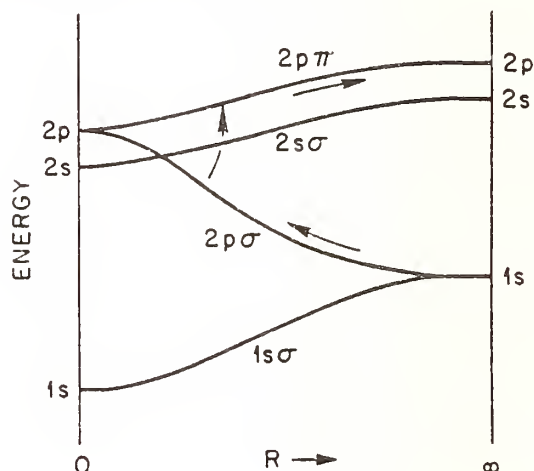
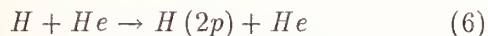


Fig. 1: Schematic energy-level diagram for H⁺-H. The binding energy of an electron moving in the field of two approaching protons is shown as a function of the internuclear separation R . For clarity, the l -degeneracy has been removed.

As is indicated in Fig. 2, the measured integral alignment⁵ is rather large at small projectile energies and close to the maximum value of + 50% permitted by Eq. (1). These measurements are thus in good agreement with theoretical calculations which properly account for this rotational coupling mechanism.⁶⁻¹⁰ Other calculations, for example

coupled-state calculations employing separated-atom electronic wavefunctions only,¹¹⁻¹³ are at lower velocities at variance with our experimental results.

A different picture emerges for the quasi-one electron system



which was investigated in an incident energy range 1-25 keV. Fig. 3 displays the measured integral alignment for this collisions system, which differs significantly from our results for $H^+ - H$ collisions. Again, as becomes obvious from a corresponding correlation diagram,¹⁷ a united-atom $2p\sigma-2p\pi$ rotational coupling provides an important mechanism for $H(2p)$ excitation in $H-He$ collisions at low incident velocities. In addition, radial couplings occur among the $2p\sigma$ and the $2s\sigma$ and $3d\sigma$ orbitals, resulting in a negative A_{20} for small incident velocities. Differential measurements show that the radial couplings are most pronounced for small impact parameters, whereas the $2p\sigma-2p\pi$ rotational coupling dominates at larger impact parameters (Fig. 4).

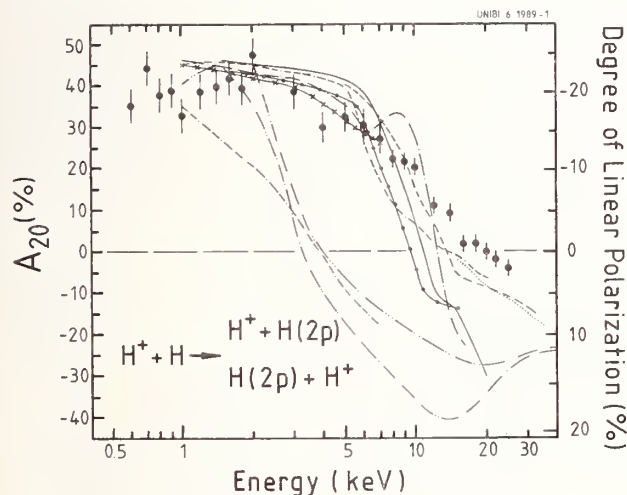


Fig. 2: Integral alignment A_{20} (left-hand scale) and degree of linear polarization P_1 (right-hand scale) for $H(2p)$ production in (\bullet) $H^+ - H$ collisions versus incident energy.⁵ Also shown are the predictions of various theoretical calculations (see text).

Towards larger velocities the integral alignment becomes positive. This result is an indication of a direct $1s-2p$ excitation process which at medium velocities favours the $H(2p_{\pm 1})$ magnetic substates; it is, however, only in qualitative agreement with optical potential calculations of Ast et al.¹⁴ and

with model calculations according to Andersen and Nielsen.¹⁵

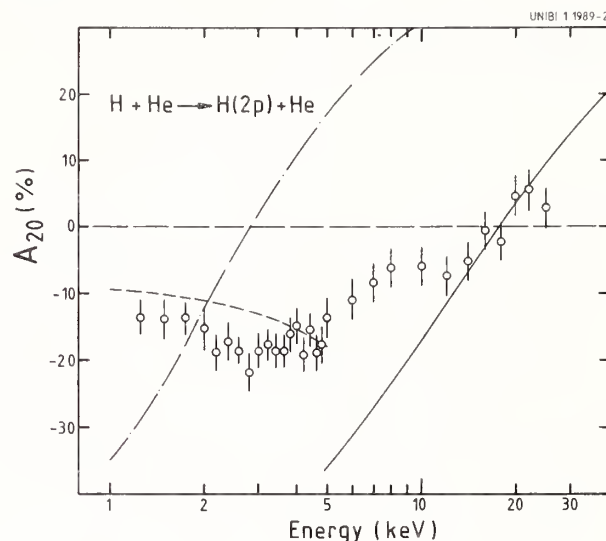


Fig. 3: Integral alignment A_{20} for $H(2p)$ production in (o) $H-He$ collisions versus incident energy.¹⁶ Also shown are theoretical calculations of Kimura and Lane¹⁷ (dashed line), optical potential calculations of Ast et al.¹⁴ (dash-dotted line), and model calculations according to Andersen and Nielsen¹⁵ (solid line).

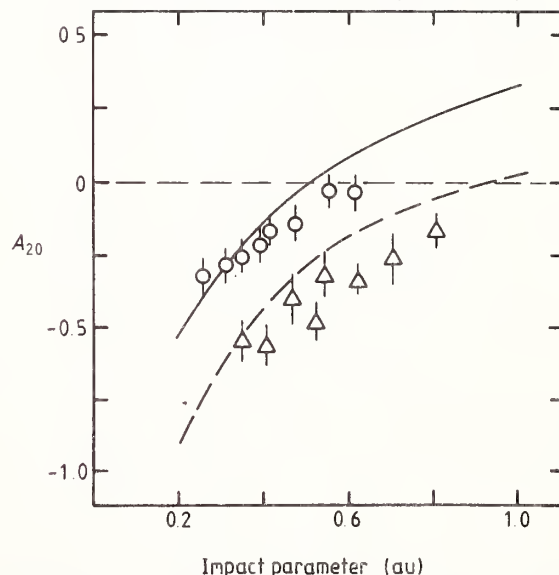


Fig. 4: Differential alignment A_{20} versus impact parameter b for $D(2p)$ production in (Δ) 2 keV and (o) 3 keV $D-He$ collisions. Also shown are corresponding calculations of Kimura and Lane¹⁷ (dashed line, solid line).

The measured orientation was only weakly depending on the impact parameter. It was observed, however, to display a rather pronounced energy dependence (Fig. 5). This behaviour is explained by the development of the adiabatic phase

$$\chi_i = -\frac{i}{\hbar v} \int E_i(R) dR, \quad (7)$$

which is different for χ_1 and χ_0 due to the different binding energies $E_i(R)$ of the quasi-molecular states along which the complex excitation amplitudes f_1 and f_0 evolve.² As the collision velocity v increases, the phase difference $\chi_1 - \chi_0$ decreases with increasing projectile energy; since the orientation is proportional to $\sin(\chi_1 - \chi_0)$ a pronounced velocity and, hence, energy dependence of $\langle L_y \rangle$ is observed.

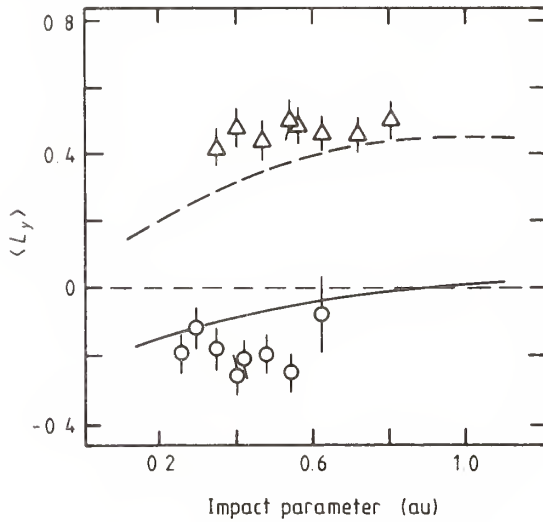
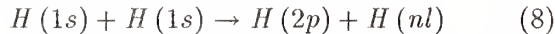


Fig. 5: Transferred angular momentum $\langle L_y \rangle$ versus impact parameter b for (Δ) 2 keV and (\circ) 3 keV D-He collisions. Dashed and solid curves are corresponding calculations of Kimura and Lane.¹⁷

The experimental results for the neutral



collision system (Fig. 6) indicate that $H(2p_0)$ and $H(2p_{\pm 1})$ states are populated with about equal probability below $E < 10$ keV. This results is at variance with recent theoretical calculations,¹⁸ where the electron wavefunction has been expanded in travelling atomic orbitals on both centers. Molecular orbitals are not included in these calculations and, hence, the above mentioned $2p\sigma$ - $2p\pi$ united

atom rotational coupling mechanism is not properly accounted for. In fact, when comparing these calculations for H-H with previous atomic orbital calculations for H^+-H collisions (e.g., Fig. 2), we note that even on a quantitative basis they predict a rather similar energy dependence of A_{20} . This points to the necessity of including united-atom wavefunctions in the calculations. The inclusion of united-atom couplings is more complicated in H-H collisions, however, where above $E > 1$ keV both the ionization and the charge exchange ($H + H \rightarrow H^+ + H^-$) channel become comparable or even larger than the $H(2p)$ excitation channel.¹⁹⁻²⁰ Recent calculations of Borondo et al.²¹ have shown that population of $H(2s)$ and $H(2p)$ states in H-H collisions is in fact influenced by a long-range radial coupling with the $\rightarrow H^+ + H^-$ charge exchange exit channel.

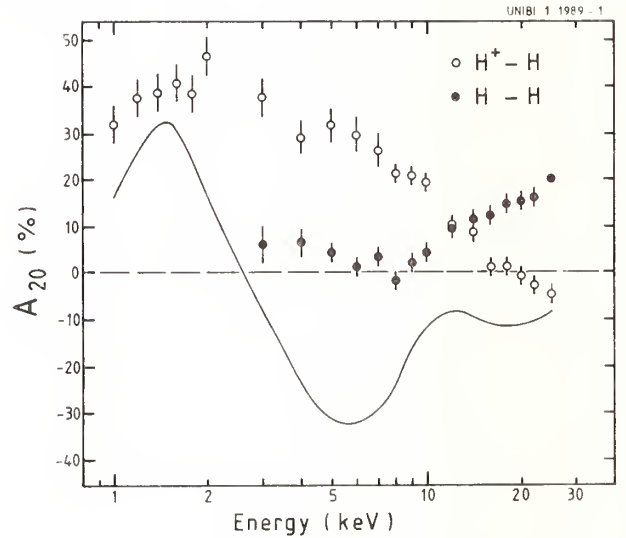
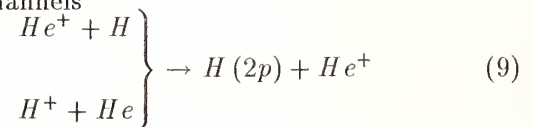


Fig. 6: Integral alignment A_{20} for $H(2p)$ production in (\circ) H^+-H and (\bullet) $H-H$ collisions versus incident energy. Also shown are theoretical calculations of Singal et al.¹⁸ for $H-H$ (solid line) collisions.

Two-electron systems, for example H-H or $(H-He)^+$, are of considerable interest as they allow an investigation of spin and, hence, of electron-electron interaction effects during the collision. For the $(H-He)^+$ system we have investigated the following two reaction channels



for which, in an independent-electron picture and at low velocities, we could expect the same A_{20} . As is

illustrated in Fig. 7, excitation to the H(2p) state in $\text{He}^+\text{-H}$ collisions occurs dominantly at small internuclear separations via couplings of the $2p\sigma$ MO with other near-degenerate MOs (for example, $2p\pi$ or $2s\sigma$). In $\text{H}^+\text{-He}$ collisions, on the other hand, H(2p) excitation is thought to arise from a two-step mechanism. In a first step a long-range radial coupling populates the charge exchange channel $\text{He}^+\text{-H}$; then the second step, as before, involves couplings of the $2p\sigma$ MO with other high-lying MOs leading to H(2p) excitation. Thus, although the two incident channels are different they appear to proceed along the same intermediate states and through the same couplings; in a one-electron picture, these states and couplings are identical for $\text{H}^+\text{-He}$ and $\text{He}^+\text{-H}$ collisions. If this picture were correct, the similarity of $\text{H}^+\text{-He}$ and $\text{He}^+\text{-H}$ would be reflected in certain characteristic signatures of the collision. For example, the alignment depends sensitively on the contributions of σ and π states to the excitation process. In a one-electron picture there is little reason why the two collision systems would produce a different alignment. In a two-electron picture, on the other hand, the different spin channels have to be considered: In $\text{H}^+\text{-He}$ collisions there exists only one (singlet) spin channel, whereas in $\text{He}^+\text{-H}$ collisions both singlet and triplet channels can contribute. Therefore, we expect a different behaviour of the two different incident channels of the $(\text{H-He})^+$ collision complex, and in turn a different alignment for $\text{H}^+\text{-He}$ and $\text{He}^+\text{-H}$.

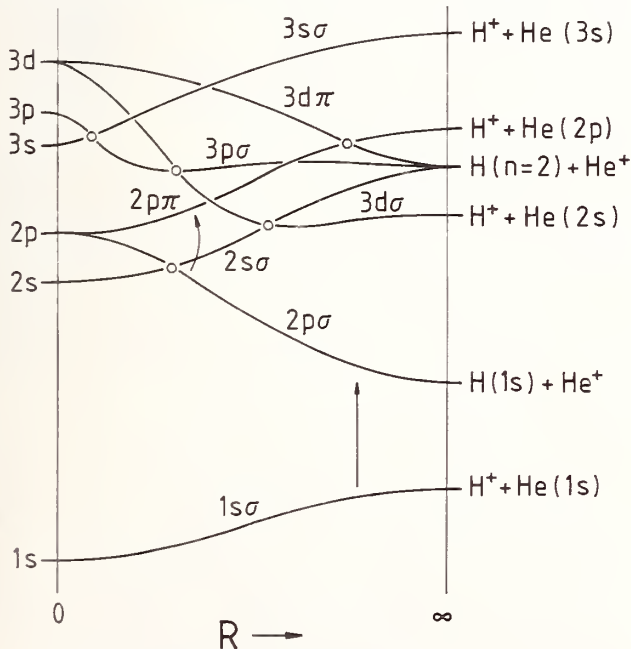


Fig. 7: Schematic (*diabatic*) energy level diagram for $(\text{H-He})^+$ collisions (singlet case).

As we have expected, a marked difference between the two different incident channels of the $(\text{H-He})^+$ collision complex is observed.²²⁻²⁴

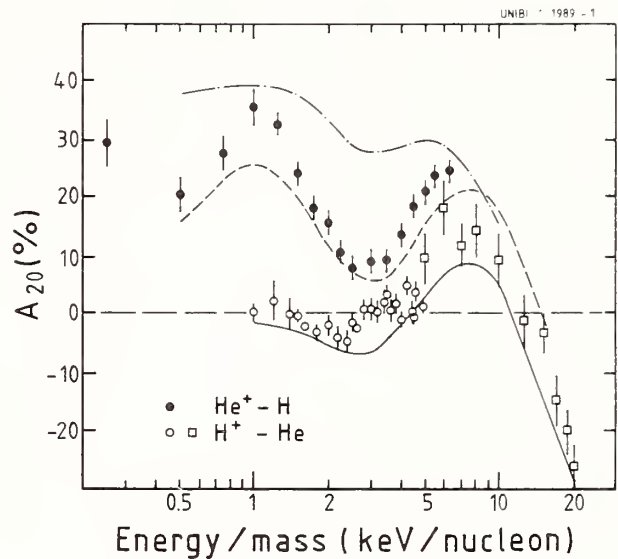


Fig. 8: Integral alignment A_{20} for H(2p) production in $\text{H}^+\text{-He}$ and $\text{He}^+\text{-H}$ collisions versus incident energy divided by the projectile mass. Experimental results for $\text{He}^+\text{-H}$ collisions (\bullet , Ref. 24) and for $\text{H}^+\text{-He}$ collisions (\circ , Ref. 22; \square , Ref. 23) are compared with corresponding theoretical calculations (dashed and solid lines, Ref. 24) and with recent calculations for $\text{He}^+\text{-H}$ by Errera et al.²⁵ (dash-dotted line).

In the following we shall discuss the origin of this difference in more detail. This is facilitated by the fact that the $(\text{H-He})^+$ collision complex has been studied quite thoroughly. In particular, recent differential measurements¹ have demonstrated that for incident $\text{H}^+\text{-He}$ collisions the $2p\sigma\text{-}2p\pi$ rotational coupling dominates at impact parameters $b \approx 1$ a.u.; this excitation mechanism populates the $\text{H}(2p_{\pm 1})$ magnetic substates (Fig. 9). At smaller b a double-rotational coupling $2p\sigma - 2p\pi - 2s\sigma$ leads to $\text{H}(2p_0)$ excitation.²⁶ This $2s\sigma$ state population is produced by the radial coupling among the $2s\sigma$ and $2p\sigma$ states around $R \approx 0.4$ a.u.. At low incident energies of a few keV, the integral populations caused by these two couplings are roughly equal; as a consequence, the integral alignment A_{20} is approximately zero. This does not hold for the reverse system $\text{He}^+\text{-H}$, where we observe a significantly larger (positive)

alignment. It indicates that the above double-rotational coupling mechanism is now of a lesser importance. This experimental result is confirmed by theoretical calculations, in which the molecular states for both singlet and triplet manifolds were obtained by the full configuration interaction method.²⁴ The most notable difference is that, for the triplet manifold, the separate atom level $H^+ + He(2^3P)$ lies lower than the $H(n=2) + He^+$ levels, while the situation is just the opposite for the singlet manifold. In the singlet case, $H(2p_{\pm 1})$ population is produced by a $2p\sigma-2p\pi$ rotational coupling, whereas $H(2p_0)$ excitation is produced by the $2p\sigma-2p\pi-2s\sigma$ coupling. At low energies, these contributions produce σ and π states with comparable strength, and the integral alignment in H^+-He collisions (pure singlet case) is small. The same couplings also operate in the triplet manifold; however, the important difference is that here they do *not* lead to excitation of the $H(2p)$ states. This is because for the triplet channel the $2p\sigma$ state, for example, does no longer correlate with the $He^+ + H(n=2)$ outgoing channel. This leads to the results that $H(2p)$ excitation in He^+-H collisions at low incident energies is dominated by a rotational coupling mechanism leading to population of outgoing π -states. It has the consequence that predominantly the $H(2p_{\pm 1})$ magnetic substates become populated, which is reflected in the positive alignment.

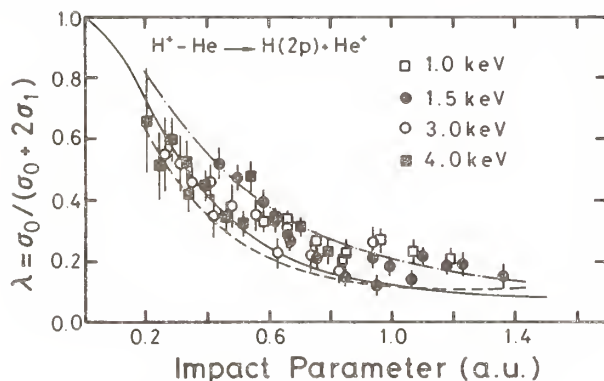


Fig. 9: Relative population of $H(2p_0)$ versus impact parameter b in H^+-He collisions at incident energies of 1–4 keV. Solid line is a theoretical calculations of Macek and Wang,²⁶ the other two curves are from Fritsch²⁷

As the incident energy increases, direct (impulsive) excitation to $H(2p)$ through $\sigma-\sigma$ couplings becomes important resulting in preferred $H(2p_0)$ population in both collision systems. This causes

the sign change of A_{20} at $\approx 15 \text{ keV/nucleon}$. Above 10 keV/nucleon the theoretical curves for H^+-He and He^+-H collisions appear to approach each other; this behaviour is not unexpected since the spin effects discussed here should be of minor importance at large collision energies.

Polarization studies in ion-molecule collisions have been performed as well. For example, the degree of linear polarization in H^+-H_2 collisions was found to be rather large ($P \approx -12\%$) around incident energies of 1–2 keV (Fig. 10).

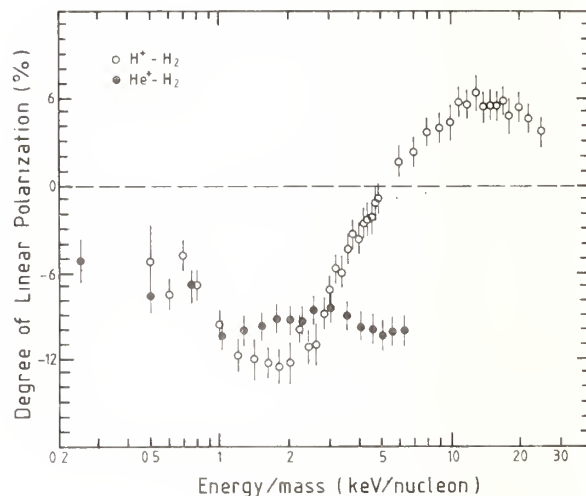


Fig. 10: Degree of linear polarization versus incident energy divided by the projectile mass for (o) H^+-H_2 and (●) He^+-H_2 collisions.²⁸

For this collision system the observed radiation should result either from projectile excitation to the $H(2p)$ state [$\rightarrow H(2p) + H_2^+$] or from dissociative excitation of the target [$\rightarrow H + H(2p) + H^+$]. Hence, assuming the emitted radiation to be due to $H(2p)$ production, this corresponds to a subshell cross section ratio $\sigma_1/\sigma_0 \approx 2$. This result is similar to H^+-H collisions where the $2p\sigma-2p\pi$ rotational coupling dominates the excitation process. In a quasi-diatomic approach one may invoke the same type of coupling, although in the triatomic picture²⁹ the two $2a'-3a'$ and $2a'-1a''$ transitions may lead to the excitation of $H(2p)$ atoms. Towards larger energies the linear polarization in H^+-H_2 collisions becomes less negative, indicating the increasing importance of (direct) excitation to the $H(2p_0)$ substate.

The experimental results for He^+-H_2 collisions display a negative linear polarization amounting to

about -10% in the range of incident energies between 4-25 keV. For this collision system dissociative target excitation to H(2p) provides the dominating process. Again, the observed magnitude of the linear polarization may be taken as an indication for a rotational coupling dominating the excitation mechanism at these energies.

Acknowledgements

The author acknowledges helpful discussions with Prof. Dr. H.O. Lutz, Prof. Dr. H. Kleinpoppen, Dipl. Phys. H. Madeheim, Dr. M. Kimura, and Dr. D. Dowek. This work was supported by the Deutsche Forschungsgemeinschaft in SFB 216.

References

1. R. Hippler, M. Faust, R. Wolf, H. Kleinpoppen, H.O. Lutz, Phys. Rev. A **37**, 4644 (1987).
2. R. Hippler, W. Harbich, M. Faust, H.O. Lutz, J. Phys. B **21**, 103 (1988).
3. U. Fano, J. Macek, Rev. Mod. Phys. **45**, 553 (1973).
4. R. Hippler, In: Fundamental Processes in Atomic Collision Physics (H. Kleinpoppen, J.S. Briggs, H.O. Lutz, Eds.), Plenum: New York (1985), p. 181; R. Hippler, In: XV ICPEAC Electronic and Atomic Collisions, Invited Papers (H.B. Gilbody, W.R. Newell, F.H. Read, A.C.H. Smith, Eds.), North-Holland: Amsterdam (1988), p. 241.
5. R. Hippler, H. Madeheim, W. Harbich, H. Kleinpoppen, H.O. Lutz, Phys. Rev. A **38**, 1662 (1988).
6. M. Kimura, W.R. Thorson, Phys. Rev. A **24**, 1780 (1981).
7. W. Fritsch, C.D. Lin, Phys. Rev. A **26**, 762 (1982); Phys. Rev. A **27**, 3361 (1983).
8. H.J. Lüdde, R.M. Dreizler, J. Phys. B **15**, 2703 (1982).
9. T.G. Winter, C.D. Lin, Phys. Rev. A **29**, 567 (1984).
10. R. Shingal, C.D. Lin, private communication (1989).
11. D. Rapp, D. Dinwiddie, J. Chem. Phys. **57**, 4919 (1972).
12. C. Gaussorgues, A. Salin, J. Phys. B **4**, 503 (1971).
13. R. Shakeshaft, Phys. Rev. A **18**, 1930 (1978).
14. J. Ast, H.J. Lüdde, R. Dreizler, J. Phys. B **21**, 4143 (1988).
15. N. Andersen, S.E. Nielsen, Adv. At. Mol. Phys. **18**, 265 (1982).
16. H. Madeheim, R. Hippler, unpublished.
17. M. Kimura, N.F. Lane, Phys. Rev. A **37**, 2900 (1988).
18. R. Shingal, B. H. Bransden, D. R. Flower, J. Phys. B **22**, 855 (1989).
19. G.W. McClure, Phys. Rev. **166**, 22 (1968).
20. M.W. Gealy, B. Van Zyl, Phys. Rev. A **36**, 3100 (1987).
21. F. Borondo, F. Martin, M. Yanez, Phys. Rev. A **35**, 60 (1987); Phys. Rev. A **36**, 3630 (1987).
22. R. Hippler, W. Harbich, M. Faust, H.O. Lutz, L. Dubé, J. Phys. B **19**, 1507 (1986).
23. P.J.O. Teubner, W.E. Kaupilla, W.L. Fite, R.J. Girnius, Phys. Rev. A **2**, 1763 (1970).
24. R. Hippler, H. Madeheim, H.O. Lutz, M. Kimura, N.F. Lane, Phys. Rev. A (1989), to be published.
25. L. F. Errera, L. Mendez, A. Riera, Z. Physik D, to be published; L. Mendez, private communication.
26. J. Macek, C. Wang, Phys. Rev. A **34**, 1787 (1986).
27. W. Fritsch, private communication.
28. D. Dowek, H. Madeheim, R. Hippler, XVI ICPEAC, Book of Abstracts (1989), and to be published.
29. V. Sidis, D. Dowek, XIII ICPEAC Electronic and Atomic Collisions, Invited Papers (J. Eichler, I.V. Hertel, N. Stolterfoht, Eds.), North-Holland: Amsterdam (1984), p. 403.

IS THE "CLASSICAL" DOUBLE SCATTERING LESS ACCURATE FOR CALIBRATING MOTT POLARIMETERS THAN RECENTLY PROPOSED METHODS?

K. Jost[†]

Physikalisches Institut, Universität, D-4400 Münster, FRG

In most experiments involving spin polarized electron beams, the degree of (transverse) polarization P of the beam is determined by a Mott analyzer.¹ In this instrument the polarized beam is scattered by a target foil of high atomic number (usually gold, $Z = 79$) at an energy E in the 100 keV region; in modern analyzers using a retarding field for energy analysis the energy is sometimes as low as 20 keV or even 150 eV.^{2,3} Due to spin orbit interaction, the scattered intensities L and R observed simultaneously by two counters under the same angle θ on the left and on the right in a plane perpendicular to P show an asymmetry

$$A = (L-R)/(L+R) = SP, \quad (1)$$

which is proportional to P . For the constant S in this relation exist a variety of names, among these the most popular ones seem to be "analyzing power" or "Sherman function". In theoretical calculations, S is a function of Z , θ and E . However, because in a real experiment multiple scattering and other disturbing effects cannot be avoided, from the experimenter's viewpoint S depends additionally on many other parameters such as foil thickness t , solid angle $\Delta\Omega$ accepted by each of the two counters and their energy resolution ΔE . In principle the inclination of the target foil with respect to the incoming beam is of importance as well.⁴ However, in order to avoid drastic instrumental asymmetries, only the "symmetric" arrangement (normal incidence) is popular for Mott analyzers (Fig. 1).

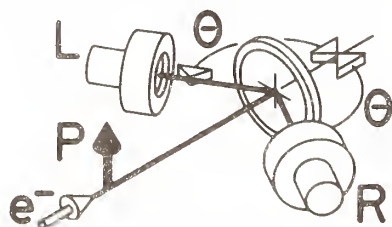


Fig. 1. Mott analyzer with symmetric foil position

As the theoretical value of S is only valid for elastic single scattering, it is important to distinguish between the effective analyzing power S_{eff} of a real analyzer and the idealized one. If S_{eff} of a Mott analyzer is known, it follows immediately from Eq. (1) that an unknown polarization can be determined by measuring the asymmetry:

$$P = A/S_{\text{eff}}. \quad (2)$$

In the following, an old and several recently proposed methods for determining S_{eff} will be discussed. At first the methods will be described neglecting disturbing effects due to imperfections of the apparatus or of the beam alignment. However, some of these methods are plagued heavily by false asymmetries and it is the main purpose of this contribution to show a strategy on how false asymmetries can be controlled.

I. CALIBRATION METHODS

A. Double scattering

The oldest⁵ and the most straightforward method to determine S_{eff} absolutely is the double scattering of electrons. This method takes advantage of the theoretically well established equality of the polarizing and analyzing power (see, e.g., Ref. 1, section 3.4.5 or Ref. 6, Fig. 15): Putting another foil in front of the Mott analyzer and scattering an unpolarized electron beam from it (Fig. 2), the polarization of the scattered beam will be S_{eff} , provided that all relevant parameters (Z , θ , E , t , normal incidence...) are the same as in the analyzer, where the "second" scattering occurs (note bene: multiple scattering occurs in both foils in like manner). Therefore, according to Eq.(2), one should obtain S^2_{eff} by measuring A . However, experience with this method shows that it is not as simple to handle as described above because of the difficulty to control spurious asymmetries (see sections II and III).

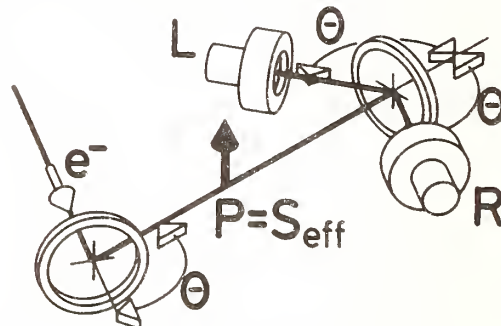


Fig. 2. Double scattering experiment

Therefore, this method is usually only applied indirectly by omitting the first scattering process. Instead, a set of foils of different thicknesses and a source of polarized electrons with unknown (but stable) polarization is used. Extrapolating the measured asymmetries to zero foil thickness and identifying the

[†] deceased

analyzing power in this case with the idealized one yields the formerly unknown P of the source and in turn the value S_{eff} of the foil actually used in the analyzer. However, this procedure has several pitfalls: (i) The extrapolation procedure is not unique⁷ because there exists no reliable theoretical guide on the dependence of S_{eff} on the foil thickness t . A much more extensive Monte Carlo calculation than the only existing one⁸ would be an invaluable help to cope with this problem. (ii) The ideal value of S is not unique either: For $E = 120$ keV and $\theta = 120^\circ$, for example, theoretical values⁹⁻¹² range from $S = -0.400$ to -0.407 , and the most accurate value obtained in a real double scattering experiment¹³ is -0.376 ± 0.008 ; i.e. between the extreme values is a difference of about 8%. (iii) An attempt to reduce the uncertainty of the first point by using extremely thin gold foils is dangerous as well: Evaporated gold tends to condense as islets¹⁴, which form no layer of homogeneous thickness below $\sim 40 \mu\text{g}/\text{cm}^2$. Therefore, apart from the irksome increase of the contribution of the backing, foils of (macroscopically) low areal density may behave like thicker ones. Taking all three problems into consideration, the overall uncertainty obtained by the extrapolation method could be even larger than the $\pm 5\%$ estimated by Fletcher et al.⁷

Because this situation is certainly not satisfactory, several alternative methods for determining S_{eff} with higher accuracy have been devised and explored recently. All these methods are based on a source of polarized electrons with easily reversible polarization and an auxiliary target between this source and the analyzer which is to be calibrated. These new methods are described in the following.

B. Optical method

In this method an auxiliary target is used, which emits circularly polarized light when it is excited with polarized electrons. In the special case of the (unresolved) $3^3\text{P} \rightarrow 2^3\text{S}_1$ transition in helium, the circular polarization of the corresponding 388.9 nm line is given by (Eqs. 10 and 11 of Ref. 15):

$$\eta_2 = (0.5 - \eta_3/6)P. \quad (3a)$$

The value of η_2 is determined by measuring the intensities of right-handed $[I(\sigma^+)]$ and left-handed $[I(\sigma^-)]$ circularly polarized light in y direction (Fig. 3):

$$\eta_2 = [I(\sigma^+) - I(\sigma^-)]/[I(\sigma^+) + I(\sigma^-)]. \quad (3b)$$

The small correction $\eta_3/6$ is due to an alignment along the z axis (Fig. 3) which the excited atomic state obtains by the collision. The value of η_3 can be determined by measuring the intensities $I(0^\circ)$ and $I(90^\circ)$ of linearly polarized light emitted in y direction:

$$\eta_3 = [I(0^\circ) - I(90^\circ)]/[I(0^\circ) + I(90^\circ)]. \quad (3c)$$

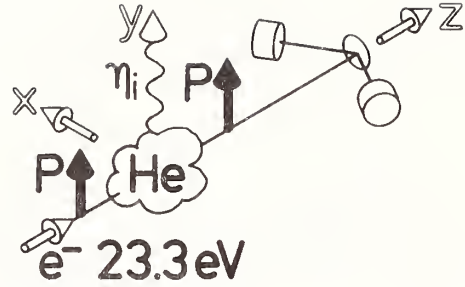


Fig. 3. Experimental arrangement for optical calibration of S_{eff} with a helium target

Eq. (3a) should be valid to high accuracy, because of the low atomic number of helium and because of its zero nuclear spin; i.e. the LS-coupling scheme used in the derivation¹⁵ is valid, spin flips can be neglected and hyperfine corrections are not required. However, note that Eq. (3a) is only valid for electron energies between 23.0 eV and 23.59 eV; below 23.0 eV the desired 3^3P level is not yet reached and above 23.59 eV the 4^3S_1 or higher states may be populated which would yield an admixture of unknown polarization to the 388.9 nm line.

The calibration of a Mott analyzer using this method is described in detail elsewhere¹⁶; by measuring η_2 and η_3 at 23.3 eV electron impact energy the polarization P of the electron source is known via Eq. (3a). The very same beam of polarized electrons is directed into a Mott analyzer, whose S_{eff} is then determined with an uncertainty in the 1% region by measuring A in Eq. (2).

C. Elastic scattering from an auxiliary target

Between a source of polarized electrons with reversible polarization P_0 and the Mott analyzer, whose S_{eff} is to be determined, an auxiliary target is introduced. This target T should show sufficiently distinct spin orbit effects such that its analyzing (or polarizing) power S_t differs from zero — the more the better — at the scattering angle and at the scattering energy chosen (usually around 100 eV). A set of scattering experiments from this target yields sufficient (or even redundant) information to extract S_{eff}^2 .

Hopster and Abraham¹⁷ used a Pt(111) crystal surface as a target to perform the (scattering) experiments shown in Fig. 4. The target surface was oriented like a mirror for 90° deflection. In the first of these experiments (Fig. 4a) the polarization P_0 is measured relatively (S_{eff} is not yet known!) by deflecting the beam electrostatically into the analyzer without using the target. The crystal was biased negatively for this purpose so that the beam was deflected without strik-

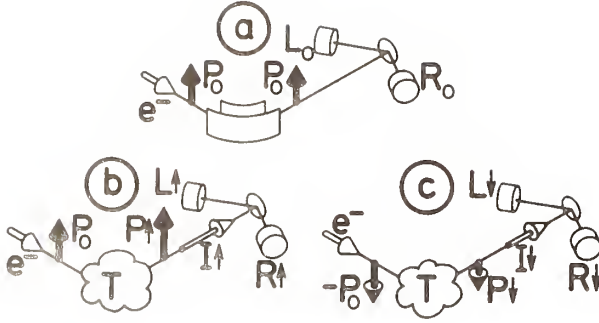


Fig. 4. Experimental arrangements with an auxiliary target T to measure a) A_0 , b) $A\uparrow, I\uparrow$ and c) $A\downarrow, I\downarrow$ (cf. Eqs. 4a-e)

ing the target. The count rates L_0 and R_0 in this experiment yield the asymmetry $A_0 = (L_0 - R_0) / (L_0 + R_0)$, which can also be expressed in terms of P_0 and S_{eff} (cf. Eq. 2):

$$A_0 = P_0 S_{eff}. \quad (4a)$$

(In practice, the experiment is repeated with reversed polarization to eliminate different counter efficiencies and the like, see section II).

The next two experiments (Figs. 4b and 4c) measure the change of the incoming polarization due to the scattering process by determining the asymmetries $A\uparrow = (L\uparrow - R\uparrow) / (L\uparrow + R\uparrow)$ and $A\downarrow = (L\downarrow - R\downarrow) / (L\downarrow + R\downarrow)$. The asymmetries $A\uparrow$ and $A\downarrow$ can also be expressed in terms of P_0 , S_t and S_{eff} because the change of a polarization by elastic scattering is well known. The general formula (Eq. 3.78 of Ref. 1) yields for the geometry shown in Fig. 4

$$A\uparrow = P\uparrow S_{eff} = \frac{P_0 + S_t}{1 + P_0 S_t} S_{eff} \quad (4b)$$

$$\text{and } A\downarrow = P\downarrow S_{eff} = \frac{-P_0 + S_t}{1 - P_0 S_t} S_{eff}. \quad (4c)$$

Simultaneously to $A\uparrow$ and $A\downarrow$, the two experiments (Figs. 4b and 4c) yield also the asymmetry $A_t = (I\uparrow - I\downarrow) / (I\uparrow + I\downarrow)$, where $I\uparrow \sim L\uparrow + R\uparrow$ and $I\downarrow \sim L\downarrow + R\downarrow$. This asymmetry is due to the analyzing power of the target and can consequently (cf. Eq. 4a) be expressed by

$$A_t = P_0 S_t. \quad (4d)$$

The four Eqs. (4a) – (4d) contain independent information on P_0 , S_t and S_{eff} . Therefore, by choosing any three of them, the desired S_{eff} can be expressed by measured asymmetries. This way, one has the choice between the following relations:

$$\begin{aligned} S_{eff}^2 &= A_0 [A\uparrow(1+A_t) - A_0] / A_t, \\ S_{eff}^2 &= A_0 [A\downarrow(1-A_t) + A_0] / A_t, \\ S_{eff}^2 &= A_0 (2A\uparrow A\downarrow + A_0 A\uparrow - A_0 A\downarrow) / (2A_0 - A\uparrow + A\downarrow), \\ S_{eff}^2 &= [(A\uparrow(1+A_t))^2 - (A\downarrow(1-A_t))^2] / 4A_t. \end{aligned} \quad (4e)$$

In Ref. 17 only the first of Eqs. (4e) is used. However, by variation of the electron energy at the target from 15 eV to 45 eV, S_t was varied as well and in this manner a set of independent determinations of S_{eff} was performed; the uncertainty is estimated to be within $\pm 2\%$. By using a mercury atomic beam instead of the solid Pt target, the same type of calibration of a Mott analyzer is described elsewhere¹⁸ (please note that in Ref. 18 the equation which is equivalent to the last one of Eqs. (4e) of the present paper contains a misprint: the last plus sign should be a minus sign).

Garcia-Rosales et al¹⁹ used a xenon atomic beam as an auxiliary target. They proposed a somewhat different set of scattering experiments which are shown in Fig. 5. In the first one (Fig. 5a), $A_0 = P_0 S_{eff}$ (Eq.

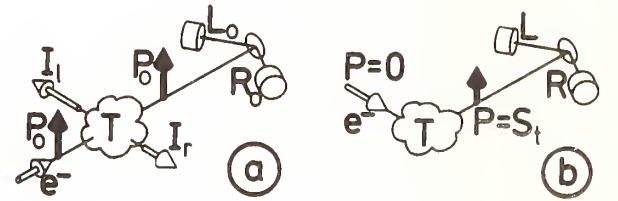


Fig. 5. Experimental arrangements with an auxiliary target T to measure a) A_0, A_t and b) A (cf. Eqs. 5a and b)

4a) and $A_t = P_0 S_t$ (Eq. 4d) are measured simultaneously. In this case, the intensities I_l and I_r (which correspond to $I\uparrow$ and $I\downarrow$ in Fig. 4) are not measured in the Mott analyzer in two different runs, but simultaneously by two spectrometers equipped with electron multipliers (not shown in Fig. 5a; the spectrometers are set to the elastic channel). The second experiment uses an approved method²⁰ to measure S_t with an unpolarized electron beam from a conventional electron gun. To be more accurate $-S_{eff}$ is assumed to be unknown – this experiment yields the asymmetry

$$A = S_t S_{eff}. \quad (5a)$$

Combining Eqs. (4a), (4d) and (5a) one obtains

$$S_{eff}^2 = \frac{A_0 A}{A_t}. \quad (5b)$$

At the moment, we will not evaluate the advantages or disadvantages of the different methods presented so far. This will be postponed until instrumental asymmetries are discussed in the next section.

II. INSTRUMENTAL ASYMMETRIES

A. Causes for instrumental asymmetries

Several situations leading to instrumental asymmetries are discussed in detail elsewhere (Ref. 1, section 8.1.2). Most people – including myself – feel bored by this topic, but exactly this seems to be the reason

that really accurate double scattering experiments could not be performed in the past because the long line of (simple) arguments had been interrupted too early. Therefore it is necessary to repeat the discussions given in Ref. 1 and to go even a step further (section III). In short: instrumental asymmetries are caused by (i) different counter efficiencies (including an unintentional difference of the solid angles accepted by the detectors or an unintentional difference of discriminator settings and the like) and/or (ii) misalignment of the incident beam (parallel shift or oblique incidence with respect to the ideal axis).

In order to facilitate the discussion, we will assume thin pencil beams, only small angular deviations ($\sin \Delta \theta = \Delta \theta$, etc.) and positional deviations which are small compared to counter distances from the foil center; in the following figures these deviations are very largely exaggerated. Furthermore, we will assume that the counters are at an angular position where the analyzing power is not changed by a small change of scattering angle ($\partial S_{\text{eff}} / \partial \theta = 0$). Finally, we will write S instead of S_{eff} for convenience. With these assumptions, it will turn out in the following that the first cause of instrumental asymmetry is harmless compared to the second one, therefore we start right away with the more difficult case.

For a moment, let us consider an unpolarized electron beam. According to Fig. 6, an obliquely incident beam which is inclined by ϵ with respect to an ideal axis and which hits the gold foil of the analyzer a distance y away from the center changes the scattered intensities detected by two ideal counters in two different ways: First, the (ideal) solid angle Ω of the white counter increases by

$$\frac{\Delta \Omega}{\Omega} = \left[\frac{\Delta h}{h} \right]^2 = 2 \frac{y}{h} \sin \theta, \quad (6)$$

and second the (ideal) scattering angle θ for the white counter is increased by (Ref. 1, Eq. 8.10):

$$\Delta \theta = -\frac{y}{h} \cos \theta + \epsilon, \quad (7)$$

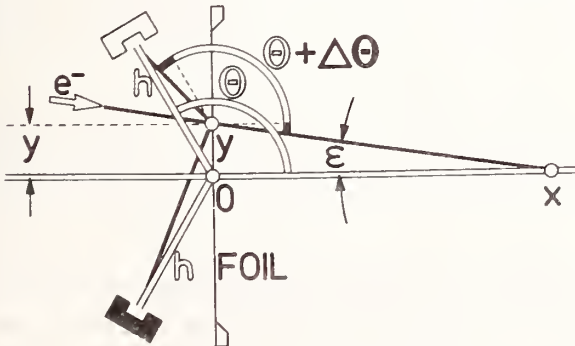


Fig. 6. Oblique incidence; x , y and ϵ are positive in the figure

which of course changes the detected intensity I which depends on θ . As the effects for the black counter have just the opposite sign, one detects a false asymmetry (even for an unpolarized electron beam!):

$$A_f = \frac{\Delta \Omega}{\Omega} + \frac{1}{I} \frac{\partial I}{\partial \theta} \Delta \theta$$

$$= 2 \frac{y}{h} \sin \theta + \Delta I_r \left[-\frac{y}{h} \cos \theta + \epsilon \right], \quad (8)$$

where $\Delta I_r = \frac{\Delta I}{I} = \frac{1}{I} \frac{\partial I}{\partial \theta}$

is the relative change of scattered intensity with scattering angle. The intensity detected in the white and black counters is proportional to $(1+A_f)$ and $(1-A_f)$, respectively.

Let us now return to a polarized electron beam whose polarization may be reversible without changing the beam position. The efficiencies of the two counters are assumed to be different now (efficiencies W and B for white and black, respectively). In the experiment shown in Fig. 7a, one measures the intensities

$$L \uparrow \sim W(1+PS)(1+A_f) \quad (9)$$

and $R \uparrow \sim B(1-PS)(1-A_f)$.

Fig. (7b) yields:

$$L \downarrow \sim W(1-PS)(1+A_f) \quad (10)$$

and $R \downarrow \sim B(1+PS)(1-A_f)$.

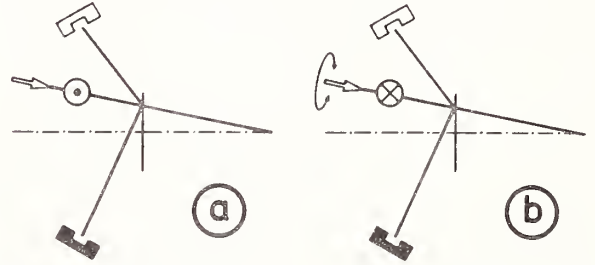


Fig. 7. Polarization reversal a) initial configuration, b) polarization reversed

Collecting the intensities with the same sign in PS and combining them in the usual way (Ref. 1, Eq. 8.6) to define $L = (L \uparrow R \downarrow)^{1/2}$ and $R = (R \uparrow L \downarrow)^{1/2}$ one obtains

$$A = \frac{L-R}{L+R} = PS, \quad (11)$$

which is the ideal result; different counter efficiencies and false asymmetries are eliminated.

Unfortunately, there are also experiments in which the incoming polarization can not be reversed. To eliminate different counter efficiencies in this case, the

counter arrangement is turned by 180° around an axis which is believed to coincide with the incoming beam. However, in general the axis of rotation and the beam axis are not quite the same and one has the situation sketched in Fig. 8. The first experiment (Fig. 8a) yields the same as Eq. (9):

$$L \uparrow \sim W(1+PS)(1+A_f) \quad (12)$$

and $R \uparrow \sim B(1-PS)(1-A_f)$.

On reversal of the counters (Fig. 8b), where the white and black counters are interchanged, one obtains

$$L' \uparrow \sim B(1+PS)(1+A_f) \quad (13)$$

and $R' \uparrow \sim W(1-PS)(1-A_f)$.

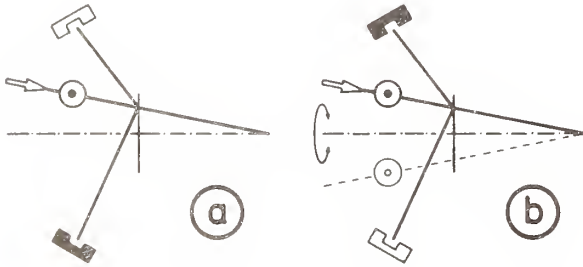


Fig. 8. Counter reversal a) initial configuration, b) counters interchanged; the dashed line shows the beam incidence which would be equivalent to Fig. 7b

Again collecting the intensities with the same sign in PS and combining them to define $L' = (L \uparrow L' \uparrow)^{1/2}$ and $R' = (R \uparrow R' \uparrow)^{1/2}$, one obtains ($A_f PS \ll 1$ neglected, compare Eq. 8.15 of Ref. 1):

$$A' = \frac{L' - R'}{L' + R'} = PS + A_f, \quad (14)$$

where the different counter efficiencies are eliminated, indeed. However, the false asymmetry A_f (Eq. 8) remains and it seems to be almost impossible to get rid of A_f , e.g. by determining it with an unpolarized electron beam, because this task would be successful only when the unpolarized beam exactly coincides with the polarized one. The encouraging result obtained by reversal of P, Eq. (11), is not obtainable by simple means when the counters are rotated. However, it will be shown in section III how this problem can be solved.

B. Influence on calibration methods

The discussion above shows that all experiments where the polarization entering the Mott analyzer can be reversed easily (without shifting the beam!) are uncritical, whereas all others bear the danger of unrec-

ognized false asymmetries. Small false asymmetries may be tolerable in experiments with modest accuracy, but definitely not when one strives for an uncertainty below a few percent. This may be illustrated by an example: in an experiment with $P = 0.3$ and $S = 0.25$, one should observe an asymmetry $A = PS = 0.075$. Assuming a counter distance $h = 30$ mm (Fig. 6) and using Rutherford scattering as a rough approximation to determine ΔI_r , Eq. 8 yields a false asymmetry A_f which reaches the 1% level of $A = PS$ when the beam has a parallel shift ($\epsilon = 0$) of only 0.02 mm or when it hits the center of the foil ($y = 0$) with an angular deviation of only 0.04° . From discussions the author knows that many people accept these arguments for thin pencil beams, but not for a beam with a diameter in the region of 10 mm, where a shift of 0.02 mm would be hardly visible. Nevertheless, a thick beam consists of a large number of thin ones and each of these is influenced by the small shift. Summing up yields therefore the same result for a thick beam as for a thin one. For the present purposes any thick beam can be represented by an infinitesimally thin one (similar to the pointlike center of mass of a huge body).

In the light of the above considerations, the optical method (section I.B) should be rather reliable, because all experiments necessary to determine S_{eff} can be performed with reversed polarization of the beam entering the Mott analyzer. All other methods have weak points with this respect: in the classical double scattering experiment performed in the 100 keV region any task to reverse the polarization after the first scattering without influencing the beam is hopeless. Considerably better off is the experiment of Hopster and Abraham¹⁷, where the beam from all three experiments (Figs. 4a-4c) passes through a spectrometer with narrow slits before it enters the Mott analyzer. Therefore one can hope — if the adjustment of the spectrometer is not touched — that the beam enters the Mott analyzer alike in all three experiments and A_f in Eq. (14) could be measured with an unpolarized beam in the arrangement of Fig. 4a when different counter efficiencies are known also via Fig. 4a with a polarized beam (Eq. 8.8 of Ref. 1). The same type of experiment¹⁸ without narrow defining slits is very likely disturbed by false asymmetries. Finally, the part of the experiment of Garcia-Rosales et al¹⁹ which is shown in Fig. 5b allows a reversal of P when the electron gun is swiveled to the mirror symmetric position in the scattering plane; however, the scattered beam should then be defined by rather narrow slits to warrant the same beam incidence into the Mott analyzer.

It should be emphasized that the accurate calibration of a Mott analyzer is meaningless when it is intended to be used later in experiments without the possibility of polarization reversal. In this case, Eq. (14) holds and the accurate knowledge of S_{eff} is easily masked by A_f .

III. MONITOR COUNTERS

The problems with false asymmetries discussed above can be overcome by introducing properly positioned monitor counters. The idea seems to be simple: two additional monitor counters are placed symmetrically at small angles where $S(\theta_m) \approx 0$. It is clear that any asymmetries observed by these monitor counters are purely instrumental. Monitor counters were popular in the past^{13, 21-23}, but strangely enough, not nowadays where higher precision in electron polarimetry is of large interest. The reason is simple: everybody who used monitor counters made the experience that the results did not really improve and often the results obtained by observing the monitor counters seemed to be more doubtful than those neglecting them. As will be explained in the following, this strange behavior of the monitor counters is caused by placing them at a wrong distance from the scattering center.

First of all, it should be emphasized that the inversion of the above statement "any asymmetries observed by these monitor counters are purely instrumental" is not allowed. That means that ideal incidence is not warranted if the monitors show no asymmetry. This statement is seemingly absurd, but it can be easily understood by looking at Eq. (8), which of course is also valid for the monitor counters if the appropriate value θ_m is inserted. Obviously, A_f vanishes if both y and ϵ are zero (ideal incidence), but it also vanishes if the effects of changing intensity due to a change of solid angle and scattering angle compensate each other. This is the case if

$$\epsilon/y = \left[\cos\theta - \frac{2 \sin\theta}{\Delta I_r} \right] / h, \quad (15)$$

because this condition is obtained from Eq. (8) by the requirement $A_f = 0$. This constant ratio ϵ/y leading to $A_f = 0$ for the monitor counters (indices m) is obtained for all beams which cross the ideal axis at a distance

$$x_m = h_m / [\cos\theta_m - 2[\Delta I_r(\theta_m)]^{-1} \sin\theta_m] \quad (16)$$

from the foil center, see Fig. 6. For the polarization counters (indices p) one obtains correspondingly $A_f = 0$ for all beams which cross the ideal axis at a distance

$$x_p = h_p / [\cos\theta_p - 2[\Delta I_r(\theta_p)]^{-1} \sin\theta_p] \quad (17)$$

from the foil center. It is an almost trivial requirement that the polarization counters should not be allowed to be disturbed by a false asymmetry when the monitor counters show $A_f = 0$. On the other hand it would be nonsense as well if the monitor counters indicate a false asymmetry when the polarization counters are not disturbed. These unpleasant contradictions can easily be avoided by making the "magic points" defined by Eqs. (16) and (17) coincide, i.e. $x_m = x_p = x_0$. This leads to the requirement for the ratio h_m/h_p of the

detector distances from the foil center to be:

$$\frac{h_m}{h_p} = \frac{\cos\theta_m - 2[\Delta I_r(\theta_m)]^{-1} \sin\theta_m}{\cos\theta_p - 2[\Delta I_r(\theta_p)]^{-1} \sin\theta_p}. \quad (18)$$

Obeying this requirement has the consequences that (i) any oblique beam passing through the common magic point x_0 defined above behaves with respect to asymmetries like an ideal (axial) one and (ii) any beam not passing through x_0 shows a false asymmetry both in the polarization counters and in the monitor counters. Moreover, it is easy to show that the false asymmetries A_{fp} and A_{fm} in the polarization and monitor counters are proportional to each other for any combination of y and ϵ :

$$A_{fp} = [\Delta I_r(\theta_p)/\Delta I_r(\theta_m)] A_{fm}, \quad (19)$$

this follows by inserting Eq. (18) into Eq. (8), which is written up for the monitor counters as well as for the polarization counters. The use of monitor counters positioned according to Eq. (18) at an angle θ_m with $S(\theta_m) = 0$ is very simple now: because A_{fm} registered by the monitor counters (Eq. 14) is independent of P and because A_{fp} in Eq. (14) is also known via Eq. (19), the true asymmetry PS can easily be extracted.

The drastic effect of a wrong ratio of h_m/h_p (i.e. $x_m \neq x_p$) is illustrated in Fig. 9: Assuming $P = 0$ and using Rutherford scattering to compute ΔI_r at $\theta_m = 45^\circ$ and $\theta_p = 120^\circ$, one obtains $h_m/h_p = 1$ (for Rutherford scattering independent of θ) and $A'_p = 0.239 A'_m$ from Eqs. (14), (18) and (19). A plot of A'_p versus A'_m , Eq. (14), yields in this case a straight line for all combinations of ϵ between -0.2° and $+0.2^\circ$ and y/h_p between -0.02 and $+0.02$ as expected. Using the same combinations of ϵ and y/h_p for the wrong distance ratio $h_m/h_p = 5$, the values of A'_p and A'_m are within the parallelogram, whose corner points are determined by the extreme combinations of ϵ and y/h_p . From this it is clear that no unique relationship between A_{fp} and A_{fm} is obtained for a wrong distance ratio. For $P \neq 0$ the straight line and the parallelogram are shifted in A'_p direction by an amount $PS(\theta_p)$, where $S(\theta_p)$ is the analyzing power of the polarization counters.

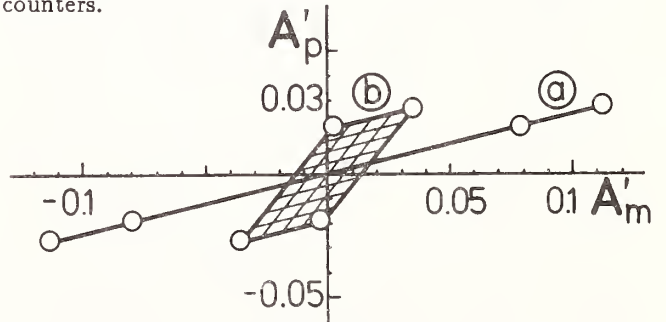


Fig. 9. Behavior of asymmetries A'_p and A'_m for a) $x_m = x_p$ and b) $x_m = 5x_p$. Extreme combinations of ϵ and y/h_p (see text) are shown as open circles

Except for van Klinken¹³, no other author has recognized the importance of the ratio h_m/h_p (Eq. 18). However, he relied on Rutherford scattering to be a reasonable approximation to determine ΔI_r . Unfortunately, this assumption is completely wrong at $\theta_p = 105^\circ$ which he chose. For determining h_m/h_p it is inevitable to measure ΔI_r at θ_p and θ_m . This inconvenience is very profitable, however, as is shown in the last section.

IV. "CLASSICAL" DOUBLE SCATTERING EXPERIMENT

Measurements of S_{eff} in dependence of the foil thickness t have been made at 50 keV and 120 keV for scattering angles of 45° , 60° , 75° , 105° , 110° , 115° , 120° , 125° and 130° . The results were presented²⁴ at the ICPEAC. The measurements (an example is shown in Fig. 10) were highly reproducible owing to the monitor counters used according the strategy explained in section III. Absolute values of S_{eff} (120°) were determined using two equal foils of $220 \mu\text{g}/\text{cm}^2$ at 120 keV and of $70 \mu\text{g}/\text{cm}^2$ at 50 keV. An analysis of the uncertainties at these calibration points shows that these are surely below 0.3%. Therefore it can be concluded that the "classical" double scattering method is by no means inferior to the recently proposed methods for calibrating S_{eff} if properly positioned monitor counters are used. Moreover, the author is convinced that the use of monitor counters in other experiments where the reversal of the polarization is difficult or impossible would largely improve the reliability of the measurements.

Finally, it should be emphasized again that more extensive Monte Carlo calculations⁸ on the dependence of S_{eff} on t would allow an accurate comparison of the ideal S (defined in the introduction) with the measurements.²⁴

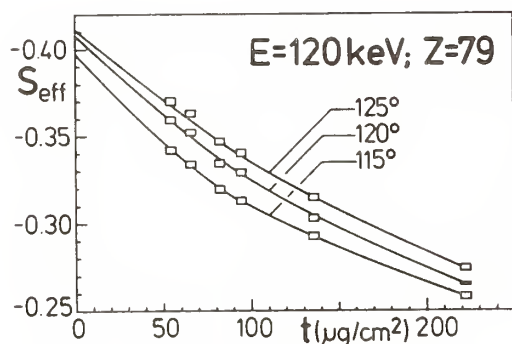


Fig. 10 S_{eff} versus foil thickness t obtained in a precise double scattering experiment²⁴. The curves are guides to the eye only. The size of the rectangles represent the experimental uncertainties

Acknowledgment: I wish to thank Professor J. Kessler and especially Dipl.-Phys. A. Gellrich for numerous fruitful discussions on the use of monitor counters. This work has been supported by the Deutsche Forschungsgemeinschaft in the Sonderforschungsbereich 216 "Polarization and Correlation in Atomic Collision Complexes".

References

- 1 J. Kessler, "Polarized Electrons", 2nd ed. (Springer, Berlin, 1985)
- 2 F.B. Dunning, L.G. Gray, J.M. Ratliff, F.C. Tang, X. Zhang and G.K. Walters, Rev. Sci. Instrum. 58, 1706 (1987)
- 3 J. Unguris, D.T. Pierce and R.J. Celotta, Rev. Sci. Instrum. 57, 1314 (1986)
- 4 H.A. Tolhoek, Rev. Mod. Phys. 28, 277 (1956), Fig. 7
- 5 N.F. Mott, Proc. Roy. Soc. A 124, 425 (1929)
- 6 K. Jost in "Physics of Ionized Gases", M.V. Kurepa, ed. (Beograd, 1972), p. 37
- 7 G.D. Fletcher, T.J. Gay and M.S. Lubell, Phys. Rev. A 34, 911 (1986)
- 8 V. Hnizdo, Nucl. Instrum. Meth. 109, 503 (1973)
- 9 S.R. Lin, Phys. Rev. A 133, 965 (1964)
- 10 G. Holzwarth and H.J. Meister, Nucl. Phys. 59, 56 (1964) and Tables... (Munich 1964)
- 11 A.W. Ross and M. Fink, Phys. Rev. A 38, 6055 (1988)
- 12 W. Bühring, private communications 1987/1989
- 13 J. van Klinken, thesis (Groningen, 1965) and Nucl. Phys. 75, 161 (1966)
- 14 L. Reimer and K. Freking, Z. Physik 184, 119 (1965)
- 15 T.J. Gay, J. Phys. B 16, L 553 (1983)
- 16 M. Uhrig, A. Beck, J. Goeke, F. Eschen, M. Sohn, G.F. Hanne, K. Jost and J. Kessler, Rev. Sci. Instrum. 60, 872 (1989)
- 17 H. Hopster and D.L. Abraham, Rev. Sci. Instrum. 59, 49 (1988)
- 18 J. Leuker and K. Jost, XVI. ICPEAC New York (1989), Abstracts of papers p. 803
- 19 C. Garcia-Rosales, H. Müller and J. Kessler, J. Phys. B 21, L 477 (1988)
- 20 K. Jost and J. Kessler, Z. Physik 195, 1 (1966)
- 21 A.R. Brosi, A.I. Galonsky, B.H. Ketelle and H.B. Willard, Nucl. Phys. 33, 353 (1962)
- 22 W. Raith in "Atomic Physics", B. Bederson, V.W. Cohen and F.M.J. Pichanick, eds. (Plenum Press, New York 1969), p. 389
- 23 G. Schönense, Phys. Rev. Letters 44, 640 (1980)
- 24 A. Gellrich, K. Jost and J. Kessler, XVI. ICPEAC New York (1989), Abstracts of papers p. 802

LOW ENERGY ELECTRON SCATTERING BY $3^2P_{3/2}$ SODIUM

L. Vučković*

Physics Department, New York University, New York, NY 10003

We have investigated partially state selective scattering amplitudes for elastic and superelastic unpolarized electron scattering by laser excited $3^2P_{3/2}$ sodium using our atom-recoil scattering apparatus¹. Higher level excitation measurements were also performed. Scattering intensity is measured with respect to polar scattering angle (θ), while preliminary measurements of azimuthal (ϕ) dependence for elastic scattering have also been performed, although a quantitative analysis for azimuthal scattering has not yet been made.

For the recoil technique post-collision observation is made on the recoil-scattered atoms. Absolute scattering cross sections are obtainable from knowledge of the ratio of the scattered to unscattered atom currents and the absolute electron number current, while the conventional crossed-beam method (observing the scattered electrons), requires knowledge of the atom number density in the interaction region, a very difficult quantity to determine reliably. At the same time, the atom-recoil technique², being suitable³ for grand-total cross section measurements, contain restrictions with respect to differential cross section observation.

Our laser excitation experiments were performed using both travelling, i.e. unidirectional, and standing, i.e. bidirectional laser radiation. A schematic diagram of the travelling wave arrangement is shown in Figure 1. The three interacting electron, atom and laser beams are mutually perpendicular, and lie along the z , y and $-x$ directions, respectively. The standing wave arrangement is also employed in the present work, but we will not discuss it here since the corresponding analysis has to be modified. Scattered

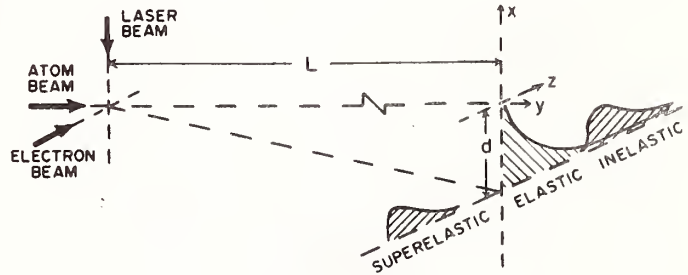


Figure 1: Schematic diagram of experiment.

atoms are measured in the detector (x, z) plane located a distance L from the interaction region perpendicular to the atom beam (y -axis).

Using a laser frequency tuned to excite only $F=2$ ground state atoms to the 3^2P state, the photon-recoiled atoms are spatially separated from the atoms that are in the off-resonant $F=1$ ground state. The displacement d of the photon-recoiled atom beam in the detector plane^{4,5} is related to the excited-state fraction f of the atoms in the interaction region by (two-level atom in resonant laser field, rate-equation approach^{6,7})

$$f = \frac{d\lambda\tau MV^2}{hlL} \quad (1)$$

where λ is the wavelength of the resonant laser radiation, τ is the lifetime of the excited states, M, V is the atom mass and speed respectively, h is Planck constant and l is the length (along y -axis) of the interaction region. In order to obtain absolute values of excited state cross sections it is necessary to obtain reliable values of f .

Both circularly polarized and linearly polarized radiation were used. The linearly polarized light had its electric vector parallel to the atom

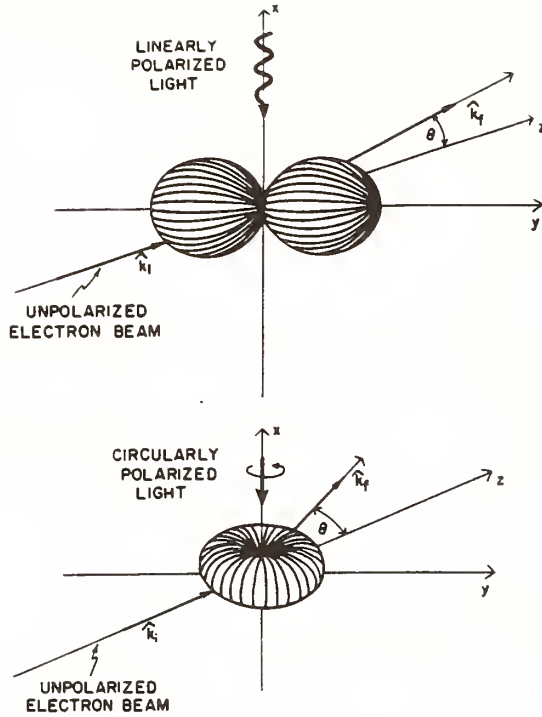


Figure 2: Sodium atom $3P$ electron charge clouds (from Ref. 11).

beam initial velocity direction (y -axis). The excited-state charge clouds prepared by the two laser polarizations, shown in Fig. 2, correspond⁶ to different combinations of $3^2P_{3/2}, F=3$ state magnetic sublevels. No analysis is made on the final atomic state.

Observations were mainly restricted to detector displacements parallel to the initial electron momentum, mv . Referring to Figure 1, the atom deflection in the detector plane due to superelastic and elastic or inelastic electron scattering result in momentum transfer to the atom beam counter to and along mv , respectively.

Kinematic analysis¹ shows that under the condition $mv \ll MV$, the x, z coordinates of the scattered atom in the detector plane are related to the polar and azimuthal angles of the scattered electron as

$$x = L\beta_k \sin \theta \sin \phi \quad (2)$$

$$z = L(\alpha - \beta_k \cos \theta) \quad (3)$$

where $\alpha = mv/MV$ and $\beta_k = mv_k/MV$. It is

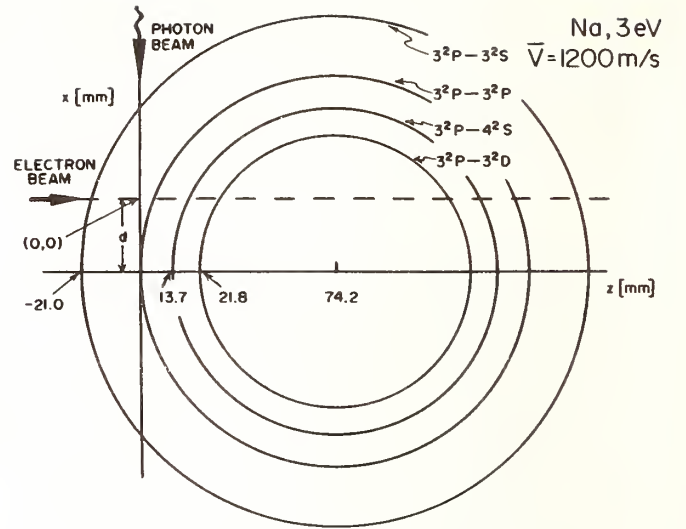


Figure 3: Projection of momentum spheres in the detector plane.

assumed that the atom is initially in the state ϵ_j (we omit the subscript j from the initial atom speed v). The subscript k refers to an electron which after scattering leaves the atom in state k , where ϵ_k is the final atomic state. This results in elastic ($\epsilon_j = \epsilon_k$), inelastic ($\epsilon_j < \epsilon_k$), or superelastic ($\epsilon_j > \epsilon_k$) scattering. Due to total momentum conservation in the interaction, elastically scattered atoms will fall on a momentum sphere with radius mv , while the radius $mv_k = mv\sqrt{1 - \Delta E/E}$ corresponds to inelastically and superelastically scattered atoms. Here E and ΔE are initial electron energy and the energy difference between initial and final atomic states, respectively. These momenta spheres projected onto the detector plane in configuration space, shown in Figure 3 for 3 eV electron scattering, correspond to circles with appropriate radii. The elastic scattering radius is $mvL/MV = \alpha L$ in the detector plane with the center at $z = \alpha L$. When the detector is placed inside a particular circle it can detect atoms scattered into channels that correspond to all momentum spheres of equal or greater radius.

The general case of the scattering process in electron-atom recoil experiments is described elsewhere³, where relations between two-

dimensional experimental parameters and the differential cross sections $\sigma(\theta)$ are quantitatively discussed. Here we recall the final relations of these analyses in order to proceed with a scattering analysis for excited species. For that purpose we define the position of the detector center to be z_D and consider only the case outside of the full dc beam shadow when all correction terms to the scattering intensity can be neglected. The scattering atom current $I_s(z_D)$ is then

$$I_s(z_D) = I_{in}(z_D) - I_{out}(z_D) \quad (4)$$

where $I_{in}(z_D)$ and $I_{out}(z_D)$ are scattering contributions into and out of the detector. Taking into account all distribution functions of the real experiment, $I_{in}(z_D)$ is defined as

$$\begin{aligned} I_{in}(z_D) &= \frac{i_0 I_0(0)}{2h\Delta x\Delta z} \int_{E_0-0.5}^{E_0+0.5} \Xi(E) dE \\ &\times \int_0^\infty \frac{V(v)}{v} dv \int_{z_1}^{z_2} Z(z) dz \int_{x_1}^{x_2} X(x) dx \\ &\times \int_{\theta_1}^{\theta_2} \sigma(\theta) \sin \theta d\theta \int_{\phi_1}^{\phi_2} d\phi \end{aligned} \quad (5)$$

where i_0 is the total electron number current, $I_0(0)$ is the atom beam current at $z_D = 0$, h is the height of electron beam, Δx and Δz are half-height and half-width of the detector, $\Xi(E)$ is the energy distribution of the electron beam, $V(v)$ is the velocity distribution of the atom beam, $X(x)$ and $Z(z)$ are vertical and horizontal beam profiles normalized to unity at the beam center, x_1 , x_2 , z_1 , z_2 are limits of integration of atom beam profiles, and

$$\theta_1 = \cos^{-1}\left(\frac{\alpha}{\beta_k} - \frac{z_D - z - \Delta z}{\beta_k L}\right), \quad (6)$$

$$\theta_2 = \cos^{-1}\left(\frac{\alpha}{\beta_k} - \frac{z_D - z + \Delta z}{\beta_k L}\right), \quad (7)$$

$$\phi_1 = -\sin^{-1} \frac{\Delta x + x}{\beta_k L \sin \theta}, \quad (8)$$

$$\phi_2 = \sin^{-1} \frac{\Delta x - x}{\beta_k L \sin \theta}. \quad (9)$$

Outside of the dc beam scattering-out contributions are generally negligible. However, this process may contribute as a consequence of a

long "tail" of the dc beam in the region where scattering-in is measured. This $I_{out}(z_D)$ contribution can be described with the simplified equation

$$I_{out}(z_D) = \frac{i_0 I_0(z_D) \sigma_T}{h \bar{V}} \quad (10)$$

where $I_0(z_D)$ is the atom beam current at z_D , \bar{V} is the average atom speed and σ_T is total scattering cross section.

The above equations describe the complete relationship between the scattering signal and the scattering cross sections for a particular channel in an atom-recoil experiment. We will now discuss under what conditions differential cross sections can be determined from such an experiment, first describing conditions of elastic scattering observation where small angle scattering is not included. The second part is related to superelectronic or inelastic scattering where small angle as well as zero-angle collisions are included.

Assume that the influence of the electron energy distribution on $\sigma(\theta)$ through the limits of integrations of θ and ϕ is negligible⁸ in the present electron energy range. Also, if the cross section is a slowly varying function of energy over the electron energy distribution then the nominal peak of that distribution is a good representation of electron energy, and the integration over that distribution is unity. With regard to the atom velocity distribution^{1,3} it is safe to take the average atom speed, when medium range angle scattering is considered.

Due to finite widths of the detector and the dc beam the detected signal is related to an integrated differential cross section over certain ranges of θ . Since θ depends nonlinearly on z (Eq. 3), when the detector is further to the right of the dc beam the overall resolution is better. The differential cross section can be taken out of the integrations in the Eq. (5), assuming there is no rapid change of $\sigma(\theta)$ with respect to the θ integration over the detector width and the changes of ϕ through the x and z integrations over the beam widths. These conditions for elastic scattering are satisfied at the detector position corresponding to θ larger than, say, 20° so that Eq.

(4) can be simplified⁹ and the differential cross section in terms of the scattering signal is

$$\sigma(\theta) = \frac{1}{I_0(0)F(\theta)} \left[\frac{h\bar{V}}{i_0} I_s(z_D) + I_0(z_D)\sigma_T \right] \quad (11)$$

where

$$F(\theta) = \frac{1}{4\Delta x \Delta z} \int_{x_1}^{x_2} X(x) dx \int_{z_1}^{z_2} Z(z) dz \quad (12)$$

$$\times \int_{\theta(z_D+\Delta z-z)}^{\theta(z_D-\Delta z-z)} \Phi(\theta, x) \sin \theta d\theta$$

and

$$\Phi(\theta, x) = 2(\sin^{-1} \frac{\Delta x - x}{\alpha L \sin \theta} + \sin^{-1} \frac{\Delta x + x}{\alpha L \sin \theta}). \quad (13)$$

Eq. (11) is generally valid for both ground state and excited state scattering processes but only outside of the *dc* beam. In practice its application is limited to the scattering angles corresponding to where the detector would start seeing 0° angle scattering for inelastic processes, in which case the scattering signal would correspond to the combination of both processes.

In the current experiment electrons are scattered by an incoherent mixture of ground- and excited-state atoms, the latter constituting a fraction *f* of the beam. Thus, the detected signal is

$$I_s(z_D) = I_s^{3S}(z_D) + I_s^{3P}(z_D) \quad (14)$$

where

$$I_s^{3S}(z_D) = \frac{i_0(1-f)}{h\bar{V}} \times [I_0(0)F(\theta)\sigma^{3S}(\theta) - I_0(z_D)\sigma_T^{3S}] \quad (15)$$

and

$$I_s^{3P}(z_D) = \frac{i_0 f}{h\bar{V}} \times [I_0(0)F(\theta)\sigma^{3P}(\theta) - I_0(z_D)\sigma_T^{3P}]. \quad (16)$$

The differential cross section for the excited-state elastic scattering is

$$\sigma^{3P}(\theta) = \frac{1}{f} [\sigma^*(\theta) - (1-f)\sigma^{3S}(\theta)] \quad (17)$$

where $\sigma^*(\theta)$ can be obtained from Eq. (11) with $\sigma(\theta)$ and σ_T replaced by $\sigma^*(\theta)$ and σ_T^* and $F(\theta)$ is calculated using the laser-deflected atom beam profiles. Here σ_T^* is defined as

$$\sigma_T^* = (1-f)\sigma_T^{3S} + f\sigma_T^{3P} \quad (18)$$

where σ_T^{3S} and σ_T^{3P} are the total 3S- and 3P-state scattering cross sections, respectively.

Superelastic scattering has an unique deflection signature, but the explicit form for the differential cross section cannot be derived since its scattering signal corresponds to small-angle scattering and the above approximations do not hold. In this angular range $\sigma(\theta)$ changes rapidly with respect to θ integration over the detector as well as the beam width, and it cannot be removed from the integrals in Eq. (5). In addition, accurate knowledge of the electron energy distribution and, even more important, atom beam velocity distribution are required. Scattering signals (Eq. (4)) for superelastic collisions contain an $I_{in}(z_D)$ contribution, described with the full Eq. (5) when the right hand side is multiplied by *f* and an $I_{out}(z_D)$ contribution described by Eq. (10) when σ_T is replaced by σ_T^* . To obtain $\sigma(\theta)$ for superelastic scattering we express¹⁰ Eq. (5) in matrix form with separated variables

$$b(z_D) = A(z_D, \theta)x(\theta) \quad (19)$$

where $b(z_D)$ is the scattering signal, $A(z_D, \theta)$ incorporates all functions included in Eq. (5) except $\sigma(\theta)$, which is represented by the vector $x(\theta)$. Due to the fact that the scattering signal in the range of measurements contain contributions from collisions in the range 0° to about 20°, $\sigma(\theta)$ can be analytically described by a function with three independent parameters. The set of parameters that produces the vector $b(z_D)$ which is in best agreement with the measured scattering signal in the full range of observation defines superelastic $\sigma(\theta)$ in the appropriate angular range.

From higher level excitation ($3^2P \rightarrow 4^2S$ and $3^2P \rightarrow 3^2D$) measurements, only the tendency of the cross sections can be extracted, due to resolution limitations even at low impact energies. For

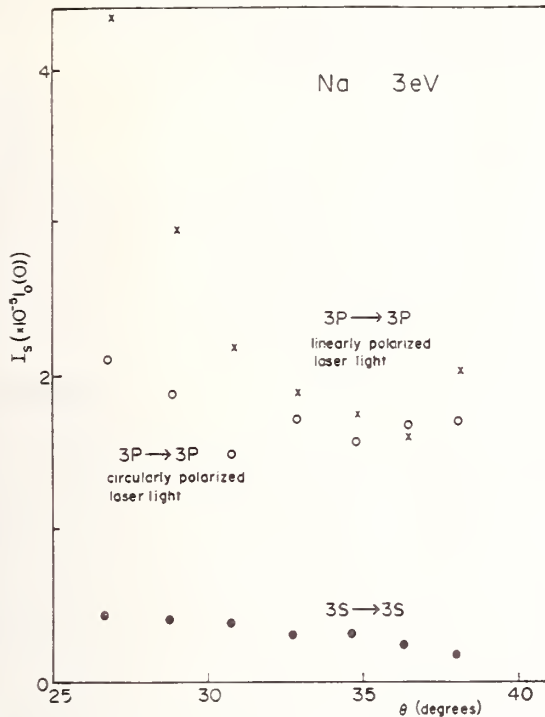


Figure 4: Elastic scattering intensity. (z_D converted into θ)

example, scattering signal at 3 eV contain contribution of 3^2S and 3^2P elastic scattering from 35° to 50° when small angle excitation peaks appear. Those peaks are partially overlapped mainly due to the atom beam velocity distribution.

Azimuthal angle dependency (Eq. 2, Fig. 3) can be studied by displacing the detector along the x -axis (changing x_D) at a fixed position of z (fixed θ). Preliminary data have been obtained for elastic ground-state scattering and elastic scattering by a superposition of ground-state and $3P$ -state sodium atoms. Observations reveal significant differences between the shape of the scattering signals for these two processes, but a quantitative analyzes will require additional effort.

Examples of the measured scattering signals are given in Figs. 4 and 5 for elastic and superelastic scattering, respectively. All experimental functions included in Eq. (5) are carefully determined. Particularly important, the atom beam velocity distribution is measured¹⁰ by laser-induced Doppler-shifted fluorescence with

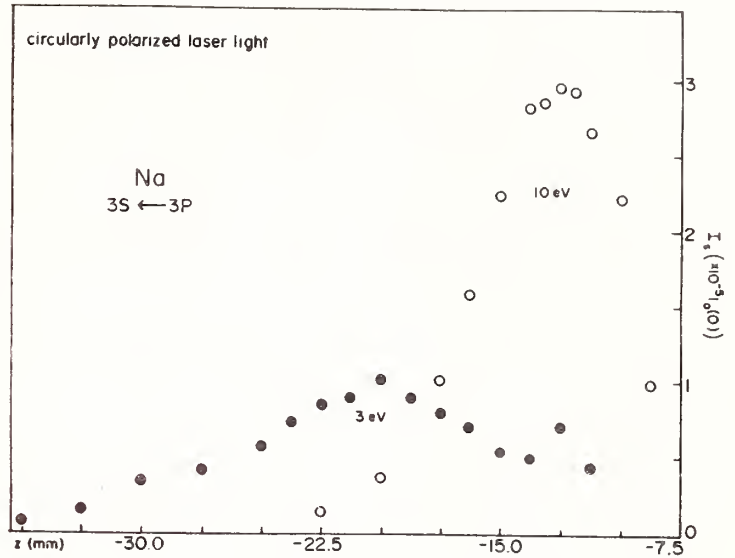


Figure 5: Superelastic scattering intensity.

absolute frequency calibration made by comparison with the zero-field hyperfine separation of the sodium atom. Alternative measurements¹ of displacement of the forward scattering peak after excitation by electron impact yield a consistent distribution. Evaluated elastic and superelastic cross sections yield information about partially state selective scattering amplitudes, which complements measurements of charge cloud alignment and orientation by other experimental groups¹¹.

Acknowledgments

This work is performed in collaboration with Prof. B. Bederson, M. Zuo, and T. Y. Jiang. Research is supported by U. S. National Science Foundation.

References

- *Permanent Address: Institute of Physics, P.O.Box 57, Belgrade, YU
- 1. B. Jaduszliwer, P. Weiss, A. Tino and B. Bederson, Phys. Rev. A **30**, 1255 (1984).
- 2. K. Rubin, J. Perel, and B. Bederson, Phys. Rev. **117**, 151 (1960).

3. L. Vušković, M. Zuo, G. F. Shen, B. Stumpf and B. Bederson, *Phys. Rev. A* **40**, 133 (1989).
4. B. Jaduszliwer, G. F. Shen, and B. Bederson, *Phys. Rev. A* **33**, 3792 (1986).
5. R. Blatt, W. Ertmer, P. Zoller, and J. H. Hall, *Phys. Rev. A* **34**, 3022 (1986).
6. I. V. Hertel and W. Stoll, in **Advances in Atomic and Molecular Physics**, edited by D. R. Bates and B. Bederson (Academic, New York, 1977), Vol. **13**, pp. 113-228.
7. N. D. Bhaskar, B. Jaduszliwer and B. Bederson, *Phys. Rev. Lett.* **38**, 14 (1977).
8. M. G. Fickes and R. C. Stern, *J. Chem. Phys.* **60**, 4710 (1974).
9. M. Zuo, T. Y. Jiang, L. Vušković, and B. Bederson, *Phys. Rev. A*, submitted for publication, 1989.
10. T. Y. Jiang, M. Zuo, L. Vušković, and B. Bederson, *Phys. Rev. A*, to be submitted, 1989.
11. N. Anderson, J. Gallagher, and I. Hertel, *Phys. Rep.* **165**, 1 (1988).

THE EFFECTS OF A FINITE SCATTERING VOLUME ON THE DETERMINATION OF ELECTRON IMPACT COHERENCE PARAMETERS

P. W. Zetner*, S. Trajmar* and G. Csanak†

*Jet Propulsion Laboratory, California Institute of Technology, Pasadena, California, USA

† Los Alamos National Laboratory, Los Alamos, New Mexico, USA

1. Introduction

In electron-atom beam-beam scattering experiments, the interaction region defined by the intersecting beams and the viewcone of the detector should be small in comparison with other characteristic dimensions of the scattering geometry and the energy and angular resolution of the apparatus should be narrow with respect to the ranges over which quantities of interest undergo significant changes. In this ideal case, the scattering signal can be assumed to originate from a point-like source and the data obtained from the measurements can be assigned to well-defined electron impact energy (E_0) and scattering angle (θ_e). In practice, the dimensions of the scattering volume and the energy and angular resolution of the apparatus are always finite and a rigorous treatment of the scattering data should take this into account. In conventional electron scattering measurements of the differential scattering cross section (DCS) these considerations, in general, cause no serious problems. The DCS can then be associated with nominal scattering angles and impact energies and represents a sum over final and average over initial experimentally indistinguishable processes. A discussion of these matters in electron scattering DCS measurements has been given, for example, by Brinkmann and Trajmar¹.

In recent years, a large body of data has accumulated in the field of electron impact induced orientation and alignment of atomic valence shells². Coherence and correlation experiments used to examine these aspects of the collision process represent a considerable refinement over conventional DCS measurements. In principle, only the scattering signal originating from an ensemble of excited atoms prepared in a well-defined quantum mechanical state is measured. The selection of this ensemble is carried out either by coincidence detection of the inelastically scattered electron and emitted photon, or by laser preparation of the excited

state atomic target and detection of the superelastically scattered electron. In both cases, a photon incidence vector and polarization vector are defined whose directions with respect to the scattering plane must be well-specified in order that unambiguous conclusions can be drawn about collision induced alignment and orientation (or, equivalently, about the electron impact coherence parameters, EICP). A rigorous evaluation of scattering data from coherence and correlation experiments should, therefore, include the convolution of the scattering angle as well as the photon direction and polarization angles with the finite angular resolution of the apparatus. Generally, however, the picture of an ideal point-like scattering has been applied to the interpretation of coherence and correlation data.

A recent study by Martus *et al.*³ does take into account the effect of averaging over the finite range of unresolved scattering angles observed by the electron detector in a measurement of the P1 polarization correlation parameter. Here, we describe a more rigorous approach to the problem of determining the influence of a finite scattering volume in electron-photon coincidence experiments and in measurements of superelastic scattering from laser-excited atoms. We treat the interaction volume as an ensemble of individual scattering points to each of which is attached a collision coordinate frame that may differ significantly from a laboratory-fixed coordinate frame. A "true" scattering plane, defined by the incident and outgoing electron momentum vectors of a collision event occurring somewhere within the ensemble can be quite different from the "nominal" scattering plane defined in the laboratory frame. The transformation of coordinate frames has extremely important consequences for the measurement of EICP and is unaccounted for by averaging over the scattering angles alone. Photon incidence and polarization vectors which are specified in the laboratory coordinate frame by spherical angles θ_ν and ϕ_ν and by polarization angle ψ_ν are given in the collision coordinate frame by angles θ_n , ϕ_n and ψ

which can, depending on the nominal scattering angle, vary radically for collision events occurring throughout the extended scattering volume. This radical behavior is expected for nominal scattering angles close to zero since the rotation of a collision frame relative to the laboratory frame for a scattering event displaced from the "nominal" scattering plane can be severe at small scattering angles. In this situation, the angular resolution of the system is no longer narrow with respect to the range over which the photon polarization vector and the photon direction vector (in particular) undergo significant variation. The extraction of EICP at these scattering angles becomes meaningless in the single-point scattering picture. Surprisingly, we have also discovered that a scattering volume of finite extent can have a dramatic influence on the measurement of EICP at scattering angles far from zero. In these cases, the range over which the photon direction and polarization vectors vary can be small compared to the angular resolution but the coincidence or superelastic scattering intensity becomes extremely sensitive to these small variations due to the behavior of the EICP themselves.

In this paper, we specifically examine the consequences of a finite scattering geometry on "in-plane" coherence experiments, i. e. polarization correlation or superelastic scattering experiments in which the incidence vector of the detected photon or the laser photon lies in the nominal scattering plane ($\phi_\nu = 0$). The "in-plane" experimental configuration is adopted in order to give direct information about spin-orbit coupling effects.

We show that a finite scattering geometry can give rise to severe distortion in the dependence of the coincidence or superelastic scattering signal intensity on the photon polarization and that this distorted behavior can be misinterpreted as arising from spin-orbit coupling effects.

2. Model Calculations

We have carried out modelling calculations in which the finite scattering volume is approximated by a distribution of discrete points. At each point, a collision coordinate frame is defined in which the theoretical formalism of da Paixão *et al.*⁴ (also Ref. (5)) is applied. This formalism can be used to describe electron-photon coincidence signal intensity for a $J = 0$ to $J = 1$ excitation or superelastic scattering signal for a $J = 1$ to $J = 0$ deexcitation. For the case of

linearly polarized photons:

$$I \sim A + B' \cos 2\psi + B'' \sin 2\psi \quad (1)$$

where the coefficients A , B' and B'' have been given^{4,5} as functions of the EICP and the photon incidence vector direction angles θ_n , ϕ_n measured in the collision coordinate frame. Implementation of the model involves carrying out the coordinate frame transformation associated with a scattering center located at position vector \vec{r}_j from the laboratory frame origin. The relation between the photon angles θ_ν , ϕ_ν , ψ_ν specified in the laboratory frame and the angles θ_n , ϕ_n , ψ in the collision frame is thereby determined as is the relation of the true scattering angle, θ_e , to the nominal scattering angle, θ_e^o . Fig. 1 presents a comparison between the collision frame associated with a scattering event located at position vector \vec{r}_j and the collision frame associated with an "ideal" scattering event taking place at the origin of the laboratory frame ($\vec{r}_j = \vec{0}$). This latter scattering event defines the nominal scattering plane and the nominal scattering angle, θ_e^o . The collision frame associated with the offset scatterer is clearly rotated with respect to the laboratory frame as evidenced by the direction of the vector \hat{Y}_{col}^j (normal to the true scattering plane) compared to $\hat{Y}_{col}^o = \hat{Y}_{lab}$ (normal to the nominal scattering plane).

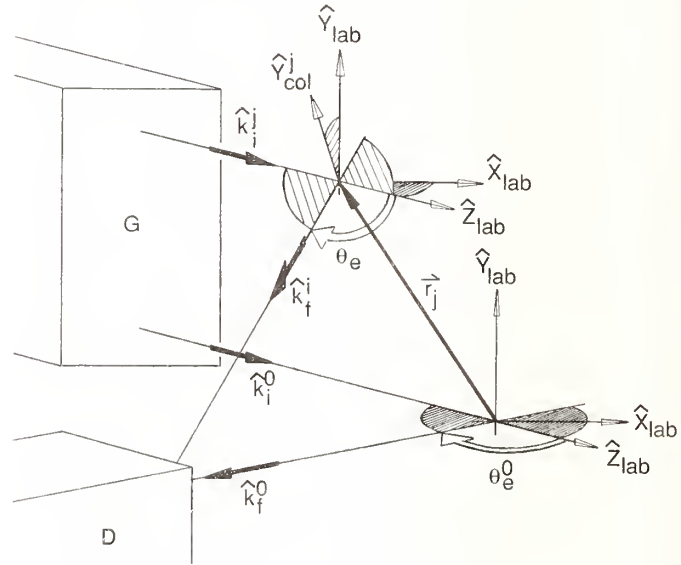


Fig. 1 Electrons emitted by the source (G) are scattered into detector (D). Collision coordinate frames associated with two different scattering events, taking place within the extended interaction volume, are shown (see text).

In our model, a weighted average of the scattering signal intensity over the distribution of scattering

centers is taken according to:

$$I_{\Sigma} = \sum_{ij} a_{ij} I_j(\hat{k}_f^i) \quad (2)$$

where I_{Σ} is the average superelastic or coincidence intensity and a_{ij} are weighting factors discussed below. The signal intensity arising from a particular collision frame is denoted $I_j(\hat{k}_f^i)$ since (for an assumed parallel incident electron beam) this frame is completely specified by the displacement vector \vec{r}_j , the nominal scattering angle, θ_e^j and the momentum vector, \hat{k}_f^i , of an electron scattered into the detector viewcone. The summation over index i in Eq. 2 represents an approximation to the effect of finite angular resolution in the electron detector. The contribution from all discrete scattering points chosen to represent the extended volume is calculated in the summation over index j . The weighting factors, a_{ij} , represent the effect of the spatial intensity distribution of the incident electron beam, the spatial response of the electron detector and the behavior of the DCS over the range of scattering angles defined by the extended scattering volume.

The sophistication of the model can be greatly increased to include, for example, the finite acceptance angle of the photon detector (or the divergence of the incident laser beam in the superelastic scattering case), the density distribution in the target gas beam and so on. We have found, however, that a relatively crude description of the scattering geometry can provide the essential aspects of the finite volume effect. In the results presented here, an array of 5 points, equidistantly spaced along a segment of the \hat{Y}_{lab} axis, was used to represent the extended scattering volume. The effect of the detector viewcone was simulated by associating 5 scattering directions with each of the 5 scattering points in the linear array. The weighting factors, a_{ij} , reflect only the spatial intensity distribution (Gaussian) of the incident electron beam.

3. Results

3.1 Superelastic Scattering from Laser-Excited $^{138}\text{Ba}(\dots 6s6p \ ^1P)$

Efforts to measure EICP for the $^{138}\text{Ba} \ ^1S_0$ to 1P_1 transition in a superelastic scattering experiment have been reported by Register *et al.*⁶. An experimental configuration was adopted in which the laser beam lay within the (nominal) scattering plane and the degree of modulation of the superelastic intensity, I_s , as a function of laser beam polarization angle, ψ_{ν} , was measured. During the course of their investigation, Register

et al. discovered that this modulation, $I_s(\psi_{\nu})$, was, unexpectedly, asymmetric with respect to $\psi_{\nu} = 0$ where $\psi_{\nu} = 0$ is defined to be the angle at which the laser beam polarization vector lies within the scattering plane. Furthermore, this asymmetry was scattering angle dependent in a regular way and was found to be reproducible despite major variations in experimental conditions. The origin of this asymmetry remained unexplained and EICP could not be extracted, with confidence, from these measurements. This led us to reinvestigate the cause of the asymmetry in more detail, both experimentally and theoretically, with special emphasis on the effects of a scattering volume of finite extent.

Superelastic scattering data can be straightforwardly analyzed by fitting Eq. 1 to the observed $I_s(\psi_{\nu})$ modulation curves. For this purpose, Eq. 1 is written in the equivalent form:

$$I_s(\psi_{\nu}) \sim 1 + \eta \cos(2\psi_{\nu} + 2\alpha) \quad (3)$$

where η is the modulation depth and α is the modulation phase shift.

For a laser beam lying in the scattering plane, theory^{4,5} predicts that $\alpha = 0$. However, the asymmetry observed by Register *et al.* and by us, in a more recent series of experiments, can be represented by a modulation phase shift which is non-zero. Fig. 2 shows the values of η and α extracted from our recent superelastic scattering measurements and the results of the corresponding model calculations for incident electrons of 30eV impact energy. These model calculations employed the theoretical EICP of Clark *et al.*⁷ which indicate that the $^{138}\text{Ba}(\dots 6s6p \ ^1P)$ state is almost purely LS coupled. It is important to note that, for a purely LS coupled state, an ideal single atom collision occurring at the origin of the laboratory frame (for laser incidence angle $\phi_{\nu} = 0$) would give $\eta = 1$ and $\alpha = 0$ at all scattering angles. Fig. 2 illustrates that serious deviations from these predicted values occur in an actual experiment and that these deviations are explained by the extended scattering volume model.

The model calculations indicate that, for a laser beam incidence vector lying in the nominal scattering plane, the phase shift differs from zero when the extended scattering volume is asymmetrically distributed in the normal direction to the nominal scattering plane. We have also verified experimentally that the deviation of α from zero is tied directly to asymmetry in the distribution of excited-state scatterers^{5,8}.

The distortion in the modulation depth, however, persists regardless of how the scattering volume is distributed. These results imply that the phase shift problem could conceivably be eliminated by ensuring a symmetrically distributed scattering source. However, EICP are extracted from the modulation depth, η , which suffers significant distortion whenever the scattering volume is finite in extent.

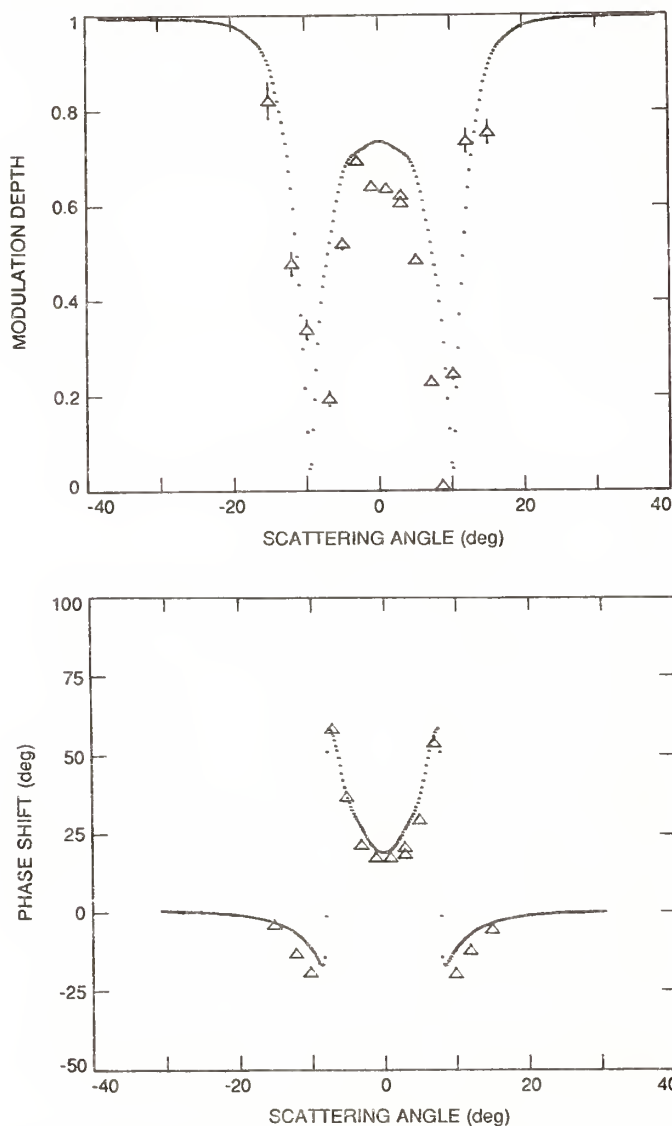


Fig. 2 Model calculations and experimental data⁸ for superelastic scattering from $^{138}\text{Ba}(\cdot\cdot 6s6p \ ^1P)$ at 30 eV. Laser beam incidence angles are $\theta_\nu = 90^\circ$; $\phi_\nu = 0^\circ$. (a) Modulation depth vs. nominal scattering angle; (b) Phase shift vs. nominal scattering angle.

Fig. 2 also reveals that the distortion in modulation depth produces relatively well-defined features which appear at specific scattering angles. For the superelastic scattering process under discussion, the

scattering angle location of these features is closely tied to the behavior of the alignment angle, γ , of the excited state charge cloud produced by the time-inverse inelastic scattering process. When this alignment angle is such that the laser photon incidence vector lies along the major axis of the charge cloud (assuming a collisionally excited "p" type orbital) then the measurement becomes extremely sensitive to extended volume effects⁵. Although it is not apparent from the figure, we have also found that the severity of the geometry-induced distortion is related directly to the shape of the charge cloud produced by the time-inverse inelastic process. In particular, when the ratio of length to width of this charge cloud is large at the "critical" alignment angle described above, then the distortion in η becomes severe. The smaller this ratio, the less sensitive the measurement becomes to extended volume effects. Of course, this ratio is given by the P_L^+ coherence parameter and we claim that, when P_L^+ is close to unity at the critical alignment angle, one can expect a strong influence of geometry on the measurement of η .

3.2 Measurements of the P4 Coherence Parameter in the Rare Gases

Conclusions about the influence of an extended scattering geometry on "laser-in-plane" superelastic scattering experiments are directly transferrable to studies concerning the P4 Stokes parameter in rare gas $J = 0$ to $J = 1$ excitations. We, therefore, extended our modelling effort to the rare gases and, in Figs. 3 through 5, the results are compared with the only P4 measurements so far available in the literature⁹. The same crude model was employed as in the case of superelastic scattering from $^{138}\text{Ba}(\cdot\cdot 6s6p \ ^1P)$. The photon detector was placed in the nominal scattering plane at 90° relative to the incident electron beam and was assumed to have infinite angular resolution. The EICP of Bartschat and Madison¹⁰ were used.

Fig. 3 shows the P4 vs. scattering angle behavior for the 1P state excitation in Ne. Dots (crosses) represent modelling calculations carried out with a finite scattering volume of 1mm (2mm) extent. The 1P state is described by pure LS coupling so that P4 is expected to be unity over all scattering angles. Near zero degrees scattering angle, the influence of a finite scattering volume reduces the P4 polarization to a minimum of about 0.8.

For the heavier rare gases, Kr and Xe, we found that, as discussed above, the shape of the modelled P4

vs. scattering angle curve was quite sensitive to the behavior of the theoretical P_ℓ^+ near the "critical" alignment angle. The model calculations plotted in Figs. 4 and 5 result from slightly modifying the P_ℓ^+ behavior predicted by Bartschat and Madison. The calculated behavior of the alignment angle was left unmodified.

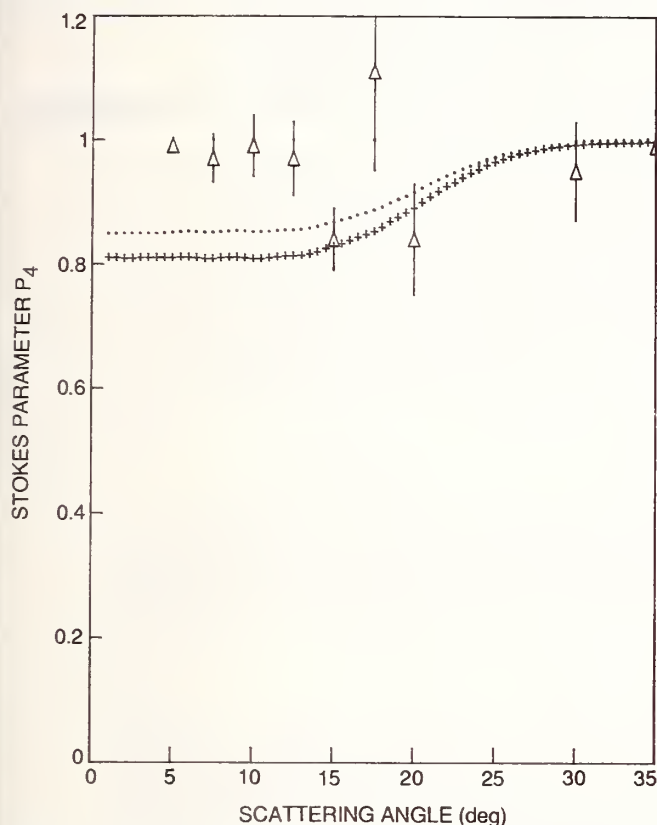


Fig. 3 Model calculations and experimental data⁹ for excitation of Ne $3s'[1/2]_1^0 1P_1$ at 80 eV impact energy.

We performed this exercise in order to check whether the experimental P_4 data, whose deviation from unity is ascribed to spin-orbit coupling effects⁹, could be fit by adjusting only the theoretically predicted behavior of P_ℓ^+ which is not associated with spin-orbit coupling. The fit of the model results to the experimental data in Figs. 4 and 5 is reasonable, suggesting that, under conditions where spin-orbit coupling effects are negligible (i.e. $\cos \varepsilon = 1$ or $\rho_{00} = 0$), extreme distortion in the P_4 measurement can occur for a particular behavior of the coherence parameters P_ℓ^+ and γ (or, equivalently, λ and χ) and a scattering volume of finite extent. The existence of an extended scattering geometry is a necessary condition for this extreme behavior in P_4 to manifest itself. This is illustrated by the fact that, for an ideal, single-point

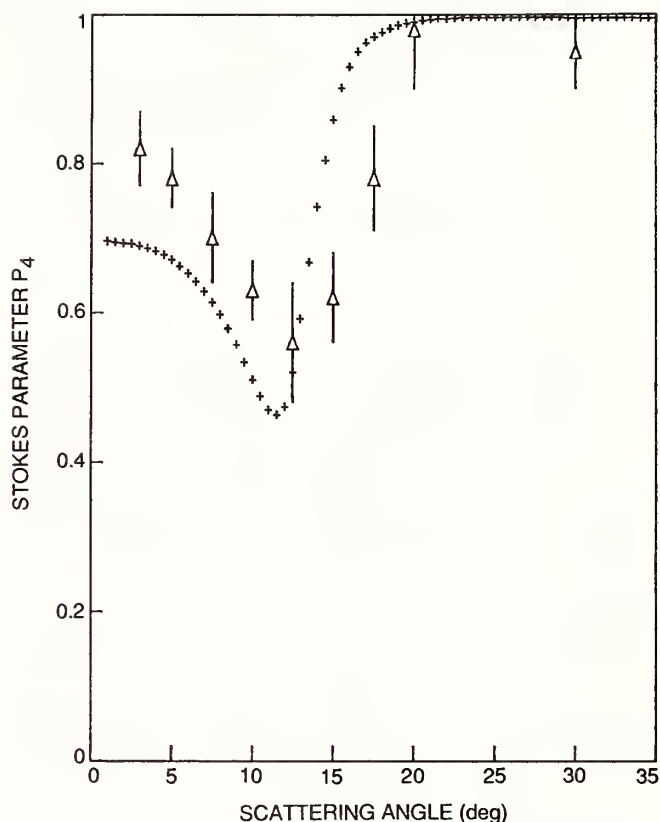


Fig. 4 Model calculations and experimental data⁹ for excitation of Kr $5s'[1/2]_1^0 1P_1$ at 60 eV.

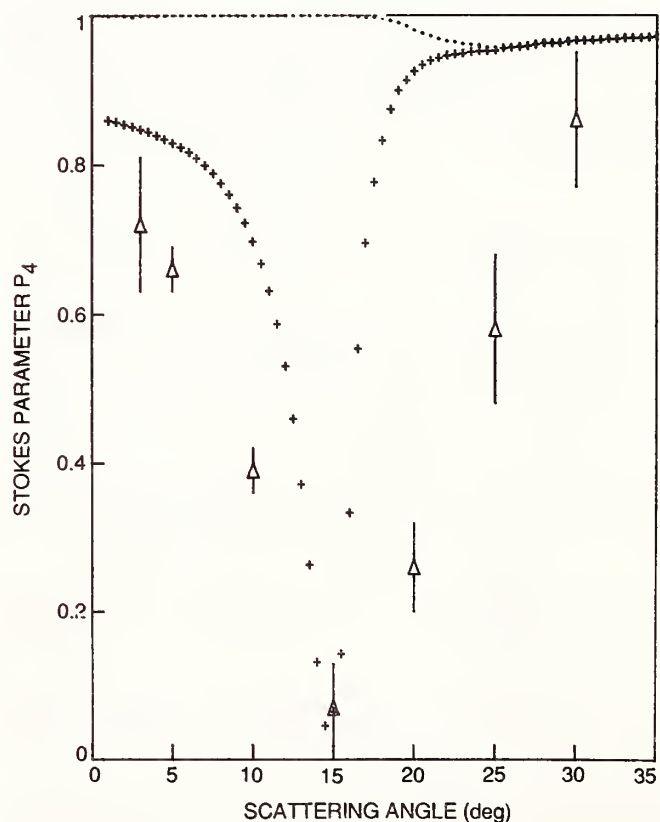


Fig. 5 Model calculations and experimental data⁹ for excitation of Xe $6s[3/2]_1^0 3P_1$ at 30 eV.

scattering at the laboratory frame origin, P_4 , in the case of Kr, is expected to be unity over the range of scattering angles studied, while, in the case of Xe, the dotted line in Fig. 5 shows the predicted behavior of P_4 .

These results will be discussed in more detail in a forthcoming publication¹¹.

Conclusions

Results of our modelling effort imply that measurements of EICP using experimental geometries in which the photon incidence vector (either laser photon in the superelastic scattering experiment or detected photon in the polarization correlation experiment) lies in the nominal scattering plane can be subject to large uncertainties. The influence of an extended scattering volume can produce severe distortion in the measured modulation depth, η , or Stokes parameter, P_4 , which can be misinterpreted as arising from spin-orbit coupling effects. The severity and location (in scattering angle) of this distortion is intimately tied to the behavior of the P_4^+ and γ parameters (or, equivalently, the λ and χ parameters).

Acknowledgements

This work was supported by the National Science Foundation, the National Aeronautics and Space Administration and the U. S. Department of Energy.

References

1. R. T. Brinkman and S. Trajmar, *J. Phys. E* **14**, 245 (1981).
2. N. Andersen, J. W. Gallagher and I. V. Hertel, *Phys. Rep.* **165**, 1 (1988).
3. K. E. Martus, K. Becker and D. H. Madison, *Phys. Rev. A* **38**, 4876 (1988).
4. F. J. da Paixão, N. T. Padial, G. Csanak and K. Blum, *Phys. Rev. Lett.* **45**, 1164 (1980).
5. P. W. Zetner, S. Trajmar and G. Csanak (to be published).
6. D. F. Register, S. Trajmar, G. Csanak, S. W. Jensen, M. A. Fineman and R. T. Poe, *Phys. Rev. A* **28**, 151 (1983).
7. R. E. H. Clark, J. Abdallah, Jr., S. P. Kramer and G. Csanak, *Phys. Rev. A* (to appear).

8. P. W. Zetner, S. Trajmar, G. Csanak and R. E. H. Clark, *Phys. Rev. A* **39**, 6022 (1989).
9. P. Plessis, M. A. Khakoo, P. Hammond, J. J. Corr and J. W. McConkey, *J. Phys. B: At. Mol. Opt. Phys.* (in press, Oct. 1988).
10. K. Bartschat and D. Madison, *J. Phys. B: At. Mol. Phys.* **20**, 5839 (1987).
11. P. W. Zetner and S. Trajmar (to be published).

SPIN DEPENDENCE IN ELECTRON IMPACT IONIZATION OF ATOMIC HYDROGEN

M.S. LUBELL, D.M. CROWE, X.Q. GUO, F.C. TANG, and A. VASILAKIS
Department of Physics, City College of CUNY, New York, NY 10031, USA

J. SLEVIN
Department of Experimental Physics, St. Patrick's College, Maynooth, Co. Kildare, Ireland

M. EMINYAN
Laboratoire de Physique Atomique, Tour 24, Université Paris VII, F-75251, Paris, France

Using beams of polarized electrons and polarized hydrogen atoms, we investigated the spin dependence in impact ionization from threshold to 500 eV. In order to provide greater insight into threshold laws for double escape, we devoted considerable attention to the energy region from 13.6 to 15.3 eV. Our measurements of the cross-section asymmetry, A_I , for electron spins antiparallel and parallel display inconsistencies with a naive application of the Wannier model. Moreover, they suggest the presence of structure, the general features of which can be reproduced by a fit of the Coulomb-dipole model. At higher energies, our asymmetry measurements appear to scale with the incident electron energy, E , according to the relation $A_I \propto E^{-0.7}$.

1. INTRODUCTION

In the context of electron-atom scattering, the electron-hydrogen collision has served for many years as one of the principal testing grounds for the development of theoretical approximation techniques. To great accuracy, the low-energy electron-hydrogen problem can be treated in a non-relativistic framework, as a consequence of which the spin-averaged scattering cross section $\bar{\sigma}$ can be expressed as¹

$$\bar{\sigma} = \frac{1}{4}|f + g|^2 + \frac{3}{4}|f - g|^2 \quad (1)$$

where $\sigma_s = |f + g|^2$ is the singlet cross section, $\sigma_t = |f - g|^2$ is the triplet cross section, and f and g are the direct and exchange amplitudes respectively. As can be seen from Eq. (1), the experimental determination of the spin-averaged cross section falls short of providing detailed knowledge of the individual amplitudes which are calculated theoretically. As a first step toward achieving the finer detail required, we have employed polarized beams to measure the spin-dependent ionization cross-section asymmetry A_I defined by

$$A_I = \frac{\sigma(\uparrow\downarrow) - \sigma(\uparrow\uparrow)}{\sigma(\uparrow\downarrow) + \sigma(\uparrow\uparrow)} \quad (2)$$

where $\sigma(\uparrow\downarrow)$ and $\sigma(\uparrow\uparrow)$ are respectively the angle-integrated ionization cross-sections for incident and atomic electron spins antiparallel and parallel. From an analysis of spin-tagged scattering, it can be shown that A_I is given by¹

$$A_I = |f||g|\cos\theta / \bar{\sigma} \quad (3)$$

where θ is the relative phase between f and g . Alternatively A_I can be expressed as

$$A_I = \frac{\sigma_s - \sigma_t}{4\bar{\sigma}} = \frac{1 - r}{1 + 3r} \quad (4)$$

where r is the ratio of the triplet to singlet cross sections.

The improved insight into the process of impact ionization provided by measurements of A_I can already be seen from exploratory studies of electron-hydrogen scattering carried out several years ago¹ with relatively primitive sources of polarized electrons and polarized hydrogen atoms. Those studies, which utilized a Fano-effect electron source and a thermal-dissociation hydrogen source, revealed previously undocumented deficiencies in virtually all theoretical models at incident electron energies below ~60 eV. Moreover, the apparent non-unity value of A_I at the ionization threshold called attention to the theoretical misconception² that all triplet states should be suppressed at threshold.³ Similar studies carried out for 90° elastic scattering and for a variety of scattering channels for the alkali atoms⁴ have proven to be equally valuable.

2. EXPERIMENTAL METHOD

The general methodology of our present experiment follows that of the earlier work¹ in that the quantity we measured was the ionization counting-rate asymmetry, Δ_I , defined by

$$\Delta_I = \frac{R(\uparrow\downarrow) - R(\uparrow\uparrow)}{R(\uparrow\downarrow) + R(\uparrow\uparrow)} \quad (5)$$

where $R(\uparrow\downarrow)$ and $R(\uparrow\uparrow)$ are the ionization counting rates, normalized to incident beam intensities and corrected for residual gas effects, for the respective antiparallel and parallel electron spin configurations. The quantities Δ_I and A_I are related by the expression¹

$$\Delta_I = A_I P_e P_H (1 - F_2) |\cos \alpha| \quad (6)$$

where P_e and P_H are respectively the electron and hydrogen polarization vectors, α is the angle between them, and F_2 is the fraction of events attributable to hydrogen molecules. In a separate study⁵ we determined that P_H had the value 0.515(5), and from a normalization of our new ionization asymmetry results to our older ones we determined that P_e had the value 0.27(2). On the basis of magnetic field studies in the interaction region, we found that we could take $|\cos \alpha|$ to be 0.995(5). The fraction of events attributable to hydrogen molecules, of course, depended upon the electron beam energy, but with a dissociation fraction of ~0.95 characterizing the hydrogen beam in the interaction region, F_2 never exceeded 0.3 over the entire energy range investigated. The residual gas pressure in the interaction was approximately 5×10^{-9} Torr.

Our experiment employed a crossed-beams geometry, as illustrated in Fig. 1. Polarized electrons were produced by photoemission from a <100> GaAs crystal^{6,7} with the use of 780-nm circularly polarized light generated from a GaAlAs diode laser and prepared by a combination of a half-wave (1/2) and a quarter-wave (1/4) retardation plate, as shown in the figure. Before reaching the interaction region, the extracted electron beam passed through a set of electrostatic electron-optical elements comprising a 90° spherical bender, a series of lenses and steerers, and a 180° hemispherical monochromator, the overall geometric orientation of which ensured that the electron polarization vector, P_e , was pointing either parallel or antiparallel to the direction of the hydrogen beam. The usable electron current, which varied between 30 and 150 nA, was monitored for normalization purposes by a Faraday cup located just beyond the interaction region.

The polarized atomic hydrogen beam⁵ originated in an rf dissociation source and underwent high-field state selection in a pair of permanent hexapole magnets which also served to focus the $m_s = +1/2$ atoms at the interaction region. Upon emerging from the second magnet, the atoms entered a small solenoidal field which adiabatically rotated their spins into a longitudinal direction either parallel or antiparallel to the direction of the hydrogen beam. Additional coils maintained the magnetic field in the longitudinal direction and trimmed it to ~100 mG at the crossed-beams interaction site. Prior to entering the interaction region, the hydrogen beam was collimated to a radial dimension of 3 mm, resulting in a usable average target density of $\sim 10^{10}$ atoms/cm³. For normalization purposes, the hydrogen beam was sampled at the end of its line by a quadrupole mass analyzer (QMA). For purposes of "real-time" background subtraction, the hydrogen beam was equipped with a mechanical chopper located between the two hexapole magnets, as shown in Fig. 1.

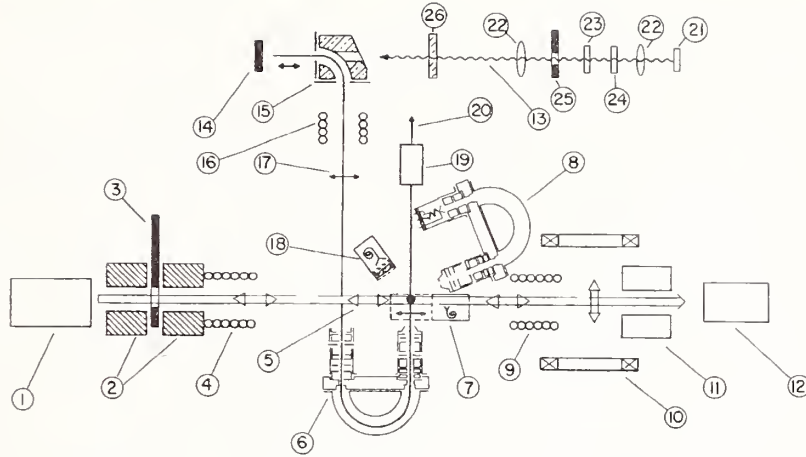


Fig. 1. Schematic layout of the experiment showing (1) hydrogen source, (2) hexapole magnets, (3) hydrogen beam chopper, (4) solenoid, (5) hydrogen polarization vector, (6) electron monochromator, (7) ion detector, (8) electron spectrometer, (9) solenoid, (10) adiabatic spin rotator, (11) Stern-Gerlach polarimeter, (12) QMA, (13) 780-nm laser light, (14) GaAs crystal, (15) 90° spherical bender, (16) solenoid, (17) electron polarization vector, (18) Lyman--alpha detector, (19) Faraday cup, (20) exit to Mott polarimeter, (21) GaAlAs diode laser, (22) lenses (23) 1/4-plate, (24) 1/2-plate, (25) laser beam flag, and (26) vacuum window. Item (11), used for the measurement of P_H , was removed for the present studies as were items (8), (18), and (20).

For ion detection, a channel electron multiplier (CEM) was used, preceded by a grid which prevented electrons or negative ions from reaching the CEM entrance cone. The grid and cone voltages were varied to ensure that the signal was free from photon contamination under the final operating conditions. In order to eliminate the influence of stray electric fields on the ions drifting downstream from the crossed beams site, the interaction region and the CEM were enclosed in a stainless steel box, the dimensions of which were chosen such that a 4π acceptance was still presented to ions having maximum recoil energy.

In carrying out the asymmetry measurements, we sought to reduce systematic effects by reversing the direction of the electron polarization at frequent intervals. To this end, under computer control, we rotated the 1/2 and 1/4 plates through 360° , the former in 8 steps of 45° and the latter in 4 steps of 90° . During data acquisition, we time ordered the retardation plate orientations to produce 8 helicity sets, each of which contained 4 circular polarizations alternating between left and right. Thus we generated 8 sets of data in each of which P_e and P_H alternated between antiparallel and parallel configurations with each configuration appearing twice. Several times we also checked for systematic effects by reversing the magnetic field in the interaction region, thereby reversing the direction of P_H .

For each of the 8 data sets, (i), within a given run, we calculated a single "real" asymmetry, $\Delta_R^{(i)}$ from the average of the rates $R(\uparrow\downarrow)_1^{(i)}$ and $R(\uparrow\downarrow)_2^{(i)}$ for the two antiparallel configurations and the average of the rates $R(\uparrow\uparrow)_1^{(i)}$ and $R(\uparrow\uparrow)_2^{(i)}$ for the two parallel configurations. In order to remove systematic effects associated with hydrogen beam instabilities and drifts in the QMA tuning, as well as spurious helicity-correlated behavior, we followed procedures similar to those used in the earlier work,¹ and for each of the data sets we generated two "false" asymmetries, $\Delta_{F\pm}^{(i)}$, in accordance with the prescription

$$\Delta_{F\pm}^{(i)} = \frac{\left[R(\uparrow\downarrow)_1^{(i)} - R(\uparrow\downarrow)_2^{(i)} \right] \pm \left[R(\uparrow\uparrow)_1^{(i)} - R(\uparrow\uparrow)_2^{(i)} \right]}{\left[R(\uparrow\downarrow)_1^{(i)} + R(\uparrow\downarrow)_2^{(i)} \right] + \left[R(\uparrow\uparrow)_1^{(i)} + R(\uparrow\uparrow)_2^{(i)} \right]}. \quad (7)$$

If any false asymmetry deviated from zero by more than 2.5 standard deviations (a 1% occurrence statistically), we deleted the entire data set to which it corresponded, an approach that is somewhat conservative but justifiable, given our goal of a $\pm 2.5\%$ relative uncertainty in the determination of Δ_I . Using this criterion, we deleted approximately 25% of our events, the vast majority of which failed the cut because of QMA tuning drifts during several isolated periods when the laboratory temperature rose to unacceptably high levels. Having made this cut, we found that each of the sixteen false asymmetries, generated in accordance with Eq. (7), was consistent with zero at the statistical level of 7×10^{-4} when

averaged over all energies examined. A slightly large value of 1.2 for a typical reduced chi-square for approximately 150 degrees of freedom, however, suggests the presence of some residual noise at a very low level.

In the course of our work, we found that the energy of the electron beam drifted slowly upward by as much as 50-75 meV during one e-folding lifetime of the GaAs crystal.⁷ We attribute this drift to the continuing change in the negative electron affinity crystal as the surface slowly degraded following each activation. Since our electron source was typified by a lifetime in excess of 400 h, the energy drift was a relatively minor problem. Nonetheless, in order to achieve a high degree of confidence, we found it useful to calibrate the beam energy every 24 to 48 h by turning off the rf power in the hydrogen source and measuring the molecular ionization rate at energies between 0.3 and 1.0 eV above threshold. For our electron energy spread, characterized by a Gaussian halfwidth, σ , of 75 meV, the convoluted ionization cross section⁸ over this energy range is nearly linear, all the vibrational and autoionizing structure remaining unresolved. We therefore were able to use a linear extrapolation of our measurements to an apparent threshold value of 15.50 eV as a means of calibrating the energy of the beam to a typical accuracy of ± 30 meV. We note that although the energy drift was substantial enough to require periodic calibration, it was sufficiently small that the polarization of the beam remained effectively unchanged. Length restrictions preclude a complete description of the method we used to determine the energy spread of the electron beam. Suffice to say that we carried out a series of ionization rate measurements of atomic hydrogen (source rf turned on) between 13.67 and 13.87 eV. From a study of the Wannier power-law^{9,10} convoluted with various assumed Gaussian energy distributions, we concluded that our beam was characterized by a Gaussian halfwidth, σ , of 75 meV, as indicated above.

In carrying out our asymmetry measurements, we accumulated data at different energies in a quasi-random sequence. In order to check for stability of operation, however, we frequently returned to the measurement of Δ_I at an energy of 15.07 eV. The results, shown in Fig. 2, indicate that our apparatus was indeed stable at a level appropriate to the accuracy of the measurements. At incident energies above the 15.43 eV molecular ionization threshold, we had to correct our asymmetry measurements for events related to molecules. We used a procedure similar to that employed in the earlier work¹ and determined the fraction of events, F_2 , due to molecules with the aid of the QMA mass-2 signals when the hydrogen source rf was on and when it was off. In the present work, we also had to make corrections for dynamic beam loading¹¹ of the interaction region because the hydrogen beam chopping frequency was relatively low (~ 0.5 Hz). With these corrections made, we calculated the atomic ionization asymmetry Δ_I^{H1} according to the general prescription $\Delta_I^{H1} = \Delta_I / (1 - F_2)$, suggested by Eq. (6).

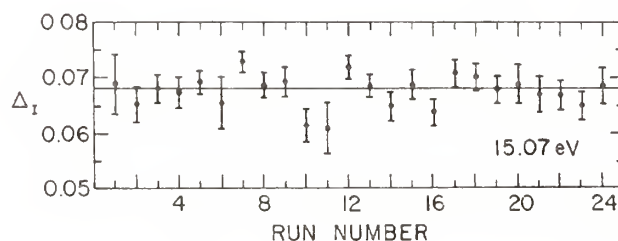


Fig.2. Stability check showing 24 separate measurements of Δ_I at 15.07 eV. The average value is 0.0682(5) with a reduced chi-square of 1.17 for 23 degrees of freedom corresponding to a confidence level of 27%.

3. RESULTS AND DISCUSSION

In Fig. 3 we present our measurements of Δ_I^{H1} for incident energies, E , between threshold and 500 eV, only two points being shown below 15 eV for purposes of clarity. We note that for incident energies above 15.1 eV, the asymmetry is represented quite well by the functional form $\Delta_I^{H1} = 0.47E^{-0.7}$, where E is expressed in eV. In order to place our asymmetry measurements on an absolute scale, we used this functional form, convoluted appropriately, to normalize our results to the data of the earlier work.

Although any individual data point in the earlier work suffers in accuracy and energy resolution by contrast with its corresponding data point in the present work, the normalization procedure involves a sufficient number of measurements that a scaling accuracy of $\pm 7\%$ in A_I is achieved. The normalization of our asymmetry data is consistent with a value of 0.27(2) for the electron polarization, P_e , which although somewhat lower than originally anticipated, is consistent with observations¹² made at a number of other laboratories for GaAs crystals operating at room temperature.

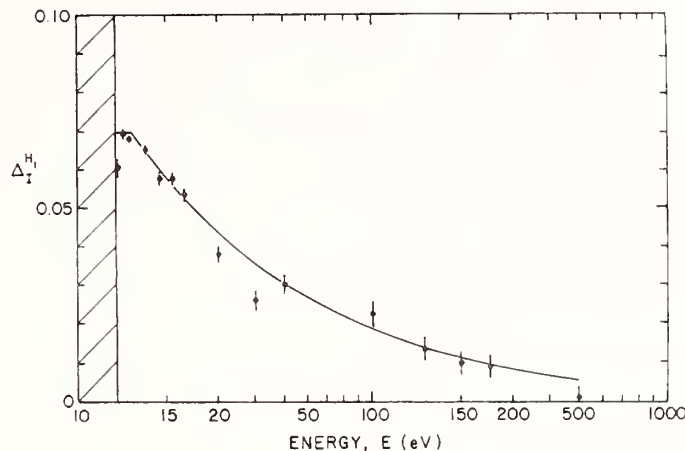


Fig.3. Measured values of ΔI^{H1} with error bars representing one standard deviation uncertainties. The solid line represents a constant value of 0.07 for the electron energy E below 15.1 eV and a power law given by $0.47E^{-0.7}$ above 15.1 eV with E expressed in eV. The hatched region at the left lies below the 13.602 eV ionization threshold.

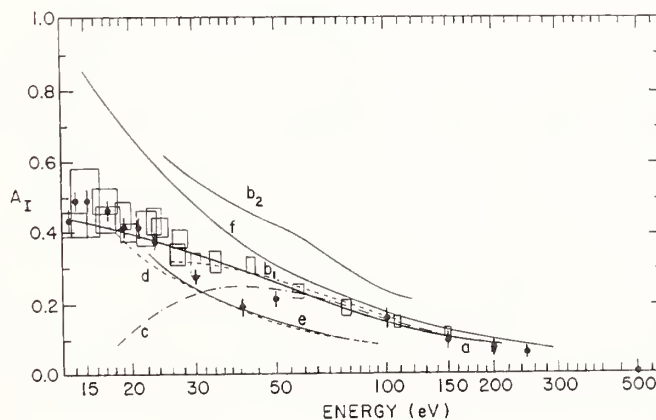


Fig.4. Summary of the asymmetry measurements A_I from the present experiment, shown as closed circles, and those of the earlier work (Ref. 1), shown as open rectangles. In the latter case, the height represents a one standard deviation uncertainty ($\pm\sigma$) while the width reflects the full-width-at-half-maximum energy spread. In the former case, the vertical error bar again represents a one standard deviation uncertainty, but the energy width of ± 75 meV is too small to be seen. The theoretical curves presented represent a sample from the literature: (a) coupled-channel distorted-wave optical potential (Ref. 13), (b₁) Born-exchange (Ref. 14), Born-exchange with exchange maximized (Ref. 14), (c) Born-exchange (Ref. 15), (d) Glauber-exchange (Ref. 16), (e) pseudostate close-coupling (Ref. 17), and (f) modified Born-Oppenheimer (Ref. 18).

Having placed our asymmetry results on an absolute scale, we can compare them with theoretical predictions. Fig. 4. provides such a comparison for a representative number of calculations, along with a display of the data from the earlier work.¹ We observe that one recent calculation by Bray, McCarthy, and Madison¹³ provides a rather good fit to the data over the full energy range down to about 20 eV. Only at

an energy of 40 eV, is there a significant discrepancy, and at this energy there is also a discrepancy between the new and old data. We have no explanation for the disagreement between the new and old data, although we note that the "knee" suggested by the new data is reminiscent of a similar structure observed for the ionization asymmetry in electron-potassium scattering.

We now turn our attention to the threshold region. In Fig. 5 we present our measurements of Δ_I for incident energies, E , between 13.67 and 15.27 eV, as well as one measurement obtained with the centroid of the beam energy at 13.57 eV, 32 meV below the laboratory threshold $E_{th}=13.602$ eV. Within the *full* region ($E_{th} \leq E < 15.27$ eV), our measurements of Δ_I are clearly inconsistent with a linear dependence on energy. A linear fit in fact yields a reduced chi-square of 5.5 for 16 degrees of freedom corresponding to a confidence level of $<10^{-11}$. It therefore appears that some structure is present, with any presumed sharp features masked by the ± 75 meV spread in the energy of the electron beam. We note that if the false asymmetries are plotted as a function of energy, no similar structure is evident.

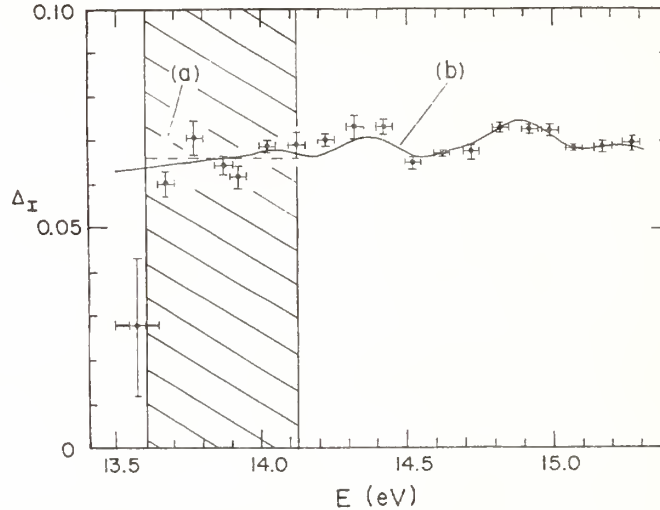


Fig. 5. Measured asymmetries Δ_I for incident electron energies between 13.57 and 15.27 eV. The vertical and horizontal error bars represent one standard deviation uncertainties. The heavy outer bar on the 13.57 eV point illustrates the characteristic energy spread of the electron beam. The curve (a) is a constant function fit in the restricted (hatched) region from threshold (13.6 eV) to ~ 14.1 eV. The curve (b) is taken from the Coulomb-dipole theory (Ref. 19) with fitted model parameters as given in the text.

It is reasonable at this point to compare our results with the predictions of ionization threshold laws. A naive approach to the Wannier law predicts that if the ^3Se and ^1Pe final states are ignored³—the latter is inaccessible in our experiment in any case— Δ_I should be constant throughout a *restricted* region, which for hydrogen has been found to extend for about 500 meV above threshold.¹⁰ Although our ± 75 meV energy spread makes precise comparisons somewhat problematic, we note that a fit of a constant function to our data within this region results in a reduced chi-square of 2.75 for 5 degrees of freedom, corresponding to a confidence level of 0.02. As a crude approximation, we can employ a linear function to test for the trend of Δ_I in the restricted region. The resulting fitted function, having a slope of $+0.019(7)$ eV⁻¹, is characterized by a reduced chi-square of 1.77 for 4 degrees of freedom, corresponding to a confidence level of 0.17. The notion that Δ_I falls with decreasing energy upon approach to threshold is reinforced by the presence of the 13.57 eV data point, which has an anomalously low value, albeit with a large uncertainty. Although this point lies slightly below threshold, it is almost unquestionably dominated by impact ionization events produced by the high-energy tail of the electron distribution and lying within ~ 50 meV of threshold. With photon contamination of the signal ruled out experimentally, the only other contribution to the 13.57 eV signal can arise from Rydberg-excited atoms with principal quantum number $n \geq 41$ which can be field-ionized²⁰ in the vicinity of the ion detector. An analysis of ionization rates slightly above threshold places a strict upper limit of 50% on such a contribution to the 13.57 eV data point. Consequently, even if all of the Rydberg contributions to the asymmetry improbably saturated at the lower bound of $-1/3$ for pure triplet excitation,¹ the value of Δ_I at 13.57 eV could still rise to only 0.065, thus confirming the positive slope suggested by the data points above threshold.

We conclude with a brief comparison of our data to the predictions of the Coulomb-dipole model as developed by Srivastava and Temkin,¹⁹ in which the partial cross sections near threshold obey the relation

$$\sigma = C [1 + (D/\alpha) \sin (\alpha \ln E + \phi)] / [\ln E' - X]^4, \quad (9)$$

where $E'=E-E_{th}$ and where the model parameters can take on different values for singlet and triplet scattering. The Coulomb-dipole prediction for Δ_I follows from Eq. (3). From curve (b) in Fig.5, which represents a fit of the prediction convoluted with our energy spread, it is evident that the Coulomb-dipole model reproduces the general features of the data over the full energy range shown. However with Δ_I/A_I taken as 0.124, the fitted set of model parameters, $\{C_I/C_S=0.321, \alpha_S=27.8, \alpha_I=12.1, X_S=4.58, X_I=4.92, D_S=-2.22, D_I=1.06, \phi_S=3.71, \phi_I=1.80\}$, results in a rather poor reduced chi-square of 2.68 for 8 degrees of freedom, corresponding to a confidence level of ~ 0.01 . We hasten to point out, however that the Coulomb-dipole model may not be *fully* valid over the 1.7 eV range to which we applied it. Moreover, it is intriguing that the confidence level of the fit worsens by several orders of magnitude if the data points are shifted in energy by 70 meV and the energy spread used in the convolution is increased by a factor of two. Nonetheless, it appears that new measurements with improved energy resolution are required if a definitive statement is to be made.

We gratefully acknowledge the financial support of the U.S. NSF, the Research Foundation of CUNY, the U.K. SERC, St Patrick's College, NATO, and the French CNRS. We also wish to thank Prof. A.R.P. Rau, Dr. A. Temkin, Prof. P.A. Souder, and Prof. K. MacAdam for a number of useful discussions.

REFERENCES

1. G.D. Fletcher *et al.*, Phys. Rev. A **31**, 2854 (1985); T.J. Gay *et al.*, Phys. Rev. A **26**, 3664 (1982); M.J. Alguard, *et al.*, Phys. Rev. Lett. **39**, 334 (1977).
2. H. Klar and W. Schlecht, J. Phys. B **9**, 1699 (1976).
3. C.H. Greene and A.R.P. Rau, Phys. Rev. Lett. **48**, 533 (1983); J. Phys. B **16**, 90 (1983).
4. See for example M.H. Kelley *et al.*, Phys. Rev. Lett. **51**, 2191 (1983); J.J. McClelland *et al.*, Phys. Rev. Lett. **55**, 688 (1985); **56**, 1362 (1986); **58**, 2198 (1987); J. Phys. B **20**, L385 (1987); Phys. Rev. A **40**, 2321 (1989); G. Baum *et al.*, J. Phys. B **14**, 4377 (1981); **18**, 531 (1985); Phys. Rev. Lett. **57**, 1855 (1986); D. Hils *et al.*, J. Phys. B **15**, 3347 (1982); P. Nass *et al.*, Z. Physik D **11**, 71 (1989).
5. N. Chan *et al.*, Z. Physik D **10**, 393 (1988).
6. F.C. Tang *et al.*, Rev. Sci. Instrum. **57**, 3004 (1986).
7. X.Q. Guo *et al.*, Rev. Sci. Instrum., in press.
8. J.W. McGowan *et al.*, Phys. Rev. **167**, 52 (1969).
9. G. Wannier, Phys. Rev. **90**, 817 (1953); A.R.P. Rau, Phys. Rev. A **4**, 207 (1971); R. Peterkop, J. Phys. B **4**, 513 (1971); T.A. Roth, Phys. Rev. A **5**, 476 (1971); H. Klar, J. Phys. B **16**, 99 (1983).
10. J.W. McGowan and E.M. Clarke, Phys. Rev. **167**, 43 (1969).
11. M.S. Lubell *et al.*, Phys. Rev. A, submitted.
12. R.J. Celotta and G. Baum, private communications.
13. I. Bray *et al.*, Phys. Rev. A, submitted.
14. R. Peterkop, Zh. Eksp. Teor. Fiz. **41**, 1938 (1961) [Sov. Phys.-JETP **14**, 1377 (1962)].
15. S. Geltman *et al.*, Proc. Phys. Soc. London **81**, 375 (1963).
16. J.E. Golden and J.H. McGuire, Phys. Rev. Lett. **32**, 1218 (1974).
17. D.F. Gallaher, J. Phys. B **7**, 362 (1974).
18. V.I. Ochkur, Zh. Eksp. Teor. Fiz. **47**, 1746 (1965) [Sov. Phys.-JETP **20**, 1175 (1965)].
19. A. Temkin, Phys. Rev. Lett. **16**, 835 (1966); **49**, 365 (1982); J. Phys. B **7**, L450 (1974); IEEE Trans. Nucl. Sci. NS-30, 1106 (1983); Phys. Rev. A **30**, 2737 (1984); A. Temkin and Y. Hahn, Phys. Rev. A **10**, 708 (1974); M.K. Srivastava and A. Temkin, Phys. Rev. A, submitted.
20. T.F. Gallagher, Rep. Prog. Phys. **51**, 143 (1988).

PROGRESS ON SPIN DETECTORS AND SPIN-POLARIZED ELECTRON SCATTERING FROM Na AT NIST

Jabez J. McClelland

Center for Atomic, Molecular, and Optical Physics, NIST, Gaithersburg, MD

Recent progress in the Electron Physics Group at NIST is discussed. Improvements have been made on the low-energy diffuse-scattering spin analyzer, reducing instrumental asymmetries and boosting the effective Sherman function. A figure of merit of 2.3×10^{-4} has been achieved. Thorium has been used as a target in a 100 keV retarding Mott spin analyzer, resulting in an effective Sherman function as high as 0.49. This increased Sherman function, together with an increased scattering intensity, results in a factor of 2 increase in the figure of merit. Good agreement is seen between experiment and theoretical predictions of the Sherman function for thorium. A hierarchical description of the T -matrix is discussed as a context for interpreting recent results on spin-polarized electron scattering from optically pumped sodium. Results are presented for elastic and superelastic scattering at 20 eV incident energy.

1 Introduction

In this paper, I would like to discuss three separate subjects. Though they may seem somewhat unrelated, they all pertain to the general theme of our work on state-selected electron-atom scattering in the Electron Physics Group at NIST. In the first two sections, I will present some recent work on the improvement of experimental techniques associated with the measurement of electron spin. Innovations in the design of a compact low-energy spin analyzer will be discussed, followed by a description of some recent work on improving the Sherman function of a Mott analyzer by using thorium as a target. In the last section, I will consider some of our latest state-selected results for 20 eV electron scattering from sodium, with particular emphasis on how they contribute to a complete picture of electron-sodium scattering.

2 Improved low energy electron spin detector

The low-energy diffuse-scattering electron spin analyzer, developed¹ in the Electron Physics Group at NIST in 1986, has led to significant advancements in the application of polarized electron studies to a large number of fields, including electron microscopy² and surface photoemission.³ The high detection efficiency of the analyzer ($I/I_0 \sim 0.01$), combined with a spin-analyzing power (effective Sherman function S_{eff}) of ~ 0.1 leads to a figure of merit $\mathcal{F} = S_{\text{eff}}^2 I/I_0$ of about 1×10^{-4} . This figure of merit is comparable with that of the best Mott detectors. The small size of the detector (about 10^{-3} m^3) makes this detector an extremely useful tool for a wide

range of applications. Figure 1a shows a sketch of the original detector design. The principle of operation is in essence the same as a conventional Mott detector—the polarized electron beam to be analyzed is incident upon a gold target, and backscattered electrons are collected with two detectors in a plane perpendicular to the component of the polarization to be measured. Two sets of detectors allow measurement of the two transverse components of the spin.

The major difference between this detector and a conventional Mott polarimeter is the ability to operate at a low energy, i.e., 150 eV, instead of 100 keV. In order to make low energy operation possible, the surface of the gold target must be kept clean. This is accomplished by operating the detector in relatively good vacuum ($\sim 10^{-9}$ Torr), and periodically evaporating a fresh gold film on the target. The high detection efficiency of the detector results from the high backscattering coefficient at 150 eV, and also from the large solid angles collected by the channelplate detectors.

Though the original design of the detector operates quite well, there are two areas in which possibilities for improvement have become evident. The improvements have been incorporated in a new design, which is now in operation.⁴

The first improvement has to do with instrumental asymmetries resulting from the sensitivity of the detector to angular and positional displacements of the incident electron beam. This problem can be particularly troublesome when the detector is used in conjunction with scanning electron microscopy, but is of concern in other applications as well, especially if the source of polarized electrons is not spatially stable. The cause of the sensitivity lies in the angular dependence of the cross section

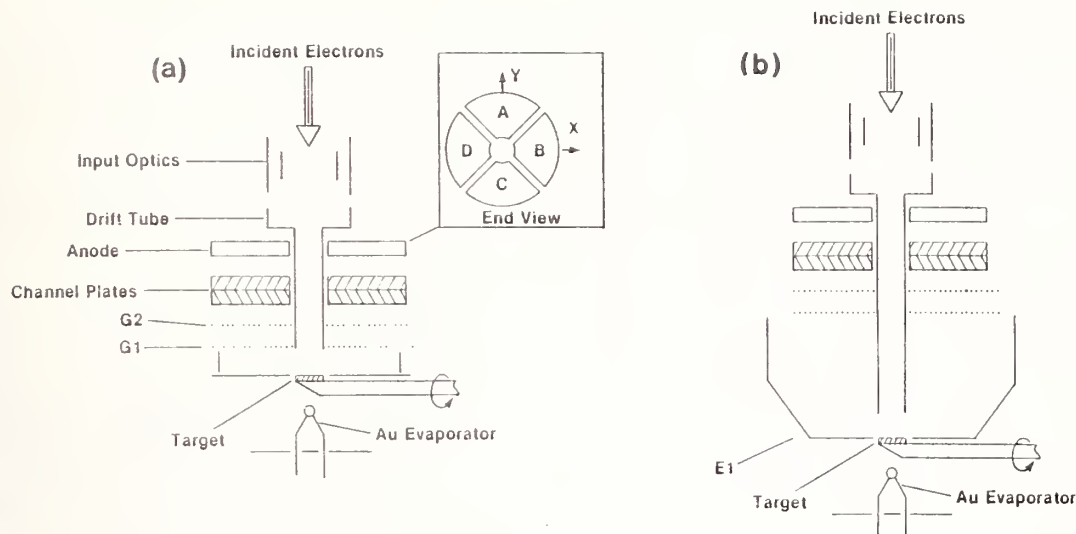


Figure 1. Low-energy diffuse-scattering electron spin analyzer. (a) Original design¹ (G1 = shield grid, G2 = retarding grid) (b) New design,⁴ showing negatively biased electrode (E1).

and the variation of the solid angles subtended by the two electron detectors as the beam is displaced.

It was found that, by altering the geometry of the detector and installing suitable optics at the input, instrumental asymmetries could be dramatically reduced. The reduction occurs because the angular dependence of the cross section and the solid angle variation can be made to cancel each other.⁵ For example, if a paraxial incident beam passes through a simple einzel lens with focus located between the lens and the target, a spatial displacement of the incident beam is converted at the target into a spatial displacement in the opposite direction plus an angular displacement. The spatial displacement will increase the intensity in the near detector, while reducing it in the far one because of solid angle effects. The angular displacement, however, will decrease the intensity in the near detector and increase it in the far one because the cross section decreases for angles farther from the backscattered direction. By correctly choosing the geometry of the detector, these two effects can be made quite linear over a large range, and so compensation involves a rather simple electron optical design process. In a detector constructed on this principle, using a simple einzel lens, we were able to obtain instrumental asymmetries as low as 0.0035/mm over a displacement of up to 4 mm.

The second improvement concerns optimization of the effective Sherman function of the detector. This was done by careful consideration of the two major influences on the effective Sherman function, i.e., the range of scattering angles over which the channelplate detectors integrate, and the range of inelastic electrons allowed to reach the channelplate detectors.

For 150 eV elastic scattering from an amorphous gold target, the Sherman function generally decreases as one goes closer to scattering in the backward direction. At 180° (full backward direction) it is identically zero by symmetry. Thus the effective Sherman function can be optimized by collecting over a selected interval of backscattering angles, usually not exceeding 150°.

In addition to its angular dependence, the Sherman function has a dependence on the amount of energy lost in scattering from the target. Elastically scattered electrons have the largest Sherman function, while inelastics have a smaller and smaller Sherman function as the energy loss increases. Thus the inclusion of inelastically scattered electrons in the set of detected electrons, though desirable for increasing I/I_0 , tends to decrease the effective Sherman function of the detector. The inelastic window must therefore be carefully controlled to balance the increased collection efficiency against the decrease in S_{eff} . To accomplish this, the detector is fitted with a retarding grid to optimize the energy range of the inelastic electrons collected.

By examining the original design of the detector (Figure 1a) it is evident that the retarding grid is not optimally designed for either the scattering angle range or the inelastic window. A suboptimal angular range is emphasized, since electrons travelling in the backward direction pass through the grid, while those travelling at smaller scattering angles (closer to 90°) are repelled because their velocity component perpendicular to the grid is reduced by $\cos \theta$. Also, because of this angular dependence of the retarding energy, the cut-off energy for inelastically scattered electrons is a strong function of scattering angle, making it impossible to choose a sin-

gle inelastic window for all angles.

These difficulties have been remedied in the new design, shown in Figure 1b, by moving the scattering target further from the channelplate detectors and adding a negatively biased electrode around the target region. With this arrangement, the trajectories of the scattered electrons from a large range of angles are made perpendicular to the retarding grid before passing through it. Thus, all scattering angles are treated more equally by the retarding grid, eliminating the emphasis on low-Sherman-function backscattered electrons, and also providing the same energy window for all scattering angles.

The results of the implementation of the new design features are a Sherman function of up to 0.15 and a figure of merit as high as 2.3×10^{-4} . This represents a significant improvement in the performance of the low energy diffuse-scattering electron spin detector, and will increase its utility in a broad range of fields.

3 Use of thorium in a Mott analyzer

As discussed in the preceding section, optimization of electron spin detectors has been a concern in our group recently. To this end, some work has also been done looking for ways to increase the effective Sherman function of a Mott analyzer. If this can be done without a corresponding loss in the detection efficiency I/I_0 , performance of the detector can be dramatically enhanced. Since the figure of merit of a detector is proportional to the square of the effective Sherman function, increasing S_{eff} has a much larger potential benefit than increasing the detection efficiency. In addition, a higher S_{eff} is advantageous independent of the figure of merit, in that instrumental asymmetries become less significant compared to a larger "real" asymmetry.

Knowing that the physical process underlying the spin sensitivity of Mott detection is the spin-orbit interaction, it is natural to search for a target that has the largest possible spin-orbit effect when electrons scatter from it. Since the spin-orbit interaction increases as the target atomic number Z gets larger, one is led to look for suitable target materials at the end of the periodic table. Thorium is a high- Z material ($Z = 90$) for which thin target discs are readily available, so we have undertaken a study of the effective Sherman function of a Mott detector using a thorium target.⁶ The results of our study are shown in Figure 2. A GaAs polarized electron source was used as a source of polarized electrons, and the Mott detector was of a 100 keV cylindrical design first developed at Rice University.⁷ The effective Sherman function was measured for a 0.09 mm thick thorium target as a function of incident electron energy over the range 20–100 keV. An energy window of 25 eV was maintained with suitable retarding voltages at the detectors.

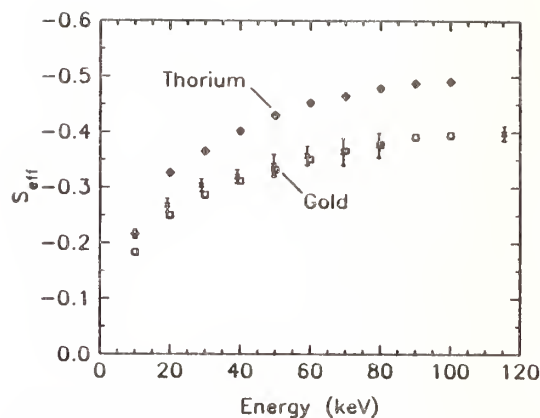


Figure 2. Effective Sherman function S_{eff} versus scattering energy. Crosses represent data of Gray *et al.*⁸

Similar measurements were done for a 1250 Å gold foil for comparison with previous gold measurements⁸ and the new thorium results. Also done, but not displayed here, were measurements of the dependence of S_{eff} on the size of the inelastic window.

The effective Sherman function for the thorium target was found to be significantly higher than it was for the gold. At 100 keV, the gold S_{eff} reaches a maximum magnitude of 0.39, while the thorium S_{eff} is as high as 0.49. At lower energies, the thorium effective Sherman function is as much as 30% higher. In addition, the scattering intensity for the thorium target was found to be about 15% greater than for the gold target. The combination of these effects results in about a factor of 2 increase in the figure of merit when thorium is used as a target.

Besides improving the effective Sherman function of the Mott analyzer, we were able to provide some interesting comparisons with theory as well. First, our incident electron beam polarization was calibrated with a measurement at 100 keV on the gold target. A value of 0.39 is generally accepted as the correct value for the Sherman function at this energy.⁸ This value allowed us to put our gold measurements on an absolute scale, after which they showed agreement with previous retarding Mott measurements,⁸ as well as with the recent theory of Ross and Fink.⁹

Comparison could then be made with similar calculations by Ross and Fink for thorium, and excellent agreement was found at 100 keV. The measured value of the Sherman function was 0.491 ± 0.009 , and the theoretical value was 0.485. Though this does not represent a fully independent absolute experimental determination of the Sherman function (a double scattering experiment is required for this), it does show good internal consistency within the theory.

The above mentioned contributions to the advancement of electron-spin polarimetry will hopefully increase the prospects for "complete" electron-atom scattering experiments, in which the polarizations of the incoming electrons, the atomic target, and the scattered electrons are all under experimental control in a single experiment. Given the large body of work in the past year alone on the improvement of spin polarimetry,^{4,6,10,11} the future for such experiments seems bright.

4 State-selected electron scattering from sodium at 20 eV

Recently, our ongoing research efforts to study electron scattering from sodium with spin-polarized electrons and atoms have produced a set of elastic scattering data at 20 eV, and a set of superelastic data at 17.9 eV incident energy. These data represent a very extensive (though not yet "complete") set of measurements which yields a broad spectrum of specific information for comparison with theory. Before discussing the results themselves, I would like to outline some thoughts on how measurements of the type we are involved in connect with theoretical calculations.

4.1 The T -matrix

Most state-of-the-art *ab initio* scattering calculations, such as close-coupling calculations, have as their most immediate output a T -matrix. This matrix, which sometimes takes the form of an S -matrix or K -matrix (i.e. reactance matrix), provides the link between an *ab initio* solution of Schrödinger's equation and the prediction of observed scattering intensities. Once a T -matrix is calculated, scattering intensities are arrived at through complex scattering amplitudes, which are generally expressed as sums over T -matrix elements with various coefficients, such as Clebsch-Gordan coefficients, spherical harmonics, etc. For example, consider the scattering amplitudes for excitation of the different M -sublevels in the sodium 3s-3p transition:*

$$f_M^S(\theta, \phi) \propto \sum_{L,l=L\pm 1} i^{L-l} (2L+1)^{1/2} \begin{pmatrix} l & 1 & L \\ -M & M & 0 \end{pmatrix} \times Y_l^{-M}(\theta, \phi) T_l^{S,L}(3s-3p) \quad (1)$$

The T -matrix itself is a multidimensional matrix with various subscripts corresponding to the different channels in a scattering process. Once the incident energy of the electron is chosen, which then becomes the energy

of the system in the solution to Schrödinger's equation, all the T -matrix elements corresponding to the various channels can in principle be calculated.

The elements of the T -matrix can be thought of in a hierarchical sense in order to facilitate keeping the multidimensional nature of the matrix in mind (see Figure 3). At the top of the hierarchy are the various energy channels open to the system. These correspond to transitions that may occur in the atomic target. There is a group of elements for each transition energetically allowed, including no transition at all (i.e., elastic scattering). For example, in sodium, we speak of the "3s-3s" channel, the "3s-3p" channel, the "3p-4s" channel, etc.

The next level of the hierarchy corresponds to the spin channels accessible to each transition in the scattering system. There may be only one channel at this level, as would be the case for scattering from a closed shell target such as helium at low energy where spin-orbit effects can be ignored, or there may be several. In the case of low-energy electron scattering from a light one-electron atom, such as hydrogen or an alkali (considered "one-electron" to a good approximation), there are two channels, the singlet and the triplet. These correspond to the two possible relative orientations of the incident electron and the target electron. In heavier atoms, where the spin-orbit interaction becomes significant and $L-S$ coupling breaks down, there may be more channels. In fact, in this case the separation between this hierarchy level and the next one down becomes less clear. For the present discussion, however, we shall ignore these effects.

The third level of the hierarchy corresponds to a series of orbital angular momentum channels. If no angular momentum is transferred between the electron and the target, this level consists simply of a series of channels corresponding to the partial waves used to describe the scattering. Each channel describes how a partial wave with a particular value of L scatters from the atom. The set of partial waves is technically infinite, but in practice is usually truncated at some large value of L .

If, however, angular momentum is transferred between the electron and the target, the angular momentum level of the hierarchy is split into two channels, corresponding to exactly how the angular momentum is transferred. For example, in the case where the atom undergoes an $S \rightarrow P$ transition, the extra unit of angular momentum can come from the L th partial wave by changing it into either an $L+1$ or an $L-1$ wave, according to the rules of addition of angular momenta. There is a partial wave series for each of these ways in which angular momentum can be transferred.

The T -matrix, then, has energy level channels, spin channels, and angular momentum channels. In order

*This expression is shown for illustrative purposes only. It may prove useful in the upcoming discussion, but the reader is referred to a text on electron scattering¹² for a discussion of all the details.

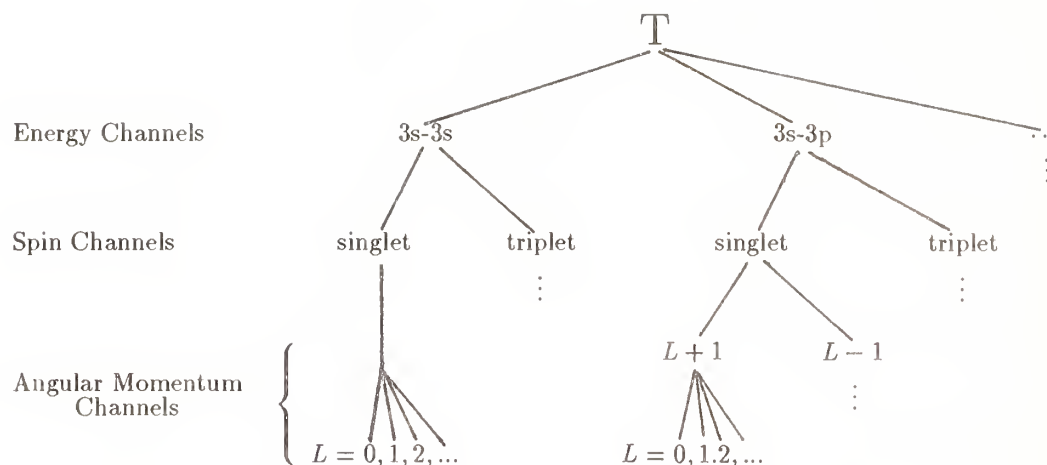


Figure 3. T -matrix hierarchy for electron-sodium scattering.

to generate a simple total scattering intensity, one must sum over all these channels. Clearly, total scattering intensities do not provide a very exacting test for theoretical predictions. Very real possibilities exist for fortuitous cancellations between the various channels, the result being good agreement between experiment and theory for the wrong reason. The only way to provide a good experimental test of a theoretical approach is to examine all elements of the T -matrix individually, to the extent that this is possible. This can only be done in state-selected scattering experiments in which all experimental variables are resolved.

Let us examine what experimental techniques can be used to probe the different hierarchies of the T -matrix. The first level, which consists of the atomic energy level channels, is in part trivial to sort out experimentally. One needs only an energy analyzer on the experiment, which is quite commonplace today. This allows measurement of the ground state elastic channel, as well as the various transition channels connecting the ground state to the excited states of the atom. The first level of the T -matrix hierarchy, however, contains many more channels than these. For a complete measurement at this level, one must also measure elastic scattering from each of the excited states, as well as inelastic scattering between different excited states. Measuring these cross sections becomes much more difficult, as it usually involves some sort of laser excitation in combination with the electron scattering experiment. Very little experimental work has been done on these other channels,^{13,14} though they represent a significant portion of the T -matrix.

The spin-channel level of the T -matrix hierarchy has received a great deal of attention lately. The spin of the incident electron can be put under experimental control through the use of a polarized electron source, the spin of

the atomic electron can be manipulated through optical pumping methods, and the spin of the scattered electron can be measured with a Mott polarimeter, as discussed in the first two sections of this paper. A large body of work has been done on investigations involving the role played by the electron spin in scattering,¹⁵ though few true "complete" measurements have been done.

The angular momentum channels in the T -matrix present somewhat of a problem for experiments. In an ideal world, one would like to be able to measure the scattering process partial wave by partial wave, examining the contribution of each individually. This is generally impossible, though it can be accomplished in a very limited sense by measuring at very low energies where only the first partial wave contributes, or by studying the somewhat analogous process of multiphoton ionization, in which selection rules limit the number of partial waves that can play a role.

By measuring the angular dependence of electron scattering intensities, however, one can obtain most of the partial wave information needed. An angle-resolved intensity is, after all, essentially a "Fourier transform" of the partial wave series, and a complete measurement over the entire angular range can be "back-transformed" to extract the coefficients for each of the individual partial waves. The coefficients are generally complex, though, so some information is lost, but the amount of information obtained is nevertheless quite substantial.

In the situation where angular momentum is transferred between the electron and the target, the angular dependence of the intensity still provides information on the individual partial wave contributions in a "Fourier transform" sense. Now, however, we also have the different transfer channels, e.g., $L+1$ and $L-1$ in a $\Delta L = 1$ transition. These can be investigated by means of align-

ment and orientation studies. In this type of study, the angular momentum state of the atom is either probed after collision in a coincidence experiment, or prepared before collision in a superelastic scattering experiment. The probabilities of exciting the different M -sublevels of the excited state, along with phase relations between the corresponding amplitudes, are measured in either case. In the coincidence measurement, the Stokes parameters of the fluorescent light are determined; in the superelastic case the atoms are optically pumped with different light polarizations. The information obtained from these studies relates directly back to the different angular momentum transfer channels in the T -matrix, by way of some Clebsch-Gordan algebra or perhaps some state-multipole formalism.

It should now be clear what is involved in generating a complete set of measurements which can verify all the predictions of an *ab initio* electron scattering calculation. One needs energy resolution to fix the target excitation channel, spin resolution to fix the spin state of the scattering system, angular resolution to determine the various partial wave contributions, and alignment/orientation information to separate the angular momentum transfer channels. A complete set of measurements entails measuring all possible elastic and inelastic excitation channels, with complete spin and angular momentum resolution. This is certainly a massive task, which any single laboratory or research group can only begin to accomplish. Nevertheless, given the large number of research efforts in this field around the world, it can be reasonably hoped that the combined results will represent significant progress toward this goal.

4.2 Experimental results

The foregoing discussion of the T -matrix has hopefully provided a reasonable context for our most recent results on electron scattering from optically pumped sodium with spin-polarized electrons. For this particular work, we have concentrated on an electron energy of 20 eV, and have measured both elastic scattering from the ground state and superelastic scattering from the first excited state ($3P$). The superelastic results involve measuring de-excitation of the $3P$ -state in order to obtain alignment and orientation information about the time-inverse inelastic $3S-3P$ excitation. Thus they were obtained with an incident energy of 17.9 eV in order to make the energy of the electrons after scattering equal to 20 eV (the excitation energy of the $3P$ -state is 2.1 eV).

Figure 4 shows the elastic scattering results, expressed in terms of a spin asymmetry as a function of scattering angle. This quantity, which highlights the spin dependence in the scattering and hence in the T -matrix, is determined by measuring intensities with incident and

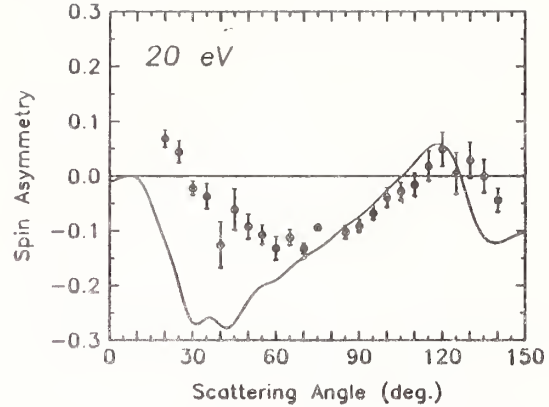


Figure 4. Spin asymmetry for elastic electron scattering from Na at 20 eV. Circles, experiment; solid line, theory of Oza.¹⁶

atomic spin either parallel or antiparallel to each other. The asymmetry is given by

$$A = P_e^{-1} P_A^{-1} \frac{I_{\uparrow\downarrow} - I_{\uparrow\uparrow}}{I_{\uparrow\downarrow} + I_{\uparrow\uparrow}}, \quad (2)$$

where P_e and P_A are the electron and atom beam polarizations, and $I_{\uparrow\downarrow}$ and $I_{\uparrow\uparrow}$ are the antiparallel and parallel intensities, respectively. Calculated in this way, the asymmetry is equivalent to a normalized difference between the singlet and triplet scattering cross sections. It can range from a value of $-1/3$ when the triplet channel dominates, to a value of $+1$ when singlet dominates. The experimental results in Figure 4 show that at this energy, the scattering is largely triplet over most of the angular range, with a slight singlet dominance at large and small angles.

Also shown in Figure 4 is the spin asymmetry from a 4-state close-coupling calculation of Oza.¹⁶ The agreement between experiment and theory is quite good at large angles, beyond about 60° , but significant differences appear at smaller angles. Below 30° , the theory still predicts a larger triplet cross section, while the experiment indicates that singlet has taken over.

Combined with an absolute determination of the differential cross section for elastic scattering from the sodium ground state, our results provide a nearly complete determination of this energy channel of the T -matrix. All that is missing is a measurement of the relative phase between the singlet and triplet scattering amplitudes, which must be determined by measuring the spin of the scattered electron while still controlling the atomic and incident electron spins.

Our superelastic results are shown in Figure 5.¹⁷ Since this energy channel involves a ΔL of 1, we must concern ourselves not only with the spin channels, but also with the angular momentum transfer channels in the T -matrix. Thus there is a larger set of parameters

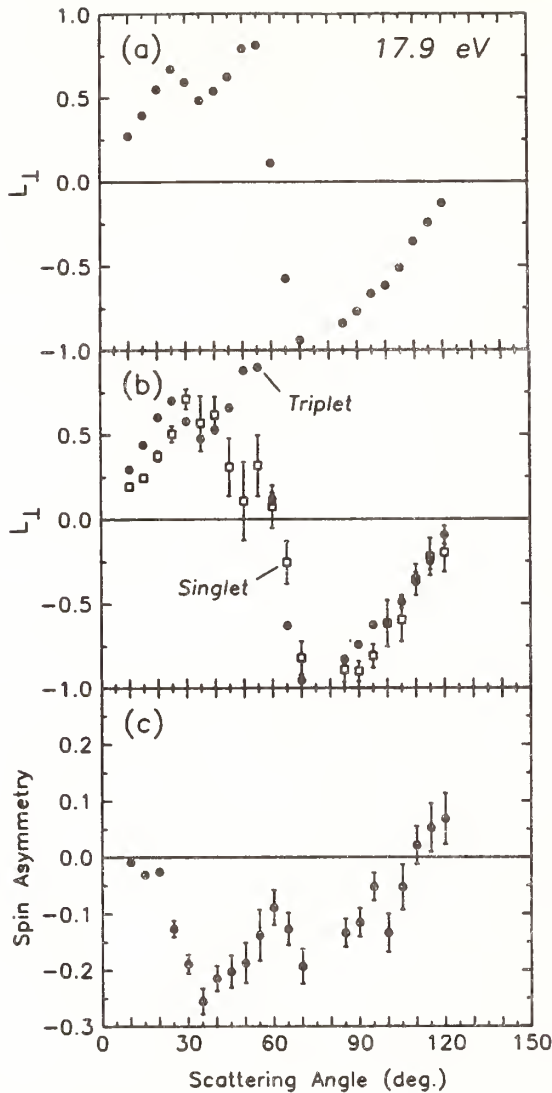


Figure 5. Superelastic electron scattering from Na at 17.9 eV. (a) L_{\perp} measured with unpolarized electrons. (b) L_{\perp} separated into singlet and triplet contributions. (c) Spin asymmetry, averaged over M_L -excitations.

that must be measured in this case. We have followed the tradition of discussing the extra parameters associated with angular momentum transfer in terms of physical quantities describing the atomic wave function.¹⁸ One such quantity is L_{\perp} , the net angular momentum transferred perpendicular to the scattering plane. By optically pumping with circularly polarized laser light incident perpendicular to the scattering plane, we can conveniently determine L_{\perp} in terms of the scattering intensities I_+ and I_- for σ^+ and σ^- polarization of the laser:

$$L_{\perp} = \frac{I_+ - I_-}{I_+ + I_-}. \quad (3)$$

Equation 3 shows that L_{\perp} is a normalized difference

between intensities associated with excitation (or de-excitation) of $M = \pm 1$ sublevels, and hence contains the necessary angular momentum transfer channel information. Phase difference information, which completes the picture for these channels, is obtained from measurements of P_{in} and γ . These physical parameters result from experiments with linearly polarized light, which we do not consider here.

Figure 5a shows our angle-resolved measurements of L_{\perp} for 17.9 eV superelastic scattering. The shape of the curve is similar to most measurements of L_{\perp} in most systems, in that it goes initially positive, crosses over to large negative values at intermediate angles, then increases toward zero at large angles. This particular curve is interesting in that it has a double positive peak at the smaller angles. At present, we do not have a theoretical curve for comparison with our experimental results.

Having separated the angular momentum transfer channels, we must now turn to the spin channels. The singlet and triplet spin channels are still an important part of this inelastic scattering channel, so they must also be resolved. The resolution is expressed by separating L_{\perp} into singlet and triplet versions L_{\perp}^S and L_{\perp}^T , and by determining the spin asymmetry (Equation 2) averaged over angular momentum transfer.¹⁹ This is accomplished experimentally by using spin-polarized incident electrons, and by virtue of the fact that the optical pumping process automatically produces a spin-polarized excited state—spin “up” with σ^+ light and spin “down” with σ^- light. The exact expressions for L_{\perp}^S , L_{\perp}^T and A in terms of scattering intensities are somewhat complicated, so they are not shown here (see Reference 19). L_{\perp}^S and L_{\perp}^T both have forms similar to L_{\perp} ; the complications arise mostly from corrections for incomplete electron beam polarization.

Figure 5b shows the experimental results for L_{\perp}^S and L_{\perp}^T . There does not appear to be much of a difference in the way angular momentum is transferred in the two spin channels, except around a scattering angle of 50°. Here we see a prominent peak in L_{\perp}^T , but no peak in L_{\perp}^S . This indicates that the second peak in the L_{\perp} curve of Figure 5a is due entirely to the triplet channel.

Though there is little difference in the way angular momentum is transferred in this inelastic channel, there is quite a large difference in the cross sections for triplet and singlet scattering. This is seen in Figure 5c, which shows the spin asymmetry. In fact, around 30°, the asymmetry almost reaches its maximal value of $-1/3$, corresponding to pure triplet scattering. It is also interesting to compare Figure 5c with Figure 4, which shows the spin asymmetry for elastic scattering. The two curves are remarkably similar over the entire angular range, the difference being only that the inelastic curve is generally larger in magnitude and has a little more

structure. This indicates that at this particular energy, the way in which the T -matrix is partitioned into spin channels is quite similar for the two energy channels.

As was the case for elastic scattering, these superelastic experiments constitute a nearly complete determination of all the accessible experimental information on a particular energy channel in the T -matrix. When combined with an absolute cross section measurement, the absolute magnitudes of all the relevant scattering amplitudes can be determined. What is missing from the superelastic measurements performed to date is once again phase difference information. Some form of phase differences are measurable by scattering unpolarized electrons from atoms excited with linearly polarized light, but the singlet and triplet contributions cannot be simply extracted from these. Combining spin-polarized incident electrons with linearly polarized optical pumping of the target is not sufficient to extract the necessary information. Measurement of the electron spin after collision, perhaps in combination with elliptically polarized optical pumping not perpendicular to the scattering plane,¹⁹ is necessary for a determination of all the phase differences.

5 Conclusion

The elastic and superelastic scattering results presented here represent a concerted effort to learn all there is to know about electron scattering from sodium at a fixed scattering energy of 20 eV. Though there is a great deal of work still to be done, we can at least say that all levels of the T -matrix (see Figure 3) have been probed in a single batch of measurements. Energy channels, spin channels and angular momentum channels have all been investigated, mostly in a "complete" sense, with the exception of phase difference information. The two major blocks of work still to be done involve measuring the cross sections for as many of the transitions in sodium as possible, and measuring with spin analysis after collision to extract the relative phases of all the various scattering amplitudes. The latter of these awaits significant breakthroughs in the efficiency of spin polarization detectors. The results described in the first two sections of this paper represent our efforts to further the field of spin polarimetry, in the hope that the truly complete experiment will be realizable in the near future.

6 Acknowledgements

Major contributions to the work described here have been made by members of the Electron Physics Group at NIST. This work is supported in part by the U.S. Department of Energy, Office of Energy Research, Division of Chemical Sciences.

References

1. J. Unguris, D.T. Pierce, and R.J. Celotta, *Rev. Sci. Instrum.* **57**, 1314 (1986).
2. D.T. Pierce, J. Unguris, and R.J. Celotta, *MRS Bulletin* **13**, 19 (1988).
3. D.T. Pierce, R.J. Celotta, M.H. Kelley, and J. Unguris, *Nucl. Inst. Meth. A.* **266**, 550 (1988).
4. M.R. Scheinfein, D.T. Pierce, J. Unguris, J.J. McClelland, R.J. Celotta, and M.H. Kelley, *Rev. Sci. Instrum.* **60**, 1 (1989).
5. A. Gellrich, K. Jost, and J. Kessler, in *Electronic and Atomic Collisions, Abstracts of Contributed Papers, ICPEAC XV*, edited by J. Geddes, H.B. Gilbody, A.E. Kingston, C.J. Latimer, and H.R.J. Latimer (1987), page 818.
6. J.J. McClelland, M.R. Scheinfein, and D.T. Pierce, *Rev. Sci. Instrum.* **60**, 683 (1989).
7. L.A. Hodge, T.J. Moravec, F.B. Dunning, and G.K. Walters, *Rev. Sci. Instrum.* **50**, 271 (1979).
8. L.G. Gray, M.W. Hart, F.B. Dunning, and G.K. Walters, *Rev. Sci. Instrum.* **55**, 88 (1984).
9. A. Ross and M. Fink, *Phys. Rev. A* **38**, 6055 (1988).
10. H. Hopster and D.L. Abraham, *Rev. Sci. Instrum.* **59**, 49 (1988).
11. M. Uhrig, A. Beck, J. Goeke, F. Eschen, M. Sohn, G.F. Hanne, K. Jost, and J. Kessler, *Rev. Sci. Instrum.* **60**, 872 (1989).
12. See, e.g., N.F. Mott and H.S.W. Massey, *The Theory of Atomic Collisions*, 3rd edition (Oxford University Press, Oxford, 1965).
13. H.W. Hermann. Ph. D. Thesis, Univ. of Kaiserslautern, 1979.
14. M. Zuo, T.Y. Jiang, L. Vuscovic, and B. Bederson, in *Electronic and Atomic Collisions, Abstracts of Contributed Papers, ICPEAC XVI*, (1989), page 132.
15. J. Kessler, *Polarized Electrons*, 2nd edition (Springer, Berlin, 1985).
16. D.H. Oza, *Phys. Rev. A* **37**, 2721 (1988).
17. J.J. McClelland, M.H. Kelley, and R.J. Celotta. To be published in *Phys. Rev. A*, 1989.
18. N. Anderson, J.W. Gallagher, and I.V. Hertel, *Phys. Rep.* **165**, 1 (1988).
19. I.V. Hertel, M.H. Kelley, and J.J. McClelland, *Z. Phys. D* **6**, 163 (1987).

COHERENCES BETWEEN AUTOIONIZING STATES OF DIFFERENT EXCITATION ENERGIES

H.G.M. Heideman

Buys Ballotlaboratorium, Rijksuniversiteit Utrecht,
P.O. Box 80 000, 3508 TA Utrecht, The Netherlands

INTRODUCTION

In the quantum dynamical description of an electron-atom collision process the final-state wavefunction of the atom can be represented as a coherent superposition of the possible atomic eigenstates. For a set of degenerate substates the coherences between these substates are readily observed by performing either a so-called angular correlation or a polarization correlation experiment. However, except in the case of quantum beats, coherences between states of different excitation energies can normally not be observed. The differences in energy between the detected particles (electrons or photons), resulting from different excited states, usually exclude practical observation of these coherences. Only when the different states can decay to the same final state can interferences and hence coherences between them be observed. Such a situation occurs, for instance, in the near-threshold excitation of autoionizing states, where the post-collision interaction may cause the energy distributions of the scattered and ejected electrons, resulting from closely separated autoionizing states, to (partly) overlap, so that coherence studies are possible.

In this paper we present the first experiment¹ where it is possible to study coherences between states that are widely separated in energy without utilizing shifting or broadening effects such as those caused by post-collision interactions. It concerns the excitation of autoionizing states of helium by electrons in the incident-energy domain where the energies of the scattered and ejected electrons are about equal. In this energy region there will be overlappings between scattered- and ejected-electron energies resulting from different autoionizing states. This provides the possibility of different autoionizing states decaying to final states (He⁺ ion + scattered electron + ejected electron) where the roles of the scattered and ejected electrons are interchanged, but which are indistinguishable. We expect that in this situation the scattered electrons from one autoionizing state will interfere with the ejected electrons from another one

and vice versa, and thus that coherences between the two states can be studied. To illustrate this we consider the excitation and subsequent autoionization of, for instance, the (2s²)¹S and (2p²)¹D autoionizing states of helium and the direct ionization process

$$e_o(E_o) + \text{He} \rightarrow \text{He}^{**}({}^1\text{S}) + e_s(E_s^{\text{S}}) \rightarrow \text{He}^+ + e_s(E_s^{\text{S}}) + e_j(E_j^{\text{S}}) \quad (1.a)$$

$$e_o(E_o) + \text{He} \rightarrow \text{He}^{**}({}^1\text{D}) + e_s(E_s^{\text{D}}) \rightarrow \text{He}^+ + e_s(E_s^{\text{D}}) + e_j(E_j^{\text{D}}) \quad (1.b)$$

$$e_o(E_o) + \text{He} \longrightarrow \text{He}^+ + e_s(E_s^{\text{C}}) + e_j(E_j^{\text{C}}) \quad (1.c)$$

where e_o , e_s and e_j denote the incident, the scattered and ejected electrons with energies E_o , E_s and E_j , respectively. The labels S, D and C refer to the two autoionizing states and the continuum, respectively. If now the incident energy E_o is chosen such that $E_s^{\text{D}} = E_j^{\text{S}}$ and $E_s^{\text{S}} = E_j^{\text{D}}$ and if electrons are detected at a fixed direction, the two final states in (1a) and (1b) are identical and we expect interferences to occur between scattered electrons from the ¹D state and ejected electrons from the ¹S state and vice versa. Of course, there is also an interfering contribution due to the direct ionization process (1c).

EXPERIMENT

Using a conventional electron spectrometer we have measured ejected-electron spectra in the incident-energy range where the effects are expected to occur. For most of the experiments the apparatus is operated in the so-called constant-energy loss mode. That is, the energy E_t of the electrons that are transmitted by the analyzer is varied along with E_o , but in such a way that the energy loss E_L , defined as $E_L = E_o - E_t$, is kept constant. Note that this general definition of E_L applies not only when scattered electrons are detected, but also when ejected electrons are detected. In the latter case $E_L = E_o - E_j^a$, where E_j^a indicates the energy of ejected electrons resulting from a particular autoionizing state a . If now the energy loss is fixed at the excitation energy of an

autoionizing state a' and we vary E_t (and E_0) we will detect at $E_t = E_j^a$ ejected electrons from a state a together with the scattered electrons resulting from the selected autoionizing state a' . This is illustrated schematically in figure 1, where the two sloping lines indicate the energies of the detected scattered electrons from the $1S$ and $1D$ states, whereas the horizontal lines represent the energies of the ejected electrons from these states. Note that interferences between scattered and ejected electrons from the same state occur at the points A and D, whereas electrons from different states interfere at B and C.

Figure 2 shows a typical measurement that clearly demonstrates interferences between scattered and ejected electrons. The spectra, which have been taken in the constant-energy-loss mode and at a detection angle of 10° with respect to the incident-beam direction, exhibit ejected-electron structures due to the $(2s^2)^1S$, $(2s2p)^3P$, $(2p^2)^1D$ and $(2s2p)^1P$ autoionizing states of helium at 57.82, 58.30, 59.90 and 60.13 eV, respectively. In the spectra (a) and (b) the energy loss was fixed at values that do not coincide with the excitation energy of any of the autoionizing states. So the structures in these spectra are caused by interference between ejected autoionization electrons and the direct ionization

continuum. As expected the two spectra look quite similar, since one would not expect the relative phases between the different autoionization processes and the direct ionization process to change much when the energy loss is changed by a few eV. In the spectra (c) and (d) the chosen energy loss coincides with the excitation energy of the $(2p^2)^1D$ and $(2s2p)^1P$ states, respectively. So in these spectra there is not only the "background" of the direct ionization, but in addition an extra "background" due to scattered electrons from $1D$ and $1P$ excitation, respectively. It is clear that the interference structures in the spectra (c) and (d) differ appreciably from those in the spectra (a) and (b). Note also the mutual differences between the spectra (c) and (d).

We attribute these differences to the fact that in

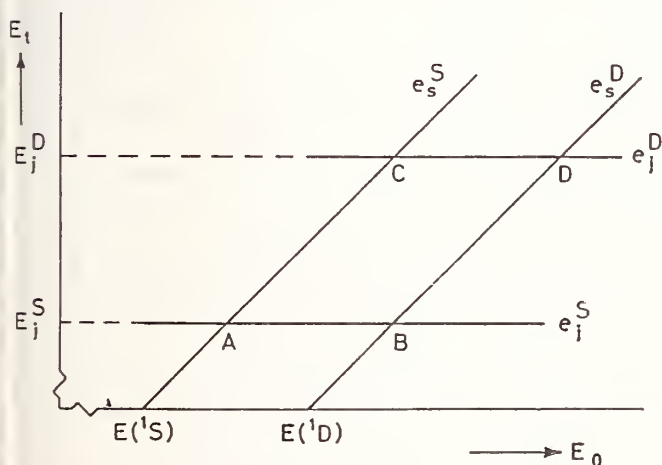


Fig. 1. Schematic diagram of the energies of the scattered and ejected electrons [resulting from excitation and subsequent decay of the $(2s^2)^1S$ and $(2p^2)^1D$ autoionizing states of helium] as a function of the incident-electron energy E_0 .

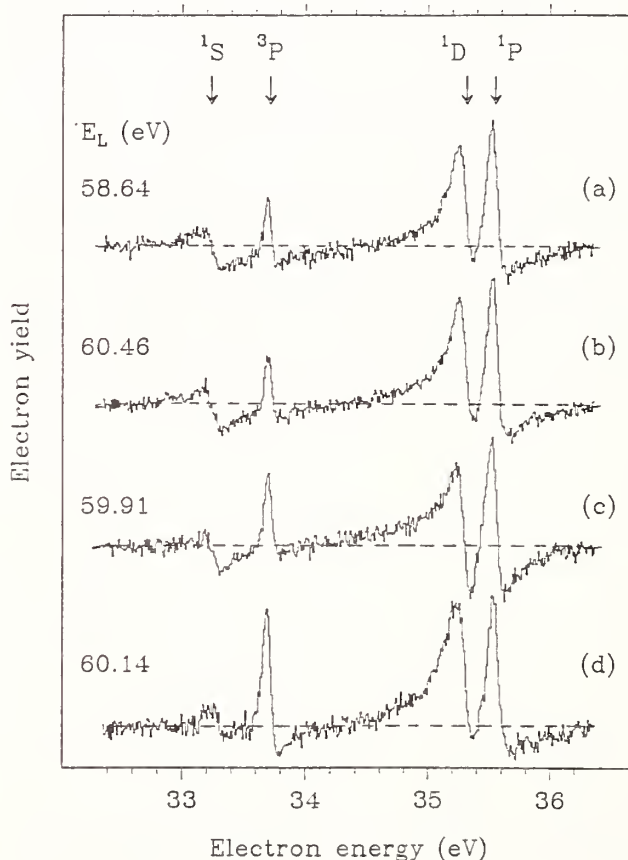


Fig. 2. Ejected-electron spectra, taken in the constant-energy-loss mode at different values of the energy loss E_L . The nominal ejected-electron energies of the four observed autoionizing states are indicated by arrows. The dashed horizontal lines indicate the "background" level.

the spectra (c) and (d) interferences occur between scattered and ejected electrons from different autoionizing states, whereas in the spectra (a) and (b) this is not the case. In absence of interference between the excitation of different autoionizing states (see reaction scheme (1)), only an extra "background" would have been added incoherently to the spectra (a) and (b) to obtain the spectra (c) and (d). The interference patterns would still look the same as in the spectra (a) and (b), only the non-interfering background would be larger. It is clear from figure 2 that this is not the case.

ANALYSIS OF THE EXPERIMENTS

For the analysis of our experiments we need a theory which is capable of describing the interaction of two discrete autoionizing states with each other and with the continuum. The simpler case of the interaction between a single discrete state and the continuum has been treated by Fano² and gives rise to the well-known Fano-profile for the autoionization resonances. We have reformulated this theory so as to account for the state-state interferences that are involved in our experiment. Based on this generalized theory we have made a parametrization of the doubly differential (with respect to energy and angle) cross section for the production of scattered and ejected electrons as resulting from processes of the type shown in the reaction scheme (1). The result is

$$\frac{d^2\sigma}{d\epsilon d\Omega} = Q^2 \times \{ 1 \quad (2.a)$$

$$+ P_a e^{-i\varphi_a} \sin\delta_a e^{-i\delta_a} + \text{c.c.} \quad (2.b)$$

$$+ P_{a'} e^{-i\varphi_{a'}} \sin\delta_{a'} e^{-i\delta_{a'}} + \text{c.c.} \quad (2.c)$$

$$+ P_{a,a'} e^{-i\varphi_{a,a'}} \sin\delta_{a,a'} e^{-i\delta_{a,a'}} + \text{c.c.} \} \quad (2.d)$$

This expression contains contributions (i) due to the direct ionization process Q^2 (assumed to be only weakly dependent on energy), (ii) due to interference between each of the discrete states a and a' and the continuum (2.b and 2.c) and (iii) due to interference between the two discrete states (2.d). The phase δ_a (and likewise $\delta_{a'}$) is defined by

$$\cot\delta_a(E) \equiv \frac{E^a - E}{\frac{1}{2}\hbar\Gamma_a} \quad (3)$$

where E is the (variable) energy of the continuum states around the discrete autoionizing state a with energy E^a and width Γ_a . The amplitudes Q , P_a , $P_{a'}$, and $P_{a,a'}$, and the phases φ_a , $\varphi_{a'}$, and $\varphi_{a,a'}$, have a clear physical meaning involving transition matrix elements for the relevant excitation and (auto)ionization processes and their phases. Far from resonances both $\sin\delta_a$ and $\sin\delta_{a'}$ are zero. When only one of them is non-zero a resonance structure arises and the parametrization (2) reduces to the Fano-formula². Only when both $\sin\delta_a$ and $\sin\delta_{a'}$ are non-zero the state-state interference term (2.d) contributes. This is the case when the scattered electrons from state a' are indistinguishable from the ejected electrons from state a and vice versa. A detailed account of the theory leading to the parametrization (2) will be given in a forthcoming publication³.

RESULTS

We have used eq. (2) to produce fits to the spectra of the type shown in figure 2. Apart from the ejected-electron spectra shown in the figures 2(c) and 2(d), with scattered electrons "in the background", we have also measured scattered-electron spectra with ejected electrons "in the background". To do this the electron spectrometer must be operated in the so-called

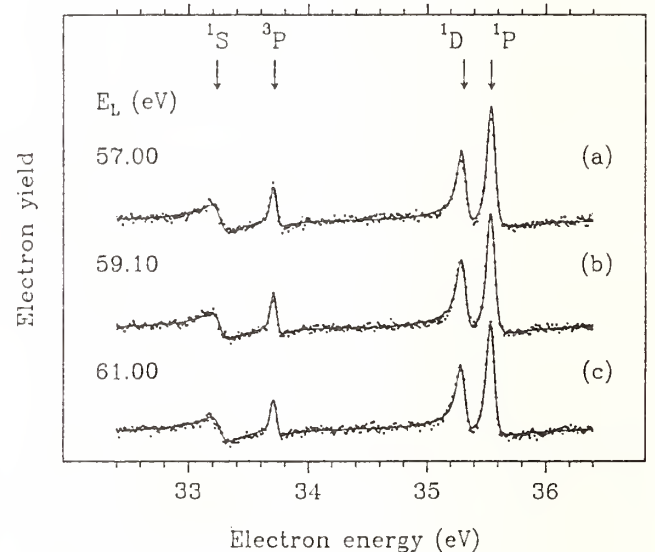


Fig. 3. Ejected-electron spectra taken at three different energy losses not coinciding with the excitation energy of any of the autoionizing states involved; thus $\sin\delta_{a'} = 0$. The full lines represent fits of eq. (2) to the experimental data (see text).

constant-transmission energy mode, where the energy loss $E_L = E_0 - E_t$ is varied along with E_0 at constant transmission energy E_t . We can now adopt the convention that in eq. (2) the quantities labeled with a refer to ejected electrons and that the quantities labeled with a' refer to scattered electrons. From the ejected-electron spectra with $\sin\delta_a = 0$, hence with no scattered electrons "in the background", we can then determine P_a and ϕ_a for each of the four autoionizing states. Figure 3 shows fits of eq. (2) to three ejected-electron spectra for different energy losses not coinciding with the excitation energy of any of the autoionizing states involved, thus with $\sin\delta_a = 0$. The fits were obtained under the restriction that the P_a and ϕ_a values for each autoionizing state be the same in all three spectra of figure 3. The quality of the fits shows that the P_a and ϕ_a indeed may be considered energy loss independent within the measured energy range. In the same way we can determine the $P_{a'}$ and $\phi_{a'}$ for each autoionizing state from the scattered-electron spectra with $\sin\delta_a = 0$, hence with no ejected electrons "in the background". We have found that these

parameters are also energy (in this case transmission energy E_t) independent within the range considered.

Our verification that the parameters P_a , $P_{a'}$, ϕ_a and $\phi_{a'}$ are energy-independent implies that the terms (2.b) and (2.c) in our cross section formula (2) are known also for ejected-electron spectra with the energy loss coinciding with the excitation energy of any of the autoionizing states, hence with scattered electrons "in the background" (or with $\sin\delta_a = 1$). Figure 4 shows ejected-electron spectra due to the lowest four autoionizing states of helium with the energy loss tuned so as to coincide with the excitation energy of the $(2p^2)^1D$ state at 59.90 eV; so there are 1D scattered electrons "in the background". The experimental data are the same in the spectra 4(a) and 4(b). The full line in spectrum (a) represents a fit with eq. (2), where the state-state interference term (2.d) is omitted and using P_a , $P_{a'}$, ϕ_a and $\phi_{a'}$ values determined as described in the previous paragraph, whereas the full line in spectrum (b) represents a fit using the complete eq. (2) with fixed values for P_a , $P_{a'}$, ϕ_a and $\phi_{a'}$, as determined above and with $P_{a,a'}$ and $\phi_{a,a'}$ as adjustable parameters. Figure 5 shows a similar measurement and fits as in figure 4, but now with the energy loss tuned to the excitation energy of the $(2s2p)^1P$ state at 60.13 eV; so here we have 1P scattered electrons "in the background". It is clear

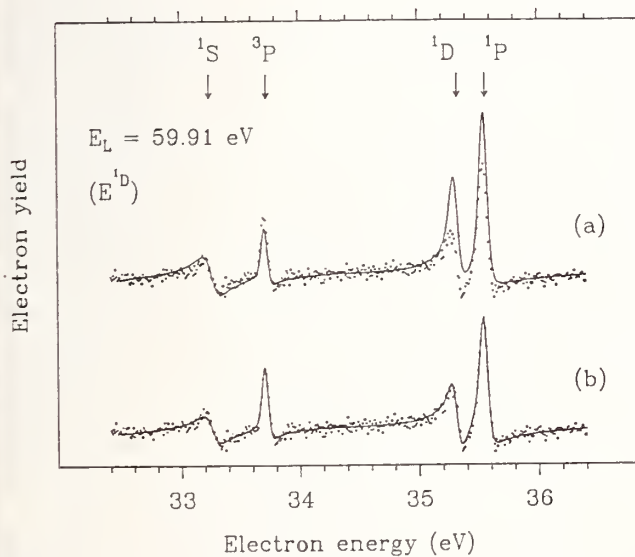


Fig. 4. Ejected-electron spectra taken at an energy loss value coinciding with the excitation energy of the $(2p^2)^1D$ state at 59.90 eV. The experimental data are the same in the spectra 4(a) and 4(b). The full line in spectrum (a) represents a fit with eq. (2), where the state-state interference term 2(d) is omitted, whereas the full line in spectrum (b) represents a fit using the complete eq. (2).

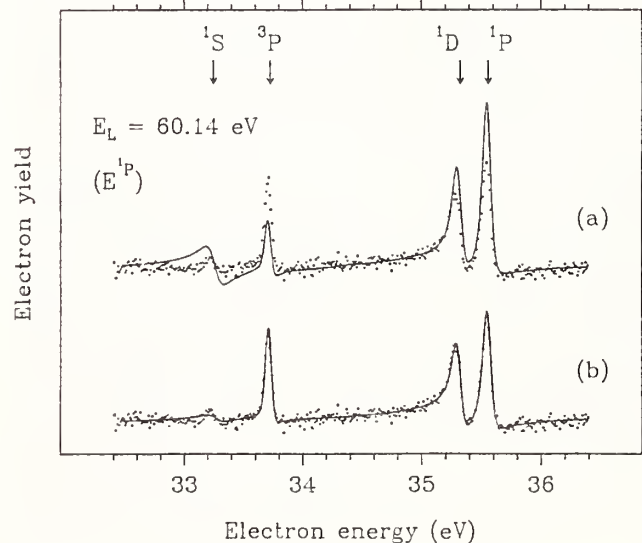


Fig. 5. Same as fig. 4 except for an energy loss value coinciding with the excitation energy of the $(2s2p)^1P$ state at 60.13 eV.

from the figures 4(b) and 5(b) that eq. (2) gives an excellent description of the observed phenomena resulting from the interference of different autoionizing states.

CONCLUSIONS

We have for the first time observed coherences between the electron impact excitation of states of different excitation energies without utilizing shifting or broadening effects, such as those caused by, for example, post-collision interactions. The method is based on the occurrence of interferences between scattered and ejected electrons resulting from the excitation of autoionizing states by electron impact. We have developed a theory which gives an excellent description of the observed interference effects.

We emphasize that our method is not restricted to coherence studies on states which are separated by a few eV, such as in the present experiment. It can in principle also be applied to states which lie several hundreds of eV apart, such as, for instance, in inner-shell excitation followed by Auger emission.

ACKNOWLEDGMENTS

I gratefully mention the fruitful cooperation with Jan van den Brink, Jaap van Eck and Gerard Nienhuis, who greatly contributed to the work presented here. This work was performed as a part of the research programme of the "Stichting voor Fundamenteel Onderzoek der Materie" (FOM) with financial support from the "Nederlandse Organisatie voor Zuiver-Wetenschappelijk Onderzoek" (ZWO).

REFERENCES

1. J.P. van den Brink, J. van Eck and H.G.M. Heideman, *Phys. Rev. Lett.* **61**, 2106 (1988).
2. U. Fano, *Phys. Rev.* **124**, 1866 (1961).
3. J.P. van den Brink, G. Nienhuis, J. van Eck and H.G.M. Heideman, *J. Phys. B: At. Mol. Opt. Phys.*, to be published (1989).

STOKES PARAMETER MEASUREMENTS IN THE HEAVY RARE GASES

J.W. McConkey*, P.J.M. van der Burgt*, J.J. Corr* and P. Plessis†

*Department of Physics, University of Windsor, Ontario, Canada

†Department of Physics, Laurentian University, Sudbury, Ontario, Canada.

INTRODUCTION

The study of electron impact excitation of atoms using the electron-photon coincidence technique has elucidated many of the processes involved in these interactions and this work has been extensively reviewed and discussed (Blum and Kleinpoppen¹, McConkey², Hanne³, Slevin⁴, Andersen et al.^{5,6}.) For the widely studied 2^1P excitation of He, LS coupling holds strictly and the spin of the continuum electron can be factored out of the problem. Thus the positive reflection symmetry, with respect to the scattering plane, of the atomic wavefunction is conserved during the collision. For the heavier noble gases LS coupling is no longer strictly valid and electron spin may play a role in the excitation. Consequently states having negative reflection symmetry with respect to the scattering plane may also be excited. In classical terms the excitation of an oscillator perpendicular to the scattering plane is now possible.

In previous communications from this laboratory (Khakoo and McConkey^{7,8}) data for the out-of-plane linear and circular Stokes parameters for Ne, Ar and Kr were presented. These enabled a study of that part of the problem to which positive reflection symmetry applies and, most significantly, the circular polarisation measurements enabled the sign of the angular momentum transfer in the collisions to be unambiguously determined for the electron scattering angles and incident energies considered. For incident electron energies in the range 60-80 eV and small scattering angles ($<30^\circ$) angular momentum transfer is positive and surprisingly similar for all the targets considered (see also McConkey et al.⁹). Measured total polarisations of close to unity suggested that essentially full coherence of this part of the excitation was occurring.

Very recently Plessis et al.¹⁰ reported the first in plane polarisation correlation Stokes parameter measurements for Kr and Xe. These enabled the so-called height parameter, ρ_{00} , of the excited-state charge clouds to be obtained and thus information on possible breakdown of reflection symmetry in the excitation process. The present work extends the work of these authors to cover a wider energy and angular range and presents details of measurements for Ne, Ar, Kr and Xe. In addition, a discussion is given of a number of experimental effects which can perturb the in-plane Stokes parameter measurements.

BASIC THEORY

The density matrix description of the excitation of the heavier noble gases leads to a formulation involving five independent parameters rather than only three for the simpler case of He. These parameters and their relation to experimentally measurable angular correlation or polarisation correlation parameters have been outlined in the reviews mentioned above. We refer in particular to Andersen et al.⁶ who provide a complete listing of formulae linking the various parameters used by different authors. The initial set of these parameters were the $\sigma, \lambda, \bar{\chi}, \cos \epsilon$ and $\cos \Delta$ parameters introduced by Blum et al.¹¹ and da Paixao et al.¹² More recently Andersen et al.^{5,6} have introduced the $\sigma, L^*, \gamma, P^*_2$ and ρ_{00} parameters which give a more transparent description of the excitation process in terms of the excited-state charge cloud characteristics. These latter parameters relate in a particularly simple way to our polarisation correlation measurements.⁸

Excitation of states having negative reflection symmetry with respect to the scattering plane can occur when the spin of the incident electron is flipped during the scattering process. Spin-flip is due to either electron exchange interaction or to spin-orbit interaction of the scattered electron in the atomic field. Spin flip by electron exchange for the $ns^2np^5(n+1)s\ ^1P_1$ resonance states of the heavier rare gases, which are represented by linear combinations of singlet and triplet LS-coupled eigenfunctions, can proceed through the triplet admixture of these states. Spin flip by spin-orbit interaction is expected to be important only for the heavier atoms.³

The ρ_{00} parameter gives the relative probability for spin flip perpendicular to the scattering plane and, in terms of charge cloud characteristics, it gives the relative height of the charge cloud. Alternatively since the excited P state radiates like a set of mutually orthogonal classical oscillators we may consider ρ_{00} as giving the relative strength of the oscillator perpendicular to the scattering plane. ρ_{00} is related to the measurable Stokes parameters by the following equation (Andersen et al.^{5,6}):

$$\rho_{00} = \frac{(1 + P_1^*)(1 - P_4)}{4 - (1 - P_1^*)(1 - P_4)} \quad (1)$$

where P_1^* and P_4 monitor the number of coincidences with photons polarised parallel to the incident electron beam minus those polarised perpendicular to this beam normalised to the total number of coincidence events, as detected by photon polarisation analysers placed above the scattering plane (P_1^*) and in the scattering plane (P_4) respectively. In a polarisation correlation experiment both in-plane and out-of-plane polarisation measurements are required to measure the effects of spin flip.

Previous experimental data which yield information on spin-flip processes are available for Kr and Xe.¹³⁻¹⁵ Theoretical calculations of the spin-flip probability (or equivalent parameters) for the heavier rare gases are limited. First-order many-body theory calculations (FOMBT) have been carried out for Ne¹⁶, Ar¹⁷ and Kr^{18,19} and in each case only spin flip due to the exchange interaction was considered. Recently Bartschat and Madison²⁰, using a distorted-wave Born approximation (DWBA), have investigated the importance of relativistic spin-dependent effects both on the description of the Ne, Ar, Kr, Xe target states and on the wavefunction of the continuum electron. For the small scattering angles involved in this work these effects were found to be very small. This is to be expected since small angle scattering represents distant collisions with small interactions.

EXPERIMENT

The experimental set-up has been described in earlier papers^{7,8,21}, therefore only the pertinent details will be given here. A schematic diagram of the apparatus is given in figure 1 of the paper by Plessis et al.¹⁰

Standard coincidence techniques are used to measure the polarisation of the photons emitted perpendicular to the scattering plane (linear and circular polarisation) as well as in the scattering plane. The in-plane linear polarisation analyser consists of a single, gold-coated mirror with an angle of incidence of 57.5° . It is situated at right angles to the incident electron beam direction. Both photons and inelastically scattered electrons are detected by channel electron multipliers (CEM). Coating the entrance cone of the photon CEM with cesium iodide significantly enhanced its detection efficiency above 100 nm²², where the resonance transitions of Ar, Kr and Xe lie.

Research purity (99.995%) neon, argon krypton and xenon were used as the target gases and were introduced into the interaction region through a single capillary. A pressure increase of 1.5×10^{-7} Torr

or less above background was maintained during data collection in order to render negligible any radiation trapping effects. An electron gun produced the electron beam and scattered electrons were energy selected by a hemispherical analyser. Electron beam currents of several μA were easily obtained with an energy resolution of approximately 600 meV (FWHM). This resolution was insufficient to resolve the $[1/2]_1^0 \text{ ns } ^1\text{P}$ and $[3/2]_1^0 \text{ ns } ^3\text{P}$ peaks (Racah notation) in Ne and Ar. The Kr peaks were only partially resolved. For the electron scattering angular range studied here, the ^1P peaks of Ne and Ar were approximately five times the intensity of the respective ^3P peaks and so for these targets the data are predominantly due to singlet excitation even though the transitions were not resolved. In Kr the contribution from the adjacent peak was less than 10% while in Xe the two peaks were completely resolved.

EXPERIMENTAL EFFECTS IN MEASURED COHERENCE PARAMETERS

The in-plane P_4 measurements can demonstrate pronounced minima at certain θ_s even though ρ_{00} (equation 1) stays relatively constant with θ_s . One reason for this is as follows. As previously mentioned, P_4 measurements correspond to the difference between the number of coincidences with photons polarised parallel to the scattering plane (incident electron beam) and the number of coincidences with photons polarised perpendicular to this plane, normalised to the total number of coincidence events. When no dipole is excited perpendicular to the scattering plane P_4 is unity. This is expected to be the case certainly for the lighter rare gases and measurements with He, Ne and Ar targets have confirmed that for these gases at small scattering angles ($< 30^\circ$) P_4 is indeed unity within experimental error. If, however, there is a dipole excited perpendicular to the scattering plane, then the measured P_4 value will depend on the charge cloud alignment. For example, when the charge cloud is aligned at 90° to the incident K vector, the P_4 detector faces the 'end' of the charge cloud and the number of detected photons polarised parallel to the scattering plane will be at a minimum. Consequently this will lead to a minimum in the P_4 measurement at this scattering angle, assuming that

the intensity of the photons polarised perpendicular to the scattering plane does not vary too greatly with scattering angle. In fact for cases where ρ_{00} varies slowly with scattering angle, the minima in the P_4 curves could act as an indicator for the scattering angle(s) at which the charge cloud is aligned perpendicular to the incident electron beam (i.e. $\gamma = |90|^\circ$).

We would point out that even if P_4 is nominally unity (no spin flip) experimental conditions can arise which can cause the actual measured value of P_4 to deviate substantially from this value. A number of potential problem areas have been identified and quantified as discussed below.

(1) Finite Acceptance Angle of Photon Detector

The finite angular acceptance of the photon detectors allows them to pick up some signal from a dipole even though it may be pointing directly towards the centre of the detector cone. This results in a slight lowering of the measured P values. As an example corrections to P_4 have been calculated using theoretical P_1^+ values²⁰ and are a maximum when the charge cloud is pointing towards the P_4 detector. At this scattering angle the largest correction factor is less than 1% of the measured value.

(2) Finite Beam Size and/or Offset

A much more serious problem arises if the effective scattering plane suffers a rotation from the nominal one. (We note that a closely-related problem has been discussed by Zetner et al²⁴ in the context of superelastic scattering of electrons by laser-excited targets). This is illustrated in Fig. 1 which indicates that if the scattering event occurs from a point displaced vertically from the nominal scattering centre, then a rotation of the scattering plane about the direction of the incident electron occurs.

The rotation angle β is related to the vertical displacement, r , from the nominal scattering centre, the distance R_c to the analyser entrance aperture, and the nominal electron scattering angle, θ_e according to

$$\tan \beta = r / (R_c \sin \theta_e). \quad (2)$$

Since the excitation process results in dipoles excited in the scattering plane then clearly, if this plane rotates, a modification to the signals observed by the photon detectors will occur. For the situation discussed above, the measured P_4 can be expressed as:

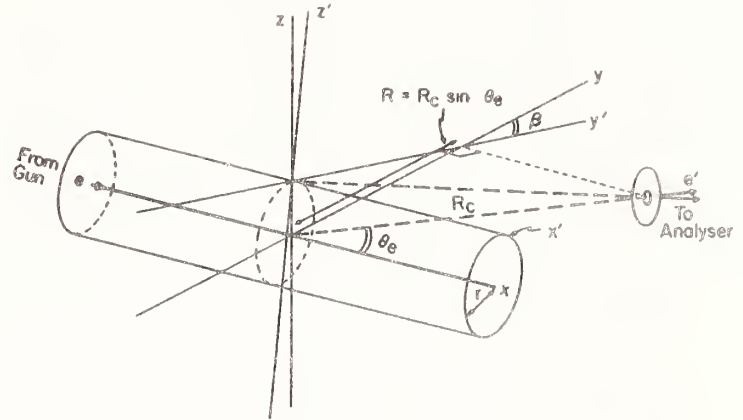


Fig. 1. Diagram illustrating the rotation, β , of the scattering plane which occurs when the scattering centre is displaced vertically.

$$P'_4 = \frac{1 - \left(\frac{1-P_1}{1+P_1} \right) \sin^2 \beta}{1 + \left(\frac{1-P_1}{1+P_1} \right) \sin^2 \beta} \quad (3)$$

where, for simplicity, effects due to the finite acceptance angle of the photon detector have been neglected.

We note incidentally, that if a dipole is excited perpendicular to the scattering plane so that $P_4 \neq 1$, then Eq. (3) must be modified to:

$$P'_4 = \frac{1 - \left(\frac{1-P_1}{1+P_1} \right) \sin^2 \beta - \left(\frac{1-P_4}{1+P_4} \right) \cos^2 \beta}{1 + \left(\frac{1-P_1}{1+P_1} \right) \sin^2 \beta + \left(\frac{1-P_4}{1+P_4} \right) \cos^2 \beta} \quad (4)$$

Although Eq. (3) relates to a rather specific scattering situation, it illustrates two important points. First, since the effect depends on $\sin^2 \beta$, it is only likely to be significant for small scattering angles ($< 20^\circ$) where β is largest. Second, we note that an amplifying effect occurs for $P_1 < 0$. For excitation of the heavier gases at intermediate energies this occurs for small electron scattering angles where β could be significant and, where, in fact our measurements are being carried out.

In practice, since any electron beam will have a finite diameter, some scattering away from the nominal scattering plane will always occur (with consequent rotation of the effective scattering plane). Small vertical displacements of the electron beam can also occur, again leading to effects similar to that discussed above.

(3) Finite Acceptance Angle of Analyser

The finite acceptance angle of the electron analyser can clearly allow scattering events to be monitored, particularly at small electron scattering angles, where the effective scattering plane is different from the nominal one. When this occurs, a modification to the measured P_4 , similar to that given by Eq. (3) will result.

(4) Scattering Angle Variation Over Scattering Volume

It is clear from Fig. 1 that if scattering occurs from a point within the electron beam but displaced from the z axis then the effective scattering angle will be altered. Similarly, if the electron beam gets displaced from the nominal x -direction within the scattering plane, θ_e will be affected. This can have significant effects since a particular Stokes parameter, or the alignment of the charge cloud, may vary rapidly with scattering angle. This particular problem as it relates to forward scattering, using an analyser with a finite acceptance angle, has been discussed by Martus et al.²³

We note that the severity of the problem introduced by the effects discussed above depends on the direction of observation. For example in-plane (P_4) measurements are particularly sensitive to beam size or offset (effect (2)) whereas out-of-plane measurements are more sensitive to effects (3) and (4).

We have carried out a variety of calculations in which we have considered all of the effects noted above. We have varied beam diameters and offsets and interaction volumes and, in some cases, have been able to reproduce experimental data points. An example of this is given in the following section.

RESULTS AND DISCUSSION

In our laboratory we have now carried out complete Stokes parameter ($P_{1,2,3,4}$) measurements on Ne, Ar, Kr and Xe at a number of energies and over a range of electron scattering angles which in some cases extends out to 50° . Some of these data have been reported previously.^{7,8,10} In this report we have only space to highlight a few points.

Of particular interest, in view of the proceeding section, are the P_4 and ρ_{00} data, some of which have been presented by Plessis et al.¹⁰ for 60 eV impact excitation of Kr $5s[3/2]_1^0$, and 50 eV impact excitation of Xe $6s[3/2]_1^0$ for scattering angles up to 30° . These indicated non-zero values for ρ_{00} at these small scattering angles suggesting that some spin-flip was occurring. As mentioned earlier, this is not

expected based on the predicted magnitude of the exchange or spin-orbit interactions at these small scattering angles.

An example of our present calculations is shown in Fig. 2 which refers to excitation of the $[1/2]_1^0 5s$ 1P state of Kr at 60 eV incident energy. The calculated data set are obtained using theoretical²⁰ Stokes parameters and are compared with an actual data set taken with our coincidence apparatus. The calculated data points were obtained assuming an electron beam radius of 1mm and a beam offset in the $-z$ direction of the same magnitude. Rather similar data were obtained if we assumed all the scattering to take place from a centre displaced 1mm in the $+z$ direction. The similarity between the calculated and experimental data strongly suggests that some net rotation of the effective scattering plane may have occurred during the experimental data taking even though careful alignment and set up procedures were followed.

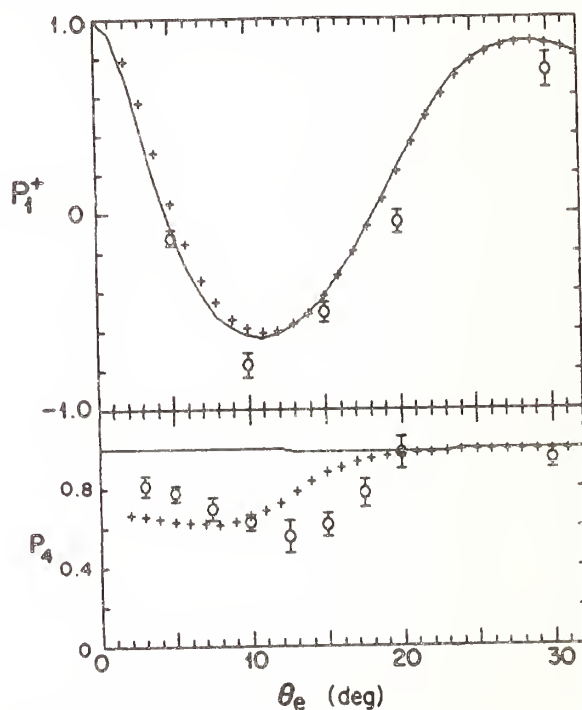


Fig. 2 Stokes parameter data for the 1P state of Kr at 60 eV impact energy. circles- experimental data; crosses-calculated data assuming conditions discussed in text; solid line - theory²⁰.

We note that the calculations show a rather small effect for P_1^+ whereas it is quite dramatic for P_4 .

In the light of this discussion we now believe that our earlier data¹⁰ may have been affected by scattering plane rotation problems and hence ρ_{00} should be considered as being effectively zero for Kr and

Xe targets in the angular range considered.

Fig. 3 shows P_1^+ , P_4 and ρ_{00} data for Ne at an incident energy of 80 eV together with theoretical data.^{17,20} These experimental data have not been corrected for any of the effects discussed in the previous section though, there is a hint of their presence in the P_4 data. In general, however, good agreement between experiment and predictions is obtained except for the highest angle P_1^+ data. A similar situation was found for Ar.

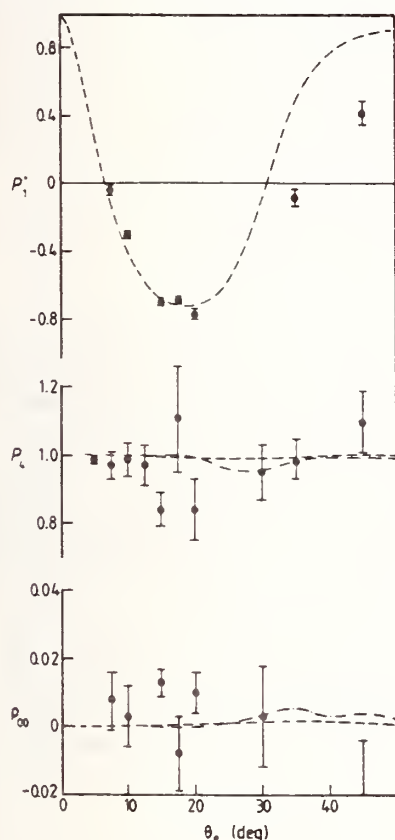


Fig. 3 Ne Stokes parameter data.

Our previous¹⁰ and more recent data taken with Xe targets have exhibited the most pronounced departures from expected P_4 and ρ_{00} values. We are not clear why the Xe data should have been more suspect to these effects than Kr or the lighter targets. Experiments are continuing to clarify this situation.

Figs. 4 and 5 show some 30 eV data for the $[3/2]_1^0$ 6s 3P state of Xe. They illustrate the very good agreement between the theoretical predictions of Bartschat and Madison²⁰ and our data for the γ and P_3^+ (angular momentum transfer) parameters under these scattering conditions. At this energy we find that our P_2^+ and P_4^+ parameters fall consistently

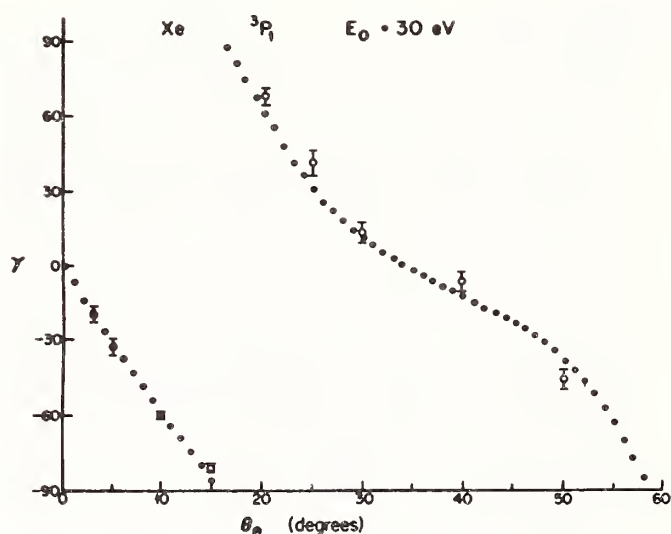


Fig. 4 Variation of charge cloud alignment angle, γ , with θ_e for 30 eV impact on Xe.

some 20% below the theoretical predictions perhaps suggesting some hyperfine relaxation caused by use of a natural Xe mixture with a significant $I \neq 0$ content.

ACKNOWLEDGEMENTS

The financial assistance of the Natural Sciences and Engineering Research Council of Canada, NATO Division of Scientific Affairs (RG686/84) and the Killam Foundation is gratefully recognised.

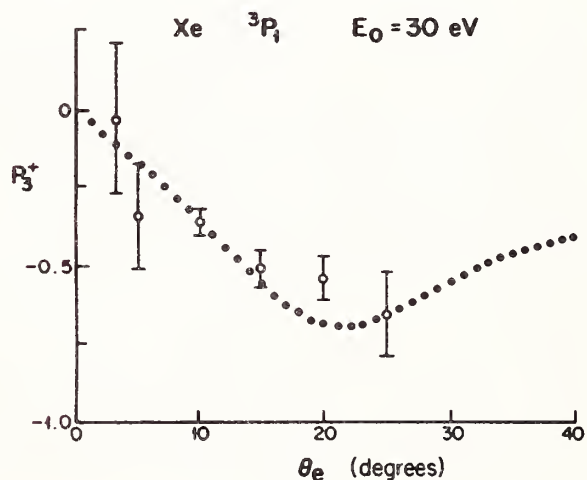


Fig. 5 Variation of circular polarization ($-L_{\perp}$) with θ_e for 30 eV impact on Xe.

REFERENCES

1. K. Blum and H. Kleinpoppen, *Phys. Rep.* 52, 203-61 (1979).
2. J.W. McConkey, *Symp. on Electron-Molecule Collisions* (Tokyo: University of Tokyo Press) Invited papers pp. 163-78 (1979).
3. G. Hanne, *Phys. Rep.* 95, 96-165 (1983).
4. J. Slevin, *Rep. Prog. Phys.* 47, 461-512 (1984).
5. N. Andersen, J.W. Gallagher and I.V. Hertel, *Proc. 14th Int. Conf. on the Physics of Electronic and Atomic Collisions* (Palo Alto) ed. D.C. Lorents, W.E. Meyerhof and J.R. Peterson (Amsterdam: North-Holland) Invited papers pp. 57-76 (1986).
6. — *Phys. Rep.* 165, 1 (1988).
7. M.A. Khakoo and J.W. McConkey, *Phys. Rev. Lett.* 57, 679-82 (1986).
8. — *J. Phys. B: At. Mol. Phys.* 20, 5541-56 (1987).
9. J.W. McConkey, P. Hammond and M.A. Khakoo, *Electronic and Atomic Collisions*, ed. H.B. Gilbody, W.R. Newell, F.H. Read and A.C.H. Smith (Amsterdam: Elsevier) pp. 105-16 (1988).
10. P. Plessis, M.A. Khakoo, P. Hammond and J.W. McConkey, *J. Phys. B: At. Mol. Opt. Phys.* 21, L483-8 (1988).
11. K. Blum, F.J. da Paixao and G. Csanak, *J. Phys. B: At. Mol. Phys.* 13, L257-61 (1980).
12. F.J. da Paixao, N.T. Padial and G. Csanak, *Phys. Rev. A* 30, 1697-713 (1984).
13. I. McGregor, D. Nils, R. Hippler, N.A. Malek, J.F. Williams, A.A. Zaidi and H. Kleinpoppen, *J. Phys. B: At. Mol. Phys.* 15, L411-4 (1982).
14. A. Danjo, T. Koike, K. Sani, H. Sugahara, A. Takahashi and H. Nishimura, *J. Phys. B: At. Mol. Phys.* 18, L595-600 (1985).
15. S.J. King, P.A. Neill and A. Crowe, *J. Phys. B: At. Mol. Phys.* 18, L589-94 (1985).
16. L.E. Machado, E. P. Leal and G. Csanak, *J. Phys. B: At. Mol. Phys.* 15, 1773-84 (1982).
17. F.J. da Paixao, N.T. Padial and G. Csanak, *Phys. Rev. A* 30, 1697-713 (1984).
18. G.D. Meneses, F.J. da Paixao and N.T. Padial, *Phys. Rev. A* 32, 156-65 (1985).
19. G.D. Meneses, F.J. da Paixao and N.T. Padial, *Phys. Rev. A* 34, 675 (1986).
20. K. Bartschat and D.H. Madison, *J. Phys. B: At. Mol. Phys.* 20, 5839-63 (1987).
21. K. Becker, H.W. Dassen, J.W. McConkey, *J. Phys. B: At. Mol. Phys.* 17, 2535-48 (1984).
22. M.C. Johnson, *Rev. Sci. Instrum.* 40, 311-5 (1969).
23. K.E. Martus, K. Becker and D.H. Madison, *Phys. Rev. A* 38, 4876 (1988).
24. P.W. Zetner, S. Trajmar, G. Csanak and R.E.H. Clark, *Phys. Rev. A*, In press (1989).

SPIN-POLARIZED ELECTRON IMPACT IONIZATION OF ATOMS

G. Baum, P. Freienstein, L. Frost, B. Granitza, W. Raith,
and H. Steidl

Fakultät für Physik, Universität Bielefeld, D-4800 Bielefeld 1
Federal Republic of Germany

In this report we describe the experimental activities at the University of Bielefeld in the area of ionizing collisions of polarized electrons and polarized atoms and discuss results which have been recently obtained. One apparatus can examine the spin dependence of total ionization cross sections, and another apparatus is capable of investigating ionization events with scattering angles, energy partitions and initial spin orientations resolved.

The spin dependence of total ionization cross sections has in the past been studied experimentally by different groups for the following atoms: hydrogen¹⁻³, lithium⁴⁻⁵, sodium⁵⁻⁷, and potassium^{8,9}. The results for these atoms are shown in Fig. 1. The spin asymmetry in ionization, A_I , is connected to the singlet (σ_s) and triplet (σ_t) parts of the total ionization cross section σ for unpolarized particles

$$\sigma = (1/4)\sigma_s + (3/4)\sigma_t,$$

by

$$A_I = (\sigma_s - \sigma_t) / (\sigma_s + 3\sigma_t),$$

All experiments used a crossed-beam arrangement to determine A_I . The polarization of the electron beam, P_e , and the polarization of the atomic beam, P_a , were measured and the observed ion rates, $N_{\uparrow\downarrow}$ and $N_{\uparrow\uparrow}$, for

antiparallel and parallel orientation of the two beam polarizations, respectively, were taken as measures of the spin dependent parts of the total ionization cross sections. It follows that

$$A_I = \frac{1}{P_e P_a} \frac{N_{\uparrow\downarrow} - N_{\uparrow\uparrow}}{N_{\uparrow\downarrow} + N_{\uparrow\uparrow}}.$$

As can be seen from Fig. 1 the asymmetries for the light atoms H, Li, and Na are very much alike. They are positive throughout the energy range studied and have a maximum of about 0.5, indicating that the singlet ionization cross sections are dominating the triplet ones. For K the asymmetry is substantial different from that of the other atoms in the region from threshold, E_I , to about $4E_I$. The reason for the reduced values is not yet known; speculations involve spin-orbit coupling effects or

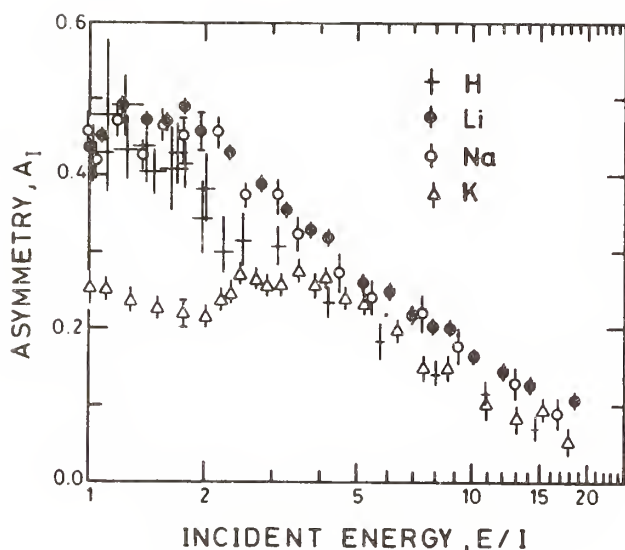


Figure 1. Energy dependence of the spin asymmetry A_1 , measured for hydrogen³ and the light alkali atoms.³ (E in units of threshold energy)

atomic structure effects because of the unfilled 3d subshell.

The threshold value of the asymmetry has attracted attention. The early experiment on H^1 could not confirm a prediction⁹ that should lead to $A_1=1$. The experiment on Li^4 then conclusively showed that singlet and triplet ionization cross section have the same energy dependence close to threshold. This also implied that, right at threshold, two-electron states with orbital angular momenta $L>0$ have to be present. This new insight gave rise to several theoretical treatments of spin, orbital angular momentum, and parity behavior near threshold.¹⁰⁻¹² Oscillations of the asymmetry were predicted¹³ but could not be found experimentally.⁷

An ab initio theoretical treatment of the ionization process at low energies from E_I to about $10 E_I$ is a formidable problem. Progress in this field can only be made by extensive interaction between theory and experiment. Progress has been obtained at high and intermediate collision energies ($E > 10 E_I$) where for hydrogen the dynamics of the unpolarized electron impact ionization is now well understood.¹⁴ At low impact energies and near threshold measurements of the triple differential cross section have been made with unpolarized electrons for helium¹⁵⁻¹⁷ and hydrogen.¹⁸ The unpolarized triple differential measurements on He ground-state atoms¹⁷ were analyzed for their singlet and triplet partial wave content up to $L=2$ waves.^{17,19} The analysis is based on models of threshold behavior and yields information on triplet contributions for the special geometric configuration of oppositely escaping electrons. Triple differential experiments with polarized particles could provide much more insight. No results exist yet. Recent close-coupling calculations²⁰ have been predicting spin asymmetries for angle-integrated double-differential ionization cross sections. Measurements are needed to aid further development.

A schematic diagram of our experimental setup for measuring spin asymmetries of total ionization cross sections is shown in Fig.2. The polarized electron beam is produced by photoemission from a (100) surface of a GaAsP crystal using circularly polarized light of a 30 mW He-Ne laser. The setup for the electron beam and the

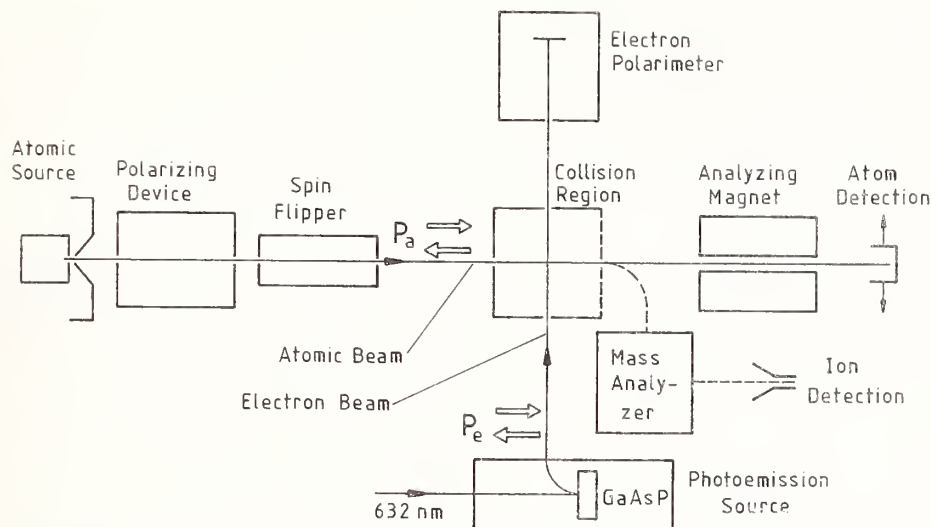


Figure 2. Schematic diagram of the apparatus to measure the asymmetry in total ionization A_I .

electron polarimeter is very similar to one described previously.²¹ The beam polarization is reversed repeatedly during data taking. The electron beam polarization is in the range of $P_e = 0.35$ to 0.40 and the electron beam intensity in the range of $I = 0.3$ to $3 \mu A$.

We recently studied the spin-polarized impact ionization of $He(2^3S)$ which, near threshold, is related to that of $He(1^1S)$, provided that the same excess energy is available in the two-electron escape process. For investigating possible relativistic effects in impact ionization and, perhaps, gaining insight into the potassium "anomaly" (Fig.1) we are working on an experiment with Cs. In Fig.2, spin flipper²², collision region, and Stern-Gerlach magnet for analyzing the beam polarization are common elements of the atomic beam line.

For the $He(2^3S)$ investigation we use a discharge source for producing the metastable beam.

As polarizing device a permanent sextupole magnet with a central stop at its exit is inserted in the beam line. Because the helium atom has no hyperfine structure this magnet is able to produce an atomic polarization of 0.9 by focussing the $m_s = +1$ substate atoms, by rejection the $m_s = -1$ atoms, and by preferentially blocking the $m_s = 0$ substate atoms with a central stop. The apparatus used to produce the spin-polarized $He(2^3S)$ beam has recently been described in detail.²³ Rydberg atoms in the metastable beam interfered with the ionization measurements. They were eliminated with the help of a strong electric field located prior to the collision region.

The cesium beam is obtained from an effusive oven arrangement which recycles the alkali metal condensed on the first collimator. With a moderate density in the scattering region ($4 \times 10^9 \text{ cm}^{-3}$) the beam can be kept continuously running for at least one week with a Cs filling of 5 g . Because of the large nuclear spin value ($I = 7/2$) and the strong hyperfine

interaction of the Cs atom, a sextupole can only yield a small spin polarization. To produce a highly spin-polarized beam we use optical pumping, following and considerably modifying recent experimental work.²⁴ Two laser diodes tuned to the $6^2S_{1/2}$ ($F=3$) \rightarrow $6^2P_{3/2}$ ($F=4$) and $6^2S_{1/2}$ ($F=4$) \rightarrow $6^2P_{3/2}$ ($F=5$) transitions, respectively, are used to pump both hyperfine sublevels of the ground state simultaneously. Because the light is circularly polarized by a quarter-wave plate only transitions with $\Delta m_F = +1$ are induced. After several pumping processes an atom is left in the $6^2S_{1/2}$ ($F=4$, $m_F = +4$) ground state. Simply reversing the sense of circular polarization of the pumping light yields the opposite atomic spin polarization. An analysis of the population distribution in the optically pumped beam is carried out by splitting it into the $m_J = +1/2, -1/2$ components in a Stern-Gerlach magnet (see Fig.3). We find nearly all atoms in one Zeeman sublevel, implying an atomic polarization of $P_a = 0.95$. The polarization direction can also be efficiently reversed with the spin flipper.

To guide the atomic spins, a magnetic field of 10^{-5} T, collinear with the atomic beam, is present in the collision region. The ions that are produced are extracted with a small electric field and directed towards a channel electron multiplier for detection. In the case of the measurements on He(2^3S) a mass analyzer, set to transmit He⁺ ions, has to be employed in order to reduce the large background of ions originating from Penning ionization of residual gas atoms at a pressure of $5 \cdot 10^{-9}$ Torr.

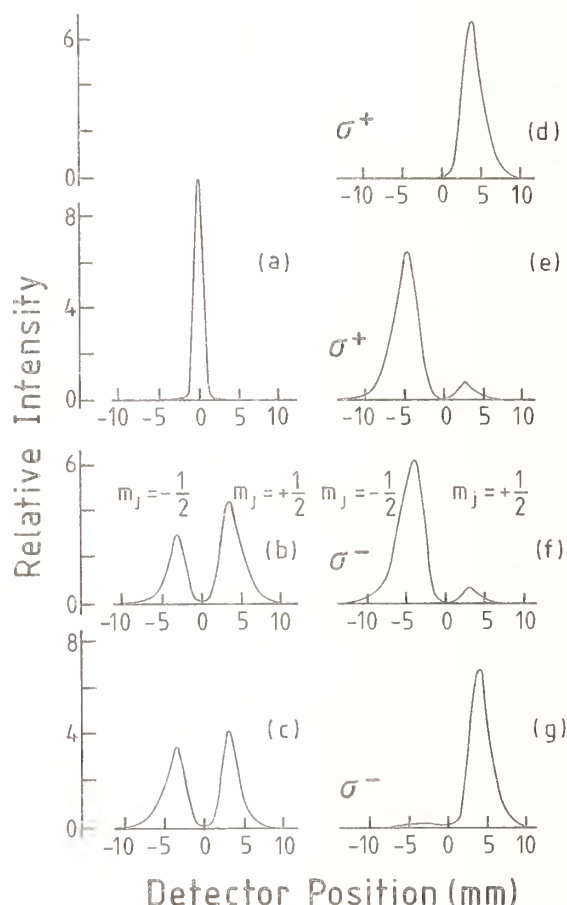


Figure 3. Stern-Gerlach profiles of the polarized Cs beam for different optical pumping conditions and different modes of the spin flipper. (a) Stern-Gerlach not activated; (b) and (c) no optical pumping, no spin flip and spin flip; (d) and (e) σ^+ pumping, no spin flip and spin flip; (f) and (g) σ^- pumping, no spin flip and spin flip, respectively.

Background measurements are made, in the case of He(2^3S) by dumping the electron beam in an upstream section of the beam pipe connecting the electron-source and collision chambers, or in the case of Cs, by blocking the atomic beam with a beam flag located 15 cm in front of the interaction region. The

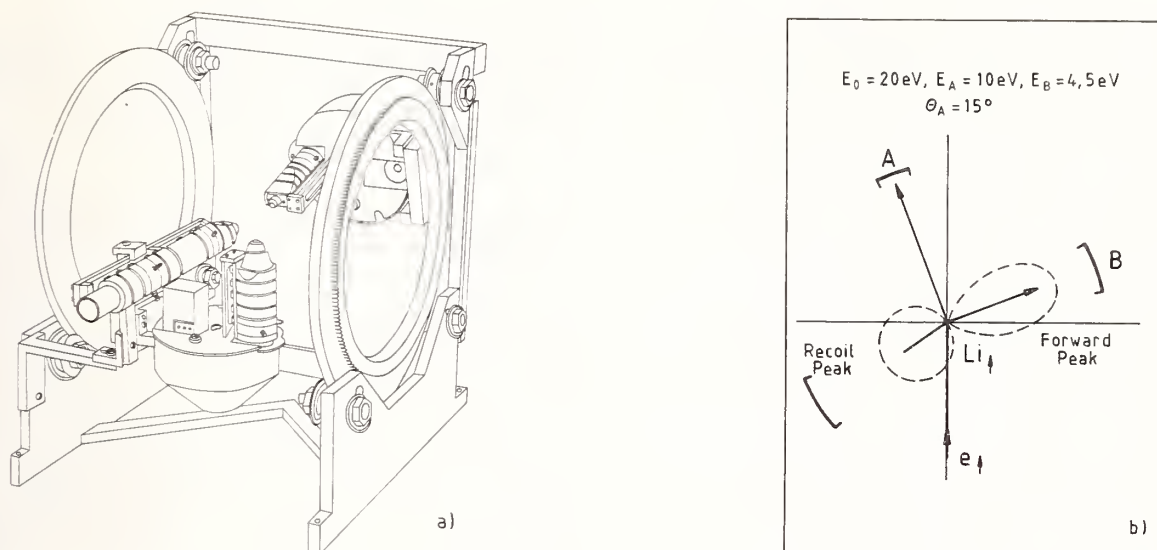


Figure 4. (a) Arrangement of the scattering geometry with the decelerating electron-beam optics and the two spectrometers, whose axis or rotation is coaxial with the lithium beam (not shown). (b) Depiction of a scattering distribution, scaled by momentum from He, with A and B indicating the angular acceptance of the "fast" and "slow" spectrometer, respectively.

energy scale is calibrated by observing the onset of ionization, $E_i = 4.8$ eV for $\text{He}(2^3\text{S})$ and 3.9 eV for Cs.

The apparatus to measure the spin asymmetry in triple differential electron impact ionization of polarized atoms, $A_{e,2e}$, also uses a crossed beam arrangement like the one shown schematically in Fig. 2. Studies are made on Li atoms. The atomic beam obtains its polarization through state selection in a permanent sextupole magnet.²¹ The polarization is limited here to $P_a(^6\text{Li}) = 0.3$. All the electron energies and momenta in an ionizing event are determined using a coplanar scattering geometry with two hemispherical electron spectrometers. The coincidence timing resolution, measured during tests on helium, is about

15 ns. The spectrometers can be rotated from $\pm 90^\circ$ to $\pm 150^\circ$, keeping a separation of $\geq 30^\circ$, and Fig. 4a shows their orientation to the crossed beams. The acceptance angles for the "fast" and "slow" electrons are $\pm 3.5^\circ$ and $\pm 10^\circ$, respectively, (see Fig. 4b) and the energy resolution is set to about 1 eV for maximum transmission. The first major investigation will be to measure the spin asymmetry in the "forward" and "recoil" peaks, near the maximum in the total ionization cross section.

Results for the spin asymmetry, A_1 , on $\text{He}(2^3\text{S})$ have been obtained recently²⁵ and are shown in Fig. 5. The asymmetry is positive throughout the energy range investigated, indicating dominance of singlet over triplet processes. The clear decrease of the asymmetry and therefore increase of

triplet processes in going towards threshold is interesting as it implies an increasing contribution from partial waves with $L > 0$. According to the analyses¹⁰⁻¹² of the structure of two electron wave functions at threshold, the following waves should be strongly presented: 1S_e , 3P_0 , 1D_e , 3F_0 , etc. These states are all expected to obey the same threshold law. Other states are suppressed in the threshold region. Therefore the growing importance of triplet states cannot be seen as a feature of the two-electron escape process. As all contributing states follow the same threshold law the asymmetry should be energy independent. In order to explain the observed decrease of A_i one has to assume an energy dependence of the initial conditions prepared in the inner reaction zone. This provides dynamical information on the ionization process.

There is only one calculation for comparison with the data (Fig. 5). Bartschat²⁶ used a distorted-wave Born-approximation (DWBA), assuming maximum interference, and included a local exchange potential. The discrepancy in the threshold region clearly indicates that interaction effects, for instance electron correlations in the exit channels, have to be treated more thoroughly. Qualitatively, the slope of A_i near threshold is also exhibited by the theory. A comparison with the experimental values for the lithium atoms⁵ is also shown. Throughout the measured energy range, the Li asymmetry values are higher by 0.05 to 0.07, but within the quoted normalization uncertainty of ± 0.05 the two data set could

still be considered to be equal. For the Li data there is an indication of a decrease of A_i towards threshold. The result of the DWBA calculation for Li is very much like the one for He(2^3S).

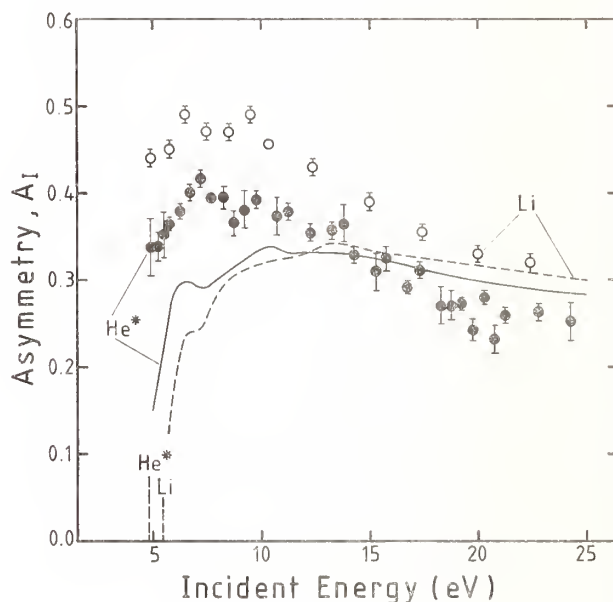


Figure 5. The energy dependence of the ionization asymmetry A_i for metastable He in the 2^3S state (He^*). The full data points are the recent experimental results²⁵, the open circles are measurements for the Li atom⁵. The full curve is the theoretical result for He^* , the broken curve is for Li. Both results are from the DWBA treatment of Bartschat.²⁶

We would like to thank Dr. K. Bartschat for communicating results prior to publication. This work was supported by the Sonderforschungsbereich 216 of the Deutsche Forschungsgemeinschaft.

References

- 1) M.J. Alguard, V.W. Hughes, M.S. Lubell, and P.F. Wainwright, *Phys.Rev.Lett.* 39, 334 (1977).
- 2) T.J. Gay, G.D. Fletcher, M.J. Alguard, V.W. Hughes, P.F. Wainwright, and M.S. Lubell, *Phys.Rev. A* 26, 3664 (1982).
- 3) G.D. Fletcher, M.J. Alguard, T.J. Gay, V.W. Hughes, P.F. Wainwright, M.S. Lubell, and W. Raith, *Phys.Rev.A* 31, 2854 (1985).
- 4) G. Baum, E. Kisker, W. Raith, U. Sillmen, and D. Zenses, *J.Phys. B* 14, 4377 (1981).
- 5) G. Baum, M. Moede, W. Raith, and W. Schröder, *J.Phys.B* 18, 531 (1985).
- 6) D. Hils, W. Jitschin, and H. Kleinpoppen, *J.Phys.B* 15, 3347 (1982).
- 7) M.H. Kelley, W.T. Rogers, R.J. Celotta, and S. Mielczarek, *Phys.Rev.Lett.* 51, 2191 (1983).
- 8) D. Hils and H. Kleinpoppen, *J.Phys.B* 11, L283 (1978).
- 9) H. Klar and W. Schlecht, *J.Phys.B* 9, 1699 (1976).
- 10) C.H. Greene and A.R.P. Rau, *Phys.Rev.Lett.* 48, 533 (1982).
- 11) A.D. Stauffer, *Phys.Lett.* 91A, 114 (1982).
- 12) C.H. Greene and A.R.P. Rau, *J.Phys.B* 16, 99 (1983).
- 13) A. Temkin, *Phys.Rev.Lett.* 49, 365 (1982); addendum: *Phys.Rev.A* 30, 2737 (1984).
- 14) H. Ehrhardt, K. Jung, G. Knoth and P. Schlemmer, *Z Phys.D* 1, 3 (1986).
- 15) E. Schubert, K. Jung, and H. Ehrhardt, *J.Phys.B* 14, 3267 (1981).
- 16) P. Fournier-Lagarde, J. Mazeau, and H. Huetz, *J.Phys.B* 17, L591 (1984).
- 17) P. Selles, A. Huetz, and J. Mazeau, *J.Phys.B* 20, 5195 (1987).
- 18) H. Ehrhardt, T. Rösel, P. Schlemmer, R. Agricola, and K. Jung, Abstract, XVI ICPEAC, New York (1989).
- 19) P.L. Altick and T. Rösel, *J.Phys.B* 21, 2635 (1988).
- 20) E.P. Curran and H.R.J. Walter, *J.Phys.B* 20, 337 (1987).
- 21) G. Baum, M. Moede, W. Raith, and U. Sillmen, *Phys.Rev.Lett.* 57, 1855 (1986).
- 22) W. Schröder and G. Baum, *J.Phys.E* 16, 52 (1983).
- 23) G. Baum, W. Raith, and H. Steidl, *Z.Phys.D* 10, 171 (1988).
- 24) R.N. Watts and C.E. Wiemann, *Opt. Commun.* 57, 45 (1986).
- 25) G. Baum, M. Fink, W. Raith, H. Steidl, and J. Taborski, Bielefeld Preprint 1989, submitted for publication.
- 26) K. Bartschat, *Physics Reports*, in press (1989), and private communication (1989).

"SPIN-ORBIT" EFFECTS IN INELASTIC ELECTRON-ATOM COLLISIONS: ARE EXPERIMENTS IN CONFLICT WITH THEORETICAL MODELS?

G.F. Hanne, University of Muenster, West Germany

1. INTRODUCTION

In the past decade numerous investigations that benefitted from progress in numerical calculations and experimental techniques have considerably promoted our quantitative understanding of spin dependent electron-atom collisions. For calculations of inelastic collisions the distorted-wave Born approximation¹⁻³ and the R-Matrix method⁴ have been improved to include effects from spin-orbit interactions, and first-order many body calculations⁵ have been performed which include intermediate-coupling schemes for excited states of noble gas targets. Experimentally, electron-photon coincidence measurements⁶⁻⁹ and experiments using polarized electrons¹⁰⁻¹² have been performed — even simultaneously¹³ — to probe the electron-atom collision process in greater detail than is possible through conventional cross section measurements. Parameters which are particularly sensitive to spin effects have been studied thoroughly to gain models that are adequate to describe spin-dependent collisions.

Even though the quantitative agreement between experimental and theoretical results is by no means perfect — in particular at electron energies between the excitation thresholds and 50 eV — we seem to understand quite well the spin phenomena that result from exchange collisions and the spin-orbit interactions. There are, however, some experimental findings — "target reflection-symmetry-breaking" collisions¹⁴ with exorbitant large relative spin-flip cross sections for large impact parameters — which are not supported by numerical calculations. These discrepancies are so large, that it seems to be a **qualitative** rather than a quantitative problem. This will be outlined in the following.

2. SPIN-DEPENDENT "FORCES" AND THEIR ACTIONS

The excitation of optically allowed transitions is, in general, dominated by direct collisions, where — in a semiclassical picture — an electron passing by an atom creates a fast-varying electric field that can excite the atom. This is possible even for rather distant collisions, and is associated with large cross sections which are peaked at forward scattering angles, clearly demonstrated by experimental and theoretical results formulated within the concept of the generalized oscillator strength.¹⁵ In contrast, the excitation of spin-forbid-

den transitions will require much closer **exchange** collisions, where the incident electron must deeply interact with the electronic cloud of the target atom. Exchange collisions are therefore more probable at small impact parameters and the resultant differential cross sections show a nearly isotropic shape (see, e.g., reference 5, figures 2–6). Moreover, if the velocity of the incident electron becomes much larger than the mean velocity of target electron with which it is exchanged, the exchange cross section becomes small and decreases — with increasing energy — much faster than the cross sections for direct scattering (for results see, e.g., references 10–12, or cf figures 4 and 8).

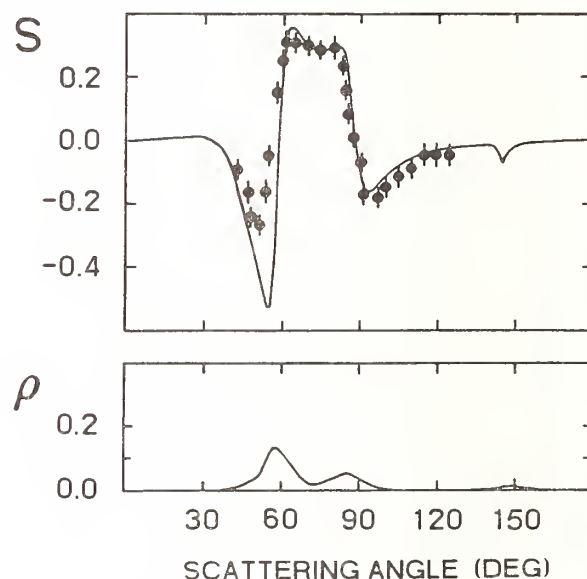


FIGURE 1. Sherman function S , and relative spin-flip cross section ρ for elastic scattering of 50 eV electrons from Xe atoms.^{16, 17}

From numerical calculations and experimental results one can conclude that the **spin-orbit interaction** of the continuum electron is a short-range force, which, compared to coulombic interactions, is generally small for low- Z targets like He ($Z = 2$), and for high- Z targets like Xe ($Z = 54$) significant spin effects are observed only if the electron comes close to the nucleus, and is thus scattered through angles $> 30^\circ$. To illustrate this we show in figure 1 experimental and theoretical results of the Sherman function $S(\theta)$ for elastic scattering of 50 eV electrons from Xe atoms.^{16, 17} $S(\theta)$ describes the left-right scattering asymmetry of polarized electrons (transverse polarization P)

$$A(\theta) = \frac{N_l - N_r}{N_l + N_r} = S(\theta) \cdot P, \quad (1)$$

where N_l and N_r are the numbers of electrons scattered to the left and to the right through the same angle θ , respectively. Also shown in figure 1 is the calculated relative cross section for spin flips along the axis of incidence,

$$\rho = \sigma(\text{SF})/\sigma, \quad (2)$$

where σ is the differential cross section, and $\sigma(\text{SF})$ is its spin flip part. Sherman function S and relative spin flip cross section ρ are related by

$$S = -2 \sqrt{\rho(1-\rho)} \sin \gamma, \quad (3)$$

where γ is the difference in the phases of the two complex scattering amplitudes (for direct and spin flip scattering) that describe elastic collisions from spinless targets.¹⁰ Equation (3) shows that, in particular for small ρ , the Sherman function is more sensitive to spin effects than the differential cross section to which, in the case of figure 1, spin-flip collisions contribute less than 15% at all scattering angles. In particular at small scattering angles ($\theta \leq 30^\circ$) the spin-flip cross section is tiny and approaches zero at $\theta = 0^\circ$. In inelastic collisions the spin-orbit interaction of the continuum electron with the nucleus has an even smaller effect because it cannot produce electronic transitions between atomic states. Hence it does not contribute to the first order of the transition amplitude.¹⁸

The spin-orbit interaction of the target electrons acts in a different way. If, like in He or Na, the fine-structure splitting is small (≤ 2 meV) it can be neglected during the short collision process (Percival-Seaton hypothesis), and LS-coupling is warranted for the entire collision system.¹⁸ If, however, the fine-structure splitting is comparable to the exchange splitting — like in Ne ($2p^5 3s$ excitation) — LS coupling does not apply for the atomic states. Thus the total spin of the collision system is not conserved even though, in Ne, the

additional spin effects are then expected — often called **spin-orbit (coupling) effects** — which, for heavy targets, are further modified by the spin-orbit interaction of the continuum electron.¹³

In the following we discuss some spin phenomena in different scattering systems studied recently in our laboratory.

3. LEFT-RIGHT SCATTERING ASYMMETRY FOR POLARIZED ELECTRONS SCATTERED SUPERELASTICALLY FROM LASER-EXCITED $\text{Na}^*(3^2P_{1/2,3/2})$ ATOMS

In this collision system ($Z = 11$ for Na) we can assume that the spin-orbit interactions during the collision process are negligible.¹² Surprisingly, however, calculations and experiments^{19,20} show that even in such a situation a strong left-right scattering or spin-up down asymmetry of polarized electrons that are scattered superelastically from unpolarized excited Na^* atoms is observed.

What is the origin of such scattering asymmetries? Let us assume, that the excited Na^* atoms are in the $3^2P_{1/2}$ state. A beam of unpolarized $2^2P_{1/2}$ atoms can be thought of as consisting of 50% with $M = 1/2$ and 50% with $M = -1/2$. For atoms with $M = 1/2$ (M is the magnetic quantum number of the total angular momentum for a quantization axis normal to the scattering plane), the orbital angular momentum is oriented mainly counterclockwise in the scattering plane, while the atomic spin is preferentially down. The situation is just the opposite for atoms with $M = -1/2$. These different orientations may cause different cross sections owing to an orbit effect (figure 2): The repulsive electron-electron Coulomb interaction may be somewhat different for electrons passing by an atom with $M = +1/2$ or $M = -1/2$, because for $M = +1/2$ continuum electron and valence electron move "parallel", and "antiparallel" for $M = -1/2$. For the sake of simplicity, let us now assume, that the cross section for $3^2P_{1/2} - 3^2S_{1/2}$ deexcitation collisions from $M = 1/2$ atoms is much larger than that for scattering from $M = -1/2$ atoms. The scattering then takes place with target atoms that are effectively spin polarized, because for $M = 1/2$ atoms the atomic spin is preferentially down (see figure 2). Consequently polarized continuum electrons show a spin-up-down scattering asymmetry because cross sections are, owing to exchange processes, in general different if the spin of the continuum electron and the atomic electron are parallel or antiparallel.

In a similar way the superelastic scattering from $2^2P_{3/2}$ atoms can be considered. Within the approximation discussed in this section we find for the spin up-down or left-right scattering asymmetry¹⁸

$$A(2^2P_{1/2}) = -2A(2^2P_{3/2}). \quad (4)$$

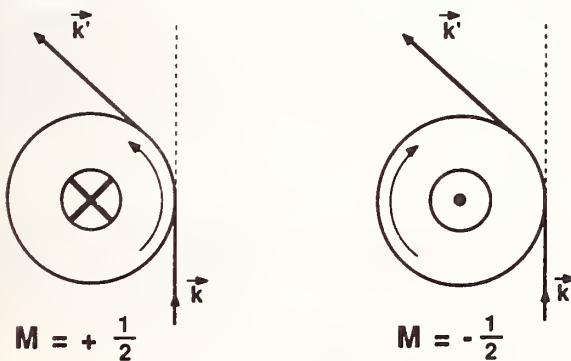


FIGURE 2. Semiclassical picture of electron scattering from $2^2P_{1/2}$ atoms.

spin-orbit interaction of the continuum electron is still negligible. In conjunction with exchange collisions

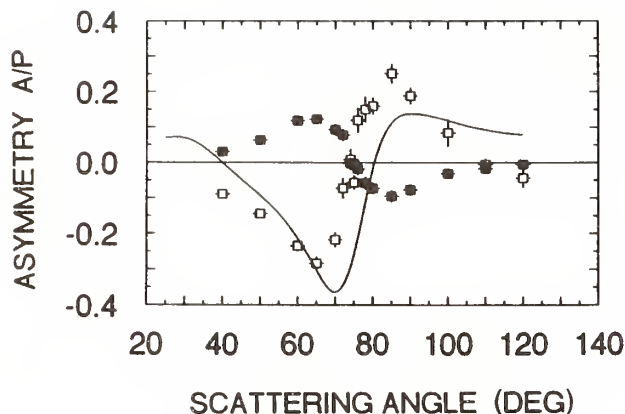


FIGURE 3. Left-right scattering asymmetry A/P for superelastic scattering of polarized 10 eV electrons from excited Na atoms. Experimental \circ ($3^2P_{1/2}$), \bullet ($3^2P_{3/2}$); two-state close-coupling calculation — ($3^2P_{1/2}$)²²

Any deviation from this relation indicates a spin-orbit effect.

Recent measurements of left-right scattering asymmetries obtained in our laboratory²¹ are shown in figure 3 together with numerical data taken from a two-state close-coupling calculation of Moores.²² There is fair agreement between the numerical and the experimental data in figure 3. Furthermore, within the statistical uncertainty, no deviation from equation (4) has been found experimentally, thus confirming the underlying model (in the calculation this model has been used, i.e., equation (4) is assumed to be valid).

4. DETERMINATION OF THE LIGHT POLARIZATION FOR OPTICAL TRANSITIONS IN CESIUM AFTER IMPACT EXCITATION BY POLARIZED ELECTRONS

Cesium atoms which are excited by collisions with slow polarized electrons show a strong circular polarization of the fluorescence light that is emitted in the direction of the electron polarization vector P_e . This is the result of a transfer of spin polarization to atomic orientation by exchange collisions.^{10, 23, 24} Such investigations have been performed recently by Nass et al²⁵ for longitudinally polarized electrons.

In the present experiment²⁶ we have measured linear and circular polarization components (Stokes parameters) using transversely polarized electrons, and consequently we have detected the photons that are emitted perpendicular to P_e , i.e. perpendicular to the incident electron beam direction. The circular polarization (Stokes parameter η_2) is defined by

$$\eta_2 = \frac{I(\sigma^+) - I(\sigma^-)}{I(\sigma^+) + I(\sigma^-)}, \quad (5)$$

where $I(\sigma^+)$ and $I(\sigma^-)$ are the intensities of light transmitted by polarization filters which fully transmit photons with positive and negative helicity, respectively.

In figure 4 are shown experimental results of η_2 of the $8^2S_{1/2} - 6^2P_{1/2}$ transition ($\lambda = 794$ nm), and of the $6^2P_{3/2} - 6^2S_{1/2}$ transition ($\lambda = 852$ nm), plotted versus electron energy. Strong circular polarization, caused by exchange collisions, has been found close to the excitation thresholds (3.01 eV and 1.46 eV, respectively). Even though the excitation of the $6^2P_{3/2}$ state is an optically allowed dipole transition the relative contribution of exchange behaves very similar to the (optically forbidden) excitation of the $8^2S_{1/2}$ state: The magnitude of the circular polarization decreases monotonically with increasing energy, and above 8 eV no significant circular polarization has been found. Numerical data from Nagy et al²⁷ for the $6^2P_{3/2} - 6^2S_{1/2}$ transition show fair agreement with the experimental data as shown in figure 4.

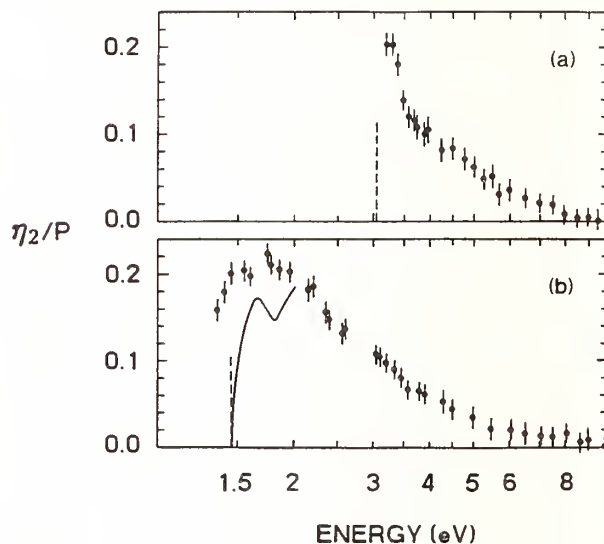


FIGURE 4. Circular polarization (Stokes parameter η_2) of light from (a) $8^2S_{1/2} - 6^2P_{1/2}$ and (b) $6^2P_{3/2} - 6^2S_{1/2}$ transitions in Cs excited by polarized electrons. Experimental \bullet ; R-matrix calculation —.²⁷ The excitation thresholds are indicated by a dashed line.

With respect to the topic discussed in this paper the linear polarization η_1 for the $6^2P_{3/2} - 6^2S_{1/2}$ transition is of special interest. This Stokes parameter is defined by

$$\eta_1 = \frac{I(45^\circ) - I(135^\circ)}{I(45^\circ) + I(135^\circ)}, \quad (6)$$

where $I(45^\circ)$ and $I(135^\circ)$ denote the fraction of intensity transmitted by a linear polarization filter which is inclined to the electron beam direction by 45° and 135° , respectively. As has been discussed by Bartschat and Blum²⁸ a nonzero value of η_1 shows directly the

influence of spin-orbit interactions during the scattering process. In figure 5 are shown experimental results for η_1 . We have found that η_1/P is very small even for inelastic collisions of electrons from cesium atoms ($Z = 55$). Bartschat, however, has pointed out that, at very low energies, a small η_1 does not necessarily mean that spin-orbit interactions and relativistic effects can be ignored in numerical calculations.²⁹

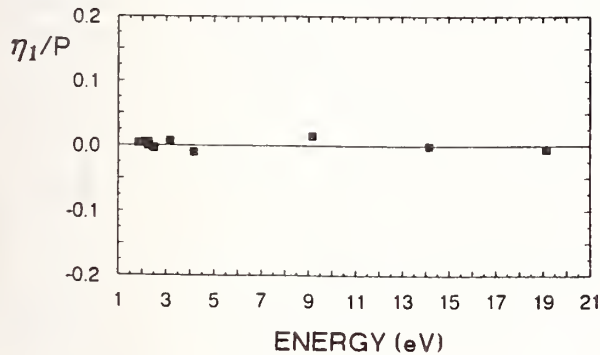


FIGURE 5. Stokes parameter η_1 for excitation of the $6^2P_{3/2} - 6^2S_{1/2}$ transition in Cs by polarized electrons.

5. SPIN-EFFECTS FOR ELECTRON-IMPACT EXCITATION OF MERCURY

For one-electron atoms like Na or Cs the atomic spin quantum number $S = 1/2$ is a well defined quantity. The situation is different for two-electron systems like excited rare gas or Hg atoms. For a sp (or ps) configuration the intermediate-coupling scheme

$$\phi(^1P_1) = \alpha \phi_{LS}(^1P_1) + \beta \phi_{LS}(^3P_1) \quad (7a)$$

$$\phi(^3P_2) = \phi_{LS}(^3P_2) \quad (7b)$$

$$\phi(^3P_1) = \alpha \phi_{LS}(^3P_1) - \beta \phi_{LS}(^1P_1) \quad (7c)$$

$$\phi(^3P_0) = \phi_{LS}(^3P_0) \quad (7d)$$

is often used. The subscript LS denotes pure Russell-Saunders states, i.e., they are coupled from the same 6s6p singlet and triplet orbitals. The intermediate coupling coefficients are, e.g., $\alpha = 0.985$ and $\beta = 0.171$ for Hg (6s6p) states², and $\alpha = 0.764$ and $\beta = 0.645$ for Xe (5p⁵6s).³

For measurements of the left-right scattering asymmetry A , cf equation (1), the intermediate coupling has the effect that a relation like¹⁸

$$A(^3P_1) = -A(^3P_2) \quad (8)$$

does not hold, in general. This is demonstrated in figure 6 where $A(^6P_{0,1,2})$ is plotted against scattering angle for electron-impact excitation of Hg at 12 eV.³⁰ Whereas equation (8) is clearly violated for $\theta < 60^\circ$ — probably because of the singlet admixture in equation (7c) — we found an approximate relation

$$A(^6P_0) = -2 A(^6P_2). \quad (9)$$

This indicates that the spin-orbit interaction of the continuum electron and differences in the radial parts of the wave functions (7b) and (7d), i.e. deviations from the intermediate coupling scheme, have only little effects.

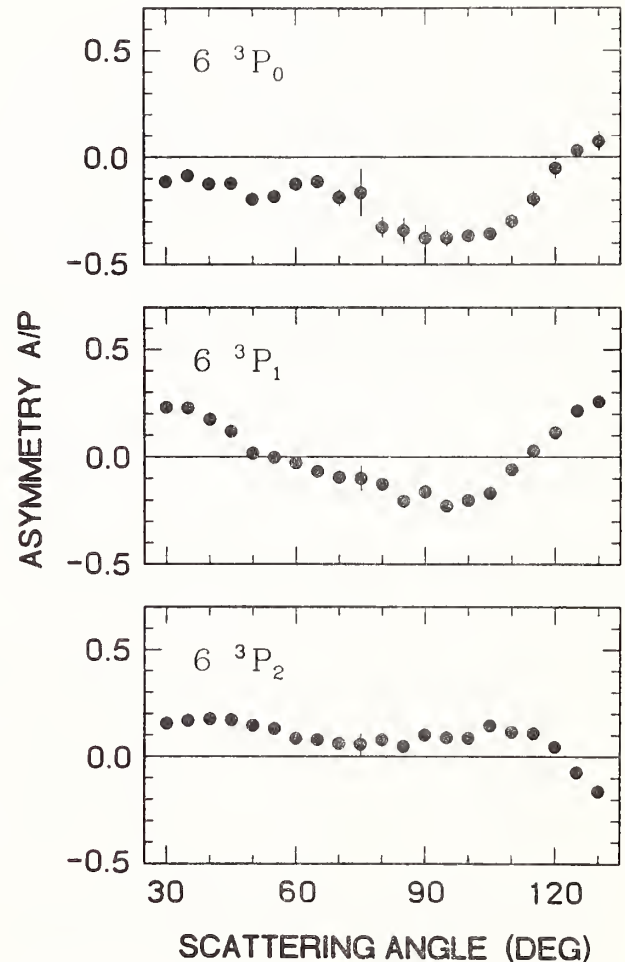


FIGURE 6. Left-right scattering asymmetry A/P for excitation of the 6^3P states of Hg by polarized electrons at $E = 12$ eV.

Whereas spin effects at large scattering angles and low energies that have been found in various experiments¹⁰⁻¹² are supported by numerical data, at least qualitatively, some experimental data seem to indicate that spin-orbit effects occur even at distant collisions and fairly high energies that are not supported by numerical results. As an example, we mention here the data of Plessis at al¹⁴ for electron-impact excitation of Xe $[3/2]^\circ_1$ at $E = 50$ eV and $\theta = 5^\circ$. In the intermediate coupling scheme the $[3/2]^\circ_1$ state corresponds to the state in equation (7c). From experimental data of P_1 and P_4 , which are linear polarization components obtained in electron-photon coincidence experiments, they determined the relative spin-flip cross section⁸

$$\rho_{00} = \frac{(1+P_1)(1-P_4)}{4-(1-P_1)(1-P_4)} \quad (10)$$

The term spin flip is here meant with respect to an axis normal to the scattering plane. The linear polarizations P_1 and P_4 are defined, similar to equation (6), by

$$P_{1,4} = \frac{I(0^\circ) - I(90^\circ)}{I(0^\circ) + I(90^\circ)}, \quad (11)$$

where P_1 is for photons that are emitted perpendicular to the scattering plane, and P_4 is for photons that are emitted perpendicular to the incident electron beam, but parallel to the scattering plane. As discussed by Anderson et al⁸, $P_4 = 1$ (and consequently $\rho_{00} = 0$) if spin flips are negligible for a $s \rightarrow p$ excitation. The experimental data of Plessis et al show values of ρ_{00} up to 0.15 for $\theta \leq 30^\circ$, whereas numerical results of Bartschat and Madison³ yield practically $\rho_{00} = 0$ ($< 5 \cdot 10^{-3}$) in this range ($E = 50$ eV, $\theta \leq 30^\circ$). Similarly, other experimental data for electron-impact excitation of rare gases^{14, 31, 32} disagree seriously with theory.^{3, 33} The relative spin-flip cross section $\rho_{00} \approx 0.2$ obtained by Murray et al⁹ for electron-impact excitation of the 6^1P_1 state of Hg ($E = 16$ eV, $\theta \leq 30^\circ$) is likewise much larger than predicted by theory.³⁴

We were interested in further experimental data for small-angle scattering and therefore we measured the linear polarization P_1 and P_4 for electron-impact excitation of the 6^3P_1 state in Hg.³⁶ Because this state has a stronger triplet character ($\alpha = 0.985$) compared to Xe $[3/2]^\circ_1$ with $\alpha = 0.764$, we expect that spin flip (by exchange) are more likely in e-Hg collisions. Moreover the spin-orbit interaction of the continuum electron is stronger in Hg ($Z = 80$) than in Xe ($Z = 54$). Hence we expect that spin-orbit (coupling) effects are stronger for excitation of Hg(6^3P_1) than for excitation of Xe $[3/2]^\circ_1$.

The experimental values of the polarizations P_1 and P_4 were corrected for depolarization by radiation trapping and hyperfine interaction. A serious problem were proper corrections for geometrical effects. The opening angle of the photon analyzer and the effective angular acceptance cone of the electron detection system (including effects from incident beam divergence and target size) had to be taken into account. In agreement with observations of Martus et al³⁵ a significant apparent depolarisation is caused by an opening angle effect of the electron analyzer if P_1 shows a strong dependence on the scattering angle. Thus a deconvolution procedure had to be included as well. Furthermore we had to correct the data for estimated misalignments of incident and scattered electron beam direction with respect to the photon emission angle. We found, in particular, that at small scattering angles $\theta_e \leq 15^\circ$ the mean orientation of the scattering plane cannot be properly estimated which resulted in large

uncertainties of the corrected data.

After all these corrections we determined the spin-flip cross section ρ_{00} from equation (10). The result is shown in figure 7 for $E = 50$ eV and $\theta < 30^\circ$. A theoretical curve (DWBA calculation from Bartschat³⁴) shows very good agreement with the experimental data. From our experiments we cannot exclude relative spin-flip cross sections of, e.g., $\rho_{00} = 0.01$ for $\theta = 0^\circ$, which still were much larger than predicted by theory. However, as indicated by figure 1 and figure 8

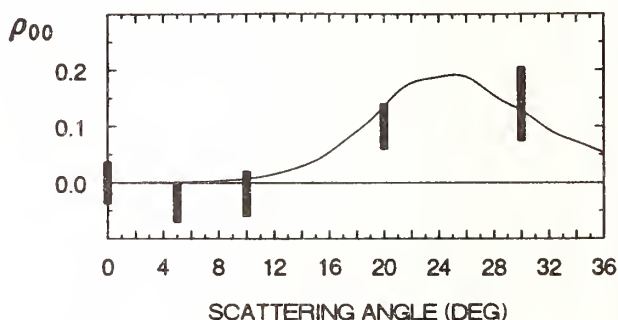


FIGURE 7. Relative spin-flip cross section ρ_{00} for electron-impact excitation of Hg (6^3P_1 state) at 50 eV. Experimental ■, ³⁶ theory — ³⁴

(which shows no excitation of the $6^3P_{0,2}$ states at energy losses of 4.67 and 5.46 eV, respectively, for $E = 50$ eV and $\theta \approx 0^\circ$) spin flips caused by either the spin-orbit interaction of the continuum electron or spin exchange are very unlikely at 50 eV and small scattering angles for the two collision systems under discussion (Hg(6^3P_1) and Xe $[3/2]^\circ_1$ excitation).

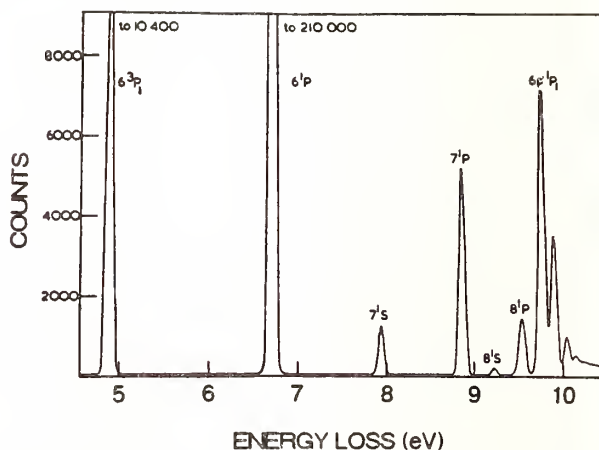


FIGURE 8. Electron-impact energy loss spectrum of Hg at $E = 50$ eV and $\theta \approx 0^\circ$

6. CONCLUSIONS

While present theoretical models underlying numerical calculations work fairly well to describe spin effects in inelastic collisions at large scattering angles

and low energies⁴ they cannot predict relative spin-flip cross sections as large as $\rho_{00} = 0.15$ experimentally obtained for small-angle inelastic scattering ($E = 50$ eV $\theta < 20^\circ$) from Xe $[3/2]_1$ excitation.¹⁴ Our experimental data (Hg(6^3P_1) excitation) agree well — even quantitatively — with theoretical data.³⁴ Because theoretical data yield values of ρ_{00} that are orders of magnitude smaller than sometimes found experimentally one explanation would be that in these cases currently used numerical procedures fail completely to describe large-impact parameter collisions and/or that some, hitherto unknown, long range spin-dependent forces are acting in these collisions. However, it is very unlikely that other, but reasonable, theoretical models will yield such large values of ρ_{00} . Thus we feel that the explanation of such data must come from elsewhere. We found it extremely difficult to control the instrumental uncertainties, in particular at very small scattering angles, during the entire accumulation time of 12 hours and longer. Thus the given error bars may still be too optimistic. A clear-cut direct experimental observation of spin-flip collisions would require an experiment of the "triple scattering" type.^{10,16,38} Such investigations, using a different experimental method, should be performed if the discrepancies, that are obtained by the electron-photon coincidence method, cannot be resolved.

Acknowledgements. The author would like to thank his coworkers in Muenster for their constructive and fruitful cooperation. This work has been supported by the Deutsche Forschungsgemeinschaft in Sonderforschungsbereich 216 Polarisation and Correlation in Atomic Collision Complexes.

References

- 1 D.H. Madison and W.N. Shelton, Phys. Rev. A7, 514 (1973)
- 2 K. Bartschat, D.H. Madison and G.F. Hanne, J. Phys. B 18, 1847 (1985)
- 3 K. Bartschat and D.H. Madison, J. Phys. B 20, 5839 (1987)
- 4 K. Bartschat and P.G. Burke, Comments At. Mol. Phys. 16, 271 (1985)
- 5 N.T. Padial, G.D. Meneses, F.J. da Paixao, G. Csanak and D.C. Cartwright, Phys. Rev. A23, 2194 (1981)
- 6 M. Erminyan, K.B. MacAdam, J. Slevin and H. Kleinpoppen, J. Phys. B 7, 1519 (1974)
- 7 J. Slevin, Rep. Prog. Phys. 47, 461 (1984)
- 8 N. Andersen, J.W. Gallagher and I.V. Hertel, Phys. Rep. 165, 1 (1988)
- 9 A.J. Murray, C.J. Webb, W.R. MacGillivray and M.C. Standage, Phys. Rev. Lett. 4, 411 (1989)
- 10 J. Kessler, Polarized electrons (2nd edn., Berlin: Springer, 1985)
- 11 W. Raith in Fundamental Processes of Atomic Dynamics (New York: Plenum 1989)
- 12 G.F. Hanne in Coherence in Atomic Collision Physics (H.J. Beyer, K. Blum and R. Hippler eds., New York: Plenum), 41 (1988)
- 13 J. Goeke, G.F. Hanne and J. Kessler, J. Phys. B 22, 1075 (1989)
- 14 P. Plessis, M.A. Khakoo, P. Hammond and J.W. McConkey, J. Phys. B 21 L483 (1988)
- 15 H.S.W. Massey and E.H.S. Burhop, Electronic and Ionic Impact Phenomena Vol. 1 (Oxford: Clarendon Press), 434 (1969)
- 16 O. Berger and J. Kessler, J. Phys. B 19, 3539 (1986)
- 17 R. Haberland, L. Fritsche and J. Noffke, Phys. Rev. A33, 2305 (1986)
- 18 G.F. Hanne, Rep. Progr. Phys. 95, 95 (1983)
- 19 G.F. Hanne, Cz. Szmytkowski and M. van der Wiel, J. Phys. B 15, L109 (1982)
- 20 J.J. McClelland, M.H. Kelley and R.J. Celotta, Phys. Rev. Lett. 55, 688 (1985)
- 21 V. Nickich, T. Hegemann and G.F. Hanne, to be published
- 22 D.L. Moores, Comput. Phys. Commun. 2, 360 (1971)
- 23 P.S. Farago and J.S. Wykes, J. Phys. B2, 747 (1969)
- 24 H. Kleinpoppen, Phys. Rev. A3, 2015 (1971)
- 25 P. Nass, M. Eller, N. Ludwig, E. Reichert and M. Webersinke, Z. Phys. D 11, 71 (1989)
- 26 F. Eschen, G.F. Hanne, K. Jost and J. Kessler, to be published
- 27 O. Nagy, K. Bartschat, K. Blum, P.G. Burke and N.S. Scott, J. Phys. B 17, L527 (1984)
- 28 K. Bartschat and K. Blum, Z. Phys. A304, 85 (1982)
- 29 K. Bartschat, J. Phys. B, to be published
- 30 H. Dümmler, M. Bartsch, H. Geesmann, G.F. Hanne and J. Kessler, to be published
- 31 A. Danjo, T. Koike, K. Sani, H. Sugahara, A. Takahashi and H. Nishimura, J. Phys. B 18, L595 (1985)
- 32 H. Nishimura, A. Danjo and A. Takahashi, J. Phys. B 19, L167 (1986)
- 33 G.D. Meneses, F.J. da Paixao and N.T. Padial, Phys. Rev. A 32, 156 (1985)
— Phys. Rev. A 34, 675 (1986)
- 34 K. Bartschat, private communication
- 35 K.E. Martus, K. Becker and D.H. Madison, Phys. Rev. A38, 4876 (1988)
- 36 T. Simon, M. Sohn and G.F. Hanne, to be published
- 37 A. Skerbele and E.N. Lassettre, J. Chem. Phys. 56, 845 (1972)
- 38 G.F. Hanne and J. Kessler, J. Phys. B9, 791 (1976)

Optical Analysis of Electron Impact Induced
Excited State-Excited State Transitions in Alkali Atoms*

Bernhard J. Stumpf, Department of Physics, University of Idaho
Moscow, ID 83843

*Supported by University of Idaho Research Council, Westinghouse Corporation for Idaho Nuclear Engineering Laboratories, and the National Science Foundation (NSF-EPSCoR).

1. INTRODUCTION

Experimental and theoretical work on inelastic atom-electron collisions has thus far concentrated on the $nS-n'L'$ problem, particularly on $nS-n'P$ electron impact induced transitions. As is documented by other contributions to this symposium much progress has been made in understanding this type of transition. Differential cross sections for magnetic sublevels with separation of direct, interference, and exchange processes and even scattering phases have been reported. An excellent review has been given by Andersen, Gallagher and Hertel.¹

On the other hand, very little work has been done on the general $nL \rightarrow n'L'$ problem when both L and L' are different from zero. Differential scattering data have been obtained by Bederson and coworkers² for $Na\ 3P \rightarrow 3P, 3D$. Stumpf and Gallagher³ have measured the angular-integrated $Na\ 3P, M_L=1 \rightarrow 3D$ cross section and estimated the $3P \rightarrow 3D$ cross section. We are currently setting up a laboratory devoted to optical study of excited state-excited state electron-alkali collisions. This paper describes the experimental method, derives the theoretical formulas that relate optical observables with collision cross sections and presents numerical results using Born and Born-Ochkur approximations.

2. METHOD

Figure 1 and 2 show the experimental method in the case of cesium: In figure 1, the $6^2S_{1/2}$ ground state is optically excited to the $6^2P_{3/2}$ ground state. Electron impact excitation from the $6^2P_{3/2}$ state to a higher $n' \ ^2D_{J'}$ state is optically analyzed by measuring total fluorescence intensity and linear polarization of the $n' \ ^2D_{J'} \rightarrow 6^2P_{J''}$ transition. As a specific example, figure 1 shows the case of impact excitation of the $7^2D_{3/2}$ state and optical detection of the $7^2D_{3/2} \rightarrow 6^2P_{1/2}$ transition. Figure 2 illustrates the principle of the experimental set-up: In a crossed beam arrangement with atom beam travelling in x-direction, electron beam and laser beam are counterpropagating along the z-axis. Total fluorescence intensity and linear polarization are measured in y-direction. The $6^2P_{3/2}$ state, initial state for electron impact excitation, is prepared as pure spin state, $|J=\frac{3}{2}, M_J=\frac{3}{2}\rangle = |L=1, S=\frac{1}{2}, M_L=1, M_S=\frac{1}{2}\rangle$, by a cw circularly polarized diode laser tuned to the $F=4 \rightarrow F'=5$ hyperfine component of the

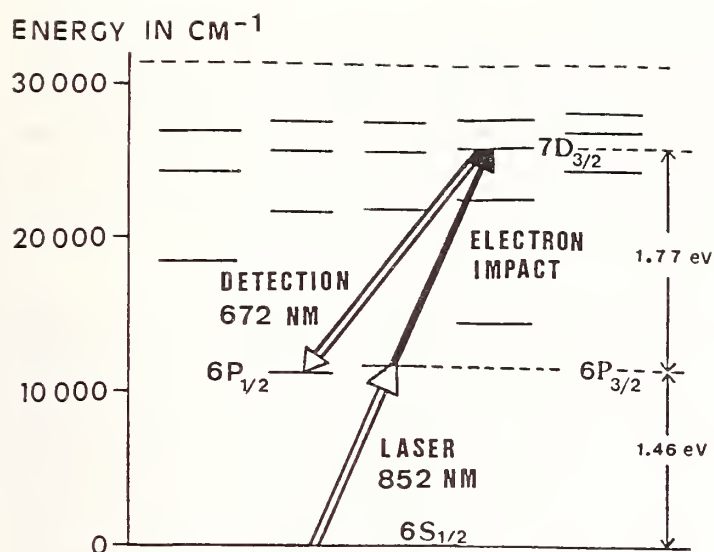


Figure 1. Cesium energy levels. Electron impact excitation of the $7\ ^2D_{3/2}$ state from the laser-excited $6\ ^2P_{3/2}$ state analyzed by optical detection of the $7\ ^2D_{3/2} \rightarrow 6\ ^2P_{1/2}$ transition.

Figure 2. Experimental arrangement.

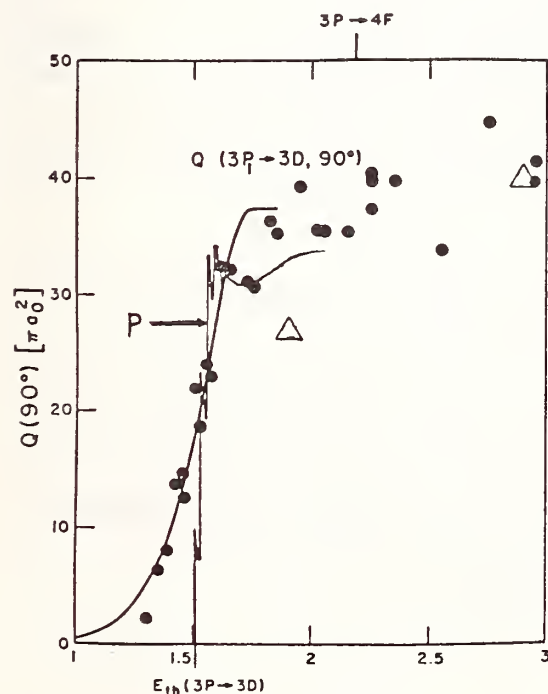
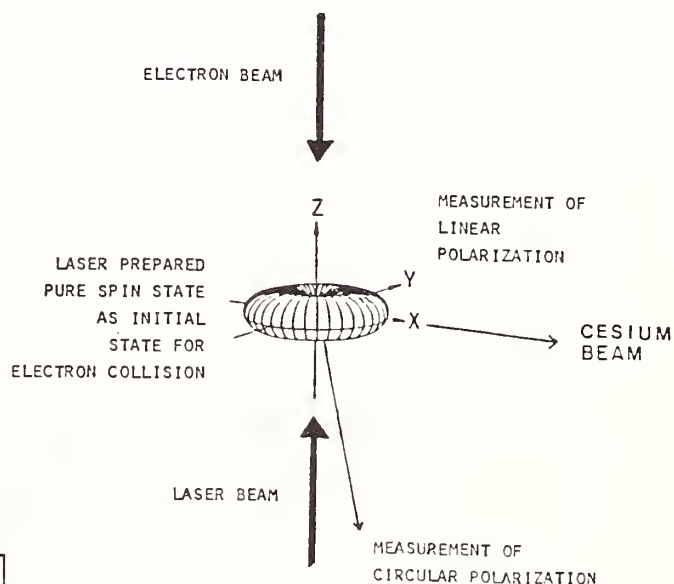


Figure 3. Experimental Na $3P, M_L=1 \rightarrow 3D$ electron impact cross section of reference 3 (●) compared with theoretical calculations of reference 4 (thin, structured line labeled "P") and reference 5 (triangles). The thick solid line is the convolution of a step function with the measured energy distribution. A detailed discussion is given in reference 3.

$6^2S_{1/2} \rightarrow 6^2P_{3/2}$ resonance transition. Measurement of the total fluorescence intensity of the $n^2D_{J'} \rightarrow 6^2P_{J''}$ transition yields, save for cascading, the $6^2P_{3/2}, M_J = \frac{3}{2} \rightarrow n^2D_{J'}$ electron impact cross section. Measurements of the linear polarization probes the magnetic sublevel population of the $n^2D_{J'}$ state and therefore $6^2P_{3/2}, M_J \rightarrow n^2D_{J'}, M_{J'}$ electron impact induced collisions.

3. NOVEL FEATURES

Two features are specific of excited state-excited state electron collisions and optical studies of these processes:

1. Both initial and final state are imbedded in a manifold of other excited states. Rich structure in cross sections, particularly for energies below the ionization limit can be expected as a consequence of resonances, cusps and flux redistribution. To illustrate this we show in figure 3 experimental data³ for the Na 3P, $M_L = 1 \rightarrow 3D$ cross section. Within the energy resolution of the experiment (0.29 eV), this cross section is a step function at threshold. Unpublished close coupling calculations by Da Paixao⁴ agree well with the experimental result. Calculations by Moores et al.⁵ are also shown. Note that figure 3 is a summary of the present status of $nL \rightarrow n'L'$ ($L, L' \neq 0$) electron impact excitation cross sections in the intermediate range of principal quantum numbers n .
2. Laser preparation as described above creates a pure quantum mechanical state, an ideal situation for collision studies. Furthermore, the laser-prepared state $|L S M_L M_S\rangle$ with $M_L = 1$ and $M_S = \frac{1}{2}$ is rather special as initial state for electron impact excitation: Differential cross sections $\sigma(LM_L = 1 \rightarrow L'M_{L'})$ and $\sigma(LM_L = 1 \rightarrow L' - M_{L'})$ are not equal! (For $nS \rightarrow n'L'$ transitions, on the other hand, $\sigma(M_{L'}) = \sigma(-M_{L'})$ always holds.) As we will show below, this simple asymmetry leads to a linear polarization that depends explicitly on electron exchange. No such explicit dependence is possible after $nS \rightarrow n'L'$ impact excitation. That measurement of the linear polarization, a very straightforward experimental procedure, yields detailed information on exchange processes, is a particularly exciting aspect of optical studies of $nL \rightarrow n'L'$ ($L, L' \neq 0$) collisions.

4. RELATIONSHIP BETWEEN OPTICAL OBSERVABLES AND COLLISIONAL CROSS SECTIONS.

Consider electron impact excitation from a single state of an alkali atom $|L S M_L M_S\rangle$ to a manifold of states $\{|L' S M_{L'} M_{S'}\rangle\}$. After impact excitation the manifold $\{|L' S M_{L'} M_{S'}\rangle\}$ recouples into a manifold $\{|J' M_{J'}\rangle\}$. After recoupling $\{|J' M_{J'}\rangle\}$ decays to a lower manifold $\{|J'' M_{J''}\rangle\}$ by photon emission. We relate light intensities for the decay $\{|J' M_{J'}\rangle\} \rightarrow \{|J'' M_{J''}\rangle\}$ to cross sections for electron impact excitation $|L S M_L M_S\rangle \rightarrow \{|L' S M_{L'} M_{S'}\rangle\}$.

Basic assumptions are:

- Axial symmetry for impact excitation, that is, off-axis scattered electrons are not observed.
- Validity of the Percival-Seaton hypothesis⁶, that is M_L $M_{L'}$ and M_S $M_{S'}$ are good quantum numbers for impact excitation $|L S M_L M_S\rangle \rightarrow |L' S M_{L'} M_{S'}\rangle$
- Fully resolved fine structure and fully unresolved hyperfine structure in the impact excited states.

The last two assumptions are obviously equivalent to the sequence $\tau_{\text{coll}} \ll \tau_{\text{fs}} \ll \tau_{J'} \ll \tau_{\text{hfs}}$ where τ_{coll} is the collisional interaction time, τ_{fs} and τ_{hfs} are the relaxation time for fine and hyperfine structure, respectively and $\tau_{J'}$ is the lifetime of an impact excited J' state. $\tau_{\text{coll}} \ll \tau_{\text{fs}}$ is a good assumption for light alkalis but a first approximation only for heavy alkalis like cesium; $\tau_{\text{fs}} \ll \tau_{J'} \ll \tau_{\text{hfs}}$ is a good assumption for alkali D states.

We then have

$$I_Z = \sum_{J'M_{J'}} Q(J'M_{J'}) \cdot A_Z(J'M_{J'})$$

$$I_X = \sum_{J'M_{J'}} Q(J'M_{J'}) A_X(J'M_{J'})$$

where I_Z and I_X are light intensities linearly polarized along the z and x-axis, $Q(J'M_{J'})$ is the angular-integrated cross section for impact excitation of the state $|J'M_{J'}\rangle$ from $|L S M_L M_S\rangle$ and $A_Z(J'M_{J'})$ and $A_X(J'M_{J'})$ are optical transition probabilities given as

$$A_Z(J'M_{J'}) = \sum_{J''} A(J'M_{J'} \rightarrow J''M_{J'})$$

$$A_X(J'M_{J'}) = \frac{1}{2} \sum_{J''} \{A(J'M_{J'} \rightarrow J''M_{J'}-1) + A(J'M_{J'} \rightarrow J''M_{J'}+1)\}$$

We use

$$Q(J'M_{J'}) = \sum_{M_L' M_{S'}} (L' S M_L' M_{S'} | L' S J' M_{J'})^2 Q(M_L' M_{S'})$$

and, for a target with $M_S = \frac{1}{2}$,

$$Q(M_L' M_{S'}) = \begin{cases} Q^d(M_L') + Q^i(M_L') & \text{for } M_{S'} = \frac{1}{2} \\ Q^e(M_L') & \text{for } M_{S'} = -\frac{1}{2} \end{cases}$$

where Q^d , Q^i , Q^e are cross sections for direct, interference and exchange excitation.⁷ We then obtain for the linear polarization, defined as,

$$P_{\text{Lin}} = \frac{I(z) - I(x)}{I(z) + I(x)} \times 100\%,$$

$$P_{\text{Lin}} = \frac{\sum_{M_{L'}} a(M_{L'}) \{Q^d(M_{L'}) + Q^i(M_{L'}) + Q^e(-M_{L'})\}}{\sum_{M_{L'}} b(M_{L'}) \{Q^d(M_{L'}) + Q^i(M_{L'}) + Q^e(-M_{L'})\}} \times 100\% \quad (1)$$

Analogously, the circular polarization

$$P_{\text{circ}} = \frac{I^{\sigma^+} - I^{\sigma^-}}{I^{\sigma^+} + I^{\sigma^-}} \times 100\%$$

is found to be

$$P_{\text{circ}} = \frac{\sum_{M_{L'}} c(M_{L'}) \{Q^d(M_{L'}) + Q^i(M_{L'}) - Q^e(-M_{L'})\}}{\sum_{M_{L'}} d(M_{L'}) \{Q^d(M_{L'}) + Q^i(M_{L'}) + Q^e(-M_{L'})\}} \times 100\% \quad (2)$$

The coefficients a , b , c , d as a function of $M_{L'}$ are given in the table below for D state impact excitation and $D \rightarrow P$ unresolved multiplet detection.

Note that Q^e is summed over $-M_{L'}$ in equation (1); this implies, in general, an explicit exchange dependence of the linear polarization. Only if the initial state has $L=0$ $Q^{d,i,e}(M_{L'}) = Q^{d,i,e}(-M_{L'})$ holds and one obtains

$$P_{\text{Lin}} = \frac{\sum_{M_{L'}} a(M_{L'}) Q(M_{L'})}{\sum_{M_{L'}} b(M_{L'}) Q(M_{L'})} \times 100\% \quad \text{for } L = 0 \quad (1a)$$

and

$$P_{\text{circ}} = \frac{\sum_{M_{L'}} c(M_{L'}) \{Q(M_{L'}) - Q^e(M_{L'})\}}{\sum_{M_{L'}} d(M_{L'}) Q(M_{L'})} \times 100\% \quad \text{for } L = 0 \quad (2a)$$

(1a) has been treated by Percival and Seaton⁶ and (2a) by Kleinpoppen⁸.

Table: Coefficients in equations (1) and (2) for D state excitation and $D \rightarrow P$ detection.

$M_{L'}$	-2	-1	0	+1	+2
a	-78	111	114	3	-150
b	174	237	238	201	150
c	-126	-39	36	99	150
d	126	63	62	99	150

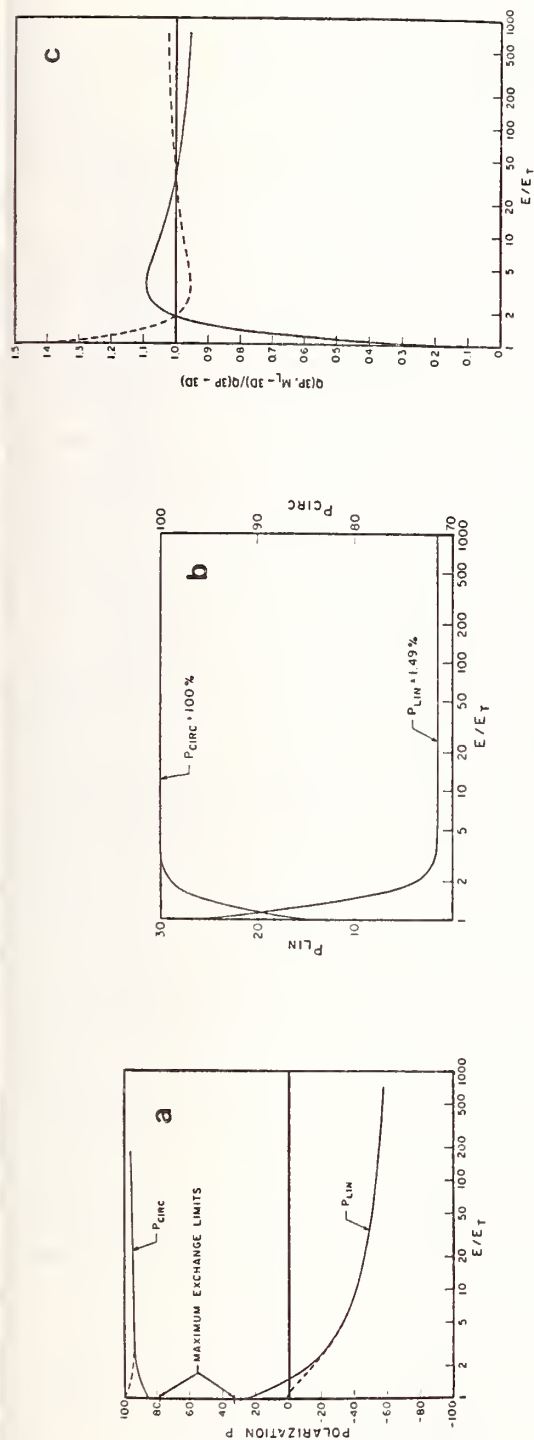


Figure 4: Na 3P, $M_L=1$, $M_S=1/2-3D$ electron impact excitation, 3D-3P unresolved multiplet detection. Electron energy E in threshold units E_T (a): Linear and circular polarization P_{LIN} and P_{CIRC} if scattered electrons are not detected; solid lines Born-Ochkur, dashed lines Born. Maximum exchange limits at threshold are 33.3% for P_{LIN} and 78.7% for P_{CIRC} . (b): Linear and circular polarization P_{LIN} and P_{CIRC} in Born-Ochkur approximation if forward scattered electrons are detected in coincidence with photons (c): Ratio of partial cross sections $Q(3P, M_L=3D)/Q(3P+3D)$ in Born approximation. Solid line $M_L=0$, dashed line $M_L=1$.

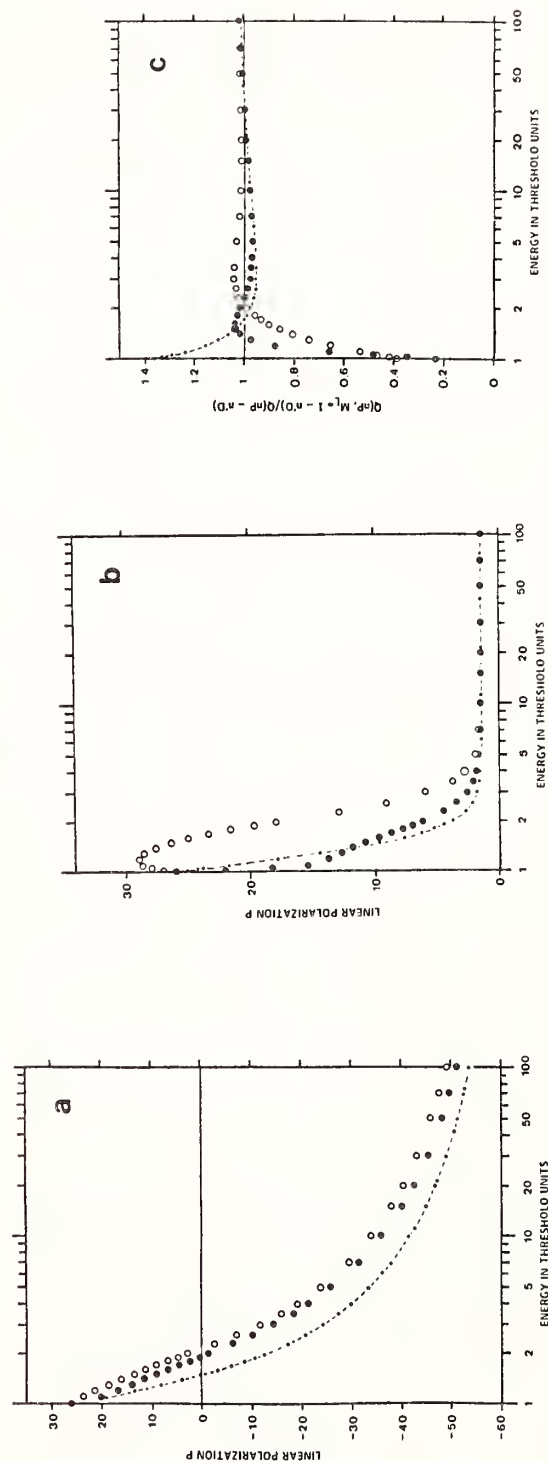


Figure 5: nL $M_L=1$, $M_S=1/2-n'L'$ impact excitation, $n'L'-nL$ unresolved multiplet detection. Open circles Rb 5p-6d; solid circles Cs 6p-7d; points with dashed line Na 3p-3d. (a): Linear polarization in Born-Ochkur approximation if scattered electrons are not detected (b): Linear polarization in Born-Ochkur approximation if forward scattered electrons are detected in coincidence with photons (c): Ratio of partial cross sections $Q(nP, M_L=1-n'D)/Q(nP-n'D)$ in Born approximation.

5. RESULTS FOR nP , $M_L = 1$, $M_S = \frac{1}{2} \rightarrow n'D$ ELECTRON IMPACT EXCITATION IN BORN AND BORN-OCKKUR APPROXIMATION

Figure 4 shows calculated results for Na $3P$, $M_L = 1$, $M_S = \frac{1}{2} \rightarrow 3D$ excitation and $3D \rightarrow 3P$ fluorescence detection, figure 5 compares these results with calculations for Rb $5P$, $M_L = 1$, $M_S = \frac{1}{2} \rightarrow 6D$ excitation/ $6D \rightarrow 5P$ detection and Cs $6P$, $M_L = 1$, $M_S = \frac{1}{2} \rightarrow 7D$ excitation/ $7D \rightarrow 6P$ detection. The comparison between Born (no exchange) and Born-Ochkur (with exchange) data in figure 4a shows the strong exchange dependence of linear and circular polarization at low energies, especially threshold. The threshold value for linear polarization is between 1.49% (no exchange) and 33.3% (maximum exchange), for circular polarization between 78.7% (maximum exchange) and 100% (no exchange), defining maximum exchange by $Q^e = \frac{4}{3}Q$. Born-Ochkur gives 26.0% and 85.2% for linear and circular polarization at threshold. Figure 5a shows that the linear polarization in Born-Ochkur approximation increases with effective quantum number of the impact excited state (Na $3D$: 2.99, Cs $7D$: 4.53, Rb $6D$ 4.68). Figure 4b shows, in Born-Ochkur approximation, linear and circular polarization for a pseudo-threshold experiment where forward scattered electrons are detected in coincidence with photons. Figure 5b indicates that such results are crucially n -dependent. Figure 4c compares, in Born approximation, the partial cross section $Q(3P, M_L = 1 \rightarrow 3D)$ with the total cross section $Q(3P \rightarrow 3D)$. Again, strong n -dependence is shown in figure 5c.

In conclusion, we have shown how optical methods can shed some first light on the yet unexplored physics of atomic excited state-excited state transitions upon electron impact. Theoretical calculations in Born and Born-Ochkur approximation have been presented.

ACKNOWLEDGMENT: The support of our graduate students Uma Krishnan, Leslie Wood and Gu Zhengang and undergraduate students Mark Dexter (now at Washington State University), Rich Alva, Russ Lawrence and Curt Martin is gratefully acknowledged.

REFERENCES:

1. N. Andersen, J. W. Gallagher and I. V. Hertel, Phys. Rep. **165**, 1 (1988).
2. M. Zuo, T. Jiang, L. Vusković, B. Stumpf and B. Bederson, Abstracts of contributed papers, XV ICPEAC, Brighton, England (1987).
3. B. Stumpf and A. Gallagher, Phys. Rev. A **32**, 3344 (1985).
4. F. J. Da Paixao, private communication.
5. D. L. Moores, D. W. Norcross and V. B. Sheorey, J. Phys. B **7**, 371 (1974).
6. I. C. Percival and M. J. Seaton, Phil. Trans. R. Soc. London A **251**, 113 (1958).
7. J. Kessler, Polarized Electrons, 2nd edition, Springer 1985.
8. H. Kleinpoppen, Phys. Rev. A **3**, 2015 (1971).

THE STEPWISE EXCITATION COINCIDENCE TECHNIQUE

M.C. Standage, W.R. MacGillivray, A.J. Murray & C.J. Webb

Division of Science and Technology, Griffith University, Nathan, Queensland 4111, Australia.

1.0 Introduction

In this paper a review is presented of a new type of electron-photon correlation technique for investigating inelastic electron-atom collisions which uses a combination of conventional electron-photon coincidence and laser excitation techniques¹. Target atoms are stepwise excited by a combination of electron and laser excitation with photons emitted from these atoms being detected in time delayed coincidence with electrons inelastically scattered during the collision process. The polarized photon correlation signals so obtained are analysed to determine the atomic collision parameters for the electron impact excited state.

Conventional electron-photon coincidence techniques have been used in electron-atom collision studies over the past sixteen years following the first coincidence experiments performed by Kleinpoppen and collaborators^{2,3}. This field has been extensively reviewed by Bium & Kleinpoppen 1979⁴, Sievin 1984⁵ and Andersen et al 1988⁶. Initial experiments made use of angular correlation measurements in the scattering plane containing the incident and scattered electron trajectories. However, even the simplest collision processes, such as the $^1S - ^1P$ excitation of a light L-S coupled atom, requires the measurement of polarized photon correlations out of the scattering plane. Where planar symmetry breaking mechanisms exist, such as strong spin-orbit interactions in heavy atoms which can cause spin-flips, measurements of polarized photon correlations are required both out of, and in the scattering plane to obtain a full measurement of all the atomic collision parameters associated with an S-P excitation.

The introduction of laser techniques to the atomic collisions field followed the development of tunable dye lasers in the early 1970's. Techniques developed included superelastic scattering⁷, atomic beam deflection⁸ and stepwise excitation techniques (MacGillivray & Standage 1988⁹). Stepwise excitation techniques have already been used in a number of non-coincidence investigations of electron-atom collision processes that have been reviewed by MacGillivray & Standage 1988. Such techniques have enabled previously inaccessible data to be obtained on

partial total cross sections for the electron impact excitation of metastable states. The narrow bandwidth available from lasers has been used in experiments in which the role of spectroscopic structure in electron-atom collision processes has been investigated. Such methods have also been used to provide data which is free from the depolarizing effects of atomic hyperfine structure. Stepwise excitation techniques have also provided a new method for investigating the electron impact excitation of VUV transitions.

One of the objectives of the research described in this paper has been to demonstrate the feasibility of using stepwise excitation coincidence techniques and to show their application to the study of the electron impact excitation of VUV transitions, which have been of such general interest in this research field. Many ground to first excited state VUV transitions of interest in atomic collision investigations are connected to higher lying transitions in the visible part of the spectrum so that stepwise excitation techniques can be widely applied. Such an excitation scheme, which combines VUV and visible transitions has already been investigated by the authors⁹ using non-coincidence techniques to measure partial total cross sections for the 6^1P_1 state of mercury. In these experiments, the initial electron excitation of the $6^1S_0 - 6^1P_1$ (185nm) VUV transition was followed by laser excitation of the $6^1P_1 - 6^1D_2$ (579nm) transition. Fluorescence was observed on the $6^1D_2 - 6^3P_1$ (313nm) transition. The lifetime of the 6^1P_1 state is short (1.3ns) while the 6^1D_2 state lifetime is 11ns. Consequently, the expected duration of the coincidence signal is of the order of 20ns. Considerable hyperfine structure is present in these transitions due to non-zero nuclear spin isotopes of mercury. However, because of the reduced Doppler width of the mercury atomic beam and the use of a single-mode dye laser, resolution of most of the spectroscopic structure of the laser excited transition was achieved so that data could be obtained free of hyperfine structure effects.

The measurement of atomic collision parameters for the 6^1P_1 state of mercury is of considerable interest because recent measurements reported for heavy atom targets, such as the rare gases, show a marked departure from light atom behaviour with the observation

of spin-flip cross sections even at relatively small scattering angles (see reference 6 for a review of this data). This effect is attributed to spin-orbit interactions between the target atom and the colliding electron. Mercury is the heaviest atom so far investigated in atomic collision studies and it has a large spin-orbit interaction, so that significant spin-flip cross sections would be anticipated.

Attention is focussed in this paper on techniques in which a complete measurement is obtained of atomic collision parameters for electron impact excitation of atoms by a non-polarized beam of electrons. To achieve this for collisions involving heavy atoms requires the measurement of four atomic collision parameters for a $^1S - ^1P$ excitation, which in a conventional coincidence experiment requires polarized photon correlation measurements to be made both perpendicular to and in the scattering plane. The laser polarization provides an additional experimental parameter which enables all atomic collision parameters to be obtained with correlation measurements made only perpendicular to the scattering plane.

2.0 Theory

MacGillivray & Standage 1988 discuss in detail the theoretical form of the stepwise coincidence signal and here only the results of such calculations are presented. A typical excitation/emission geometry is shown in figure 1 together with a typical energy level diagram for a stepwise excitation experiment. Atoms in a

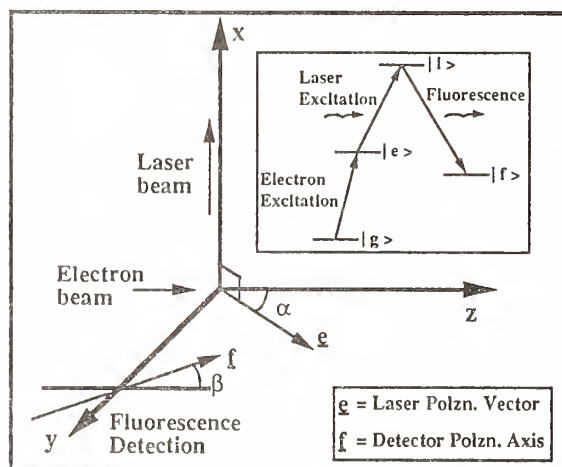


Fig. 1 The Excitation / Emission Geometry.
Inset : Energy Level Diagram.

$J = 0$ ground state are first excited by electron impact to a $J = 1$ excited state and then by laser excitation to a higher $J = 2$ state. Fluorescence is detected from the stepwise excited atoms as they spontaneously decay back to a $J = 1$ state. A mutually orthogonal excitation/emission geometry is shown in which laser and electron beams travel along the x and z directions, respectively and the x-z plane is the scattering plane. Fluorescence is detected along the y direction.

The stepwise coincidence signal is expressed in terms of Stokes parameters as $P_1 = (I_0 - I_{90})/I$, $P_2 = (I_{45} - I_{135})/I$, $P_3 = (I_{RHC} - I_{LHC})/I$, where I is the total intensity and the linear polarizer angle is given with respect to the z direction.

For collisions which involve heavy atoms with strong spin-orbit interactions, four atomic collision parameters are required to describe the electron impact excitation of an $S - P$ transition. In the collision frame, where the quantization direction is taken as parallel to the incident electron beam direction, the density matrix elements of the P state may be parameterized as

$$\begin{aligned} \lambda &= \rho_{00}/\sigma, & \cos\chi &= \text{Re}\rho_{10}/(\rho_{00}\rho_{11})^{1/2} \\ \sin\phi &= \text{Im}\rho_{10}/(\rho_{00}\rho_{11})^{1/2}, & \cos\delta &= \rho_{1-1}/\rho_{11} \\ \sigma &= \rho_{00} + 2\rho_{11} \end{aligned} \quad (1)$$

where diagonal density matrix elements represent differential cross sections for magnetic sublevels and off-diagonal elements represent excited state coherences produced by the collision process. σ is the differential cross section. In the natural frame the quantization axis is taken perpendicular to the scattering plane and the four independent parameters normally used are ρ_{00} , the normalized spin-flip cross section, L_L , the angular momentum transferred to the atom during the collision, γ , the tilt angle of the major axis of the atomic charge cloud to the incident electron beam direction and P_L , the polarization of the charge cloud measured perpendicular to the scattering plane.

The coherent nature of the excitation is characterized by the coherence parameter μ , which is given by the expression¹⁰

$$\mu = \sqrt{\frac{P_2^2 + P_3^2}{1 - P_1^2}} = \sqrt{\frac{2}{1 - \cos\delta}} (\cos^2\alpha + \sin^2\phi) \quad (2)$$

and the vector polarization parameter $|P| = (P_L^2 + P_\perp^2)^{1/2}$, where $|P| \geq |\mu| \geq 0$. It should be noted that the expression for $|P|$ differs from that normally used in the literature by a factor $2/(1 - \cos\delta)$ which arises when it is correctly derived using the expression given above. It is this expression that properly satisfies the inequality. Although the coherence parameter is frame dependent, whereas $|P|$ is not, and for this reason $|P|$ has been favoured as the measure of coherence, the coherence parameter can provide a more stringent test of the coherent character of the collision process by virtue of the inequality stated above. This has recently been noted in work on the comparison of superelastic and coincidence experiments on sodium¹¹.

Consideration has to be given to the atom-light interaction, which if it can be regarded as a weak interaction involving only single photon processes, then enables analytical expressions to be obtained for the stepwise coincidence signal. For the geometry and excitation/emission scheme described above, it can be shown that these signals are given by⁹

$$IP_1 = \lambda \left[\frac{27}{2} - 6\cos^2\alpha \right] + \frac{9}{2}\cos 2\alpha + \frac{9}{2}(1-\lambda)\cos\delta$$

$$IP_2 = -3(5 - \cos 2\alpha)[\lambda(1-\lambda)]^{1/2}\cos\alpha \quad (3)$$

$$IP_3 = 9(3 + \cos 2\alpha)[\lambda(1-\lambda)]^{1/2}\sin\phi$$

$$I = \lambda(6\cos^2\alpha + \frac{17}{2}) + (5\cos^2\alpha + \frac{17}{2}) + \frac{1}{2}(1-\lambda)(8\sin^2\alpha - 9)\cos\delta$$

where α is the laser polarization angle. In the event that the atom-light interaction is strong, then a quantum electrodynamical treatment is required. Space does not allow a detailed discussion of the QED calculation here (for a discussion see references 9 and 12), but results from calculations are considered in Section 3.0.

It can be seen from the above equations that the additional experimental parameter provided by the laser polarization enables more information to be obtained than would be possible with the same geometry and a conventional coincidence experiment. The parameters λ and δ may be determined provided measurements of P_1 are made for two laser polarizations such as $\alpha = 0^\circ$ and 90° . The remaining parameters $\cos\alpha$ and $\sin\phi$ may then be

determined from measurements of P_2 and P_3 . As mentioned in Section 1.0, conventional coincidence measurements of these parameters require an additional linear polarization measurement in the scattering plane.

3.0 Experiment

A schematic diagram of the apparatus is shown in figure 2.

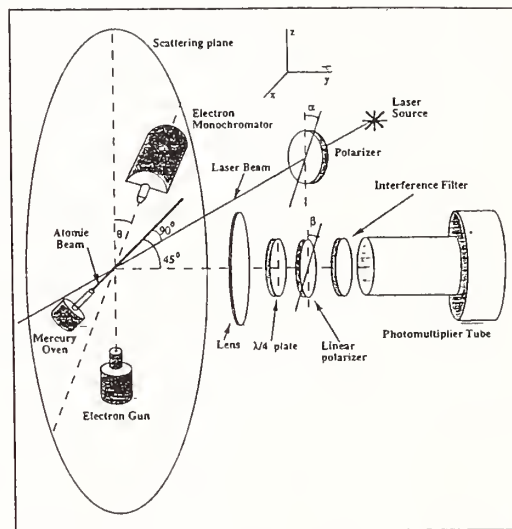


Fig. 2 Schematic of the Experimental Apparatus.

The apparatus is the same as for a conventional coincidence experiment with the addition of a laser system to provide the optical excitation step. The electron gun is of a two stage aperture lens design with a tungsten filament as the electron source. The gun was operated at 16.0 eV with a beam current of 500 nA and an energy halfwidth of 500 meV. The electron analyzer was of a standard cylindrical design with an aperture lens fitted on the input to accurately image the interaction region into the analyzer. The acceptance solid angle of the analyzer was 0.01 sr. A quartz lens imaged light from the interaction region into an optical detection system mounted inside the vacuum system to maximize its efficiency. The system consisted of an externally rotatable linear or circular polarization analyzer and an interference filter and a cooled photomultiplier tube. The acceptance solid angle of the system was 0.50 sr.

An atomic beam oven produced an effusive beam of atoms with an estimated density of $(2-5) \times 10^{16}$ atoms/m³.

within the interaction region. The dimensions of the interaction region were determined experimentally by performing conventional electron-photon coincidence measurements on mercury atoms excited by direct electron impact to the nearly degenerate manifold of singlet and triplet 6D states with photon detection at 579 nm along a direction perpendicular to the atomic beam. The size of the laser beam was chosen to match the dimensions of the interaction region.

An actively stabilized cw ring laser was used with a jitter bandwidth of about 1 MHz. Typical laser powers in the interaction region were 350 mW with the laser beam having a $1/e$ diameter of 2.5 mm. The 579 nm transition of mercury which was excited by the laser has extensive hyperfine structure, most of which was resolved in this experiment. The laser was tuned to the zero-nuclear-spin isotope peak which enabled data to be obtained free from the depolarizing effects of hyperfine structure that would be present in conventional coincidence data.

Careful attention was given to possible sources systematic errors caused by stray fields and radiation trapping. Helmholtz coils and mu-metal shielding was used to reduce stray magnetic fields to 10^{-6} T. The 185 nm transition of Hg has a short lifetime and a correspondingly strong absorption coefficient so that the presence of radiation trapping has to be considered. We found that it was possible to induce significant radiation trapping at higher pressures as evidenced by increased decay times for stepwise coincidence signals and accordingly operated the experiment at tank pressures that reduced such effects to the level at which a small correction of a few percent was applied to the data. It should be noted that in this experiment, the use of stepwise excitation confines radiation trapping to the region of the interaction volume illuminated by the laser beam, thereby limiting this source of systematic error.

Figure 3a shows a stepwise coincidence signal obtained with the polarizer in the photon detector removed. Standard coincidence techniques were used to obtain the signal. The electron analyzer was tuned to the 6^1P_1 peak of the inelastically scattered electron energy loss spectrum. Real coincidences can only involve

313 nm photons emitted by stepwise excited atoms which have previously scattered an electron from the 6^1P_1 level that is detected by the electron analyzer. The total run time to accumulate this signal was 12 hours with a 6^1P_1 inelastic electron countrate of 15 kHz and a photon countrate of 130 Hz. The photomultiplier tube dark countrate was 10 Hz and the countrate from direct electron excitation of the $6^1,^3D$ states of Hg, which have transitions to lower states at approximately 313 nm, was 30 Hz.

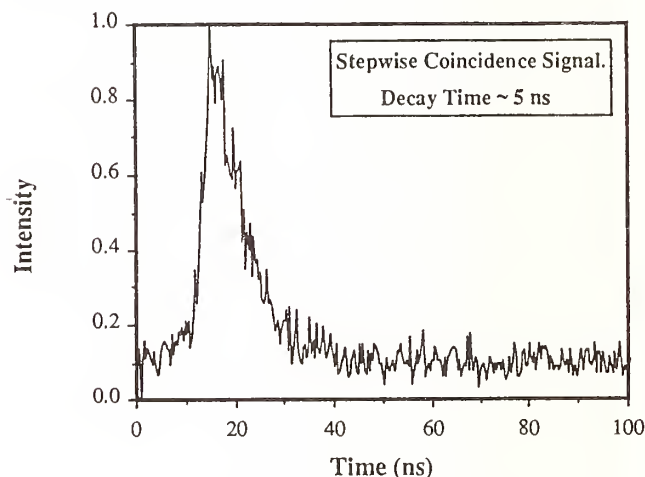


Fig. 3(a). The Stepwise Coincidence Signal.

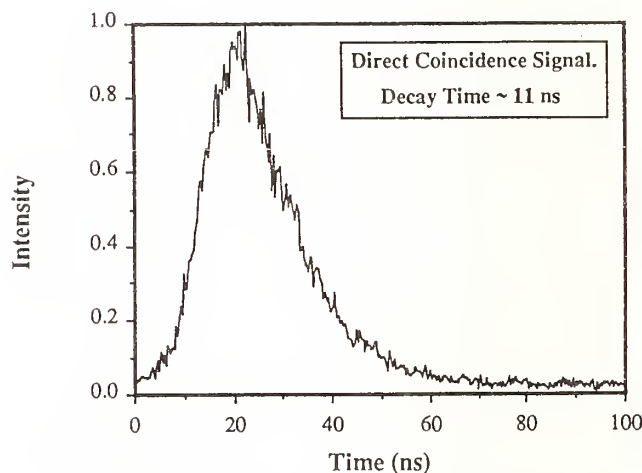


Fig. 3(b). The Direct Coincidence Signal.

Qualitatively similar coincidence signals were obtained when a linear or circular polarization element was placed in the photon detector. Measurements of the Stokes parameters were obtained from coincidence signals that were normalized to the number of scattered electrons detected during a run. Many runs of short duration were recorded and statistically analyzed to minimize systematic errors that might arise because of drifts in experimental parameters.

4.0 Results and Discussion

Before considering the results obtained from measurements of atomic collision parameters, we consider more closely evidence that a weak excitation treatment of the data obtained in this experiment is adequate. If this is the case, then the coincidence data may be analyzed using the analytic expressions of equation 3. Figure 3b shows a direct coincidence signal obtained by tuning the electron analyzer to the $6^1P_1 - 6^1D_2$ inelastic scattering peak. The expected lifetime for the direct coincidence signal is about 11 ns, which is what is observed, however the striking feature of the stepwise coincidence signal is that it has a decay time of only 5 ns. The expected decay time for this signal under weak excitation conditions is similar to the direct signal, approximately 11 ns.

Some results are now considered from an extensive series of QED calculations we have performed to model the interaction of strong laser light with the laser excited transition. The QED model produces time resolved population and coherence data for both the upper and lower states of this transition. In practice, the shape of the coincidence signal is found to be relatively independent of the precise values of the atomic collision parameters, whereas the total integrated area of the signal does depend on their values. For the purpose of a comparison with the weak excitation case, arbitrary initial values of the atomic collision parameters of $\lambda = \cos\theta = \cos\alpha = \sin\phi = 0.5$ were used to calculate the curves shown in Figure 4. The laser intensity was assumed to be constant over the laser beam which was assumed to have a diameter of 2.5 mm and calculations were performed for 1 mW power to simulate weak excitation conditions and at 1000 mW power to represent strong excitation conditions. The decay time

for the 1 mW signal is approximately 11 ns whereas the 1000 mW signal has a 1.5 ns decay time. Some evidence of a Rabi nutation can be seen on the 1000 mW signal with a corresponding Rabi frequency for the $6^1P_1 - 6^1D_2$ (579nm) transition of Hg of 130 MHz.

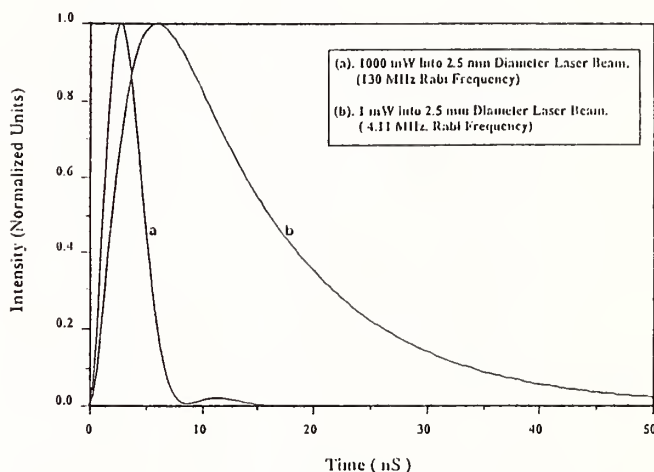


Fig. 4. Time Resolved Stepwise Coincidence Intensity.

The cause of this enhanced decay rate is the coupling by the laser of the upper excited state, with a lifetime of 11 ns to the lower excited state, with a much shorter (1.3 ns) lifetime.

When the effect of the Gaussian laser beam intensity profile is included, the result is that the range of Rabi frequencies present removes the oscillations from the signals and increases the decay time. When the Doppler spread of the atomic beam is also included and the laser beam parameters are adjusted to match the experimental conditions used, good agreement is obtained with the measured decay time.

When the same calculation is applied to determine the behaviour of the Stokes parameters, the variation from the weak excitation result is between 2% and 5%, depending on which parameter is chosen. It can be seen that in spite of the presence of factors which quite strongly influence the decay rate of the stepwise coincidence signal, little change occurs in the Stokes parameters.

Scattering Angle	$\theta_s = +10^\circ$	$\theta_s = +20^\circ$	$\theta_s = +30^\circ$
Collision Frame			
λ	0.47 ± 0.04	0.43 ± 0.08	0.36 ± 0.06
$\cos \delta$	-0.01 ± 0.15	-0.08 ± 0.40	-0.24 ± 0.21
$\cos \chi$	-0.13 ± 0.09	0.05 ± 0.12	0.42 ± 0.25
$\sin \phi$	-0.05 ± 0.03	-0.03 ± 0.02	-0.08 ± 0.05
$ \mu_{xz} $	0.14 ± 0.08	0.06 ± 0.10	0.43 ± 0.25
P	0.34 ± 0.07	0.18 ± 0.07	0.55 ± 0.31
Natural Frame			
P_{00}	0.26 ± 0.05	0.26 ± 0.16	0.24 ± 0.10
P_{11}^+	0.33 ± 0.07	0.18 ± 0.07	0.54 ± 0.31
γ	$+16^\circ (+10^\circ -20^\circ)$	$-10^\circ (+34^\circ -15^\circ)$	$-48^\circ (+6^\circ -31^\circ)$
L_L^+	$+0.06 \pm 0.03$	$+0.04 \pm 0.03$	$+0.10 \pm 0.07$

Table 1 The Atomic Collision Parameters

Table 1 shows data obtained for collision frame and natural frame parameters for three electron scattering angles and an incident electron energy of 16.0 ± 0.5 eV. Experimental uncertainties are one standard deviation and $\pm 1.5^\circ$ in the electron scattering angle. The data was obtained for negative electron scattering angles i.e. the electron detector lay in the $(-x, z)$ quadrant of the scattering plane. Sign changes have been applied to collision parameters, where appropriate, to correspond to positive electron scattering angle.

The data clearly shows a breakdown of positive reflection symmetry with respect to the scattering plane with the spin-flip cross section $P_{00} > 0$ and $\cos \delta = -1$. The angular momentum transferred in the collision is small and the coherence and total polarization parameters show a marked loss of coherence in the collision process. Not surprisingly, the data shows a marked departure from that expected for light-atom collisions and, particularly with respect to spin-flip cross sections, reflects the behaviour found in electron - heavy rare gas collisions.

5.0 Conclusion

We have seen that the introduction of a laser excitation step between the initial electron impact excitation process and the final fluorescent emission process enables the unique properties of laser light to be utilized in coincidence experiments. The laser

polarization may be used as an additional experimental parameter to reduce the number of measurements required to fully determine the atomic collision parameters. The spectral resolution may enable the effect of spectroscopic structure on the measurement of atomic collision parameters to be eliminated. The optical power of the laser light enables a satisfactory stepwise signal to be generated even when a very rapid decay rate exists for the electron-impact excited transition. A tightly collimated laser beam allows the interaction volume to be accurately defined and confines radiation trapping to this volume, thereby minimizing such effects.

In the case of electron excited VUV transitions, the main advantage of the stepwise excitation technique lies in the transfer of polarization measurements to wavelengths at which standard optical components can be used.

Finally, stepwise excitation techniques open up the possibility of applying coincidence techniques to the investigation of the electron-impact excitation of metastable states.

Although the stepwise excitation technique has the obvious practical disadvantage that a laser system is required in addition to the usual electron scattering apparatus, the advantages outlined above will hopefully encourage more researchers to consider using such techniques.

References

- ¹A.J. Murray, C.J. Webb, W.R. MacGillivray & M.C. Standage, Phys. Rev. Lett. 62, 411 (1989).
- ²M. Emynan, K.B. MacAdam, J. Sievin & H. Kleinpoppen, Phys. Rev. Lett. 31, 576 (1973).
- ³----- J. Phys.B., 7, 1519 (1974).
- ⁴K. Blum & H. Kleinpoppen, Phys. Rep. 52, 203 (1979).
- ⁵J. Slevin, Rep. Prog. Phys. 47, 461 (1984).
- ⁶N. Andersen, J.W. Gallagher & I.V. Hertel, Phys. Rep. 165, 1 (1988).
- ⁷I.V. Hertel & W. Stoll in 'Advances in Atomic and Molecular Physics' eds D.R. Bates & B. Bederson (Acad. Press, N.Y. 1977) 13, 113.
- ⁸B. Jaduszliwer, G.F. Shen, J-L Cai & B. Bedersen, Phys. Rev. A. 31, 1157 (1985).
- ⁹W.R. MacGillivray & M.C. Standage, Phys. Rep. 168, 1 (1988).
- ¹⁰A.J. Murray, C.J. Webb, W.R. MacGillivray & M.C. Standage, in preparation (1989).
- ¹¹P.M. Farrell, C.J. Webb, W.R. MacGillivray & M.C. Standage, submitted to J. Phys.B., (1989).
- ¹²P.M. Farrell, W.R. MacGillivray & M.C. Standage, Phys. Rev. A., 37, 4240 (1988).

SUMMARY OF SYMPOSIUM PROCEEDINGS-
SOME IMPRESSIONS AND OBSERVATIONS

Benjamin Bederson
Physics Department
New York University
New York, N. Y. 10003, U.S.A.

Being invited to present the closing talk at a specialized symposium is a mixed blessing at best. Is one supposed to distill the essence of the previous talks and present a global, definitive overview that effectively summarizes for posterity the important material already offered by the previous speakers? Or should one use the previous talks as a springboard, to offer a projection of what is to come at the next such symposium? Either of these extremes requires a presumptuousness that I don't particularly wish to assume. On the other hand, knowing that I would be giving this talk resulted in the obligation to listen to all the talks presented (I noticed that many other attendees did the same even without the unique incentive that drove me.) Accordingly I feel that I can assume the luxury of offering remarks that convey impressions as opposed to definitive value judgements.

At least I have the advantage over my late NYU colleague Werner Brandt, who was in a similar position at a symposium on beam-solid interactions held in Tokyo some years ago. Werner had simply neglected to obtain the required visitor's visa, and so was refused access to the meeting, being forced to stay during the entire meeting

at the airport. I understand that he did finally get clearance to attend the meeting on its last day. He gave the final talk as scheduled, anyway.

While listening to the several talks presented at this meeting and although they covered a quite wide range of subject matter, both theoretical and experimental, it was not too difficult to identify the common thread that ran through most if not all of the talks. It is, in my opinion, the appeal this kind of work has to those wishing to effect as close a connection between fundamental theory, computational techniques, and experiment as is currently possible. And despite the fact that there was not an overwhelming number of talks--only about two dozen--virtually all aspects of current activity were covered to one degree or another. (I should add that the relatively leisurely pace of the meeting allowed each talk to be long enough to be understandable to the non-expert, for the most part.) In fact in considering what can be accomplished by the application of the state-of-the-art experimental techniques discussed here one cannot help but be impressed by the virtually unique role this field is playing in collision

physics, and this statement applies equally well in atomic, nuclear, and high energy collision studies.

Before discussing some of the specifics of the new work that surfaced at the meeting, I would like to address the points singled out for special mention by Joachim Kessler in his introductory talk, and for which he expressed a hope that these would be resolved during the meeting.

First Prof. Kessler raised the question: should there be a conference such as this one every two years, a strong argument in favor being that it is correlated and coherent with the biennial ICPEAC. But as he points out this is not a sufficient condition for a positive response. There has to be an overdriving scientific purpose that is not already satisfied in another way (say at the ICPEAC itself). Based on what happened at this meeting, I agree with Prof. Kessler that the answer is yes, although some minor suggestions for variations will be offered at the end of this paper.

Also, Prof. Kessler mentions the experiment of the JPL group (Trajmar et al) on laser-excited barium that revealed an unexpected asymmetry of scattered electrons with respect to a direction along the electric vector of the exciting laser beam, when linearly polarized. They could not make the asymmetry disappear despite many efforts to discover systematic errors by elaborate variations of experimental parameters (in this as with other specific papers I refer the reader to the

original symposium articles for reference citations). The conclusion of the JPL workers at the time was that either there remained an as yet unrevealed systematic error or there was a true asymmetry that reflected some not-understood breakdown of collision theory. The JPL talk definitely answers this question in favor of the former (to most everybody's regret, I'm sure). The problem concerns the subtle influence of imperfect angular alignment on the polarization detection. The effort put into this work by the JPL group will likely help others in identifying similar systematic deviations from nominally mutually perpendicular crossed beams.

A related discussion on overlap integrals and sensitivity to orientation of the scattering plane with respect to the detection system was given by Prof. McConkey (Windsor). I refer the reader to the penultimate paragraph of the section of that article entitled "Finite beam size and/or offset" for their important conclusions.

A second, also "technical" question raised by Kessler concerned the assumed accuracy of electron polarization determination by Mott scattering. Two papers at the meeting addressed this question, one by a University of Missouri group (Khakoo et al), and the other by the Munster group. This talk was originally to have been given by K. Jost but as we know he unfortunately passed away just before the ICPEAC, so the paper was given by A. Gellrich. As can be seen from both these papers, the last word has yet

to be spoken on this subject. The conservative view expressed by the Munster group, reinforced by the earlier systematic investigations of Fletcher et al, to the effect that current Mott analyzers generally can yield accuracies of perhaps 5%, remains the safest one to date. Future improvement, particularly when calibration to a simpler physical situation, i.e., polarization of helium impact radiation, is promising but yet remains to be definitively established. A third paper, by the NIST group (McClelland) is interesting for a different reason since it takes an alternate approach using low voltages to the design of a Mott analyzer (see the McClelland paper for details).

Several other issues of specific interest or should we say that presented potential traps for experimentalists were raised at the meeting. One concerned radiation trapping (Standage et al)--always a possible problem in dealing with resonant radiation--, and another with background time-dependent pressure effects caused by mechanical beam chopping (Lubell).

I found it very interesting to note that all four of these experimental problems have challenged collision physicists to one degree or another throughout the history of crossed-beam research (radiation trapping: Mitchell and Zemansky; Mott scattering: Mott and Massey; "overlap integral" effects in angular distributions: Massey and Burhop; pressure-modulation effects due to beam-chopping: Fite). This is characteristic

of a developing field of research; old problems surface in a new context. The sophistication of the present research generation is of such a level that many familiar problems, seemingly put to rest, rear their ugly heads once again.

There is one final point I would like to address related to Joachim's talk. He points out, and correctly, that "it is usually the cross sections that are the weakest point" (in determining the complete set of observables in a scattering experiment). Again, this is a characteristic common to many branches of physics. Absolute values of anything are the most difficult quantities to determine and this includes but is not restricted to absolute cross sections. The field of coherence and correlation in a certain sense skirts this problem, since often the relevant quantities are ratios: ratios of polarizations, or scattering signals, for example. In determining ratios absolute densities of targets and absolute intensities of signals are not required. It is for this reason that some of the data obtained herein are intrinsically more accurate and reliable than in the supposedly less demanding integrated or summed cross sections of more conventional techniques. Thus theorists can be presented with data that they can be reasonably confident will not change radically with time. (Although of course there are exceptions!) And it must also be borne in mind that the complete experiment requires knowledge of the absolute cross section, in addition to the fundamental parameters that are

the principal focus of this meeting. My colleague Prof. Leposava (Lepsha) Vuskovic addressed this problem in her talk; I will not elaborate on it here.

So much for the follow-up on the Kessler introductory talk. I would like to make several further observations that do not refer to specific presentations before addressing some of these. I was struck by the apparant ubiquitousness of one particular article that was referred to in perhaps half of all the talks presented--the recent review by Andersen, Gallagher, and Hertel. Even the conference logo, showing a laser-excited S to P charge cloud in an alkali, comes from that article. Further, although the article was really intended as a compendium of experimental data on polarization and correlation, the part of the article that was generally quoted was only the first few pages, which summarizes with great clarity one currently generally accepted way of looking at correlation (in particular Stokes parameters and reference frames) and coherence phenomena (L_1 and λ), in simple atomic systems. I suspect that in addition to the useful presentation of the relation of observables to atomic and collision parameters, a principal reason for the appeal of this article is that physicists like to think pictorially, and it has some gorgeous sketches that give at least the illusion that the excitation process can be quite readily visualised in terms of charge clouds, quantization axes, and scattering angles. As a corollary to this, now that

this field has reached a certain advanced level in both theory and experiment, some conceptually simple unifying and "obvious" features can now be recognized (of course these are simple generally speaking only after the fact). An example is the explanation of the left-right asymmetry for polarized electrons scattered superelastically from laser-excited sodium. See in particular the discussion in Sect. 3 of the Hanne article, and the accompanying Fig. 2.

Now for some specifics. Of the 23 research talks 14 were primarily experimental, 5 were theoretical, and 4 were devoted primarily to experimental "technology" for want of a better word. It is probably fair to state that no revolutionary experimental or theoretical concepts were introduced, the meeting being devoted primarily to the fruitful exploitation of methods that are by now reasonably well-understood. Certain trends and significant developments did surface--the ones I happen to single out do naturally reflect my own predelictions rather than some absolute judgments about what is particularly important or not important. The field, which traditionally concerned itself primarily with electron-atom collision has for some time broadened to include heavy particle collisions. However, while 19 of the papers were dedicated primarily to electron collisions, including several that concerned general theory that could also apply to heavy particle collisions, there were only 3 involving atom-atom collisions (I'll get to the 23rd paper later). It would

probably surprise no one were the ratio of heavy-heavy to light-heavy particle collisions to be substantially larger in Adelaide two years from now. This development was nicely highlighted by the two papers, one theoretical (Masnou-Seeuws) and the other experimental (Meijer), on the associative ionization reaction in laser-excited $\text{Na}(3p) + \text{Na}(3p)$. These papers were concerned with the observation and analysis of the dependence of the reaction on laser polarization which determines the charge cloud alignment of the reaction constituents just as in electron-atom collisions, though with greater complexity. Hippler (Bielefeld) reported measurements of alignment and orientation parameters of atomic hydrogen 2p excitation either by direct or by charge-changing collisions.

Computational physics was represented by two impressive papers from Los Alamos. The first was a general discussion of the development of atomic structure and collision codes by Clark and the second a talk more specifically directed at the use of such codes to calculate electron-impact coherence parameters and spin-polarization functions using first order many body theory (FOMBT) and distorted wave approximation schemes (DWBA) (Cartwright). It appears that according to Clark such codes can now be accessed by modem, even from NYU. This is an intriguing development-- will experimentalists be able, at last, to make serious efforts at calculating cross sections and coherence and correlation parameters? We will doubtless hear more of this at Adelaide.

Still, the more fundamental question remains: how reliable are the actual theoretical bases for these codes? Among the liveliest discussions at the symposium were those related to the two "schools" of theory represented, with FOMBT and DWBA on the one hand, and close-coupling methods on the other. These latter were ably represented by Ian McCarthy (Flinders) and his US colleague, Don Madison. The experimental data at the symposium produced no well-defined winner. For example, Prof. Crowe (Belfast) presented data for P and D excitation of ground state helium that did not agree well with FOMBT and DWBA, but on the other hand similar data in krypton did much better. Crowe suggests that this may be due to the somewhat smoother central potential offered to the exciting electron by the fatter krypton atom. The traditional reliability of close coupling in dealing with low energy collisions in the alkalis continued unabated, with data of the NIST group (McClelland) on polarized electron scattering and of the Flinders group (Teubner) on orientation and alignment, both using sodium. At the moment I would call it a tie, with FOMBT and DWBA being more successful (and much more economical with respect to computer time) at higher energies, and with close coupling being more appropriate as one goes to lower energies. Also, close coupling may work better with the alkalis because, being single valence electron atoms, their electric dipole matrix elements tend to converge relatively rapidly while the rare gas closed shell atoms present a smoother

potential more suited for the Los Alamos models.

The situation with regard to spin-tagged electron impact ionization of atoms seems to be well in hand, with the comprehensive measurements of the Bielefeld group (Baum). Data for atomic hydrogen and the lighter alkalis, as well as of metastable helium (lithium-like) were presented. Only a calculation using DWBA by Bartschat could be compared with their lithium and metastable helium data, and these are in reasonable, qualitative agreement. The possibility of oscillations in the spin asymmetry close to threshold seems to have been put to rest. Prof. McCarthy pointed out the importance of establishing the correct boundary conditions for ionization reactions, whose final product contains three charged bodies. He noted that Brauner, Briggs and Klar have recently succeeded in establishing the exact three-body boundary condition for this problem. I hope we will be hearing more about this at the next symposium.

Inner shell correlation experiments were reported by Prof. Stefani (Rome, now at Camerino), the only talk that was devoted primarily to other than outer-shell excitations. An interesting experiment was described by Heideman (Utrecht), in which he observed coherence effects in autoionization of states with significantly different excitation energies. Prof. Stumpf (Moscow, Idaho) discussed experiments in progress on optical analysis of electron excitation of laser-

excited alkali atoms. Standage (Griffith, Australia), also employing laser-excited atoms in related work, described his measurements of stepwise excitation. In all I counted seven papers that used lasers to prepare, i.e., excite, atoms (almost exclusively sodium to 3P, excepting barium by JPL) to perform either superelastic, elastic (Vuskovic) or inelastic measurements. There were no papers that described laser-assisted collisions, i.e., using high-intensity lasers.

Professor Fano gave a talk concerned with the dynamics of the excitation process--the physics behind the observations of polarization phenomena. This is related to the qualitative discussion by Hanne of the so-called "propensity" describing the relation between the orientation of atomic momentum before collision with respect to the projectile's angular momentum, measured with respect to the atomic nucleus. I should like to particularly call to your attention references 5 and 7 of Prof. Fano's article. They refer to honors B. S. theses by R. Venugapalan and J. Bohn respectively. It appears as though the University of Chicago continues to attract first-class undergraduates, not to mention the fact that it requires an unusually gifted mentor to inspire such work--no surprise, in this case!

The twenty third paper, by Prof. Duncan (Stirling) was not about collisions at all, being a study of polarization correlation effects in the two-photon decay of metastable deuterium, although by stretching the point you might talk yourself into it (the

inverse reaction would be a three body (two photon) collision to excite deuterium to the 2S state). This work is the second paper from Stirling on the use of atomic systems to test Bell's inequality, that is, the validity of quantum mechanics. Duncan, Kleinpopp et al had already performed such a measurement that supplemented the original Aspect et al work. The present experiment was undertaken to check out a loophole suggested by Selleri and coworkers, but the results still bear out the predictions of quantum mechanics. Doubtless other loopholes will surface in the future; these will have to be addressed as they appear. The point here is that the techniques being developed to address the problems of specific interest to this symposium may very well be adapted to other areas of equal interest and importance.

Finally, to take up the point raised by Prof. Kessler at the end of his paper--from what we have learned in the present symposium how would I propose to organize the next one? Again, I can't rally the chutzpa (read, presumption) to offer such an outline--it is better to just wait and see what develops. I certainly would not be surprised to see more papers on heavy particle collisions, certainly more papers involving laser-prepared collision targets, and maybe even some work on laser-assisted collisions, and perhaps a paper or two involving exotic collision partners, particularly positrons. Very likely still more accurate measurement of scattering amplitudes either

through the L_{\perp} , γ or λ , χ approaches will be forthcoming, to approach ever closer to the "perfect scattering experiment". In this connection it should be noted that one can go even beyond this ideal, in simple electron-atom collisions, because of the possibility of overdetermination of collision parameters through the performance of more than the required number of independent experiments. (Purists can argue that if the parameters are overdetermined the experiments cannot be all independent. This is true only if time-independent scattering theory as we understand it represents a completed description of the scattering process. Future precision experiments will play a role in deciding, in fact, if this is actually the case.) I would most assuredly like to see a more elaborate face-off arranged with a larger group of theorists to discuss not only inevitably improved computational techniques, but more fundamental theoretical talks as well. And finally it is always important when experts meet to address the highly specialized but crucial technical questions that determine in the last analysis the reliability of experimental results, as was noted at the beginning of this paper. I hope that there will be more of this at Adelaide, although perhaps we don't have to force our theoretical colleagues to sit through some of the more nitty-gritty discussion that will inevitably occur.

List of Attendees

J. Abdallah	Los Alamos National Laboratory, USA
N. Andersen	University of Aarhus, Denmark
K. Bartschat	Drake University, USA
W. Batelaan	University of Utrecht, The Netherlands
G. Baum	University of Bielefeld, FRG
K. Becker	City College of CUNY, USA
B. Bederson	New York University, USA
J.A. Brand	University of Missouri, Rolla, USA
S. Buckman	Australia National University
L. Bureyea	USSR Academy of Sciences, USSR
D.C. Cartwright	Los Alamos National Laboratory, USA
R.E.H. Clark	Los Alamos National Laboratory, USA
J.J. Corr	University of Windsor, Canada
A. Crowe	Queen's University of Belfast, UK
D.M. Crowe	City College of CUNY, USA
G. Csanak	Los Alamos National Laboratory, USA
A.J. Duncan	University of Sterling, UK
U. Fano	University of Chicago, USA
T.J. Gay	University of Missouri, Rolla, USA
X.Q. Guo	City College of CUNY, USA
G.F. Hanne	University of Munster, FRG
H.G.M. Heideman	University of Utrecht, The Netherlands
R. Hippler	University of Bielefeld, FRG
K-N. Huang	Institute of Atomic and Molecular Science, Taiwan
A. Jain	Florida State University, USA
T.Y. Jiang	New York University, USA
M.H. Kelley	N.I.S.T., Gaithersburg, USA
J. Kessler	University of Munster, FRG
M.A. Khakoo	University of Missouri, Rolla, USA
H. Kleinpoppen	University of Sterling, UK
C.J. Liu	Argonne National Laboratory, USA
M.S. Lubell	City College of CUNY, USA
W.R. MacGillivray	Griffith University, Australia
L.E. Machado	University of Sao Carlos, Brazil
D.H. Madison	University of Missouri, Rolla, USA

E.J. Mansky II	Georgia Tech., USA
B. Marinkovic	Institute of Physics, Belgrade, Yugoslavia
K.E. Martus	City College of CUNY, USA
F. Masnou-Seeuws	Universite de Paris-Sud, France
K.C. Mathur	University of Roorkee, India
I. McCarthy	Flinders University, Australia
J.J. McClelland	N.I.S.T., Gaithersburg, USA
J.W. McConkey	University of Windsor, Canada
R. McEachran	York University, Canada
H.A.J. Meijer	University of Kaiserslautern, FRG
U. Muller	University of Saarlandes, FRG
P.A. Neill	University of Nevada, Reno, USA
S.E. Nielsen	University of Copenhagen, Denmark
J. Ratliff	Jet Propulsion Laboratory, USA
E. Reichert	University of Mainz, FRG
H.R. Sadeghpour	JILA-University of Colorado, USA
S. Sarkar	Indian Association for the Cultivation of Science, India
R. Siegel	City College of CUNY, USA
M.C. Standage	Griffith University, Australia
G. Stefani	Universita' di Camerino, Italy
H. Steidl	University of Bielefeld, FRG
B.J. Stumpf	University of Idaho, Moscow, USA
P.J.O. Teubner	Flinders University, Australia
S. Trajmar	JPL-Caltech, USA
J.P. van den Brink	University of Utrecht, The Netherlands
P.J.M. van der Burgt	University of Windsor, Canada
L. Vušković	NYU, USA/Institute of Physics, Belgrade, Yugoslavia
K. Wijayaratna	University of Missouri, Rolla, USA
J.F. Williams	University of Western Australia
P.W.. Zetner	JPL-Caltech, USA
Y. Zheng	Flinders University, Australia

BIBLIOGRAPHIC DATA SHEET

1. PUBLICATION OR REPORT NUMBER
NIST/SP-789

2. PERFORMING ORGANIZATION REPORT NUMBER

3. PUBLICATION DATE
June 1990

4. TITLE AND SUBTITLE

Proceedings of the International Symposium on Correlation and Polarization in
Electronic and Atomic Collisions

5. AUTHOR(S)

P.A. Neill, K.H. Becker and M.H. Kelley

6. PERFORMING ORGANIZATION (IF JOINT OR OTHER THAN NIST, SEE INSTRUCTIONS)

U.S. DEPARTMENT OF COMMERCE
NATIONAL INSTITUTE OF STANDARDS AND TECHNOLOGY
GAITHERSBURG, MD 20899

7. CONTRACT/GRANT NUMBER

8. TYPE OF REPORT AND PERIOD COVERED

9. SPONSORING ORGANIZATION NAME AND COMPLETE ADDRESS (STREET, CITY, STATE, ZIP)

Electron Physics Group
Electron and Optical Physics Division
Building 220, Room B206
N.I.S.T., Gaithersburg, Maryland 20899

10. SUPPLEMENTARY NOTES

11. ABSTRACT (A 200-WORD OR LESS FACTUAL SUMMARY OF MOST SIGNIFICANT INFORMATION. IF DOCUMENT INCLUDES A SIGNIFICANT BIBLIOGRAPHY OR LITERATURE SURVEY, MENTION IT HERE.)

The International Symposium on Correlation and Polarization in Electronic and Atomic Collisions was held at the Stevens Institute of Technology, Hoboken, New Jersey on August 2-4, 1989. The previous meeting, held in Belfast, UK (1987), extended the scope of the Symposium to include ion-atom and atom-atom collisions. This was reflected in the Symposium title which was modified to replace the term "electron-atom collisions" with "electronic and atomic collisions." The Hoboken meeting maintained this expanded area and included several talks in more loosely related areas. The attendance of 66 scientists represented 16 countries and the talks described the work of 23 research groups from 9 countries.

12. KEY WORDS (6 TO 12 ENTRIES; ALPHABETICAL ORDER; CAPITALIZE ONLY PROPER NAMES; AND SEPARATE KEY WORDS BY SEMICOLONS)

alignment; coherence; correlation; electronic and atomic collisions; electron-photon
coincidence; orientation; polarization; scattering

13. AVAILABILITY

- | | |
|-------------------------------------|---|
| <input checked="" type="checkbox"/> | UNLIMITED |
| <input type="checkbox"/> | FOR OFFICIAL DISTRIBUTION. DO NOT RELEASE TO NATIONAL TECHNICAL INFORMATION SERVICE (NTIS). |
| <input checked="" type="checkbox"/> | ORDER FROM SUPERINTENDENT OF DOCUMENTS, U.S. GOVERNMENT PRINTING OFFICE,
WASHINGTON, DC 20402. |
| <input checked="" type="checkbox"/> | ORDER FROM NATIONAL TECHNICAL INFORMATION SERVICE (NTIS), SPRINGFIELD, VA 22161. |

14. NUMBER OF PRINTED PAGES

163

15. PRICE





NIST *Technical Publications*

Periodical

Journal of Research of the National Institute of Standards and Technology—Reports NIST research and development in those disciplines of the physical and engineering sciences in which the Institute is active. These include physics, chemistry, engineering, mathematics, and computer sciences. Papers cover a broad range of subjects, with major emphasis on measurement methodology and the basic technology underlying standardization. Also included from time to time are survey articles on topics closely related to the Institute's technical and scientific programs. Issued six times a year.

Nonperiodicals

Monographs—Major contributions to the technical literature on various subjects related to the Institute's scientific and technical activities.

Handbooks—Recommended codes of engineering and industrial practice (including safety codes) developed in cooperation with interested industries, professional organizations, and regulatory bodies.

Special Publications—Include proceedings of conferences sponsored by NIST, NIST annual reports, and other special publications appropriate to this grouping such as wall charts, pocket cards, and bibliographies.

Applied Mathematics Series—Mathematical tables, manuals, and studies of special interest to physicists, engineers, chemists, biologists, mathematicians, computer programmers, and others engaged in scientific and technical work.

National Standard Reference Data Series—Provides quantitative data on the physical and chemical properties of materials, compiled from the world's literature and critically evaluated. Developed under a worldwide program coordinated by NIST under the authority of the National Standard Data Act (Public Law 90-396). NOTE: The Journal of Physical and Chemical Reference Data (JPCRD) is published quarterly for NIST by the American Chemical Society (ACS) and the American Institute of Physics (AIP). Subscriptions, reprints, and supplements are available from ACS, 1155 Sixteenth St., NW., Washington, DC 20056.

Building Science Series—Disseminates technical information developed at the Institute on building materials, components, systems, and whole structures. The series presents research results, test methods, and performance criteria related to the structural and environmental functions and the durability and safety characteristics of building elements and systems.

Technical Notes—Studies or reports which are complete in themselves but restrictive in their treatment of a subject. Analogous to monographs but not so comprehensive in scope or definitive in treatment of the subject area. Often serve as a vehicle for final reports of work performed at NIST under the sponsorship of other government agencies.

Voluntary Product Standards—Developed under procedures published by the Department of Commerce in Part 10, Title 15, of the Code of Federal Regulations. The standards establish nationally recognized requirements for products, and provide all concerned interests with a basis for common understanding of the characteristics of the products. NIST administers this program as a supplement to the activities of the private sector standardizing organizations.

Consumer Information Series—Practical information, based on NIST research and experience, covering areas of interest to the consumer. Easily understandable language and illustrations provide useful background knowledge for shopping in today's technological marketplace.

Order the above NIST publications from: Superintendent of Documents, Government Printing Office, Washington, DC 20402.

Order the following NIST publications—FIPS and NISTIRs—from the National Technical Information Service, Springfield, VA 22161.

Federal Information Processing Standards Publications (FIPS PUB)—Publications in this series collectively constitute the Federal Information Processing Standards Register. The Register serves as the official source of information in the Federal Government regarding standards issued by NIST pursuant to the Federal Property and Administrative Services Act of 1949 as amended, Public Law 89-306 (79 Stat. 1127), and as implemented by Executive Order 11717 (38 FR 12315, dated May 11, 1973) and Part 6 of Title 15 CFR (Code of Federal Regulations).

NIST Interagency Reports (NISTIR)—A special series of interim or final reports on work performed by NIST for outside sponsors (both government and non-government). In general, initial distribution is handled by the sponsor; public distribution is by the National Technical Information Service, Springfield, VA 22161, in paper copy or microfiche form.

U.S. Department of Commerce
National Institute of Standards and Technology
(formerly National Bureau of Standards)
Gaithersburg, MD 20899

Official Business
Penalty for Private Use \$300